Carbon stock and carbon turnover of boreal and temperate forests

Dissertation

zur Erlangung des akademischen Grades doctor rerum naturalium

(Dr. rer. nat.)

vorgelegt dem Rat der Chemisch-Geowissenschaftlichen Fakultät der Friedrich-Schiller-Universität Jena

von M.Sc. Martin Thurner

geboren am 07.02.1987 in Greiz

Gutachter:

1. Prof. Dr. Christiane Schmullius
   Friedrich-Schiller-Universität Jena
2. Associate Prof. Dr. Christian Beer
   Stockholm University
3. Prof. Dr. Dieter Gerten
   Potsdam-Institut für Klimafolgenforschung und Humboldt-Universität zu Berlin

Tag der Verteidigung: 08.06.2016

Allein ein ganzes Menschenalter würde nicht hinreichen, jedes Meisterstück der göttlichen Kunst in dem Reich der Natur nur zu erzählen, viel weniger, nach Würde zu betrachten.

Carl von Linné

Next Page:
Pristine boreal and temperate forest ecosystems and different mortality processes and agents (bark beetle infestations, caterpillar infestations, fire, frost, permafrost freezing and thawing, wind)
in Harz National Park and Rhön Biosphere Reserve (Germany), Bayerischer Wald / Sumava National Park (Germany / Czech Republic), La Gomera (Islas Canarias, Spain), Madeira (Portugal), Parque Nacional Alerce Andino, Reserva Nacional Lago Jeinimeini / Future Patagonia National Park and Reserva Nacional Tamango (Patagonia, Chile), Svyatoy Nos Peninsula / Baikal (Buryatia, Russia) and Tura (Central Siberia, Russia)

Danksagung

An dieser Stelle möchte ich allen Personen danken, die mir bei der Erstellung dieser Arbeit hilfreich zur Seite standen. Mein ganz besonderer Dank gebührt Dr. Christian Beer für die hervorragende Betreuung der Arbeit zunächst am Max-Planck-Institut für Biogeochemie und später an der Stockholm University. Ohne seine zahlreichen Anregungen und seine geduldige Unterstützung wäre diese Dissertation nicht möglich gewesen. Dr. Nuno Carvalhais danke ich für die Mitbetreuung dieser Arbeit und die ausgiebigen Diskussionen, die wesentlich zur Vertiefung der Analysen beitrugen. Ebenfalls danken möchte ich Prof. Dr. Christiane Schmullius für die Erstbetreuung der Promotion, ihre immerwährende Unterstützung und dafür, dass sie im Verlauf des Studiums mein Interesse an der Fernerkundung geweckt hat.

Für ihre Beiträge zu den veröffentlichten und noch unveröffentlichten Manuskripten, die im Rahmen meiner Doktorarbeit entstanden, danke ich Bernhard Ahrens, Christian Beer, Nuno Carvalhais, Philippe Ciais, Matthias Forkel, Andrew Friend, Akihiko Ito, Axel Kleidon, Elisabeth Kompter, Shaun Levick, Mark Lomas, Shaun Quegan, Tim Tito Rademacher, Maurizio Santoro, Sibyll Schaphoff, Dmitry Schepaschenko, Christiane Schmullius, Anatoly Shvidenko, Markus Tum, Andy Wiltshire und Thomas Wutzler. Für die hervorragenden Diskussionen, die Unterstützung und die angenehme Zeit am MPI für Biogeochemie möchte ich darüber hinaus Dr. Markus Reichstein und dem gesamten Department Biogeochemical Integration danken. Besonders bedanken möchte ich mich für die immer gute Atmosphäre in „unserem“ schönen Büro bei Altug Ekici, Matthias Forkel, Sonja Kaiser und Thijs Koelen. Weiterhin danke ich für die Unterstützung anderer Angehöriger des MPI, insbesondere der IT-Abteilung.

Für die gemeinsame schöne Zeit am Department of Environmental Science and Analytical Chemistry an der Stockholm University und allgemein in Stockholm danke ich Tina Bayer, Christian Beer, Matthias Brakebusch, Altug Ekici, Maria Norman, Philipp und Lena Porada sowie Erna Scherwin. Außerdem danke ich meinen Freunden, die während der zurückliegenden vier Jahre für die nötige Ablenkung und Aufmunterung sorgten und auf die ich mich während der gesamten Promotion immer verlassen konnte. Dabei seien vor allem Altug, Frederik, Hannes, Hans, Maik, Marius, Matthias, Misha, Robert B. und Robert W. erwähnt. Nicht zuletzt danke ich meiner Mutter Violetta, die mir immer optimale Bedingungen für meine Ausbildung ermöglichte und mich stets in jeglicher Hinsicht unterstützte, sowie meinem Onkel Frank, meiner Tante Angelika und meinen Großeltern Hedwig und Jakob.

Vorwort

Diese Dissertation basiert auf wissenschaftlichen Untersuchungen, die im Zeitraum Juni 2011 - Mai 2014 am Max-Planck-Institut für Biogeochemie und im Zeitraum Juni 2014 - April 2016 an der Stockholm University durchgeführt wurden. Wesentliche Bestandteile dieser Arbeit, insbesondere der Methoden- und Ergebnis-Kapitel 2-4, sind auch in wissenschaftlichen Publikationen in internationalen Zeitschriften verwendet worden bzw. sind dafür vorgesehen. Im Rahmen dieser Dissertation werden diese Untersuchungen in einen Gesamtzusammenhang eingeordnet und neu aufbereitet. Nachfolgend sind die drei zugehörigen veröffentlichten Publikationen aufgeführt, aus denen Textpassagen und Abbildungen entnommen wurden.

Thurner M, Beer C, Santoro M, Carvalhais N, Wutzler T, Schepaschenko D, Shvidenko A, Kompter E, Ahrens B, Levick SR, Schmullius C (2014) Carbon stock and density of northern boreal and temperate forests. Global Ecology and Biogeography, **23**, 297-310. (Chapter 2)

Thurner M, Beer C, Carvalhais N, Forkel M, Santoro M, Tum M, Schmullius C (2016) Large-scale variation in boreal and temperate forest carbon turnover rate related to climate. Geophysical Research Letters, **43**, 4576-4585. (Chapter 3)

Thurner M, Beer C, Ciais P, Friend AD, Ito A, Kleidon A, Lomas MR, Quegan S, Rademacher TT, Schaphoff S, Tum M, Wiltshire A, Carvalhais N (2017) Evaluation of climate-related carbon turnover processes in global vegetation models for boreal and temperate forests. Global Change Biology, doi:10.1111/gcb.13660. (Chapter 4)

Die folgenden Publikationen mit Bezug zum erweiterten Themenbereich dieser Dissertation sind darüber hinaus während der Arbeit an der Dissertation von mir mitverfasst worden:

Carvalhais N, Forkel M, Khomik M, Bellarby J, Jung M, Migliavacca M, Mu M, Saatchi S, Santoro M, Thurner M, Weber U, Ahrens B, Beer C, Cescatti A,

Randerson JT, Reichstein M (2014) Global covariation of carbon turnover times with climate in terrestrial ecosystems. Nature, **514**, 213-217.

Forkel M, Carvalhais N, Schaphoff S, von Bloh W, Migliavacca M, Thurner M, Thonicke K (2014) Identifying environmental controls on vegetation greenness phenology through model-data integration. Biogeosciences, **11**, 7025-7050.

Santoro M, Beaudoin A, Beer C, Cartus O, Fransson JES, Hall RJ, Pathe C, Schmullius C, Schepaschenko D, Shvidenko A, Thurner M, Wegmüller U (2015) Forest growing stock volume of the northern hemisphere: spatially explicit estimates for 2010 derived from Envisat ASAR data. Remote Sensing of Environment, **168**, 316-334.

Die folgende Publikation ist während der Arbeit an der Dissertation von mir mitverfasst worden, steht jedoch nicht im direkten Bezug zum Thema der Dissertation:

Doktor D, Lausch A, Spengler D, Thurner M (2014) Extraction of plant physiological status from hyperspectral signatures using machine learning methods. Remote Sensing, **6**, 12, 12247-12274.

Deutsche Kurzfassung der Arbeit

Wissenschaftlicher Hintergrund:

Der Klimawandel ist eine bedeutende Gefahr für die Umwelt und die Gesellschaft des 21. Jahrhunderts. In der Vergangenheit haben Wälder als Kohlenstoffsenken gewirkt, indem sie Kohlendioxid (CO_2) aus der Atmosphäre gebunden haben und somit die Auswirkungen des Klimawandels milderten. Angesichts der wahrscheinlich erhöhten Waldmortalität unter zukünftigen Klimabedingungen ist eine fortbestehende Kohlenstoffsenke in der terrestrischen Vegetation jedoch höchst unsicher. In dieser Hinsicht ist es von entscheidender Bedeutung, den Zustand und Wandel des Kohlenstoffbestands in Wäldern zu überwachen. Frühere Abschätzungen der Kohlenstoffbestände in borealen und gemäßigten Wäldern wurden üblicherweise von auf nationale Werte hochskalierten Waldinventurdaten abgeleitet, und gehen deshalb mit einer geringen räumlichen Auflösung und hohen verbleibenden Unsicherheit einher. Darüber hinaus sind die bedeutendsten Faktoren, die die räumlichen Muster des Wald-Kohlenstoffumsatzes auf großer räumlicher Skala bestimmen, nicht bekannt, da sie in räumlich begrenzten Geländestudien nur schwer beobachtet werden können.

Forschungsziele:

Das übergreifende Ziel dieser Arbeit ist es, unser Wissen über die räumliche Verbreitung der Kohlenstoffbestände und des Kohlenstoffumsatzes in den borealen und gemäßigten Wäldern der nördlichen Hemisphäre zu erweitern. Es kann in die folgenden wissenschaftlichen Ziele untergliedert werden:

(I) Die Ableitung einer räumlich expliziten Kohlenstoffdichtekarte einschließlich ihrer Unsicherheit.

(II) Die Untersuchung der räumlichen Zusammenhänge zwischen beobachtungsbasierter Kohlenstoffumsatzrate und Klimavariablen.

(III) Die Evaluierung verfügbarer globaler Vegetationsmodelle hinsichtlich ihrer Fähigkeit, die beobachteten räumlichen Zusammenhänge zwischen Kohlenstoffumsatzrate und Klima wiederzugeben.

Methoden:

Radarfernerkundungsdaten, die das Stammvolumen der borealen und gemäßigten Wälder der gesamten Nordhalbkugel (30-80°N) bei einer räumlichen Auflösung von 0.01° quantifizieren, sind kürzlich verfügbar geworden. Mithilfe von

forstinventurbasierten Datenbanken, die Informationen zur Holzdichte und zu allometrischen Beziehungen zwischen Biomasse-Kompartimenten bereithalten, kann das Stammvolumen in Kohlenstoffbestände umgerechnet werden, einschließlich Stamm-, Ast-, Laub- bzw. Nadel- und Wurzelbiomasse. Eine damit einhergehende Abschätzung der Unsicherheit der abgeleiteten Kohlenstoffbestände stellt eine wertvolle Information bereit, indem sie deren Verlässlichkeit quantifiziert und eine Integration mit globalen Vegetationsmodellen erleichtert. Zusätzlich wird das abgeleitete Produkt evaluiert, indem es mit hochskalierten Biomassedaten aus der Forstinventur auf regionaler Ebene verglichen wird. Basierend auf der Kohlenstoffdichtekarte können die Kohlenstoffbestände und -dichten für die abgedeckten Waldbiome und Kontinente ermittelt und mit früheren groben Abschätzungen verglichen werden. Zusammen mit verschiedenen fernerkundungsbasierten Produkten zur Nettoprimärproduktion wird aus der Kohlenstoffdichtekarte nachfolgend die Kohlenstoffumsatzrate auf einer räumlichen Auflösung von 0,5° abgeleitet. Auch dieses Produkt stellt räumlich explizite Informationen bereit und ist somit das erste seiner Art. Daraufhin werden die räumlichen Beziehungen zwischen der Kohlenstoffumsatzrate und einer umfangreichen Auswahl von Klimavariablen in ausgewählten borealen und gemäßigten Waldregionen untersucht. Außerdem werden die beobachteten Zusammenhänge auf plausible (Mortalitäts-) Prozesse und Ursachen zurückgeführt. Schließlich werden globale Vegetationsmodelle hinsichtlich ihrer Fähigkeit, die beobachteten räumlichen Muster in der Kohlenstoffumsatzrate und deren Beziehungen zum Klima zu reproduzieren, bewertet. Zu diesem Zweck werden die simulierte Biomasse und Nettoprimärproduktion von sieben verschiedenen Modellen (HYBRID4, JeDi, JULES, LPJml, ORCHIDEE, SDGVM, VISIT) auf einer räumlichen Auflösung von 0,5° verwendet. Darüber hinaus werden Mittelwerte für die abgedeckten Biome sowie Korrelationen zwischen Modellen und Beobachtungen ermittelt und in Bezug auf die Kohlenstoffumsatzrate, die Nettoprimärproduktion und die Biomasse verglichen. Abweichungen von den Beobachtungen deuten dabei auf fehlende oder vereinfachte Mortalitätsprozesse in derzeitigen globalen Vegetationsmodellen hin.

Hauptergebnisse:

Im Jahr 2010 waren 40.7 ± 15.7 PgC in borealen, 24.5 ± 9.4 PgC in gemäßigten Laub- und Misch- sowie 14.5 ± 4.8 PgC in gemäßigten Nadelwäldern gespeichert. Insgesamt summieren sich diese Werte auf 79.8 ± 29.9 PgC in den nördlichen borealen und gemäßigten Wäldern. Bezüglich der Kohlenstoffdichte enthalten gemäßigte

Nadelwälder durchschnittlich 6.21 ± 2.07 kgC m^{-2}, gefolgt von gemäßigten Laub- und Mischwäldern mit 5.80 ± 2.21 kgC m^{-2} und borealen Wäldern mit 4.00 ± 1.54 kgC m^{-2}. Der Vergleich der Kohlenstoffdichtekarte mit den hochskalierten Forstinventurdaten ergab eine hohe Übereinstimmung auf regionaler Skala (r^2 = 0.70–0.90). In borealen Wäldern steht die Kohlenstoffumsatzrate in räumlicher Beziehung mit der Winterlänge und Wintertemperatur, was auf direkte und indirekte Effekte von Frost-Stress auf die Waldmortalität hinweist. In gemäßigten Wäldern hingegen erklären klimatische Bedingungen, die Trockenstress und den Ausbruch von Insektenepidemien und Krankheitserregern begünstigen, die räumliche Variation der Kohlenstoffumsatzrate. Globale Vegetationsmodelle sind nur begrenzt in der Lage, die beobachteten räumlichen Muster in der Kohlenstoffumsatzrate wiederzugeben. Dies liegt sowohl in der Unsicherheit der simulierten Nettoprimärproduktion als auch in Unzulänglichkeiten der berücksichtigten Mortalitätsprozesse begründet. Bezüglich der Nettoprimärproduktion sind die meisten Modellergebnisse innerhalb von 20 % der beobachtungsbasierten Mittelwerte in borealen und gemäßigten Wäldern, obwohl die Korrelation zwischen Modellen und Beobachtungen oft gering ist ($r \leq 0.65$), mit wenigen Ausnahmen mäßiger Korrelation. Die Korrelation zwischen modellierter und beobachteter Biomasse und Kohlenstoffumsatzrate ist sogar noch wesentlich geringer. Die Abweichungen von der beobachtungsbasierten Kohlenstoffumsatzrate reichen von -61.5 % bis -6.6 % in borealen und von -60.3 % bis 10.3 % in gemäßigten Wäldern. Sie können hauptsächlich auf massive Überschätzungen der Biomasse zurückgeführt werden.

Schlussfolgerungen:

Mithilfe von Radarfernerkundungsdaten konnten neue Richtwerte der absoluten Menge und räumlichen Verteilung des Kohlenstoffbestands in borealen und gemäßigten Wäldern der Nordhemisphäre ermittelt werden. Eine vergleichbare Kohlenstoffdichtekarte war bisher nicht verfügbar und ist zum Beispiel für die Integration mit globalen Vegetationsmodellen von großem Wert. In dieser Arbeit konnte die Bedeutung von Fernerkundungsprodukten, die Aufschluss über die Vegetationsstruktur und -dynamik geben, für ein verbessertes Verständnis des Kohlenstoffkreislaufs in Wäldern demonstriert werden. Erstmals konnten die Auswirkungen zusammenwirkender Mortalitätsprozesse und deren Bedeutung auf grober Skala erforscht werden, wobei die gesamte Vielfältigkeit dieser Prozesse (Streufall, Hintergrundmortalität und alle Arten von Störungen) auf Landschaftsskala über lange Zeiträume erfasst wurde. Die Abbildung von Mortalitätsmechanismen

(Frost-Stress, Trockenstress, Insektenepidemien) in globalen Vegetationsmodellen müssen verbessert werden, um mit den beobachteten räumlichen Mustern der Kohlenstoffbestände besser übereinzustimmen und schlussendlich eine verbesserte Vorhersage der zukünftigen Rückwirkungen des terrestrischen Kohlenstoffkreislaufs auf das Klima und veränderte Klimabedingungen zu ermöglichen.

Executive Summary

Background:

Climate change is a major threat for the environment and society in the 21st century. In the past, forests have been acting as a carbon sink, sequestering atmospheric CO_2 and thus mitigating climate change effects. However, in view of likely intensified forest mortality under future climate conditions, a continued carbon sink in the terrestrial vegetation is highly uncertain. In this respect, it is of critical importance to monitor the state of and changes in forest carbon stock. Earlier estimates of boreal and temperate forest carbon stock were usually based on up-scaling of forest inventory data to national estimates, involving a poor spatial resolution and high remaining uncertainty. Moreover, the most important drivers underlying the spatial patterns of broad-scale forest carbon turnover are unknown, since they can hardly be observed by plot-level field studies alone.

Research objectives:

The general objective of this thesis is to increase our knowledge on the spatial distribution of carbon stock and carbon turnover in Northern Hemisphere boreal and temperate forests. This overall objective comprises the following research objectives:

(I) The derivation of a spatially explicit carbon density map including uncertainties.

(II) The investigation of spatial relationships between observation based forest carbon turnover rate (k) and climate variables.

(III) The evaluation of available global vegetation models (GVMs) concerning their ability to reproduce observed spatial relationships between k and climate.

Methods:

At a spatial resolution of 0.01°, radar remote sensing data of forest growing stock volume (GSV) became recently available, covering the entire Northern Hemisphere boreal and temperate forests (30-80°N). By applying forest inventory based databases on wood density and biomass allometry, stem volume can be converted to carbon stock, including stem, branch, foliage and root carbon. Corresponding uncertainty provides very relevant information concerning the reliability of the product and facilitates integration with GVMs. In addition, the derived product is evaluated with respect to up-

scaled forest inventory biomass data at regional scales. Carbon stocks and densities are derived for different forest biomes and continents and compared to former existing rough estimates. Together with different remote sensing based products on net primary production (NPP), the carbon density map is subsequently used to derive for the first time spatially explicit estimates of *k* at 0.5° resolution. The spatial relationships between *k* and an extensive selection climate variables are investigated in selected boreal and temperate forest transects. Furthermore, the observed relationships are attributed to plausible underlying (mortality) processes and agents. Finally, GVMs are evaluated concerning their ability to reproduce observed spatial patterns in *k* and the relations to climate. For this purpose, simulated biomass and NPP are obtained from seven different models (HYBRID4, JeDi, JULES, LPJml, ORCHIDEE, SDGVM, VISIT) applied at 0.5° spatial resolution. In addition, biome average values and correlations are compared between models and observations regarding *k*, NPP and biomass. Deviations from observations are used to identify and discuss missing or oversimplified mortality processes in current GVMs.

Main Results:

In 2010, 40.7 ± 15.7 PgC are stored in boreal forests (BFT), whereas temperate broadleaf and mixed forests (TBMF) and temperate conifer forests (TCF) contain 24.5 ± 9.4 PgC and 14.5 ± 4.8 PgC, respectively. In total, these numbers add up to 79.8 ± 29.9 PgC stored in northern boreal and temperate forests. In terms of carbon density, 6.21 ± 2.07 kgC m^{-2} are retained in TCF and 5.80 ± 2.21 kgC m^{-2} in TBMF, whereas BFT have a mean carbon density of 4.00 ± 1.54 kgC m^{-2}. The evaluation of the resulting carbon density map revealed strong agreement at regional scale (r^2 = 0.70–0.90). In boreal forests, the spatial variation of *k* is found to be related to winter length and temperature, indicating direct and indirect frost damage effects on forest mortality. In temperate forests, in contrast, climatic conditions favouring drought stress and insect or pathogen outbreak related mortality can explain the spatial variation in *k*. GVMs are able to reproduce the observed spatial patterns of *k* only to a limited extent, due to both uncertainties in simulated NPP and shortcomings regarding the implemented mortality processes. Concerning NPP, most of the models are within 20 % of observed overall averages for boreal and temperate forests, although correlation between models and observations is often weak ($r \leq 0.65$) with only few exceptions of moderate correlation. Correlations are even much weaker regarding biomass and *k*. Deviations from observation based *k* range from -61.5 % to -6.6 % in boreal and from -60.3 % to 10.3 %

in temperate forests, and can be attributed mostly to severe overestimations of observed biomass.

Main Conclusions:

The radar remote sensing data allowed for benchmarking the absolute amount and spatial distribution of Northern Hemisphere boreal and temperate forest carbon stock. Such a carbon density map has been missing before and is of great value for instance for integration purposes with GVMs. The significance of remote sensing products related to vegetation structure and dynamics for an improved understanding of the carbon cycle in forests has been demonstrated. For the first time the effects of interacting mortality processes and their relevance at continental scale could be investigated, capturing the whole variety of turnover processes (litterfall, background mortality, and all kinds of disturbances) at landscape scale over long time periods. The representations of mortality mechanisms (frost stress, drought stress, insect epidemics) in GVMs need to be improved in order to better match observed carbon stock spatial patterns and finally enable a better informed prediction of future land carbon cycle feedbacks to climate change.

Content

Figures

Tables

Abbreviations

AIC	Akaike's information criterion
AMT	Annual mean temperature
AR5	Fifth Assessment Report
ASAR	Advanced Synthetic Aperture Radar
BETHY	Biosphere Energy Transfer Hydrology
BFT	Boreal forests (biome)
BIOCLIM	Bioclimatic variables
CH_4	Methane
CMIP3/CMIP5	$3^{rd}/5^{th}$ Coupled Model Intercomparison Project
C	Carbon
CLIMDEX	Climate extreme variables
CO_2	Carbon dioxide
DGVMs	Dynamic global vegetation models
DLR	German Aerospace Center (Deutsche Zentrum für Luft- und Raumfahrt)
Envisat	Environmental Satellite
ESA	European Space Agency
ESMs	Earth System Models
fAPAR	Fraction of Absorbed Photosynthetically Active Radiation
FIA	Forest Inventory and Analysis
FD	Number of frost days
GAM	Generalized additive models
GFED4	Global Fire Emissions Database
GHG-AFOLU	Greenhouse Gases in Agriculture, Forestry and Other Land Uses
GLAS	Geoscience Laser Altimeter System
GLC2000	Global Land Cover for the Year 2000
GPP	Gross primary production
GSL	Growing season length
GSV	Growing stock volume
GVMs	Global vegetation models
HadGEM2-ES	Met Office Hadley Centre Global Environment Model version 2 – Earth System
HWSD	Harmonized World Soil Database
IAMs	Integrated Assessment Models

ICESat	Ice, Cloud, and land Elevation Satellite
ID	Number of icing days
IIASA	International Institute for Applied Systems Analysis
InSAR	Interferometric synthetic aperture radar
IPCC	Intergovernmental Panel on Climate Change
ISI-MIP	Inter-Sectoral Impact Model Intercomparison Project
ISO	Isothermality
JRC	Joint Research Centre
k	Forest carbon turnover rate
LAI	Leaf area index
LiDAR	Light detection and ranging
MEF	Modelling efficiency
MODIS	Moderate-resolution Imaging Spectroradiometer
MPI	Max-Planck-Institute
N	Nitrogen
N_2O	Nitrous oxide
NASA	National Aeronautics and Space Administration
NBCD2000	United States National Biomass and Carbon Dataset for the year 2000
NBP	Net biome production
NEE	Net ecosystem exchange
NEP	Net ecosystem production
NPP	Net primary production
PFTs	Plant functional types
r	Pearson correlation coefficient
R_a	Autotrophic respiration
Radar	Radio detection and ranging
RCPs	Representative Concentration Pathways
REDD+	Reducing Emissions from Deforestation and Degradation and the role of conservation, sustainable management of forests and enhancement of forest carbon stocks in developing countries
R_h	Heterotrophic respiration
RMSE	Root mean square error
RSE	Residual standard error
SAR	Synthetic aperture radar
SD	Number of summer days

SPII	Simple precipitation intensity index
SRTM	Shuttle Radar Topography Mission
TBMF	Temperate broadleaf / mixed forests (biome)
TCF	Temperate conifer forests (biome)
TCM	Minimum temperature of coldest month
TCQ	Mean temperature of coldest quarter
TDQ	Mean temperature of driest quarter
TN	Number of tropical nights
TS	Temperature seasonality
TWarmQ	Mean temperature of warmest quarter
TWM	Maximum temperature of warmest month
USDA	United States Department of Agriculture
VCF	Vegetation Continuous Field
VOC	Volatile organic compound
WATCH	Water and Global Change programme
WD10	Maximum length of warm (maximum temperature ≥ 10°C) –dry (no precipitation) periods
WHRC	Woods Hole Research Center

CHAPTER 1

Introduction

Forests are of inestimable ecological, social, economic and political value. Ecological – because they sequester carbon dioxide (CO_2) from the atmosphere and thus mitigate global warming, because they interact not only with the carbon cycle, but also with the energy and water cycles by means of their albedo and evapotranspiration, and because they provide the habitat for an enormous biodiversity of animals and plants. Social – since forests can serve as recreational areas. Economic – as a provider of wood products (Bonan, 2008). And now even political – in the context of the "Reducing Emissions from Deforestation and Degradation and the role of conservation, sustainable management of forests and enhancement of forest carbon stocks in developing countries" (REDD+) scheme (UN-REDD, 2011).

However, there are huge uncertainties associated with the estimated amount of carbon (C) stored in the World's forests, both in vegetation and soils (Ciais *et al.*, 2013). We hardly know the magnitude and spatial variation of changes in forest carbon stocks, either through climate change effects or direct human intervention (Pan *et al.*, 2011). We also do not know the importance of processes determining forest mortality and carbon turnover at a global scale, despite evidence of severe forest mortality due to drought and heat (Allen *et al.*, 2010, 2015) and caused by intensified climate extremes in general (Reichstein *et al.*, 2013). The work documented in this thesis is a step forward to answer some of these open questions more precisely. A step forward to understand the threat of climate change to forest ecosystems and the potential of forests to mitigate rising atmospheric CO_2 caused by fossil fuel emissions over the long term.

In the following, the interactions between climate and the forest carbon cycle in light of climate change conditions are described. Forest carbon turnover rate (k) is introduced as a key ecosystem property to characterize the long-term dynamics of the forest carbon cycle and its response to climate change. Subsequently, an overview on available information on forest carbon stocks and net primary production (NPP) from forest

inventory and remote sensing data as well as from global vegetation models (GVMs) is given. Based on this state of knowledge, the need for research and objectives of this work arise.

1.1 Climate change

Climate change is a major threat for the environment and society in the 21st century. The Intergovernmental Panel on Climate Change (IPCC) reports summarize the current scientific knowledge and provide the basis for political decisions. According to the most recent report, the Fifth Assessment Report (AR5), atmospheric CO_2 has been increasing continuously from 278 ppm before the industrial age (value from about 1750) to 390.5 ppm in 2011. This increase can be attributed with very high confidence to fossil-fuel (coal, oil, gas) and cement emissions (Ciais *et al.*, 2013). In addition to CO_2, also the concentrations of other greenhouse gases in the atmosphere, most importantly methane (CH_4) and nitrous oxide (N_2O), have been increasing as a consequence of human-induced emissions, land-use change and feedback mechanisms of climate change.

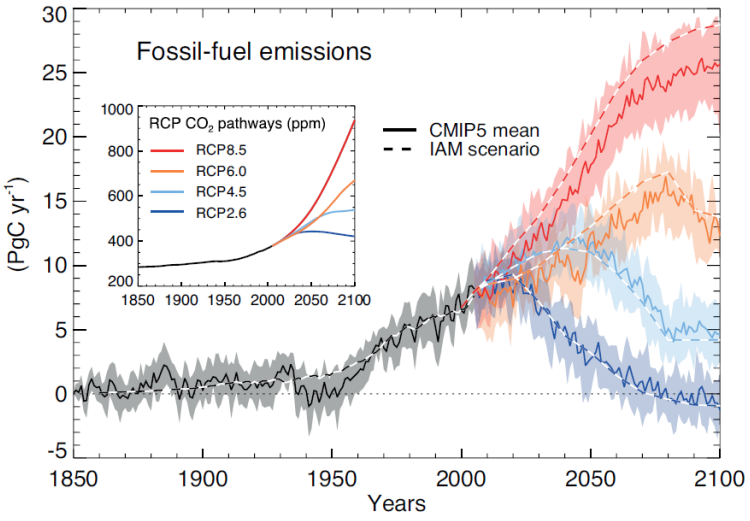

Fig. 1.1: Fossil-fuel emission rate in PgC y^{-1} simulated by CMIP5 ESMs (solid lines with standard deviation) and IAMs (dashed lines) for the historical period (1860-2005) and for four RCP scenarios until 2100. The small inner figure shows the corresponding simulated increase in atmospheric CO_2 in ppm (Ciais *et al.*, 2013, p.527).

Different scenarios of future emissions, the so-called Representative Concentration Pathways (RCPs), are generated by Integrated Assessment Models (IAMs). These RCPs assume four different scenarios of the peak or stabilization value of the radiative forcing

within the 21st century, including not only forcing from CO_2, but also from other greenhouse gases and from land use change (RCP2.6: peak at 3 W m^{-2} followed by stabilization at 2.6 W m^{-2} by 2100, RCP4.5 and RCP6.0: stabilization at 4.5 and 6 W m^{-2} respectively around 2100, RCP8.5: 8.5 W m^{-2} by 2100 followed by further increase; Moss *et al.*, 2010; van Vuuren *et al.*, 2011; in Cubasch *et al.*, 2013; Fig. 1.1). The occurrence of the scenarios is dependent on the development of society and economy.

These RCPs can be used to drive Earth System Models (ESMs), which simulate the carbon cycle between and within atmosphere, ocean and land. Such models, as applied for example within the 5th Coupled Model Intercomparison Project (CMIP5), allow for the interaction of physical processes with biogeochemical cycles. For instance, feedbacks between the CO_2 balance and air temperature are represented. Anthropogenic greenhouse gas emissions likely contributed between 0.5 and 1.3°C to the observed global mean surface warming of 0.6°C during 1951-2010 (Bindoff *et al.*, 2013). With the help of ESMs, it can be shown that increases in global mean surface temperature anomaly can very likely be explained by forcings caused by anthropogenic emissions in addition to natural forcings, but not by natural forcings alone (Jones *et al.*, 2013; Knutson *et al.*, 2013; in Bindoff *et al.*, 2013; Fig. 1.2). Natural forcings comprise most importantly changes in solar irradiance and volcanic eruptions (Myhre *et al.*, 2013).

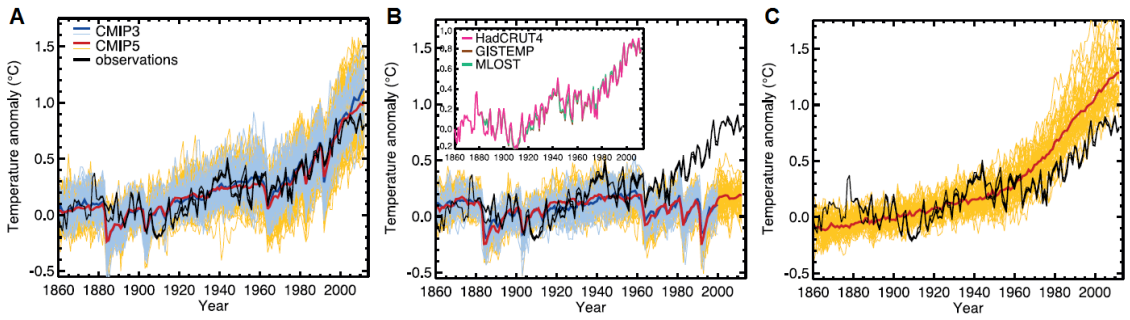

Fig. 1.2: Observed global mean surface temperature anomalies (black lines; with respect to 1880-1919) compared to CMIP3 (thin blue lines; average = thick blue line) and CMIP5 (thin yellow lines; average = thick red line) model simulations considering anthropogenic and natural forcings (A), natural forcings only (B) and anthropogenic forcings only (C). In the inset to (B) the three observational datasets (Hadley Centre/Climatic Research Unit gridded surface temperature data set 4 (HadCRUT4), Goddard Institute of Space Studies Surface Temperature Analysis (GISTEMP), and Merged Land–Ocean Surface Temperature Analysis (MLOST)) are separated (Jones *et al.*, 2013; Knutson *et al.*, 2013; in Bindoff *et al.*, 2013, p.879).

In addition to mean surface temperature, climate change is expected to affect also temperature and precipitation extremes. CMIP5 models driven by the extreme RCP8.5 scenario forecast a decrease in cold and an increase in warm temperature extremes in the end of the 21st century. In the Northern Hemisphere boreal regions, the decrease in cold temperature extremes is particularly remarkable, whereas in temperate regions the strongest increase in warm temperature extremes is predicted. Across both these regions, an important decline in the number of frost days is projected accordingly. In terms of the water cycle, the duration of drought events is simulated to increase in the Mediterranean, opposite to a decrease in the high latitudes of the Northern Hemisphere (Sillmann *et al.*, 2013; in Collins *et al.*, 2013; Fig. 1.3).

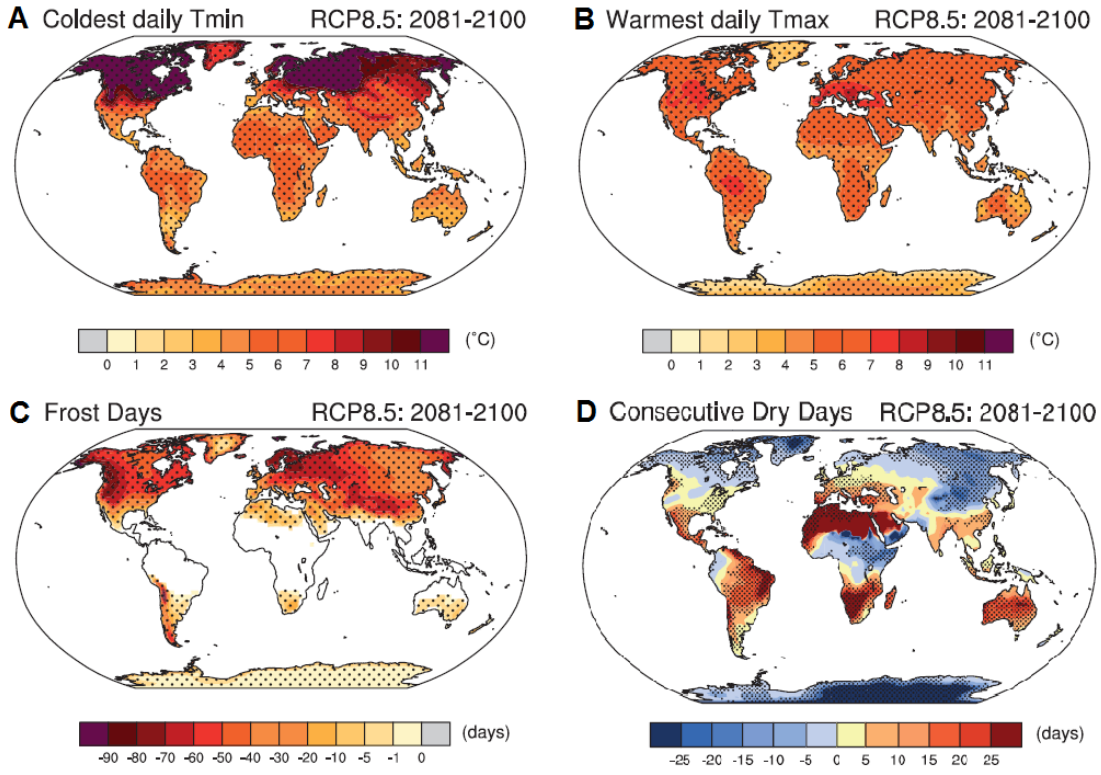

Fig. 1.3: Projected changes in annual minimum of daily minimum temperature (A), annual maximum of daily maximum temperature (B), annual number of frost days (minimum temperature < 0°C; C) and annual maximum consecutive dry days (precipitation < 1 mm; D) during 2081-2100 compared to 1981-2000 by CMIP5 models, applying the RCP8.5 scenario. Stippling indicates grid cells with significant changes at the 5 % level (Sillmann *et al.*, 2013; in Collins *et al.*, 2013, p. 1067/1083).

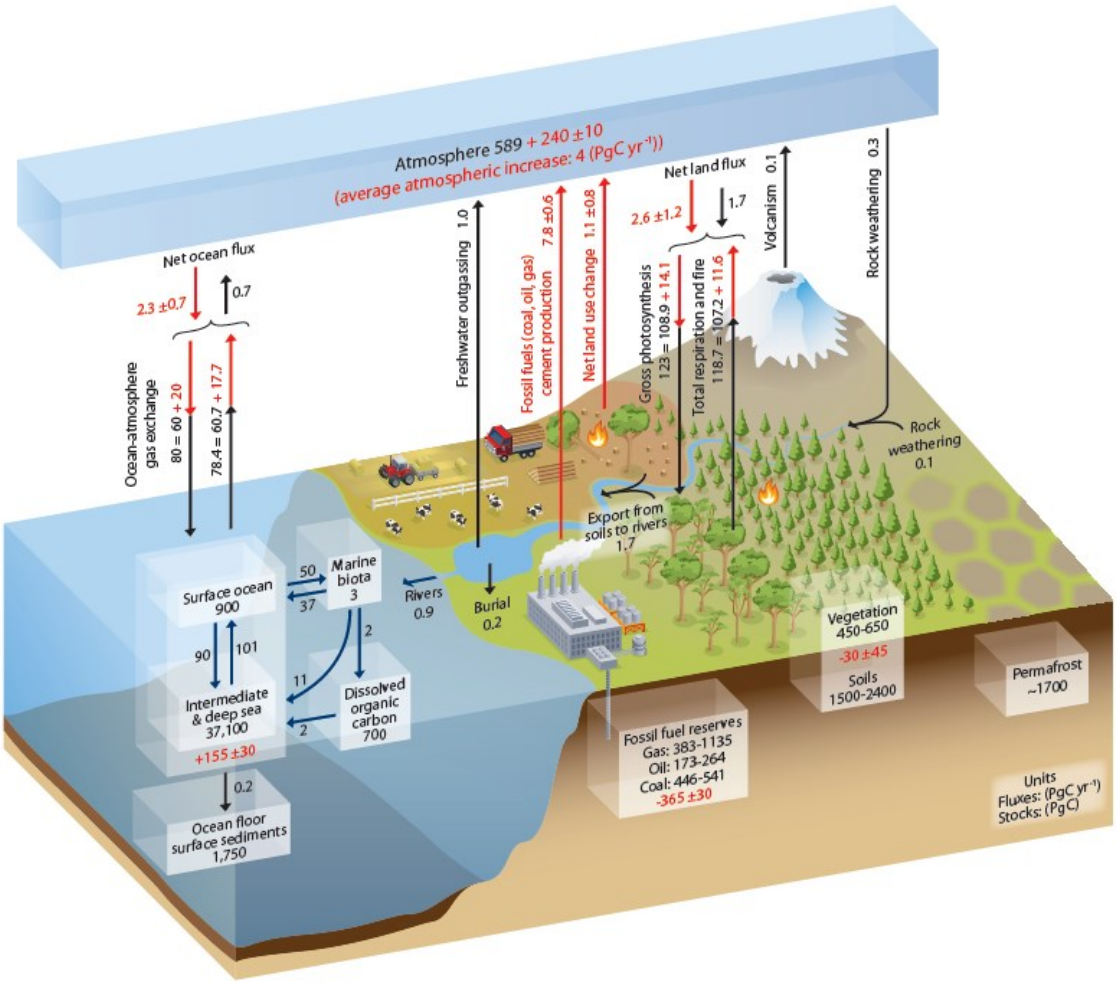

Fig. 1.4: The global carbon cycle. Black numbers and arrows represent stocks [PgC] and fluxes [PgC yr^{-1}] estimated for the time prior to the Industrial Era (1750). Red numbers and arrows indicate human induced fluxes averaged over the 2000–2009 time period. Red numbers in the carbon stocks denote cumulative changes of anthropogenic carbon over the Industrial Period 1750–2011. Uncertainties are given as 90% confidence intervals. (Ciais *et al.*, 2013, p. 471)

In the atmosphere, carbon is mostly bound in CO_2 (828 PgC). The increase in atmospheric CO_2 by fossil fuel emissions and land use change has been partly counteracted by the carbon fixation in the land (vegetation, soil, and freshwater) and ocean reservoirs (Ciais *et al.*, 2013; Le Quéré *et al.*, 2015; Fig. 1.4). Both land carbon stock and flux estimates are highly uncertain due to difficulties to sufficiently cover the spatial (and temporal) heterogeneity and complexity of vegetation and soil carbon stocks and fluxes with measurements. These uncertainties make it necessary to infer the global land carbon sink as the residual of anthropogenic CO_2 emissions, the land use change flux and the uptake of CO_2 in the atmosphere and the ocean, instead of a direct estimation. Based on this method, it has been inferred that the land surface has been

acting as a carbon sink during 1750-2011, gaining in total 160 ± 90 PgC (Ciais *et al.*, 2013). This carbon sink has been attributed to different processes, including the fertilization effect of enhanced atmospheric CO_2 on photosynthesis (e.g. Sitch *et al.*, 2008, 2015), the fertilization effect of nitrogen (N) on plant productivity as a consequence of increased N deposition (e.g. Norby, 1998), direct climate effects on plant productivity (e.g. Nemani *et al.*, 2003), and forest regrowth and afforestation (e.g. Pan *et al.*, 2011). Hence, the land carbon cycle acts as a negative feedback to climate change. However, the sustainability of this carbon sink is under debate. Coupled climate- carbon cycle models show large discrepancies in the projected development of the land carbon uptake until 2100 (Friedlingstein *et al.*, 2006; Ahlström *et al.*, 2012).

1.2 The carbon cycle in forest ecosystems

While forest ecosystems cover around 30 % of the land surface, they are supposed to store approximately 45 % of the carbon sequestered in land ecosystems and at present act as a carbon sink of increased atmospheric CO_2 (Bonan *et al.*, 2008). A spatially more detailed study based on up-scaled forest inventory data has further quantified the carbon stocks and carbon sinks across all forest ecosystems (Pan *et al.*, 2011; Fig. 1.5). According to these estimates boreal and temperate forests store relatively similar amounts of carbon in living vegetation, whereas a much larger amount of carbon is sequestered in the soils of boreal compared to temperate forests (Table 1.1). Both boreal and temperate forests have been acting as carbon sinks during 1990-2007.

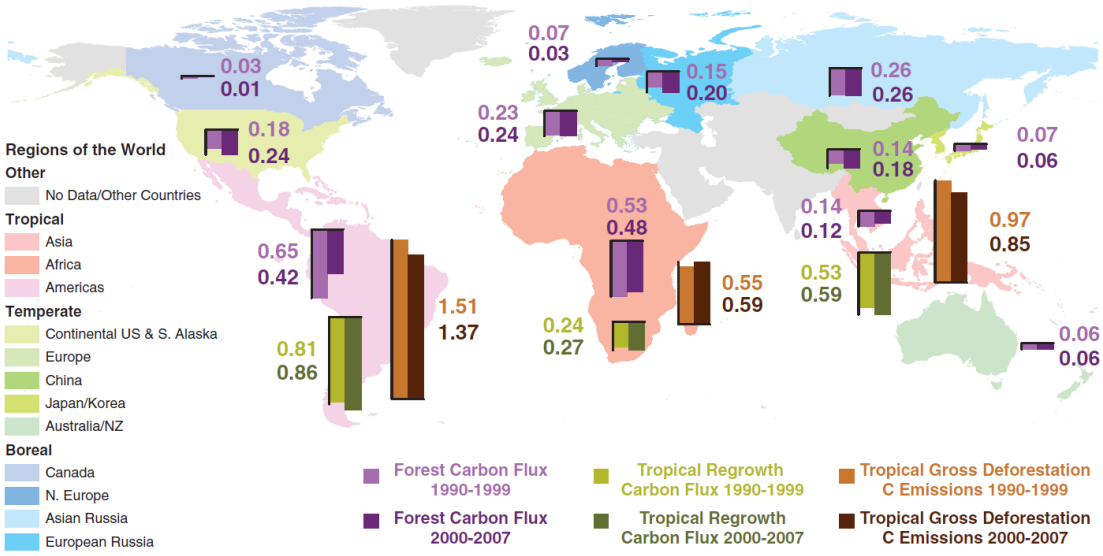

Fig. 1.5: Forest carbon sinks (downwards) and sources (upwards) [PgC yr^{-1}] (Pan *et al.*, 2011, p. 991)

Table 1.1: Area, carbon stocks and carbon sinks of boreal and temperate forests (Pan *et al.*, 2011)

	Boreal forests	Temperate forests
Area	1135 Mha	767 Mha
Living biomass carbon stocks	53.9 PgC	46.6 PgC
Dead wood carbon stocks	16.1 PgC	3.3 PgC
Litter carbon stocks	27.0 PgC	12.1 PgC
Soil carbon stocks	174.5 PgC	56.7 PgC
Total carbon stocks	271.5 ± 22.5 PgC	118.6 ± 6.3 PgC
Total carbon density	239.2 MgC ha^{-1}	154.7 MgC ha^{-1}
Carbon sink (1990-2007)	0.50 ± 0.08 PgC y^{-1}	0.72 ± 0.08 PgC y^{-1}

Opposite to their negative feedback on the carbon cycle, the comparably low albedo of forest ecosystems is a positive climate forcing. This is especially true for boreal forests, which have a significantly lower albedo than other boreal land covers particularly in case of snow cover. The importance of other biophysical effects like the cooling potential from evapotranspiration in forest ecosystems is less well understood, but considered more important in tropical than in temperate or boreal forests (Bonan *et al.*, 2008).

Forests assimilate carbon by the process of photosynthesis, and this uptake of CO_2 at the ecosystem scale is called gross primary production (GPP). A fraction of the assimilated carbon is required for plant growth and maintenance and thus lost to the atmosphere by autotrophic respiration (R_a). The remaining net uptake of CO_2 is called NPP (Chapin *et al.*, 2002):

$$NPP = GPP - R_a \qquad \text{(Eq. 1.1)}$$

NPP is distributed to different tree compartments, namely stem, branch, root (fine and coarse) and foliage carbon pools. This process is called carbon allocation, resulting in a specific allometry between biomass compartments dependent on allocation fractions. Carbon allocation is a function of the most limiting resource(s) in an ecosystem. Proportionally more carbon is distributed either to the foliage (light limited ecosystem) or to the roots (soil water or nutrient limited ecosystem) in order to maximize the capacity to absorb the limiting resource(s) (Chapin *et al.*, 2002).

Due to senescence and tree mortality, plant material is transferred to the litter pool (litterfall), and finally decomposed and added to the soil pool. Soil organic carbon is further decomposed by microbes and other soil organisms, and the carbon is again released by heterotrophic respiration (R_h) to the atmosphere, whereas R_h in turn makes minerals available for production processes. Furthermore, parts of NPP are consumed by animals (herbivory) and transferred partly to the atmosphere (animal respiration as a part of R_h), partly to the soil this way. Net ecosystem production (NEP) describes the net accumulation of carbon by an ecosystem (Chapin *et al.*, 2002):

$$NEP = NPP \pm F_{lateral} - (R_h + F_{disturbances} + F_{leaching} + F_{VOC} + F_{CH4}) \qquad \text{(Eq. 1.2)}$$

At large (i.e., regional) spatial scales, NEP equals net biome production (NBP). In addition to NPP and R_h, also other important components of NEP need to be considered. Most importantly, episodically occurring disturbances (deforestation, fire, $F_{disturbances}$) can release huge amounts of carbon in a short time. Other processes contributing to NEP are leaching of carbon from the soil to the groundwater and streams ($F_{leaching}$), carbon losses by volatile organic compound (VOC) emissions from plants to the atmosphere (F_{VOC}), methane emissions from the soil to the atmosphere (F_{CH4}), and lateral transport (gain by deposition or loss by erosion) of carbon between ecosystems ($F_{lateral}$). Between disturbance events, climate-dependent NPP and R_h are the processes determining NEP, but nevertheless NEP is more strongly influenced by time since disturbance than by climate (Chapin *et al.*, 2002).
The carbon balance of forest vegetation can also be considered separately from the soil (Fig. 1.6):

$$\frac{\Delta Biomass}{\Delta t} = NPP - \left(F_{litterfall} + F_{rootExudates} + F_{herbivory} + F_{VOC} + F_{disturbances}\right) \qquad \text{(Eq. 1.3)}$$

The change in vegetation biomass ($\Delta Biomass$) over time (Δt) is the difference of the net carbon influx (NPP; photosynthesis minus plant respiratory costs) and the carbon outflux. The carbon outflux is the sum of a variety of processes occurring at different timescales, and includes litterfall ($F_{litterfall}$), carbon exuded by roots or transferred to microbes in a symbiotic relationship with roots (e.g. mycorrhizae; $F_{rootExudates}$), herbivory ($F_{herbivory}$), emissions of VOCs (F_{VOC}), and disturbances ($F_{disturbances}$). Again, typically

litterfall is the largest carbon loss from plants, but episodic disturbances can have a very important impact when they occur (Chapin *et al.*, 2002).

While litterfall accounts for senescence of tree components and also individual tree mortality, transferring carbon from the vegetation to the litter and subsequently the soil pool, disturbance by deforestation or fire immediately remove the carbon from the entire forest ecosystem. There are many different mechanisms which are considered to lead to tree mortality, and they can both act as large-scale disturbances and at individual scale. Examples are mortality induced by drought, frost, insects or pathogens, and wind throw (for a detailed discussion of these mortality mechanisms, please refer to Chapter 5.2). In contrast to deforestation and fire, these processes transfer carbon from the vegetation to the litter pool. Individual tree mortality can also occur as a result of competition between individuals for resources (light, water, nutrients) (e.g. Das *et al.*, 2011), or physical tree mortality as a consequence of uprooting, snapping, or crushing by falling surrounding trees or wood or root rot (Holzwarth *et al.*, 2013). Individual tree mortality due to senescence may be caused by no longer sustainable demands on water and nutrient supply with increasing size, but also genetic controls cannot be ruled out (Penuelas, 2005).

Climate and atmospheric CO_2 are important drivers of the carbon cycle in forest ecosystems (cf. Fig. 1.6). In experiments (e.g. Zak *et al.*, 2011) and models (e.g. Sitch *et al.*, 2008, 2015), elevated CO_2 has been shown to have a fertilization effect on photosynthesis, leading to higher productivity. However, this effect is supposed to be limited by the availability of nutrients, mostly by N in boreal and temperate forests (e.g. Goll *et al.*, 2012). Increased temperature as well has been reported to have a positive feedback on NPP (Nemani *et al.*, 2003) on the one hand, but also causes increased soil respiration (Bond-Lamberty & Thomson, 2010) on the other hand. The relative importance of these feedbacks is largely unknown, but models suggest an increase in both NPP and NEP caused by changes in climate in high latitudes. Effects of rising temperature may be very heterogeneous in space, and in addition are coupled to changes in the water cycle (Friedlingstein *et al.*, 2006). Moreover, rising mean temperatures and the expected increased frequency and severity of climate extremes (Reichstein *et al.*, 2013) influence the carbon cycle by their effects on forest mortality (see Chapter 5.2). Disturbances and vegetation dynamics (establishment, growth, competition, disturbances) in general, including their response and feedback to climate change, belong to the most critical processes not properly taken into account by models as identified by the IPCC report (Ciais *et al.*, 2013).

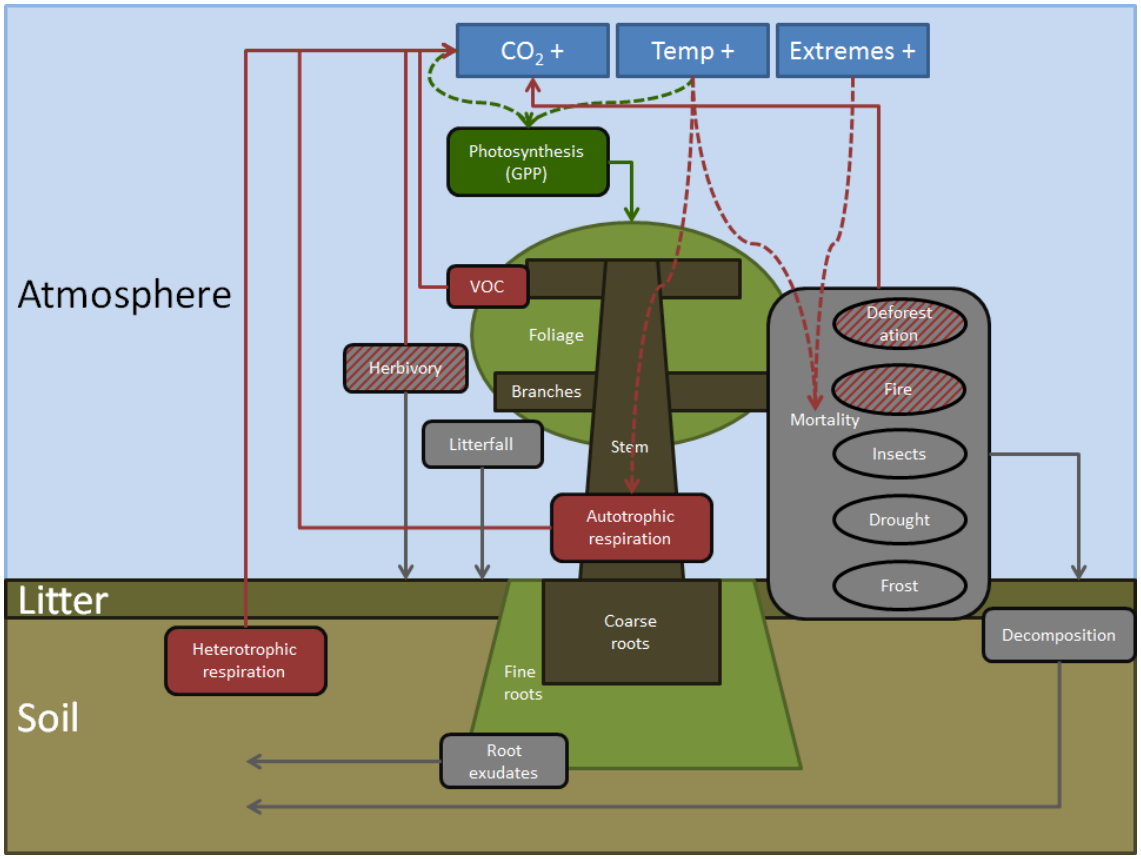

Fig. 1.6: The carbon cycle in forest ecosystems and its feedback to increasing atmospheric CO_2 content, increasing temperatures and intensified climate extremes. Green boxes and solid green arrows indicate carbon fluxes from the atmosphere to the vegetation. Red boxes and solid red arrows indicate carbon fluxes from the vegetation or the soil to the atmosphere. Grey boxes and arrows indicate carbon fluxes from the vegetation to the soil. Negative feedbacks are indicated by dashed green arrows. Positive feedbacks are indicated by dashed red arrows.

1.3 Carbon turnover rate as a key ecosystem property

The vegetation carbon turnover rate describes the fraction of carbon lost from the vegetation during a specific time, usually per year. It equals the reciprocal of carbon turnover time, which approximates carbon residence time (denoting the average time a carbon atom is stored in vegetation biomass) under steady state conditions (Bolin & Rodhe, 1973; Rodhe, 1992) and in general if long-term averages are considered (Schwartz, 1979). Uncertainties have been found to be larger in the climate change response of carbon residence time than of NPP (Friend *et al.*, 2014; Fig. 1.7). Applying a set of GVMs participating in the Inter-Sectoral Impact Model Intercomparison Project (ISI-MIP; Warszawski *et al.*, 2014) for different climate scenarios predicted by a range of general circulation models, an increase of 52-477 PgC stored in vegetation is

simulated in case the mean global land surface temperature rises by 4°C. Although models agree on a continued carbon sink effect in the first half of the simulation period (until 2100), there are important differences between models and according to some of them, the land vegetation may turn into a carbon source towards the end of this century. Importantly, these differences are mostly due to disagreements in the modelled carbon residence time. While all models except HYBRID agree on continued increases in NPP mainly due to CO_2 fertilization effects on photosynthesis, different carbon turnover and mortality implementations contribute to larger differences in the simulated carbon residence time (Friend *et al.*, 2014).

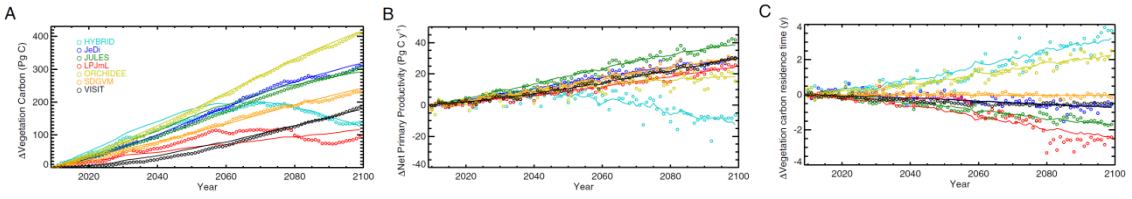

Fig. 1.7: Changes in global vegetation carbon stocks (A), NPP (B) and vegetation carbon residence time (C) projected by GVMs participating in ISI-MIP, applying the HadGEM2-ES RCP 8.5 climate and CO_2 scenario (Friend *et al.*, 2014, p. 3282)

Here specifically the vegetation carbon turnover rate in forest ecosystems is of interest. The vegetation carbon turnover rate concept accounts for several processes that control the time at which carbon is lost from the vegetation, such as background mortality (including litterfall, root exudates and herbivory), mortality by disturbances, and forest management. Unfortunately these outflux processes are difficult to measure, especially over large areas and during long timespans. However, under the assumption of steady state, the influx (NPP) to the forest carbon reservoir (Biomass) is balanced with its outflux, and the forest carbon turnover rate (k) can be derived from the flux and the reservoir size:

$$k = \frac{NPP}{Biomass} \qquad \text{(Eq. 1.4)}$$

A similar concept has been used to study total ecosystem turnover time, integrating over both vegetation and soil (Carvalhais *et al.*, 2014). Based on this approach, it has been shown that total ecosystem carbon turnover time covaries more strongly with precipitation globally than considered in ESMs, which also show large discrepancies

between each other (Fig. 1.8). However, in Northern Hemisphere boreal ecosystems, the mean of the model ensemble matches the observations relatively well in terms of their partial correlation to precipitation. In Northern Hemisphere temperate ecosystems, the observed negative correlation between residence time and precipitation is more pronounced compared to the models. In contrast, the models simulate a much stronger negative correlation between residence time and temperature than found in the observations in Northern Hemisphere boreal and temperate ecosystems. In general, these correlations are mainly driven by soil carbon and less by vegetation carbon (Carvalhais *et al.*, 2014). A detailed study focusing on vegetation carbon turnover rate and its relation to climate is essential to understand the underlying processes concerning the vegetation component of turnover rate, separated from the soil component. In addition, forest ecosystems may behave differently from non-forest ecosystems and it is important to investigate them separately.

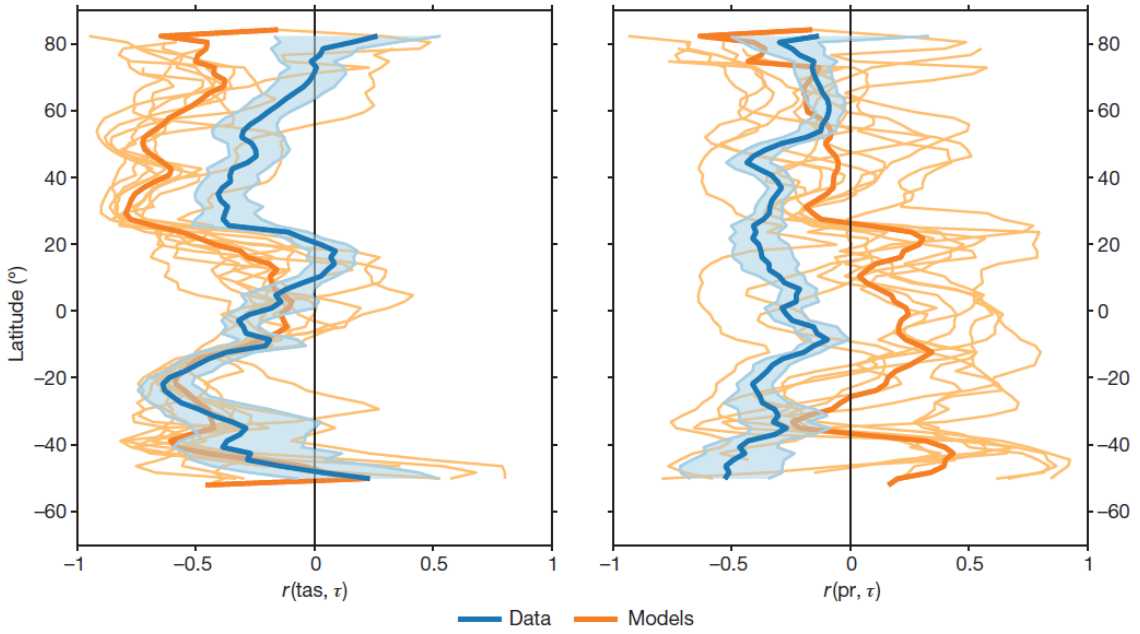

Fig. 1.8: Latitudinal gradients in the partial correlation between observed and modelled ecosystem carbon turnover time and temperature (left) and precipitation (right; Carvalhais *et al.*, 2014, p. 215)

In the tropics, a six-fold variation (23–129 years) in woody biomass residence time has been observed based on a collection of field studies (Galbraith *et al.*, 2013; Fig. 1.9). Although the median of woody biomass residence time was very similar in observations and between vegetation models (ca. 50 years), the range of modelled values is large (20-200 years). The common usage of a constant residence time value within models does

not reflect the observed spatial variability, which was found to be more related to edaphic than climatic conditions (Galbraith *et al.*, 2013). In a modelling study, Delbart *et al.* (2010) demonstrate the improvements in simulated biomass spatial variation in the Amazonian tropical forest after the introduction of a relationship between mortality rate and productivity. In contrast, outside the tropics studies on the spatial patterns of forest mortality or carbon turnover rates have been hampered by the unavailability of spatially consistent data on forest biomass in the past (Thurner *et al.*, 2014). The recently available BIOMASAR-II growing stock volume (GSV) product (Santoro *et al.*, 2011; Santoro *et al.*, 2015) together with remote sensing based NPP products (see Chapter 1.4) allow for the first time for an investigation of the spatial variation in *k* and its relation to environmental variables in Northern Hemisphere boreal and temperate forests.

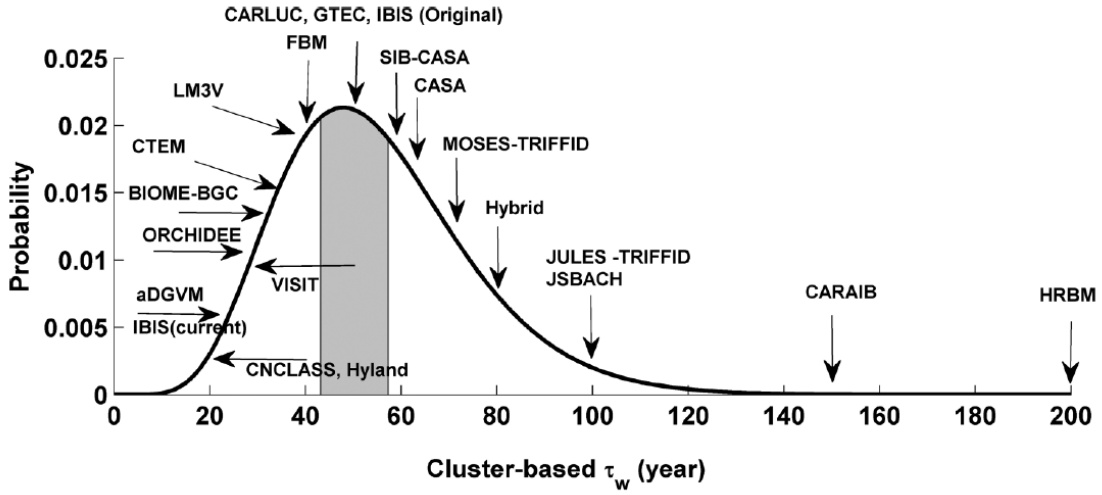

Fig. 1.9: Observed distribution of woody biomass residence time versus the baseline woody biomass residence time assumed in vegetation models in tropical forests. The grey shaded area represents the bootstrapped 95% confidence interval of the observed median (Galbraith *et al.*, 2013, p. 152)

1.4 Forest carbon stock and NPP estimates

In general, NPP increases with mean annual temperature and annual precipitation across boreal and temperate forests. However, these relationships seem to saturate at temperatures higher than 10°C and precipitation of more than 1500 mm. In addition, in ecosystems limited by temperature (< 5°C) or precipitation (< 800 mm), no increases in NPP with these climate variables have been found based on a database of measured and modelled NPP estimates (Luyssaert *et al.*, 2007). NPP has been reported to be

controlled by temperature mostly in boreal ecosystems (Beer *et al.*, 2006), whereas in temperate ecosystems radiation and temperature in winter, temperature in spring and precipitation in summer govern NPP during the seasons of the year (Running *et al.*, 2004). Similar relationships are also considered in GVMs, with soil moisture rather than precipitation directly determining NPP (Cramer *et al.*, 1999). The spatial patterns of biomass (or carbon stocks), however, have not been investigated across boreal and temperate forests due to the absence of observations sufficiently covering the spatial heterogeneity of these ecosystems, both from forest inventories and from remote sensing. Such studies have been possible only for selected regions. For instance, Beer *et al.* (2006) have been looking at the spatial gradients (55-75°N) in both biomass and NPP in Krasnoyarsk Kray, a study region in Siberia, comparing up-scaled forest inventory data and results from a GVM accounting for permafrost related processes. Since measurements are missing and forest dynamics are one of the key uncertainties in GVMs, also models can hardly provide new insights on the spatial patterns of biomass and their climate dependency. The limited available information from forest inventories, remote sensing and GVMs, on which this current knowledge is based on, are introduced in detail in the following.

1.4.1 Forest inventory data

Detailed forest inventory data on GSV or carbon stocks as well as on NPP are often available from national forest inventory initiatives. For example, the United States Department of Agriculture (USDA) Forest Service Forest Inventory and Analysis (FIA; USDA, 2012) provides field-based datasets for the entire US, aggregated for every county. For Europe, only statistics at a national scale (EFI, 2005) are available to the public. Such data are usually not released together with their exact geographical measurement location and can thus not be used for spatially explicit comparisons at high resolution to other data products, e.g. from remote sensing. However, in many national forest inventories remote sensing data are used to up-scale and interpolate inventory-based measurements to spatially continuous gridded data products. For the US, the United States National Biomass and Carbon Dataset for the year 2000 (NBCD2000; Kellndorfer *et al.*, 2010, 2012) was produced by the Woods Hole Research Center (WHRC) and provides a benchmark map of aboveground wood carbon covering the conterminous United States at high spatial resolution (30 m). It has been derived from FIA measurements, up-scaled using interferometric synthetic aperture

radar (InSAR) data from the Shuttle Radar Topography Mission (SRTM) and optical Landsat data (Kellndorfer *et al*., 2010, 2012). A similar product, but at 250 m resolution and using remote sensing data from the Moderate-resolution Imaging Spectroradiometer (MODIS), is also available covering Canada's forests (Beaudoin *et al.*, 2014). For Russia, different forest characteristics (e.g. GSV, biomass, NPP, species composition, age) are available at up to 1 km resolution from the International Institute for Applied Systems Analysis (IIASA; Shvidenko *et al*., 2010; Schepaschenko *et al*., 2011), but comparison can be requested only and is usually performed in an aggregated version at coarser grid resolution or forest enterprise scale. Further up-scaled GSV and biomass field data are provided to the public also from other national forest inventories, for example Sweden (Reese *et al.*, 2003) and Finland (Metla, 2013).

In order to convert GSV to carbon stocks, forest inventory data on wood density, biomass allometry and the carbon content of vegetation are required. Field measurements of wood density are collected in the Global Wood Density Database (Chave *et al.*, 2009; Zanne *et al.*, 2009) for a wide range of species. Biomass allometry measurements are available from the Joint Research Centre (JRC) "Greenhouse Gases in Agriculture, Forestry and Other Land Uses" (GHG-AFOLU) Biomass Compartment Database (JRC, 2009), integrating measurements from Cannell (1982), Keith *et al.* (2009) and Usoltsev (2001). In this database, stem, branch, root and foliage biomass fractions are well represented especially for tree species native to Northern Hemisphere boreal and temperate forests. The carbon content of vegetation is often assumed 50 % of vegetation mass, however, exploring available databases, Thomas & Martin (2012) present considerable variations in vegetation carbon content across tree species and tissue types. Further web-based databases on biomass allometry (GlobAllomeTree; Henry *et al.*, 2013) and on plant traits in general (TRY; Kattge *et al.*, 2011) have been developed recently and are extended continuously. Another more simplified approach to convert GSV to carbon stocks relies on applying biomass expansion factors to infer carbon stocks from GSV, which are based on empirical relationships derived from field measurements (Somogyi *et al.*, 2008; Teobaldelli *et al.*, 2009; Guo *et al.*, 2010). Such conversions are dependent on tree species, among other factors. Tree species maps at high spatial resolution exist for Europe (Köble & Seufert, 2001), and a comparable global product at a similar level of detail is strongly required.

Direct measurements of NPP are difficult to obtain due to the complexity of the carbon balance of forest vegetation (cf. Eq. 1.3). NPP is not only distributed to foliage, stem, branches, roots, reproductive parts, and understory, but also lost by herbivory, root

exudates, VOC, litterfall, and disturbances. An extensive collection of NPP and also biomass measurements from different studies is contained in the Luyssaert database (Luyssaert *et al.*, 2007). However, NPP measurements differ in the consideration of NPP components, and in the measurement methodology. Due to the difficulties to capture all these components, especially belowground, measurements of NPP partly rely on indirect methods and are likely underestimating the actual NPP (Clark *et al.*, 2001). Similarly, belowground biomass usually can be retrieved only indirectly and is thus highly uncertain. In general, databases of NPP or biomass measurements at selected locations are always limited in their spatial coverage and representativeness, since the distribution of measurement sites is often biased towards more easily accessible and undisturbed forests. Hence, measurements cannot capture all processes at the landscape scale, in particular vegetation dynamics. For such problems, the application of the spatial information from remote sensing observations or GVMs is beneficial.

1.4.2 Spatial data from remote sensing

Remote sensing data come with the advantage of their spatial coverage of large areas at relatively low cost and with the potential of multi-temporal standardized observations. Different techniques are most promising for the retrieval of NPP and biomass information. While NPP is best derived from optical vegetation properties detectable with optical remote sensing sensors, radio detection and ranging (Radar) and light detection and ranging (LiDAR) remote sensing signals are better related to structural vegetation properties like forest biomass, GSV, or height. One important global remote sensing based NPP product has been derived from the MODIS sensor (Running *et al.*, 2004; Zhao *et al.*, 2005; Zhao & Running, 2010). While it is possible to retrieve information on the fraction of absorbed photosynthetically active radiation (fAPAR) and the leaf area index (LAI) of the vegetation from optical remote sensing, a photosynthesis and respiration model needs to be applied in order to finally derive NPP (Heinsch *et al.*, 2003). Recently BETHY/DLR (Wißkirchen *et al.,* 2013), a global NPP product with improved thematic resolution, has become available, applying a state-of-the-art biosphere model mainly driven by remote sensing derived biophysical variables. BETHY/DLR integrates remote sensing data (LAI time series from SPOT-VEGETATION, land cover, albedo, digital elevation model, atmospheric CO_2 concentrations), meteorological as well as soil data and the Biosphere Energy Transfer Hydrology (BETHY) (Knorr, 2000; Knorr & Kattge, 2005) model, simulating gross

primary productivity and plant respiration. It has been recently developed at the German Aerospace Center (DLR).

Radar remote sensing is capable to measure biomass or GSV, since the radar backscatter is directly related to the vegetation structure. However, other confounding influences from (soil and vegetation) moisture or topography need to be accounted for in the retrieval model (Santoro *et al.*, 2011). An overview on a selection of present and future spaceborne synthetic aperture radar (SAR) sensors available for biomass estimation is given in Table 1.2. The wavelength (C-band = 7.5 – 3.75 cm; L-band = 30 – 15 cm; P-band = 100 – 30 cm) determines the size of objects which can be detected, with longer wavelengths better related to larger objects like tree stems, increasing the sensitivity to biomass and biomass change. Multiple polarizations carry different information on forest and ground structure and their combined use has the potential to improve the biomass estimates, especially when applied together with information on forest height obtained from interferometric radar (Le Toan *et al.*, 2011).

Table 1.2: Selection of available present and future spaceborne SAR sensors for biomass estimation. Single (S), Double (D) or Full (F) polarization.

Satellite/Sensor	Agency	Operating time	Band	Polarization	Ref.
ALOS/PALSAR	JAXA	2006-11 / 2014-	L	S,D / S,D,F	Rosenqvist *et al.* (2007)
BIOMASS	ESA	2020-	P	F	Le Toan *et al.* (2011)
Envisat/ASAR	ESA	2002-2012	C	S,D	e.g. applied by Santoro *et al.* (2011)
Sentinel-1	ESA	2014-	C	S,D	Torres *et al.* (2012)

For the tropics, wall-to-wall biomass maps recently became available based on fusion approaches of spaceborne LiDAR (from the Geoscience Laser Altimeter System (GLAS) onboard of the National Aeronautics and Space Administration (NASA) Ice, Cloud, and land Elevation Satellite (ICESat)) and multispectral (Baccini *et al.*, 2012) as well as radar data (Saatchi *et al.*, 2011). Nevertheless, the calibration of the vegetation height measured by the LiDAR signal to forest biomass relied on up-scaled inventory data from ground plots. Outside the tropics, however, comparable spatially extensive products have been lacking so far. This shortcoming recently has been overcome by the

derivation of GSV from Environmental Satellite (Envisat) / Advanced Synthetic Aperture Radar (ASAR) C-band data (Santoro *et al.*, 2011, 2015).

1.4.3 Global vegetation models

GVMs simulate the interactions between energy, water and biogeochemical cycles in land ecosystems. The carbon cycle in the vegetation is represented by establishment, productivity, respiration, carbon allocation, and carbon turnover processes in response to changes in climate and atmospheric CO_2. Forced with climate scenarios, such models provide the means to investigate not only the past and present state of the land carbon cycle, but also its future development. In addition, dynamic GVMs (DGVMs) simulate changes in the spatial distribution of vegetation cover. A huge variety of GVMs and several intercomparison studies exist. For instance, seven GVMs participated in the ISI-MIP (Warszawski *et al.*, 2014), including HYBRID4 (Friend *et al.*, 1997; Friend & White, 2000), JeDi (Pavlick *et al.*, 2013), JULES (Clark *et al.*, 2011), LPJml (Sitch *et al.*, 2003), ORCHIDEE (Krinner *et al.*, 2005; Delbart *et al.*, 2010), SDGVM (Woodward & Lomas, 2004) and VISIT (Ito & Oikawa, 2002; Inatomi *et al.*, 2010).

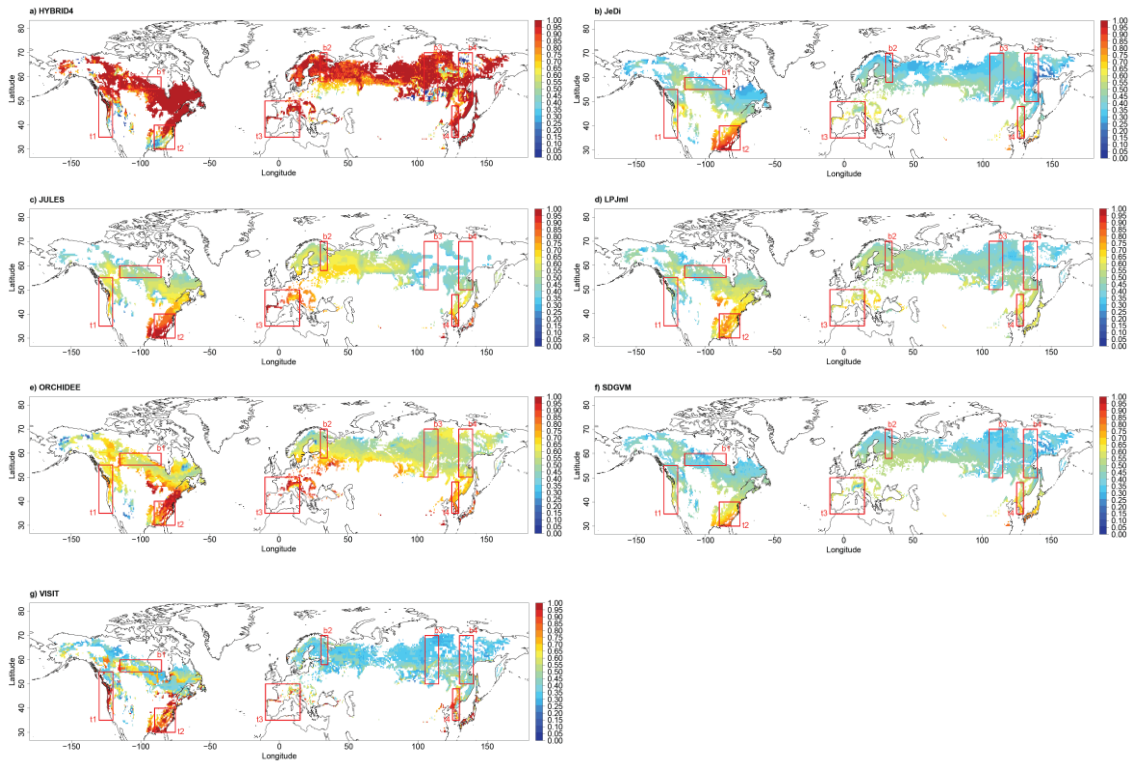

Fig. 1.10: Spatial patterns of 2000-2004 average NPP [kgC m^{-2} y^{-1}] simulated by ISI-MIP GVMs (a) HYBRID4, b) JeDi, c) JULES, d) LPJml, e) ORCHIDEE, f) SDGVM, g) VISIT), including areas with at least 40 % forest cover and at least 1 kg C m^{-2} biomass. Red boxes show selected transects (cf. Table 3.1).

With the exception of HYBRID4, these models agree relatively well in terms of the spatial patterns of simulated NPP (Fig. 1.10). GVMs share relatively similar photosynthesis and stomatal conductance models, for instance based on Farquhar *et al.* (1980) and Collatz *et al.* (1991, 1992). Nevertheless, especially the dependencies of plant respiration (e.g. Atkin & Tjoelker, 2003; Piao *et al.*, 2010; Smith & Dukes, 2013) and allocation fractions to carbon pools (e.g. Friedlingstein *et al.*, 1999; Litton *et al.*, 2007; Wolf *et al.*, 2011) on environmental conditions are not entirely understood at the spatial and temporal scales usually applied in global long-term runs of GVMs. In contrast, GPP and its relation to climate is relatively well known at a global scale (Luyssaert *et al.*, 2007; Beer *et al.*, 2010), but there is still considerable uncertainty in simulated GPP between models and compared to observations (Schaefer *et al.*, 2012; Piao *et al.*, 2013).

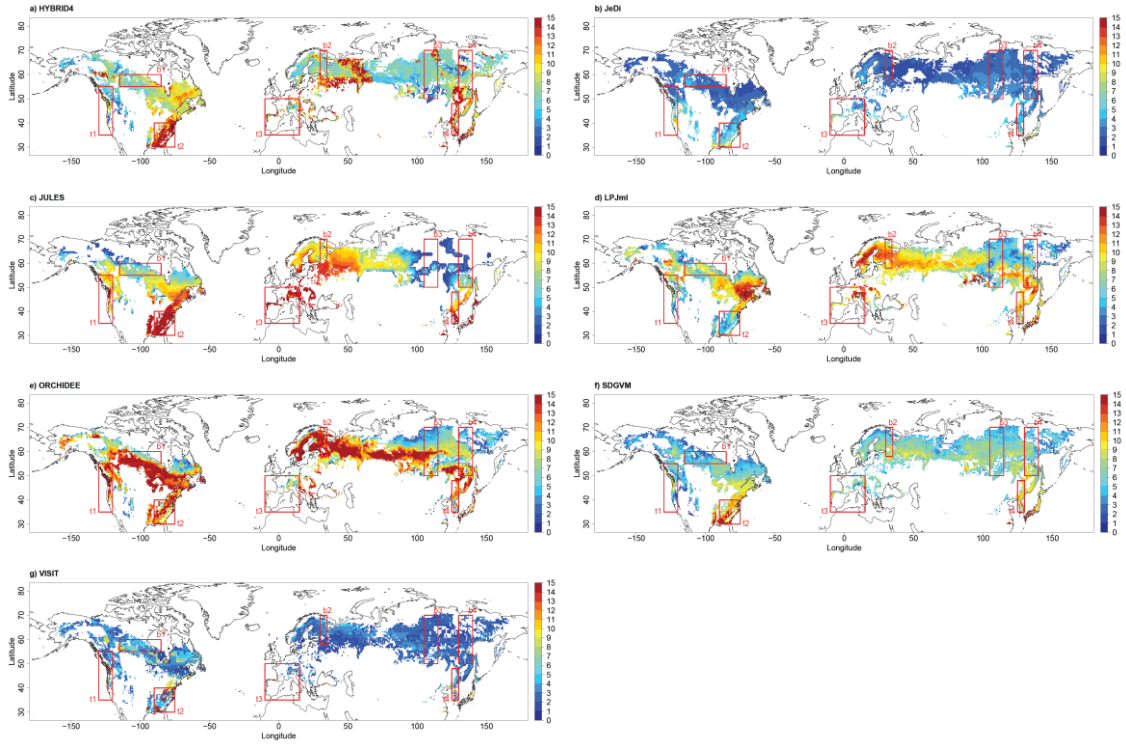

Fig. 1.11: Spatial patterns of biomass in 2004 [kgC m-2] simulated by ISI-MIP GVMs (a) HYBRID4, b) JeDi, c) JULES, d) LPJml, e) ORCHIDEE, f) SDGVM, g) VISIT), including areas with at least 40 % forest cover and at least 1 kg C m-2 biomass. Red boxes show selected transects (cf. Table 3.1).

With respect to biomass, the differences in the spatial patterns between models are much more pronounced (Fig. 1.11). The higher uncertainty in modelled biomass compared to NPP is mainly caused by a huge variety of implemented turnover processes

in these models (Friend *et al.*, 2014). In addition to PFT- and compartment-specific constant background turnover rates, considered processes include mortality due to competition, fire, low growth efficiency or NPP, and heat stress (cf. Chapter 4.1). Furthermore, in some models phenology is affected by drought and/or frost stress. An overview on different mortality implementations in GVMs is also given in McDowell *et al.* (2011), including further mechanisms like size or age thresholds and carbon starvation. This diversity in considered turnover processes reflects the knowledge gap on the importance of mortality mechanisms at a global scale (McDowell *et al.*, 2011).

1.5 Research objectives and questions

The general objective of this thesis is to increase our knowledge on the spatial distribution of carbon stocks and carbon turnover in Northern Hemisphere boreal and temperate forests. In order to address the presented need for research, this overall objective can be divided into the following research objectives:

(I) Derivation of a spatially explicit carbon density map including uncertainties (Chapter 2)

At a spatial resolution of 0.01°, BIOMASAR-II GSV data cover the entire Northern Hemisphere boreal and temperate forests (30-80°N). By applying forest inventory based databases on wood density and biomass allometry, GSV can be converted to carbon stocks, including stem, branch, foliage and root carbon. Corresponding uncertainty provides very relevant information concerning the reliability of the product and facilitates integration with GVMs. In addition, the dataset is evaluated with respect to up-scaled forest inventory biomass data at regional scales. Such a carbon density map has been missing before and for the first time allows consistently quantifying the carbon stored in Northern Hemisphere boreal and temperate forests based on spatially explicit remote sensing data. Carbon stocks and densities are derived for different forest biomes and continents and compared to former existing rough estimates.

(II) Investigation of spatial relationships between observation based forest carbon turnover rate (k) and climatic variables (Chapter 3)

Together with different remote sensing based NPP products, the carbon density map is used to derive for the first time *k* at 0.5° resolution. The spatial relationships between *k* and a set of climate variables are investigated in selected boreal and temperate forest transects. Furthermore, the observed relationships are attributed to plausible underlying (mortality) processes and agents. Additional analyses examine the influence of confounding factors, including soil conditions, fires, gradients in tree cover, possible relationships between biomass allometry and climate as well as the uncertainty in NPP products, on the results.

(III) Intercomparison of available GVMs concerning their ability to reproduce observation based spatial relationships between *k* and climate (Chapter 4)

Simulated biomass and NPP are obtained from GVMs applied at 0.5° spatial resolution within ISI-MIP. *k* is derived in a similar way for both models (HYBRID4, JeDi, JULES, LPJml, ORCHIDEE, SDGVM, VISIT) and observations in order to allow for maximum comparability. The ability of these GVMs to reproduce observed spatial relationships between *k* and climate is evaluated. In addition, biome average values and correlations are compared between models and observations for *k*, NPP and biomass. While the influence of already implemented mortality schemes on modelled *k* and its relation to climate is investigated, deviations from observations are used to identify and discuss missing mortality processes in current GVMs. In addition, the impacts of the steady state assumption, of forest management effects and of the considered NPP timespans on the results are assessed.

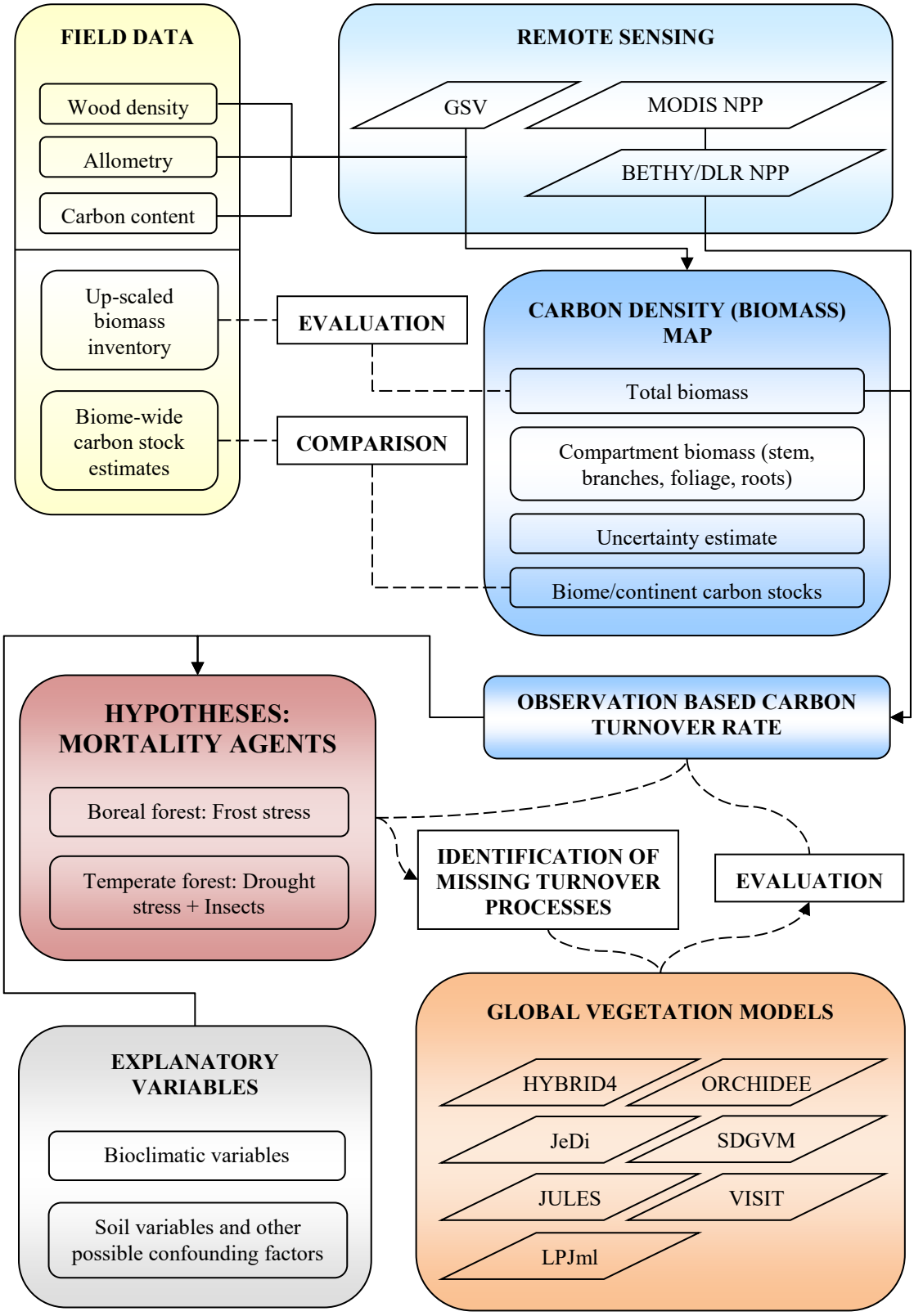

Fig. 1.12: Methodical concept

The methodical concept of this thesis, as described above, is also visualized in Fig. 1.12. Based on the formulated objectives the central research questions of this dissertation are:

(1) How much carbon is currently stored in Northern Hemisphere boreal and temperate forests? How are forest carbon stock and density spatially distributed? (Chapter 2)

(2) How is the spatial variation in boreal and temperate forest carbon turnover rate related to climate? Which mortality agents are responsible for the observed relationships? (Chapter 3)

(3) Are the observation based relationships between turnover rate and climate reproduced by GVMs? Which climate-related mortality processes are represented in GVMs and which are required for an improved simulation of turnover rate spatial patterns? (Chapter 4)

These questions are investigated within the following three chapters. Implications of the results are discussed in the context of the literature and an outlook on future improvements is given (Chapter 5). Finally, the major results of this thesis are summarized with respect to the research questions (Chapter 6).

CHAPTER 2

Carbon stock and density of northern boreal and temperate forests

Within this chapter, the derivation of a spatially explicit forest carbon density map at 0.01° resolution from GSV data originating from Envisat/ASAR is described. For this purpose, information on wood density and allometric relationships are required and can be derived from available inventory databases. A detailed evaluation of the resulting carbon density map with respect to up-scaled forest inventory data is implemented at regional scale. In addition, a complementary uncertainty estimate is calculated, giving valuable information for instance for model-data-integration purposes. Finally, the carbon density map is used to infer carbon stock and density estimates for Northern Hemisphere boreal and temperate forests.

2.1 GSV data

GSV denotes the volume of tree stems per area. Santoro *et al.* (2015) estimated spatially explicit GSV for the Northern Hemisphere boreal and temperate forests (30-80°N), covering North-America, Europe and Asia, with a resolution of 0.01° (Fig. 2.1). By applying the so-called BIOMASAR algorithm (Santoro *et al.*, 2011), GSV is derived from large numbers of observations by the ASAR instrument on-board the Envisat satellite, acquired in ScanSAR mode, making use of radar backscatter intensity. The estimation accuracy is substantially improved by the combination of multiple data acquisitions compared to the sole use of single images (Santoro *et al.*, 2011). The GSV estimated from the SAR data is determined by the wavelength of the ASAR instrument (C-band, 5.6 cm) and related to the forest structural and dielectric properties. Objects with a size smaller than the wavelength as well as objects containing frozen water are transparent to the radar signal. A distinctive characteristic of the BIOMASAR algorithm is its independency on *in situ* data, since the GSV range is calibrated for each estimation

region (tile) based on the radar backscatter of unvegetated and dense forest areas (training of a water-cloud-like backscatter model). The pre-processing algorithm also accounts for speckle filtering and the correction of topographic effects (Santoro *et al.*, 2011).

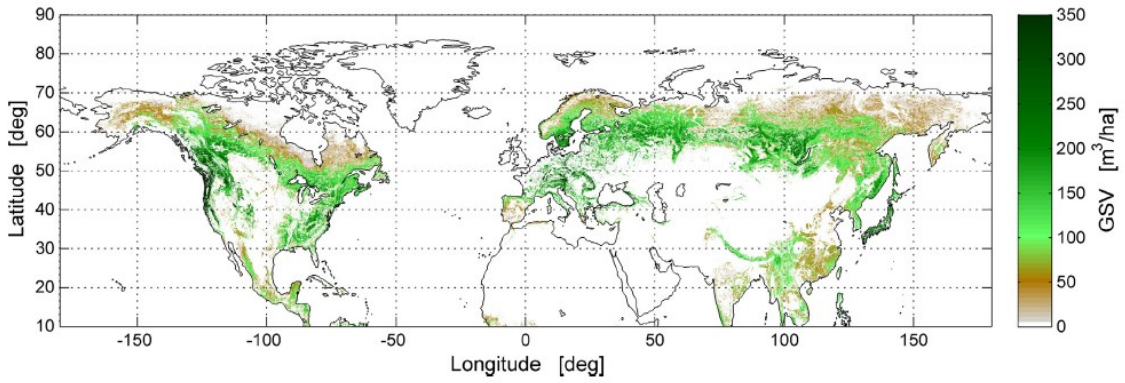

Fig. 2.1: Forest GSV [m^3 ha^{-1}] in 2010 estimated from Envisat/ASAR by the BIOMASAR algorithm (Santoro *et al.*, 2015). Non-forest areas have been masked out by GLC2000 (Bartholomé & Belward, 2005).

By combining in a weighted approach individual GSV estimates from primarily winter-time ASAR data, the GSV estimation procedure extracts the maximum in terms of signal related to GSV in the radar data (Santoro *et al.*, 2011). In other words, the effect of soil moisture on the radar signal is as small as possible under such conditions. Stumps are accounted for in the ASAR GSV estimate as long as they are seen by the signal, i.e., their size is larger than the wavelength and they are standing. GSV estimates might also contain a necromass component if this is directly sensed by the radar. These aspects have not been quantified so far though. The BIOMASAR algorithm retrieves GSV regardless of the vegetation type. To ensure that the biomass estimates correspond to forest only, non-forest areas were masked out beforehand according to the Global Land Cover for the Year 2000 (GLC2000) land use - land cover map (Bartholomé & Belward, 2005; available from JRC, 2003; cf. Table 2.1).

The multi-temporal SAR dataset was acquired between October 2009 and February 2011, thus containing information on the state of vegetation structure in the year 2010. GSV was mapped without saturation up to 300 m^3 ha^{-1}. Above this level the retrieved GSV was characterized by a tendency to saturate, i.e., increasing underestimation for increasing GSV. However, less than 1 % of the pixels in the study area had a GSV above this value (Santoro *et al.*, 2011, 2015). The uncertainty of GSV estimates was

quantified to be 10 % originally (Santoro *et al.*, 2011). Later, a spatially explicit uncertainty estimate was obtained, indicating higher uncertainties (< 30% for approximately 80% of the forest area). While in boreal regions the uncertainty was usually found to be below 10 % even in high density forests due to a high number of data acquisitions usable by the algorithm (Fig. 2.2A), the uncertainty can increase to much higher values in case of less available observations, like especially in some temperate forest areas (Fig. 2.2B; Santoro *et al.*, 2015). These more precise uncertainty estimates unfortunately could not be used in the uncertainty analysis carried out here (cf. Chapter 2.2), since they have been only available after completion of this work. In addition, the spatial coverage of the GSV product has been extended to northern subtropical forests recently (10-80°N). Compared to forest inventory data up-scaled to regional scales, the relative root mean square error (RMSE) was found to be between 12 and 45 %, with 29 % on average (Santoro *et al.*, 2015).

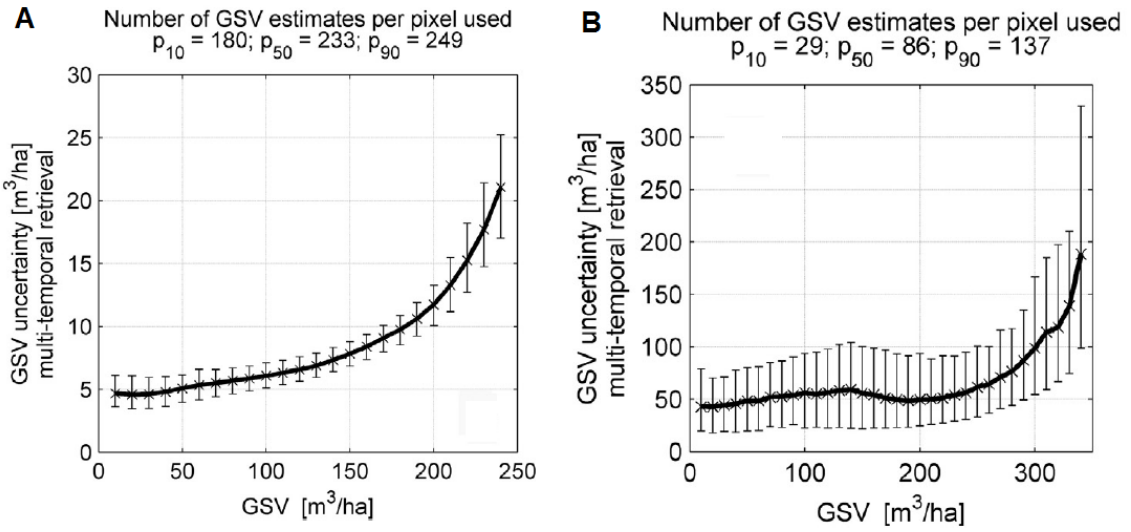

Fig. 2.2: Distribution of the uncertainty in GSV as a function of retrieved GSV, shown for sample estimation regions (1° x 1° tiles) in (A) boreal forest in Central Siberia and (B) temperate forest in the Southern Appalachian region in the USA. Retrieved GSV is grouped in 10 m^3 ha^{-1} wide intervals, for each of which the average uncertainty (crosses) and the range between the 10^{th} and the 90^{th} percentile of the uncertainty (vertical bars) are displayed. The spatial variation of the number of single-image GSV estimates used in the multi-temporal combination across the tile is reported in form of percentiles (p10, p50 and p90) (Santoro *et al.*, 2015).

2.2 Derivation of a carbon density map from GSV data

Forest carbon density, the spatial distribution of carbon stocks per area, accounting for all major tree compartments (stem, branches, roots, foliage), is inferred from GSV. Such information is relevant for informing and evaluating carbon cycle models and in general for the assessment of the role of forests within the global carbon cycle (cf. Chapter 1.2). In order to derive total carbon density from GSV, in the first instance additional information on wood density from the Global Wood Density Database (Chave *et al.*, 2009; Zanne *et al.*, 2009) allowed for conversion to stem biomass (Fig. 2.3). Subsequently, allometric relationships extracted from the JRC GHG-AFOLU Biomass Compartment Database (JRC, 2009) were used to estimate branch, root, and foliage biomass in addition. Finally, the carbon content in the vegetation determines the conversion from biomass to carbon density.

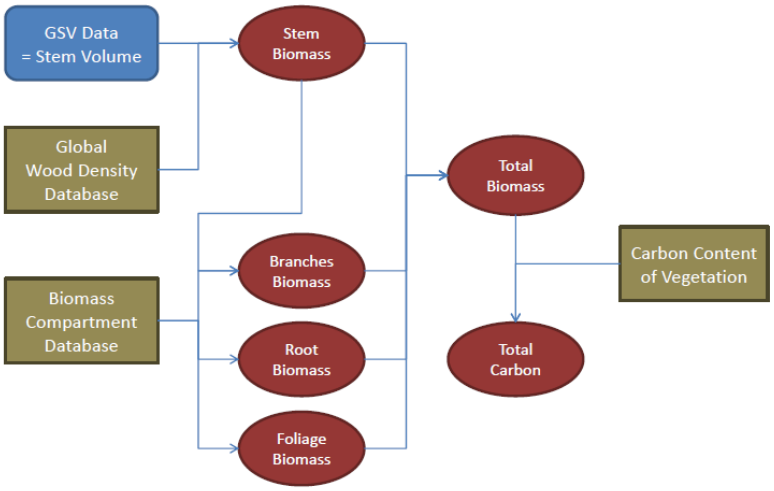

Fig. 2.3: Processing algorithm

While the Global Wood Density Database contains information on wood density, the JRC Biomass Compartment Database includes measurements of the absolute amounts of compartment biomass, both over a wide range of species and sufficiently covering the study area. The Global Wood Density Database consists of more than 16,000 entries, covering more than 8000 tree species. The JRC Biomass Compartment Database is also giving additional information on latitude/longitude, tree age, diameter, height and density amongst others.

Table 2.1: GLC2000 classes and their aggregation to leaf types

No.	Class	Leaf Type
1	Tree Cover, broadleaf, evergreen	broadleaf forest
2	Tree Cover, broadleaf, deciduous, closed	
3	Tree Cover, broadleaf, deciduous, open	
4	Tree Cover, needleleaf, evergreen	needleleaf evergreen forest
5	Tree Cover, needleleaf, deciduous	needleleaf deciduous forest
6	Tree Cover, mixed leaf type	mixed forest
7	Tree Cover, regularly flooded, fresh water	
8	Tree Cover, regularly flooded, saline water	
9	Mosaic: Tree cover / Other natural vegetation	
10	Tree Cover, burnt	
11	Shrub Cover, closed-open, evergreen	non-forest
12	Shrub Cover, closed-open, deciduous	
13	Herbaceous Cover, closed-open	
14	Sparse Herbaceous or sparse Shrub Cover	
15	Regularly flooded Shrub and/or Herbaceous Cover	
16	Cultivated and managed areas	
17	Mosaic: Cropland / Tree Cover / Other natural vegetation	
18	Mosaic: Cropland / Shrub or Grass Cover	
19	Bare Areas	
20	Water Bodies	
21	Snow and Ice	
22	Artificial surfaces and associated areas	

As there is no detailed tree species map covering the whole study area available, information contained in those databases had to be aggregated to the level of leaf types (broadleaf, needleleaf deciduous, needleleaf evergreen forest). GLC2000 was used to distinguish between those leaf types. It assigns one of 22 different land cover classes to each pixel. These classes were summarized to broadleaf, needleleaf deciduous, needleleaf evergreen, mixed forest and non-forest (Table 2.1). GLC2000 with its

original resolution of 1 km was reprojected using nearest neighbor resampling to 0.01° in order to match the resolution of the GSV map.
In addition to the total carbon density map, an uncertainty estimate was derived for each pixel. Here uncertainty is referred to in terms of the standard deviation of the biomass value. All the steps of the processing algorithm contribute to the overall uncertainty, including:
(i) uncertainty of the BIOMASAR GSV estimates;
(ii) uncertainty of the GLC2000 land use - land cover classification;
(iii) uncertainty of wood density data;
(iv) uncertainty of biomass compartment data;
(v) uncertainty of the carbon content in vegetation.

The relative error of GSV estimates related to the retrieval algorithm (i) was quantified by Santoro *et al.* (2011) to be on average 10 %. The uncertainty of GLC2000 land cover (ii) could not be accounted for in this analysis, since its quantification is hardly possible. It is assumed to slightly affect the spatial distribution of uncertainties, but their overall range only to a minor extent. The land cover classification potentially introduces uncertainty by applying a wood density or an allometric relation for the wrong leaf type. In addition, sub-pixel heterogeneity in land cover is not covered by GLC2000. The consideration of the uncertainty in wood density (iii) and biomass allometry (iv) is described in detail in the following subchapters (2.2.1 and 2.2.2). The uncertainty of the carbon content of vegetation (v) was considered negligible compared to the magnitude of the other uncertainties. Error propagation was implemented following Taylor (1997), applying a Gaussian error propagation (GEP) approach. Its use in ecological studies has been demonstrated by Lo (2005) for a similar application. It was found to be especially beneficial when implying step-by-step calculations or different scales, both of which are as well relevant to the work presented here.

2.2.1 Wood density

In a first step, stem biomass (SB) was derived from GSV using information on wood density (WD) from the Global Wood Density Database as follows:

$$SB = GSV \cdot WD \qquad \text{(Eq. 2.1)}$$

All the entries for different tree species contained in the database were summarized to tree genera and leaf types, finally. In the absence of a global tree species map, no weighting according to the occurrence of tree species could be implemented. Investigations concentrated on the most common genera in boreal and temperate forests, including *Abies, Acer, Alnus, Betula, Fagus, Fraxinus, Larix, Picea, Pinus, Populus, Quercus, Tilia* and *Tsuga*. For each pixel of the GSV map stem biomass was calculated following Eq. (2.1). Mean wood density per leaf type was applied according to the leaf type distribution derived from the GLC2000 land cover map (cf. Table 2.1).

The standard deviation of wood density for different leaf types, containing its variance between species, could be used to quantify its uncertainty (iii). Uncertainty of stem biomass (u_{SB}) can be calculated from the relative error of GSV (i; $u_{GSV} = 10\% \cdot GSV$) and the standard deviation of wood density (u_{WD}). These uncertainties can be assumed to be independent and random, and u_{SB} can be calculated as follows ($\frac{dSB}{dGSV}$ denotes the partial derivative of SB with respect to GSV):

$$u_{SB} = \sqrt{\left(\frac{dSB}{dGSV} \cdot u_{GSV}\right)^2 + \left(\frac{dSB}{dWD} \cdot u_{WD}\right)^2} = \sqrt{\left(WD \cdot u_{GSV}\right)^2 + \left(GSV \cdot u_{WD}\right)^2} \qquad \text{(Eq. 2.2)}$$

The mean values and standard deviations of wood density for different leaf types are summarized in Table 2.2. Corresponding boxplots show the median values and quartiles not only across leaf types, but also more detailed across tree genera (Fig. 2.4). As the differences between mean and median values are negligible, the mean values can be considered to describe the distributions of wood density sufficiently well. Thus, they were used to calculate stem biomass following Eq. (2.1). When summarized to leaf types, especially the wood density of broadleaf trees varies considerably between tree species. In this processing step, the uncertainty introduced by the Global Wood Density Database is relatively large for broadleaf trees. In terms of their mean value, broadleaf trees have the highest wood density and thus a higher biomass per volume, followed by needleleaf deciduous and needleleaf evergreen trees.

Table 2.2: Wood density mean and standard deviation obtained from the Global Wood Density Database (Chave *et al*., 2009; Zanne *et al*., 2009) for different leaf types

Forest Leaf Type	Broadleaf	Needleleaf Deciduous	Needleleaf Evergreen
Mean Wood Density [g cm^{-3}]	0.570	0.464	0.411
Standard Deviation of Wood Density [g cm^{-3}]	0.150	0.057	0.066

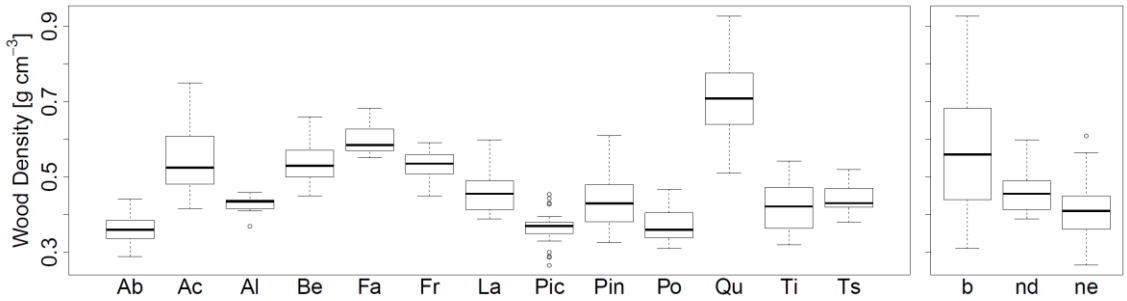

Fig. 2.4: Variance in wood density [g cm^{-3}] measurements contained in the Global Wood Density Database **(**Chave *et al*., 2009; Zanne *et al*., 2009) across tree genera (left; Ab = *Abies*, Ac = *Acer*, Al = *Alnus*, Be = *Betula*, Fa = *Fagus*, Fr = *Fraxinus*, La = *Larix*, Pic = *Picea*, Pin = *Pinus*, Po = *Populus*, Qu = *Quercus*, Ti = *Tilia*, Ts = *Tsuga*) and leaf types (right; b = broadleaf, nd = needleleaf deciduous, ne = needleleaf evergreen). The Box-Whisker-Plots show the median and the interquartile range of values. The whiskers extend up to the most extreme data point which is no more than 1.5 times the interquartile range away from the box. Outliers are drawn as circles.

2.2.2 Allometric relationships

In a second step, allometric relationships at leaf type level between stem biomass and the other required biomass compartments (BC; including branches, foliage, and roots) were derived by fitting root functions to the Biomass Compartment Database. Nonlinear models of the following form were fitted using generalized least square regression (Pinheiro & Bates, 2000):

$$BC = a \cdot SB^{\frac{1}{b}} \quad \text{(Eq. 2.3)}$$

The model form is similar to allometric relationships used by Zianis *et al.* (2005) and Wutzler *et al.* (2008), although here stem biomass is used instead of tree diameter as a predictor. Branch, root and foliage biomass were calculated in this manner. These

relationships were applied to the stem biomass map resulting in maps of the other biomass compartments. The coefficients a and b in Eq. (2.3) were again derived per leaf type. Then, the GLC2000 land cover map was applied once more to estimate biomass compartments for the different leaf types. *Abies, Alnus, Betula, Fagus, Larix, Picea, Pinus, Populus, Quercus* and *Tsuga* could be included in this analysis. Unfortunately, for *Acer, Fraxinus and Tilia* no sufficient information (at least 10 database entries) on root biomass was available in the database.

The uncertainty introduced by the relationship between biomass compartments (iv), which is caused by the variation of allometric functions within leaf types, was estimated from the variance of residuals of the model fit by applying a Generalized Model (Pinheiro & Bates, 2000; Zuur *et al.*, 2009). This kind of model allowed the increase of the variance of residuals with increasing covariate, in this case the stem biomass. Hence an increasing uncertainty in branch, root and foliage biomass could be modelled with increasing stem biomass.

The uncertainty of branch biomass (u_{BB}) for given stem biomass consists of the propagated uncertainty of stem biomass and the uncertainty of the fitted relationship between those two variables ($u_{BB=f(SB)}$; cf. Taylor, 1997, p. 190), which is caused by the uncertainty of the Biomass Compartment Database. Again, these uncertainties can be assumed to be independent and random:

$$u_{BB} = \sqrt{\left(\frac{dBB}{dSB} \cdot u_{SB}\right)^2 + u_{BB=f(SB)}^2} = \sqrt{\left(\frac{a}{b} \cdot SB^{\frac{1}{b}-1} \cdot u_{SB}\right)^2 + u_{BB=f(SB)}^2} \quad \text{(Eq. 2.4)}$$

The derivatives are evaluated at given stem biomass and estimated model parameters. The uncertainty of the allometric function can be derived from the Generalized Model, quantifying the uncertainty introduced by the influence of species, climate, tree age and possible other factors on this allometric relation. It does however not fully account for the uncertainty arising from measurement errors, especially since these observations are often not based on “real measurements”, which would be particularly complicated in case of root biomass (Clark *et al.*, 2001; Mokany *et al.*, 2006), but themselves derived from allometric scaling calibrated to specific regions and species (e.g. Jenkins *et al.*, 2003). The variance of the residuals is expressed in dependence of the residual standard error (RSE) and rising with the power of the absolute value of the covariate (SB). The parameter δ is fitted by the model (Pinheiro & Bates, 2000; Zuur *et al.*, 2009):

$$u^2_{BB=f(SB)} = RSE^2 \cdot |SB|^{2\delta} \qquad \text{(Eq. 2.5)}$$

The uncertainty of root (u_{RB}) and foliage (u_{FB}) biomass can be derived in the same way.

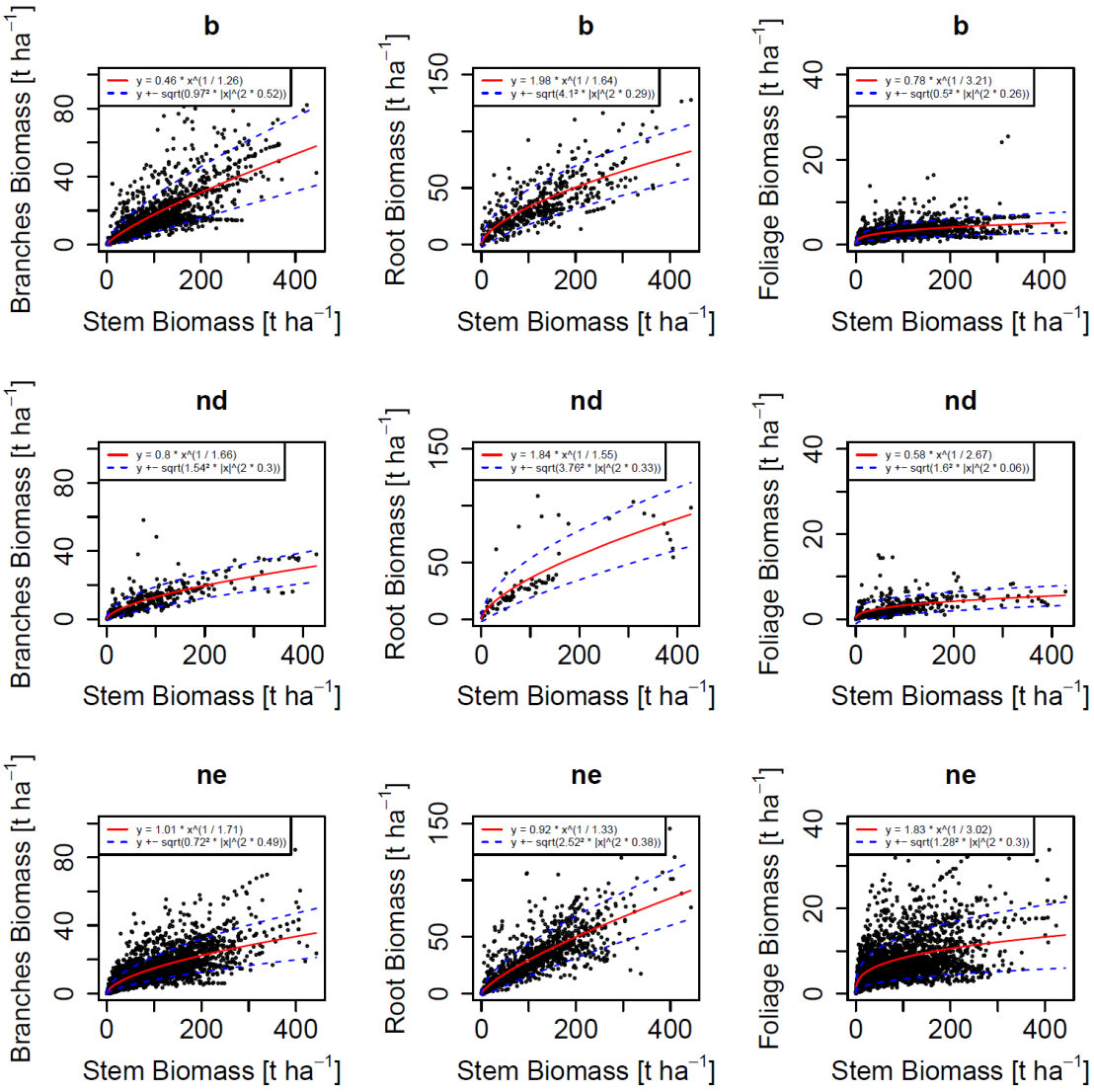

Fig. 2.5: Fitted allometric relationships between stem, branch, root and foliage biomass [t ha^{-1}] using the Global Biomass Compartment Database (JRC, 2009) (b = broadleaf, nd = needleleaf deciduous, ne = needleleaf evergreen; central solid line = functional relationship, upper and lower bound = uncertainty bound of the fitted relationship (standard deviation of the residuals, see Eq. (2.5))

The fitted allometric relationships between branch, root and foliage biomass to stem biomass are visualized in Fig. 2.5. While an increasing stem biomass is able to support the growth of more branches and also leaves, at the same time more biomass has to be

allocated to roots in order to supply water and nutrients for increasing maintenance and growth needs. These findings are consistent with the pipe model (Shinozaki *et al.*, 1964). Increasing resource competition with increasing stand biomass is responsible for the non-linearity of the relationship. The database contained trees with a stem biomass up to about 400 t ha^{-1}. While broadleaf trees were found to be able to support higher branch biomass, needleleaf evergreen trees have higher foliage biomass compared to the other leaf types. However, at a 95 % confidence interval, these findings were not significant, besides a significantly higher multiplier in the allometric relation between foliage and stem biomass for needleleaf evergreen trees compared to broadleaf trees. The modelled relationship of root biomass to stem biomass was not significantly different between leaf types. Relative uncertainty introduced in this processing step is highest for inferring foliage biomass from stem biomass, especially for needleleaf deciduous trees with low stem biomass values. Again, a breakdown into tree species instead of leaf types would reduce the uncertainty in the allometric relationships (not shown), but this is hampered by the lack of a global tree species map. Unfortunately, the derived allometric relationships cannot be directly compared to the literature, since usually tree diameter instead of stem biomass is used as a predictor (Zianis *et al.*, 2005; Wutzler *et al.*, 2008).

Generalized additive models (GAM; Hastie & Tibshirani, 1990; Wood, 2006) were used to test the influence of different predictor variables on the modelling of branch, root and foliage biomass. Model accuracy was quantified in terms of adjusted R^2, root mean square error (RMSE), and Akaike's information criterion (AIC; Akaike, 1974). Nonparametric GAM were employed because of their ability to account also for nonlinear relationships, including numerical as well as factorial predictor variables. A total of ten model setups were implemented, using different combinations of predictor variables:

(I) Stem biomass

(II) Stem biomass + leaf type (broadleaf, needleleaf deciduous, needleleaf evergreen)

(III) Stem biomass + tree genus (*Abies, Alnus, Betula, Fagus, Larix, Picea, Pinus, Populus* and *Quercus*)

(IV) Stem biomass + climate (Köppen-Geiger climate classification; updated version, data from Kottek *et al.*, 2006)

(V) Stem biomass + leaf type + climate

(VI) Stem biomass + tree genus + climate

(VII) Stem biomass + stand age

(VIII) Stem biomass + stand density

(IX) Stem biomass + leaf type + climate + stand age + stand density

(X) Stem biomass + tree genus + climate + stand age + stand density

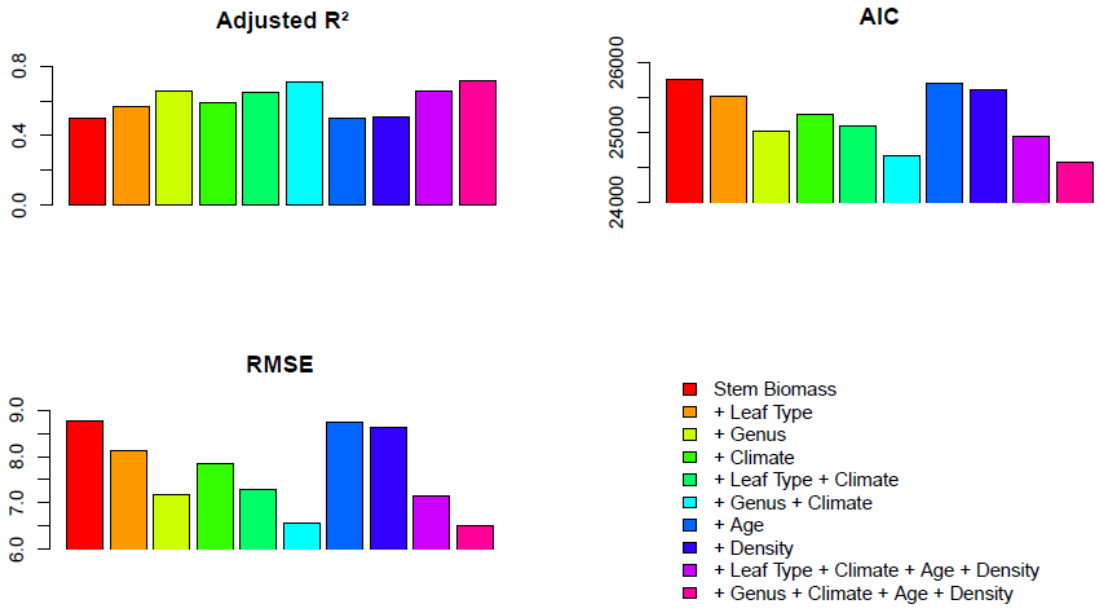

Fig. 2.6: Generalized additive model (GAM) results modelling branch biomass using different sets of predictors (AIC = Akaike's information criterion; RMSE = root mean square error)

Branch biomass, root biomass, foliage biomass, stem biomass, leaf type, tree genus, stand age and stand density could be extracted from the Biomass Compartment Database. The comparison of these different sets of predictors for modelling of the allometric relationships reveals that the applied algorithm could be further improved by the availability of a consistent global tree species map. E.g. modelling of branch biomass out of stem biomass using a GAM was significantly improved (in terms of adjusted R^2, RMSE, and AIC) when information on tree genus were taken into account (model III; Fig. 2.6). In contrast, the approach used here could only make use of leaf type information in addition to the stem biomass (model II). Results were similar for root and foliage biomass (not shown). Such improvements would lead to a more precise biomass estimate and to a reduction of the uncertainty of the resulting total carbon map. In addition, the consideration of different climate zones (model IV-VI) could further improve the modelling of allometric relationships. This would require more extensive

and standardized measurements of biomass compartments, covering all important tree species across all the different climate zones. In contrast, tree age (model VII) and tree density (model VIII) did not have much effect on GAM results.

2.2.3 Compartment and total carbon density maps

Finally, total biomass (TB) was inferred as the sum of the biomass compartments stem, branch (BB), root (RB) and foliage biomass (FB):

$$TB = SB + BB + RB + FB \qquad \text{(Eq. 2.6)}$$

The carbon content in vegetation varies between leaf type and biomes (Thomas & Martin, 2012); however, variations between plant tissues are of minor importance. The observed difference between broad- and needleleaf species was taken into account when converting TB to total carbon (TC) stocks:

$$TC = 0.488 \cdot TB \text{ for temperate / boreal broadleaf tree species} \qquad \text{(Eq. 2.7)}$$

$$TC = 0.508 \cdot TB \text{ for temperate / boreal needleleaf tree species} \qquad \text{(Eq. 2.8)}$$

As the uncertainties of the biomass compartments cannot be considered to be independent (they are all calculated out of stem biomass; i.e., if the uncertainty of stem biomass increases, also the uncertainty of the other biomass compartments will increase), the uncertainty of their sum (u_{TB}) has to be calculated as the sum of the original uncertainties:

$$u_{TB} = u_{SB} + u_{BB} + u_{RB} + u_{FB} \qquad \text{(Eq. 2.9)}$$

Finally, the uncertainty of total biomass was propagated in order to derive the uncertainty of total carbon, assuming negligible uncertainty of carbon content (v):

$$u_{TC} = \frac{dTC}{dTB} \cdot u_{TB} = 0.488 \cdot u_{TB} \text{ for temperate / boreal broadleaf tree species} \qquad \text{(Eq. 2.10)}$$

$$u_{TC} = \frac{dTC}{dTB} \cdot u_{TB} = 0.508 \cdot u_{TB} \text{ for temperate / boreal needleleaf tree species} \qquad \text{(Eq. 2.11)}$$

In addition to TB, also the individual compartments SB, BB, RB, and FB have been converted to carbon stocks by applying the above factors. Stem, branch, root, and foliage carbon density are shown in Figs. 2.7-2.10. The differences in spatial patterns follow the distributions of leaf types in GLC2000 and can be explained by the differences between leaf types in modelled compartment relationships (cf. Fig. 2.5). The relative uncertainty of stem carbon is below 20 % in most areas, except for broadleaf trees, where the high variation in wood density causes higher uncertainties (cf. Fig. 2.4). Modelling of branch and particularly root and foliage carbon introduces additional uncertainty, which is highest (in relative terms) in low biomass areas (mostly northern taiga). But as the total carbon map is dominated by stem biomass, while the other compartments account only for a small proportion of total carbon, the overall relative uncertainty of the final map (Fig. 2.11) is within a very satisfactory range.

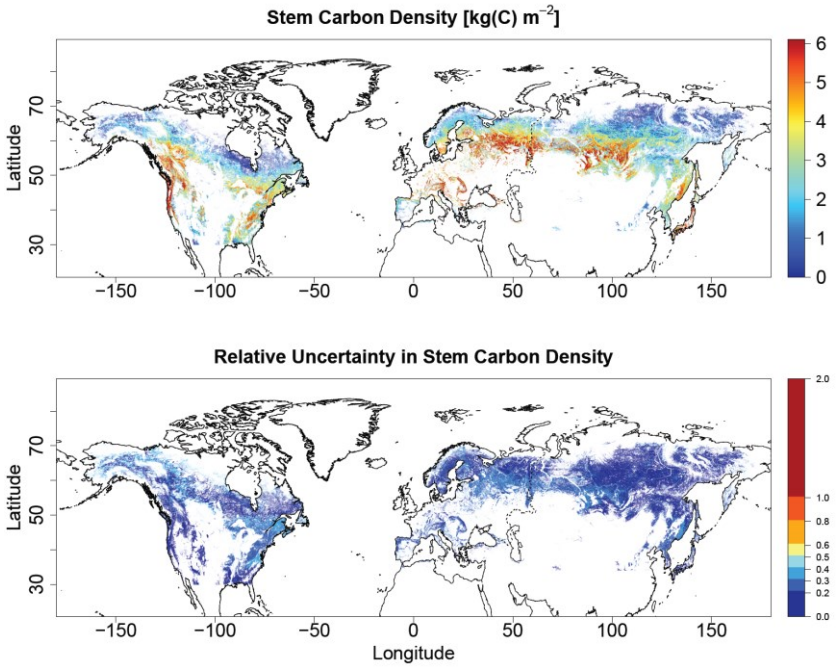

Fig. 2.7: Spatial distribution of stem carbon density in Northern Hemisphere boreal and temperate forests and its corresponding relative uncertainty (a value of 1 means 100 % uncertainty). Non-forest is masked out according to the GLC2000 land-use/land-cover map. The dashed black line indicates the boundary between Europe and Asia (data from ESRI, 2008) used for the estimation of continental carbon stocks.

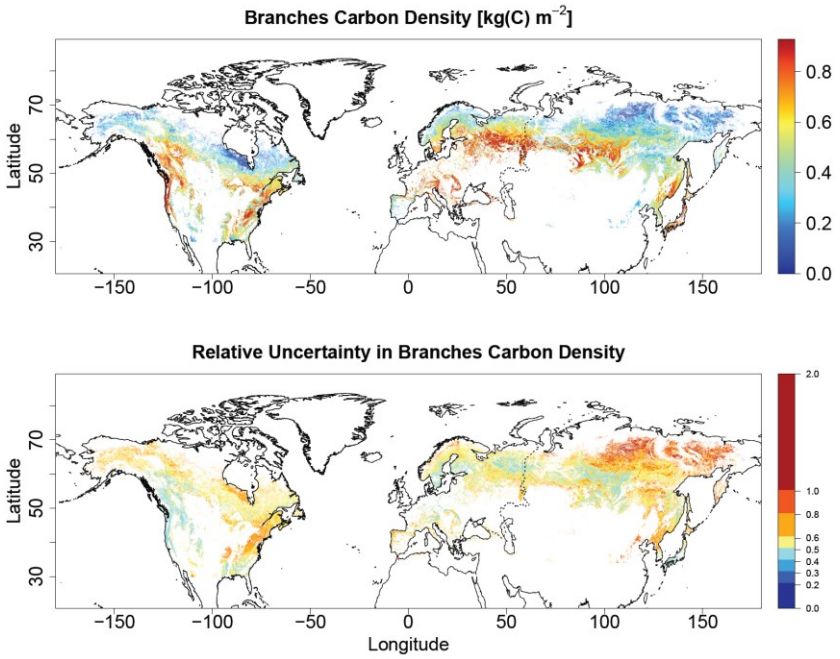

Fig. 2.8: Spatial distribution of branch carbon density in Northern Hemisphere boreal and temperate forests and its corresponding relative uncertainty (a value of 1 means 100 % uncertainty). Non-forest is masked out according to the GLC2000 land-use/land-cover map. The dashed black line indicates the boundary between Europe and Asia (data from ESRI, 2008) used for the estimation of continental carbon stocks.

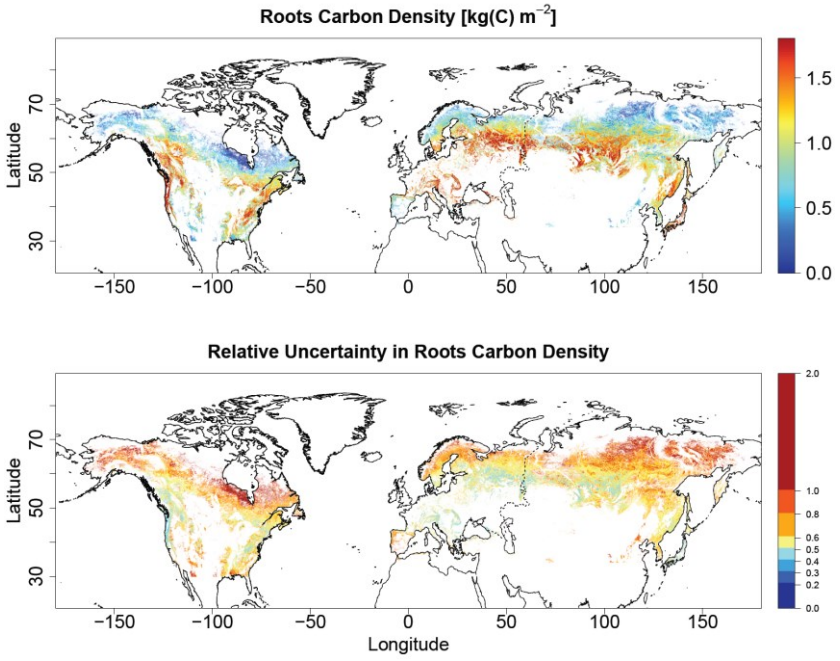

Fig. 2.9: Spatial distribution of root carbon density in Northern Hemisphere boreal and temperate forests and its corresponding relative uncertainty (a value of 1 means 100 % uncertainty). Non-forest is masked out according to the GLC2000 land-use/land-cover map. The dashed black line indicates the boundary between Europe and Asia (data from ESRI, 2008) used for the estimation of continental carbon stocks.

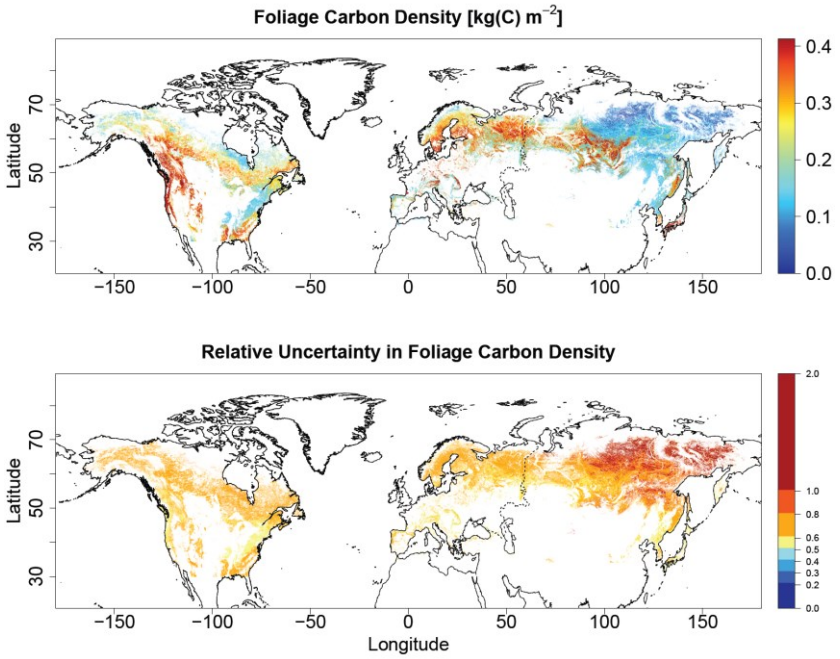

Fig. 2.10: Spatial distribution of foliage carbon density in Northern Hemisphere boreal and temperate forests and its corresponding relative uncertainty (a value of 1 means 100 % uncertainty). Non-forest is masked out according to the GLC2000 land-use/land-cover map. The dashed black line indicates the boundary between Europe and Asia (data from ESRI, 2008) used for the estimation of continental carbon stocks.

Most of the forests with the highest total carbon content per area (> 8 kgC m^{-2}) are situated along the Rocky Mountains in Northwest Canada and the USA, the European mountains (both mostly temperate coniferous forest), European Russia, southern Central Siberia (temperate broadleaf and mixed forests, southern boreal forests) and Japan (mostly temperate broadleaf and mixed forests; Fig. 2.11). In the boreal zone, forest carbon decreases to the North along a latitudinal gradient. The spatial patterns give information e.g. on potential carbon loss due to disturbances or potential wood availability to man. Corresponding relative uncertainty is most often between 20 % and 40 %, especially in high biomass areas. Lowest relative uncertainties are estimated in the high biomass density regions of Northwest Canada and the USA, Central Siberia, most European mountain ranges and Japan. The relative uncertainty of this modelling approach increases in the northern taiga, where very low biomass is situated.

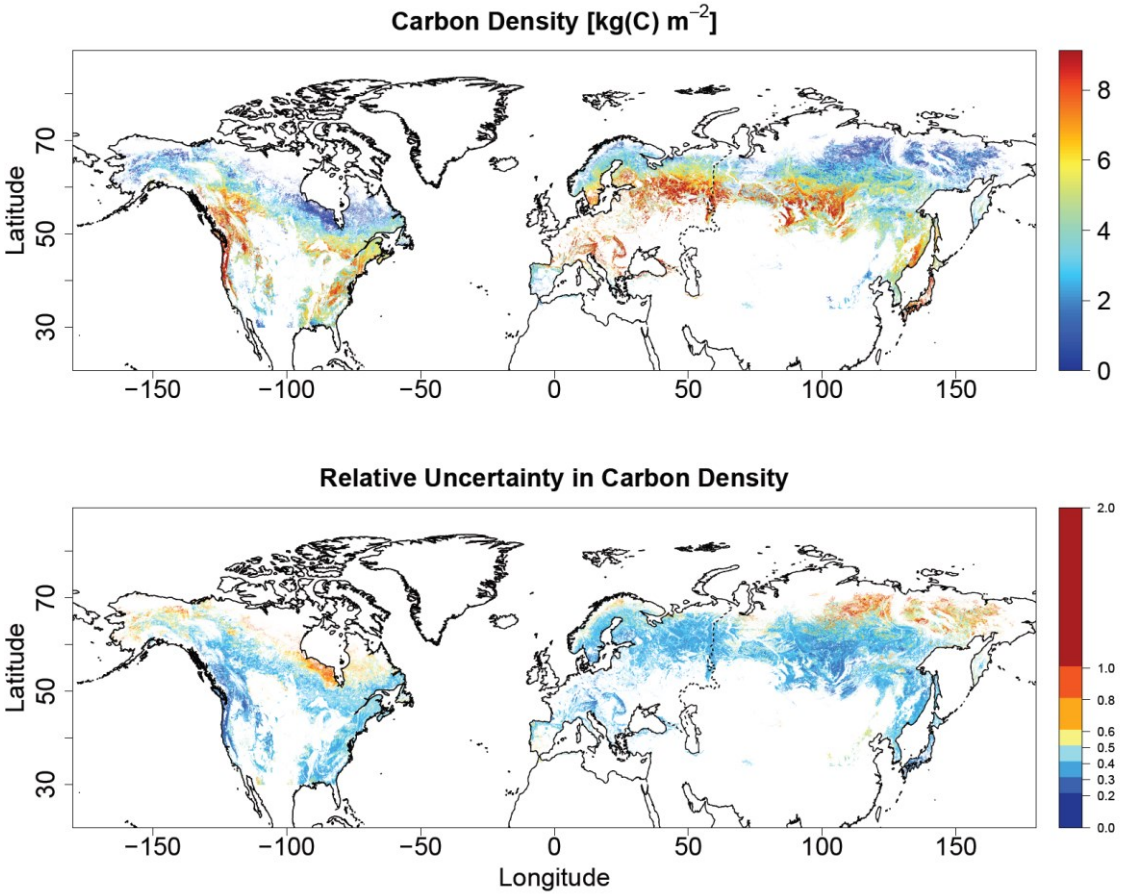

Fig. 2.11: Spatial distribution of total forest carbon density (tree stems + branches + roots + foliage) in Northern Hemisphere boreal and temperate forests and its corresponding relative uncertainty (a value of 1 corresponds to 100% uncertainty). Non-forest is masked out according to the GLC2000 land-use/land-cover map. The dashed black line indicates the boundary between Europe and Asia (data from ESRI, 2008) used for the estimation of continental carbon stocks.

Alternatively to the presented methodology, total biomass (as the sum of all compartments) could also be derived directly from stem biomass. In that way, an overestimation of the uncertainty, which had to be calculated as the sum of the uncertainties of the compartments, can be avoided. A direct estimation of total biomass (Fig. 2.12, left) would result in very similar total biomass estimates (Fig. 2.12, centre), but would decrease the uncertainty estimate considerably (Fig. 2.12, right). However, a separate estimation of biomass compartment biomass has been preferred, since this approach can provide useful information for applications requiring such detailed data, for instance model-data-integration uses, and avoids inconsistencies between the estimated biomass compartments and the total biomass.

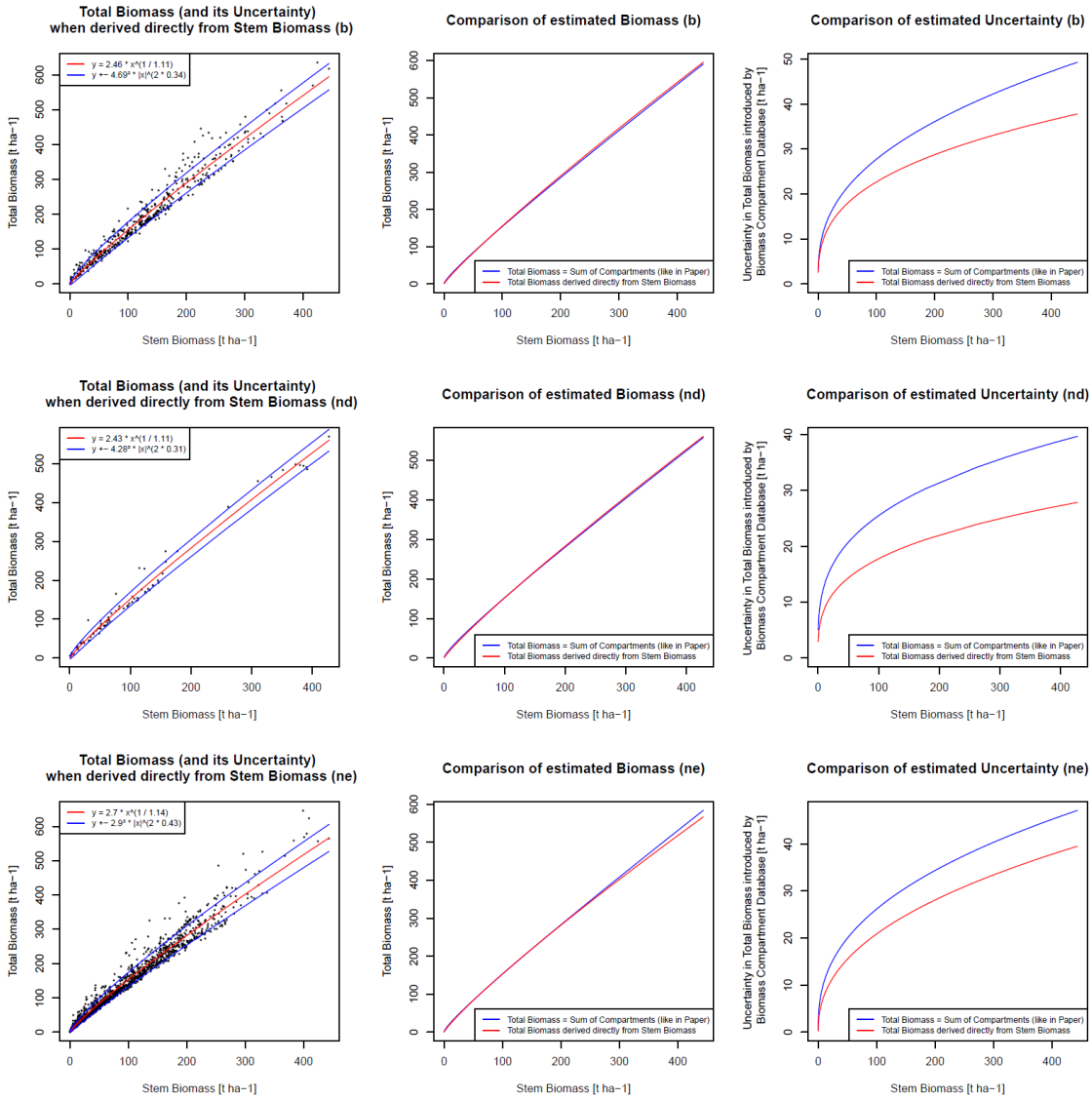

Fig. 2.12: Total biomass (and its corresponding uncertainty) [t ha^{-1}] when derived directly from stem biomass (left; central red line = functional relationship, upper and lower bound = uncertainty bound of the fitted relationship (standard deviation of the residuals, see Eq. (2.5))). Comparison of the estimated biomass between the two approaches (centre). Comparison of the estimated uncertainty between the two approaches (right). b = broadleaf, nd = needleleaf deciduous, ne = needleleaf evergreen.

2.3 Evaluation

The produced total carbon density map was evaluated against different independent datasets, covering an exhaustive range of ecosystems and forest structures. For intercomparison, Russian forest enterprise data (Shvidenko *et al.*, 2010; Schepaschenko *et al.*, 2011), the United States National Biomass and Carbon Dataset for the year 2000 (NBCD2000; Kellndorfer *et al.*, 2010; Kellndorfer *et al.*, 2012) and European national statistics (EFI, 2005) were used. The evaluation was implemented at regional scale

(Russian forest enterprises, US counties, European countries), since plot-level data would not represent the entire grid cell covered by the radar remote sensing signal and are thus hardly useful for a direct comparison. Instead, existing up-scaled estimates based on forest inventory data are used, demonstrating the validity at a larger scale which is useful for a number of applications, e.g. for integration with GVMs.

The Russian land cover dataset produced by IIASA (Shvidenko *et al.*, 2010; Schepaschenko *et al.*, 2011) is based on integration of forest inventory data and other relevant information. The dataset contains detailed forest characteristics, biomass among other things, at 1 km resolution. Intercomparison was performed for approximately 1600 forest enterprises with an average area of 9132.3 km^2, ranging from 2.8 to 550,074.0 km^2. While forest enterprises are usually small in densely populated territories in European Russia, they cover very large areas in remote territories of Siberia.

NBCD2000 (Kellndorfer *et al.*, 2012) was produced by the WHRC and can be seen as a benchmark map covering the conterminous United States. Combining USDA Forest Service FIA (USDA, 2012) and remote sensing data (InSAR data from SRTM and optical Landsat data), a high-resolution (30 m) raster dataset of aboveground wood carbon is available (Kellndorfer *et al.*, 2010, 2012). Aggregated biomass values could be compared for more than 3000 counties with an average area of 2405.7 km^2, ranging from 0.8 to 52,109.4 km^2. The comparison at the level of forest enterprises, counties or countries ensures a comparison to original forest inventory data and is not affected by the spatial variability introduced by other remote sensing data into the reference datasets.

The implemented intercomparison shows strong agreement to up-scaled inventory data and demonstrates the accuracy of the derived carbon density map. For Russia, the estimated carbon density at forest enterprise level agrees well with IIASA data (r^2 = 0.78, RMSE = 1.13 kgC m^{-2}; Fig. 2.13A). In a more detailed investigation no significant differences in this relationship were found for different bioclimatic zones in Russia (Fig. 2.14). For the USA, the comparison of aggregated values at county level shows strong agreement with the WHRC NBCD 2000 dataset (r^2 = 0.90, RMSE = 0.54 kgC m^{-2}; Fig. 2.13B). For European countries, evaluation results are comparable (r^2 = 0.70, RMSE = 0.87 kgC m^{-2}; Fig. 2.13C). While there is no systematic error apparent from the intercomparison in Russia, at least not in the Southern and Central taiga, the presented carbon density product might slightly underestimate high carbon densities, as can be seen from the evaluation results for US and European data. This indicates a saturation

effect probably related to the shortcomings of the C-band radar backscatter in high density forests; however, the GSV derived with the BIOMASAR algorithm was found to saturate only above 300 m^3 ha^{-1} (Santoro *et al.*, 2011).

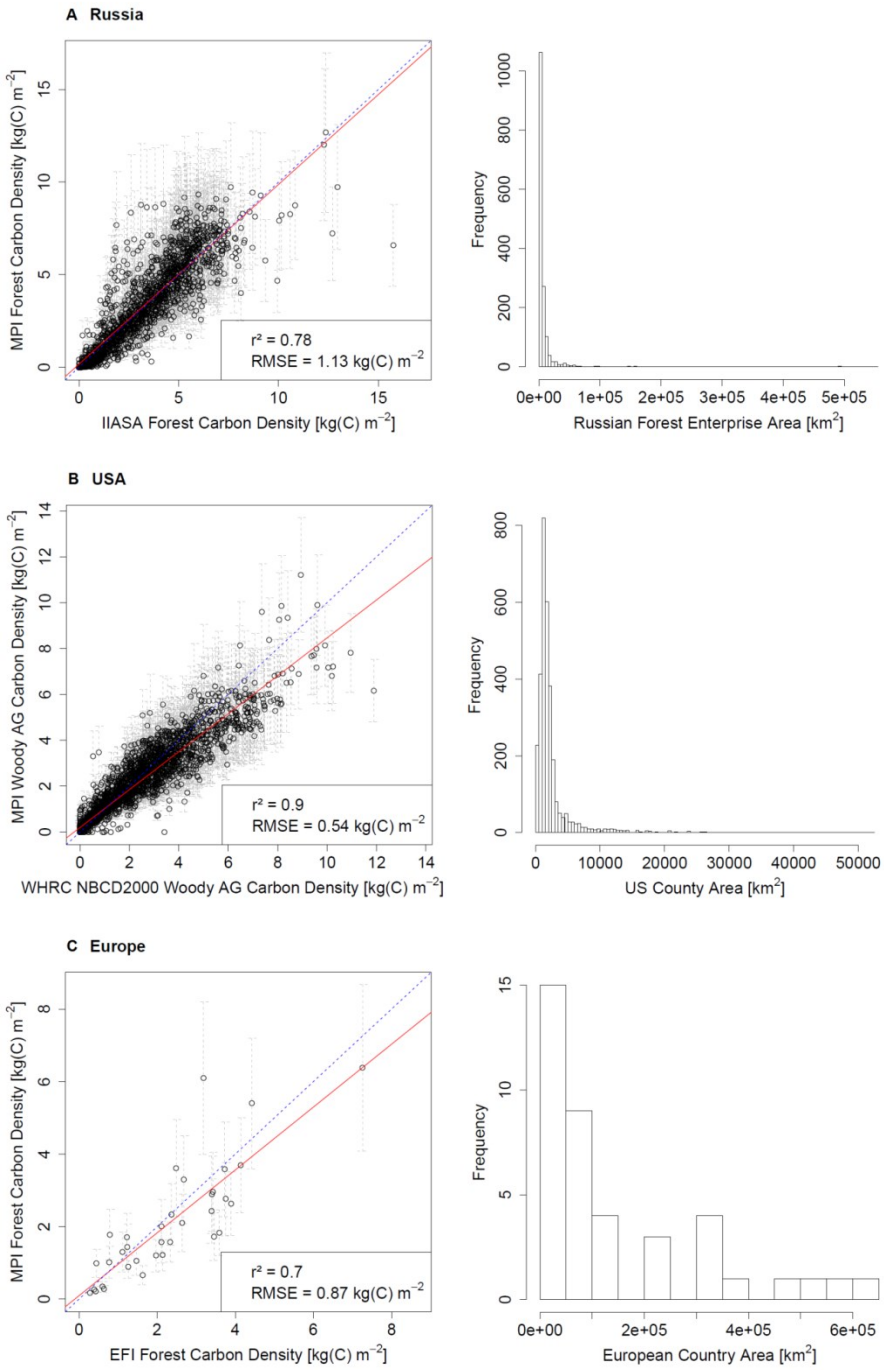

Fig. 2.13: Intercomparison of carbon density data from this study (MPI) and (A) IIASA forest enterprise (Shvidenko *et al.*, 2010; Schepaschenko *et al.*, 2011), (B) WHRC NBCD2000 US county (Kellndorfer *et al.*, 2010, 2012), and (C) EFI European country (EFI, 2005) carbon density data. The dashed line is the 1-to-1 line. The solid line is the linear regression line. Please note: Here carbon density is calculated per total (enterprise/county/country) area, not per forest area, due to differences in the estimated forest area between products. Corresponding histograms show the spatial scale at which evaluation took place.

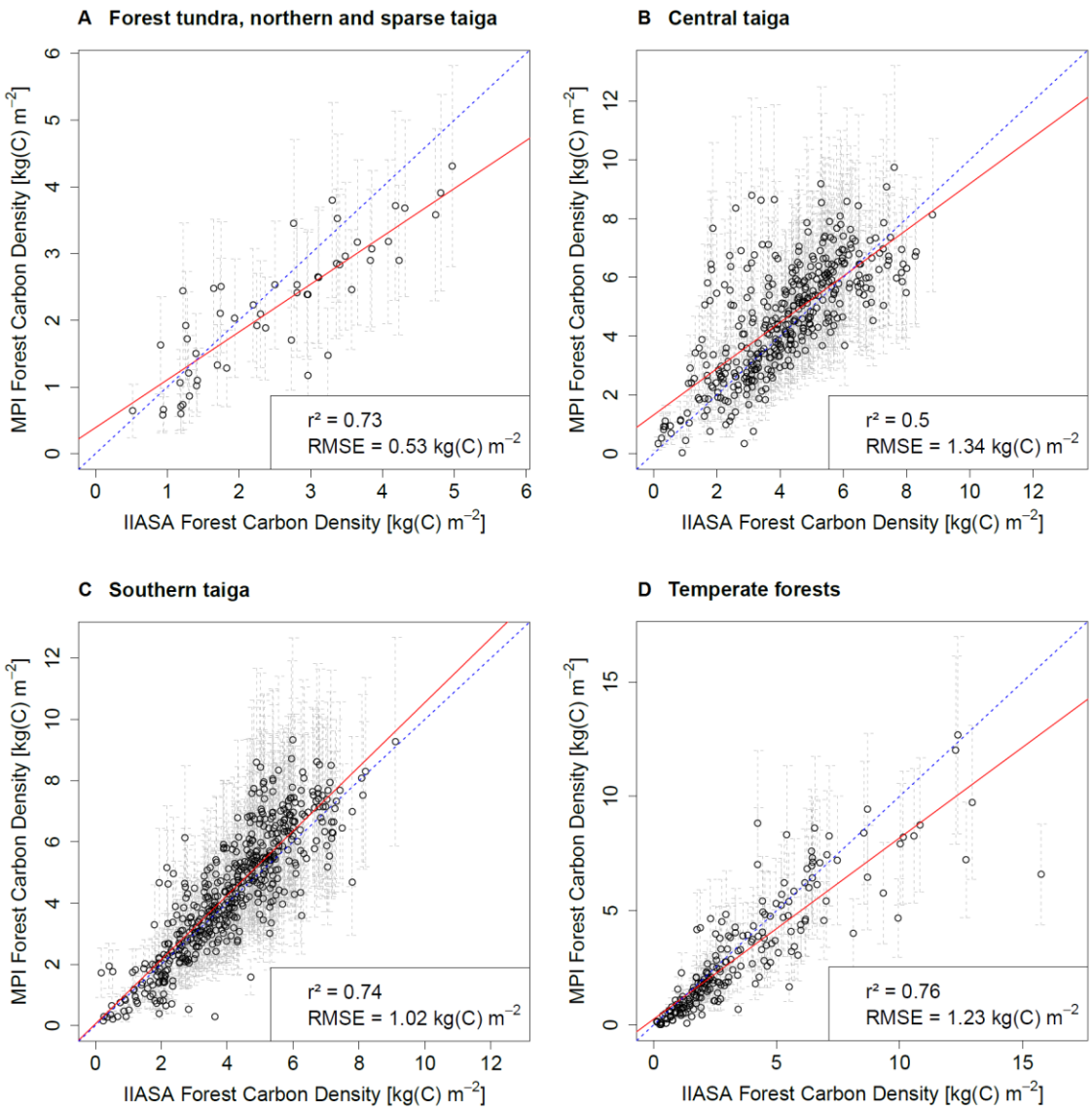

Fig. 2.14: Intercomparison of this study's (MPI) and IIASA forest enterprise carbon density data (Shvidenko *et al.*, 2010; Schepaschenko *et al.*, 2011) for different bioclimatic zones in Russia.

2.4 Boreal and temperate forest carbon stock and density

Based on the total carbon density map, boreal and temperate forest carbon stock and carbon density were estimated across three continents, North-America, Europe and Asia. Biomes were extracted according to Olson *et al.* (2001), including boreal forests (BFT), temperate broadleaf / mixed forests (TBMF) and temperate conifer forests (TCF). Continental boundaries were defined according to ESRI (2008). The land cover map GLC2000 was used as a forest mask in order to specify forest area. GLC2000 considers a pixel containing more than 15 % tree cover as forest (Bartholomé &

Belward, 2005). When deriving biomass estimates at a coarser spatial scale, the actual area of each grid cell was explicitly taken into account, assuming the Earth to be a perfect sphere. The carbon stock and its corresponding uncertainty of biomes and continents were calculated as the sum of the absolute biomass and uncertainties of the corresponding pixel values, respectively. In order to derive the carbon density and its uncertainty per biome and continent, the carbon stock and its uncertainty were divided by the covered forest area.

In 2010, the boreal and temperate forests of the Northern Hemisphere (30°N – 80°N) stored about 79.8 ± 29.9 PgC (Table 2.3) and their mean carbon density was 4.76 ± 1.78 kgC m^{-2} forest area (Table 2.4). Most of the forest carbon in the Northern Hemisphere is stored in BFT (40.7 ± 15.7 PgC), while TBMF and TCF account for 24.5 ± 9.4 PgC and 14.5 ± 4.8 PgC, respectively (Table 2.3). In terms of carbon density, a non-significant ($p = 0.95$) trend of more carbon per forest area stored in TBMF (5.80 ± 2.21 kgC m^{-2}) and TCF (6.21 ± 2.07 kgC m^{-2}) compared to BFT (4.00 ± 1.54 kgC m^{-2}; Table 2.4) is found. The uncertainty of these estimates is the sum of the uncertainties of all 0.01° pixels and is within the range of 30 - 40 %.

Table 2.3: Estimated mean and uncertainty of total forest carbon for North America, Europe and Asia across 3 different biomes (TBMF = Temperate Broadleaf and Mixed Forests, TCF = Temperate Conifer Forests, BFT = Boreal Forests / Taiga)

Total Forest Carbon [PgC]	N-America	Europe	Asia	Sum of 3 Continents
TBMF	9.7 ± 3.8	8.6 ± 3.1	6.2 ± 2.4	24.5 ± 9.4
TCF	10.1 ± 3.3	1.5 ± 0.5	2.9 ± 1.1	14.5 ± 4.8
BFT	8.9 ± 3.7	9.8 ± 3.6	22.1 ± 8.3	40.7 ± 15.7
Sum of 3 Biomes	28.7 ± 10.8	19.9 ± 7.3	31.2 ± 11.8	79.8 ± 29.9

Forest biome carbon stock and density values were also obtained more detailed for North America, Europe and Asia (see Tables 2.3, 2.4 and Fig. 2.15). Asian BFT account for the largest carbon stock within the investigated biomes. Concerning carbon density, TBMF were found to have a higher carbon density than TCF in Asia, in contrast to the other two continents. European forests exhibit a higher carbon density across all the three biomes compared to North America and Asia. Due to the conservative approach of estimating uncertainty, many of these findings are not significant at the 95 % confidence

interval. However, some of the reported results are significant. Carbon stocks (Table 2.3) in TCF are significantly smaller in Europe and Asia compared to North America. On the other hand, carbon stocks in BFT are significantly higher in Asia in comparison to Europe and North America. In Europe, there is significantly less carbon stored in TCF than in TBMF and BFT, while in Asia carbon stocks were found to be significantly higher in BFT than in TBMF and TCF. Carbon density (Table 2.4) is significantly higher in European versus North American BFT. In North America, carbon density was found to be significantly higher in TBMF and TCF compared to BFT.

Table 2.4: Estimated mean and uncertainty of carbon density for North America, Europe and Asia across 3 different biomes (TBMF = Temperate Broadleaf and Mixed Forests, TCF = Temperate Conifer Forests, BFT = Boreal Forests / Taiga)

Carbon Density [kgC m^{-2} Forest]	N-America	Europe	Asia	Mean of 3 Continents
TBMF	5.42 ± 2.14	6.70 ± 2.46	5.38 ± 2.05	5.80 ± 2.21
TCF	6.42 ± 2.07	7.60 ± 2.62	5.13 ± 1.86	6.21 ± 2.07
BFT	2.99 ± 1.26	5.47 ± 2.04	4.07 ± 1.53	4.00 ± 1.54
Mean of 3 Biomes	4.53 ± 1.71	6.08 ± 2.24	4.36 ± 1.64	4.76 ± 1.78

While European forest carbon stocks are relatively small compared to the other continents, the carbon density is higher in Europe across all the three biomes compared to North America and Asia. These patterns are also visible in Fig. 2.16, which shows carbon density per forest area aggregated to a regional scale (0.5° pixel size). Carbon stocks per area forest are estimated to be high for instance in Central Europe while relative to total land the carbon density is small there (cf. Fig. 2.11) since the European landscape is dominated by agricultural areas. Average biomass density is higher in Europe probably due to the influence of favourable climatic conditions, forest management activities and protection areas. Such information is important e.g. for a comparison to process-oriented ecosystem models, such as GVMs, which are often operated at coarser spatial resolutions like 0.5°.

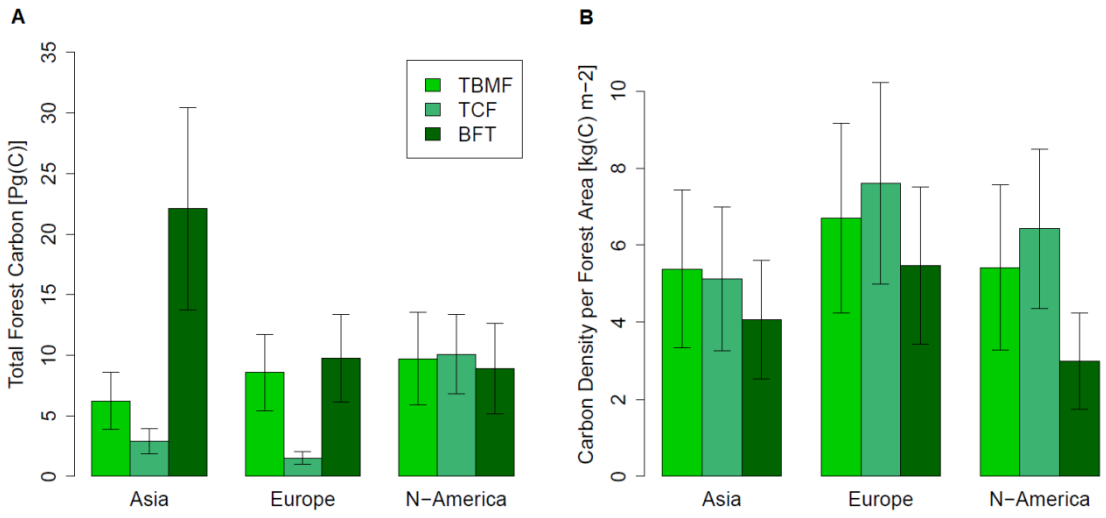

Fig. 2.15: (A) Total carbon stored in Northern Hemisphere forests (TBMF, temperate broadleaf and mixed forests; TCF, temperate conifer forests; BFT, boreal forests/taiga) and (B) their corresponding carbon density.

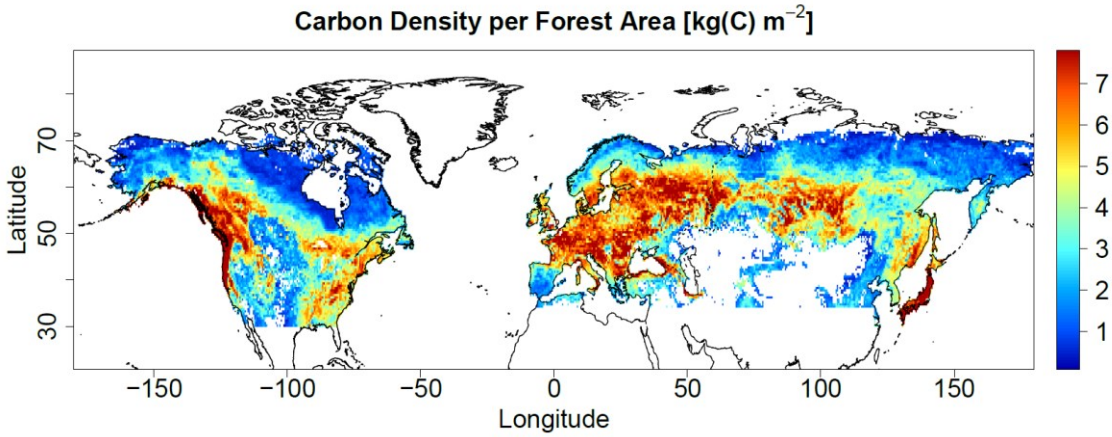

Fig. 2.16: Spatial distribution of carbon density per forest area in Northern Hemisphere boreal and temperate forests (aggregated to 0.5° resolution). The dashed black line indicates the boundary between Europe and Asia (data from ESRI, 2008) used for the estimation of continental carbon stocks.

CHAPTER 3

Large-scale variation in forest carbon turnover rate and its relation to climate

Following Chapter 1.3, forest carbon turnover rate (k) can be derived as the ratio of NPP and biomass under the assumption of steady state (cf. Eq. 1.4). Forest biomass (also called carbon density in Chapter 2; Thurner *et al.*, 2014; Santoro *et al.*, 2011, 2015) and NPP (Running *et al.*, 2004; Zhao *et al.*, 2005; Zhao & Running, 2010) products based on remote sensing data are used to calculate the average k at 0.5° spatial resolution during 2001-2010, covering boreal and temperate forests of the Northern Hemisphere (30-80°N). Therefore, and in contrast to plot-level field studies, the presented approach allows for a spatially comprehensive analysis over large areas. Furthermore, the data matches the required spatial scale at which processes are represented in current GVMs, circumventing uncertainty related to up-scaling of field study results. In order to shed light on the underlying drivers of k, the spatial gradients in k are related to spatial gradients in environmental variables, with special emphasis on climate variables. Observed relationships are explained by climate effects on forest mortality, but also possible confounding factors are discussed in detail.

3.1 Derivation of turnover rate from remote sensing based NPP and biomass

The MODIS MOD17 product provides information on NPP globally with a spatial resolution of 1 km (Collection 5 version 55; Running *et al.*, 2004; Zhao *et al.*, 2005; Zhao & Running, 2010; obtained from http://www.ntsg.umt.edu/project/mod17), necessitating its re-projection to geographic coordinates at 0.01° resolution. Average long-term NPP was derived for the period 2001-2010 in order to decrease the influence of inter-annual variability. This NPP product is based on several satellite-derived (MODIS fAPAR, land cover, LAI) and meteorological input datasets and accounts for GPP as well as maintenance and growth respiration of woody components and living

tissue (for details see Heinsch *et al.*, 2003). In addition to MODIS NPP, another NPP product (BETHY/DLR; Wißkirchen *et al.*, 2013; cf. Chapter 3.4.1) and an additional proxy of NPP derived from a data-driven estimate of GPP (Beer *et al.*, 2010; cf. Chapter 3.4.2) are used for comparison purposes in order to minimize effects of the NPP uncertainty and to test the robustness of the observed spatial patterns in k and their relationship to climatic indices. Although both MODIS and BETHY/DLR NPP products include models of gross primary productivity and plant respiration, their main drivers are biophysical variables obtained from remote sensing, particularly fAPAR and LAI.

MODIS NPP shows distinct spatial gradients corresponding to temperature, precipitation, and radiation (Fig. 3.1). In general, NPP increases with annual temperature and precipitation, although in ecosystems limited by either temperature or precipitation this relationship has not been observed using a comprehensive database of direct NPP measurements (Luyssaert *et al.*, 2007). While in boreal regions NPP is mostly limited by temperature, in temperate forests radiation and temperature in winter, temperature in spring and precipitation in summer are the climatic factors determining the upper bound of NPP (Running *et al.*, 2004). Similar temperature and precipitation driven gradients in NPP are reproduced by GVMs (Cramer *et al.*, 1999).

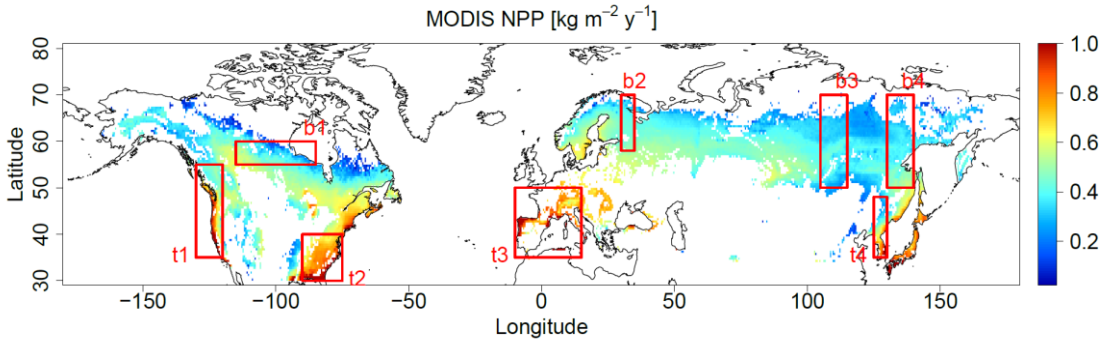

Fig. 3.1: Spatial patterns of MODIS NPP [kg m^{-2} y^{-1}], for all areas with at least 40 % forest cover (according to GLC2000 land cover dataset; additional use of MODIS MOD12 land cover classification). Red boxes show selected transects (Table 3.1).

Both biomass (or carbon density; cf. Chapter 2) and NPP datasets were aggregated to 0.5° resolution prior to calculating k, taking into account only forested pixels according to the GLC2000 land-use/land-cover map (cf. Table 2.1). Additionally, the MODIS MOD12 land cover classification (Friedl *et al.*, 2010) was used for division between forest and non-forest in order to consider only grid cells where the MODIS NPP product

has been derived from parameters calibrated to forest biomes (Heinsch *et al.*, 2003). Non-forest pixels were masked out already before aggregation, and only 0.5° grid cells containing at least 40 % forest covered grid cells at 0.01° (according to GLC2000) were considered to be dominated by forest and included in the analysis. Aggregation to 0.5° was performed in order to reduce the influence of uncertainties of the biomass, NPP and land cover products at their original spatial scale.

Large-scale forest *k* shows clear spatial gradients especially towards the northern edges of boreal and towards the southern edges of temperate forests (Fig. 3.2). In those regions, the estimated *k* can increase to values greater than 0.2 y^{-1}, but is mostly below 0.15 y^{-1}, with a mean turnover rate of 0.092 y^{-1} in Northern Hemisphere boreal and temperate forests. In the following, spatial gradients in *k* and their relation to climate variables are studied in detail along selected transects, four each in boreal (b1-b4) and temperate forests (t1-t4; Table 3.1).

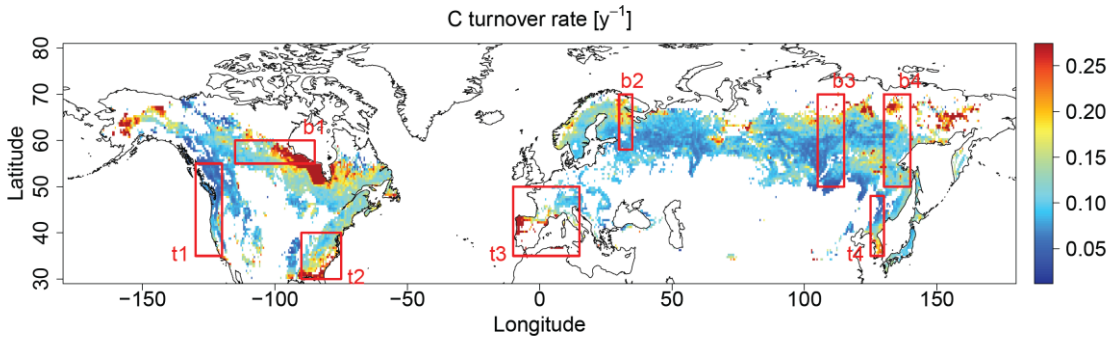

Fig. 3.2: Spatial patterns of *k* [y^{-1}] as the ratio of MODIS NPP over biomass, for all areas with at least 40 % forest cover (according to GLC2000 land cover dataset; additional use of MODIS MOD12 land cover classification). Red boxes show selected transects (Table 3.1).

The observed gradients in *k* differ substantially from those in NPP, especially in boreal forests they occur in opposite directions (Fig. 3.2 vs. Fig. 3.1). The spatial variation in *k* in the investigated boreal forest transects is mostly originating from a higher variation in biomass, while the variation in NPP is comparatively lower (Table 3.2). On the other hand, no consistent difference between the variation in NPP and the variation in biomass in the selected temperate forest transects becomes apparent (Table 3.2). When interpreting spatial patterns of *k*, it is important to keep in mind that NPP directly influences biomass accumulation. In the absence of climate-dependent turnover processes, the climate-driven NPP patterns are propagated to patterns in biomass. Thus,

spatial differences in the NPP/biomass ratio can be explained by effects of turnover processes on biomass, including both complete mortality of individual trees and senescence of tree components (implying woody biomass and living tissue), known as litterfall.

Table 3.1: Selected transects (b1-b4: boreal forest transects, t1-t4: temperate forest transects)

	Name	Major regions	Longitude [°]	Latitude [°]
b1	Canada	North-Eastern Alberta, Northern Saskatchewan, Manitoba and Ontario	-115 / -85	55 / 60
b2	Karelia / Western Russia	Murmansk, Karelia, Leningrad, Novgorod	30 / 35	58 / 70
b3	Central Siberia / Baikal	Western Sakha (Yakutia), Eastern Irkutsk, Buryatia, Western Zabaykalsk	105 / 115	50 / 70
b4	Eastern Siberia	Eastern Sakha (Yakutia), Khabarovsk	130 / 140	50 / 70
t1	Western North-America	Southern British Columbia, Western Washington State, Oregon and California	-130 / -120	35 / 55
t2	South-Eastern North-America	South-Eastern Illinois, Southern Indiana and Ohio, Kentucky, West Virginia, Virginia, Tennessee, North Carolina, South Carolina, Eastern Mississippi, Alabama, Georgia	-90 / -75	30 / 40
t3	South-Western Europe	France, Southern Germany, Switzerland, Austria, Slovenia, Italy, Spain, Portugal, Northern coast of Morocco, Algeria and Tunisia	-10 / 15	35 / 50
t4	North-Eastern China / Korea	Southern Heilongjiang, Jilin, North-Korea, South-Korea	125 / 130	35 / 48

Table 3.2: Variation coefficient (VC = standard deviation / mean) of *k*, NPP and biomass in the selected boreal and temperate forest transects

Transect	VC turnover rate	VC NPP	VC biomass
b1	0.717	0.298	0.605
b2	0.406	0.126	0.465
b3	0.497	0.151	0.388
b4	0.417	0.200	0.337
t1	0.475	0.377	0.305
t2	0.448	0.204	0.252
t3	0.693	0.274	0.368
t4	0.525	0.417	0.152

3.2 Comparison to inventory based estimates

In the absence of other studies integrating over both woody and living tissue (including foliage and fine roots) above- and belowground, the variance in *k* ((area weighted) median = 0.095 y^{-1}, first quartile = 0.076 y^{-1}, third quartile = 0.120 y^{-1}) was compared to the variance in *k* derived from the Luyssaert database (Luyssaert *et al.*, 2007) (median = 0.053 y^{-1}, first quartile = 0.034 y^{-1}, third quartile = 0.090 y^{-1}), integrating over boreal and temperate forests in the whole study area (Fig. 3.3). Although this evaluation seems to indicate an overestimation of *k* estimated here, a comparison to the Luyssaert database has its own shortcomings. Most importantly, in contrast to a remote sensing based *k*, the Luyssaert database and also other collections of field measurements do not capture the variety of turnover processes (litterfall, background mortality and all kinds of disturbances) at landscape scale over long time periods. Field measurements are unlikely to be representative for a 0.5° grid cell and can potentially be biased if they are implemented in largely undisturbed forests. In addition, the Luyssaert database is biased in the spatial distribution of measurement sites. Not many measurements are taken in areas where the highest *k* are observed here, potentially leading to an underestimation of the median *k* (Fig. 3.4). Thus, in addition to biases in the applied NPP and biomass datasets, the possible overestimation of the remote sensing based *k* could likely be explained also by other reasons related to the reference dataset. Overall, there is no sufficient data available for an independent field based evaluation of the estimated large-scale spatial patterns of *k*. Nevertheless, different NPP products and proxies can

be applied in order to test their influence on the results (cf. Chapter 3.4), and, together with the uncertainty in biomass (available from Thurner *et al.*, 2014; cf. Chapter 2.2), allow for a first-order uncertainty estimate of *k* (cf. Chapter 3.5).

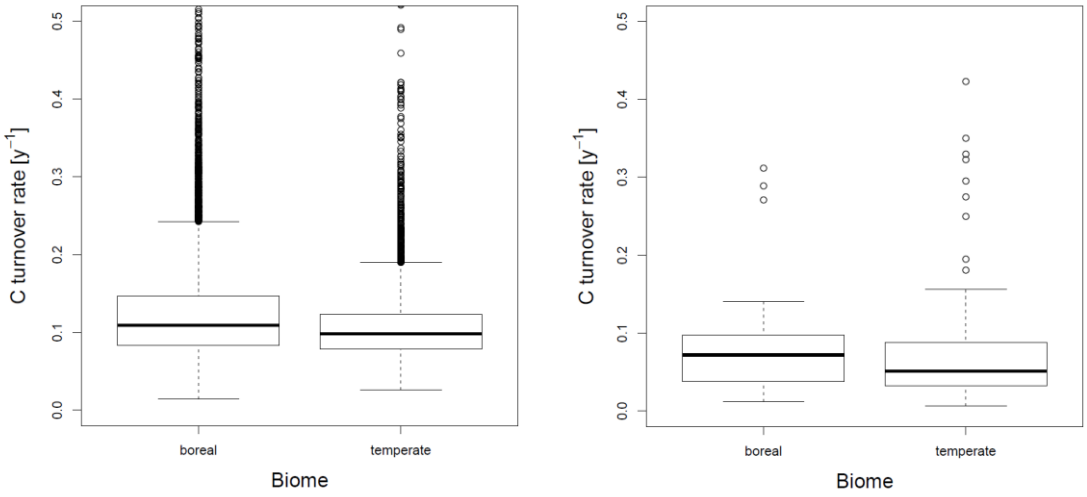

Fig. 3.3: Variance in *k* derived from MODIS NPP and BIOMASAR carbon density (left) and estimated from the Luyssaert database (Luyssaert *et al.*, 2007) (right)

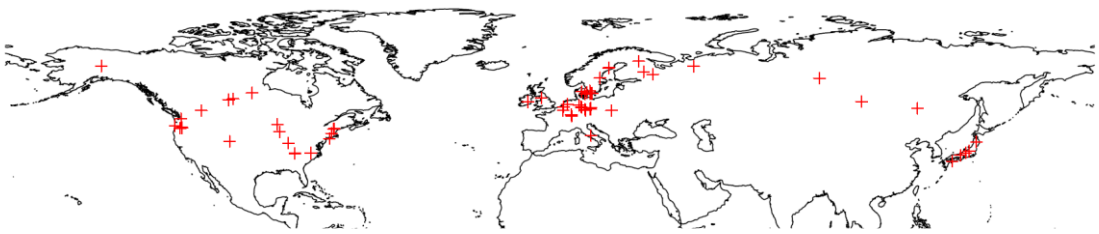

Fig. 3.4: Spatial representativeness of NPP and biomass estimates in Northern boreal and temperate forests available from the Luyssaert database (Luyssaert *et al.*, 2007)

Furthermore, the applied remote sensing NPP products and proxies can be evaluated against up-scaled forest inventory NPP estimates at the scale of the administrative units in Russia (Shvidenko *et al.*, 2007a). The administrative units represent republics, krays, oblasts, cities of federal significance, an autonomous oblast and autonomous okrugs of Russia. Both intercomparisons in absolute and relative (per area of the administrative unit) NPP units indicate that all the three applied NPP products (MODIS NPP, BETHY/DLR NPP) or proxies (GPP/2) might overestimate high NPP values (Fig. 3.5). However, an overestimation of low absolute or relative NPP values does not become

apparent. These results indicate that the gradients observed in *k* cannot be caused by a gradually increasing overestimation of NPP estimates by MODIS, BETHY/DLR or GPP/2 with decreasing NPP. The reliability of the applied biomass product has been demonstrated in Chapter 2.3.

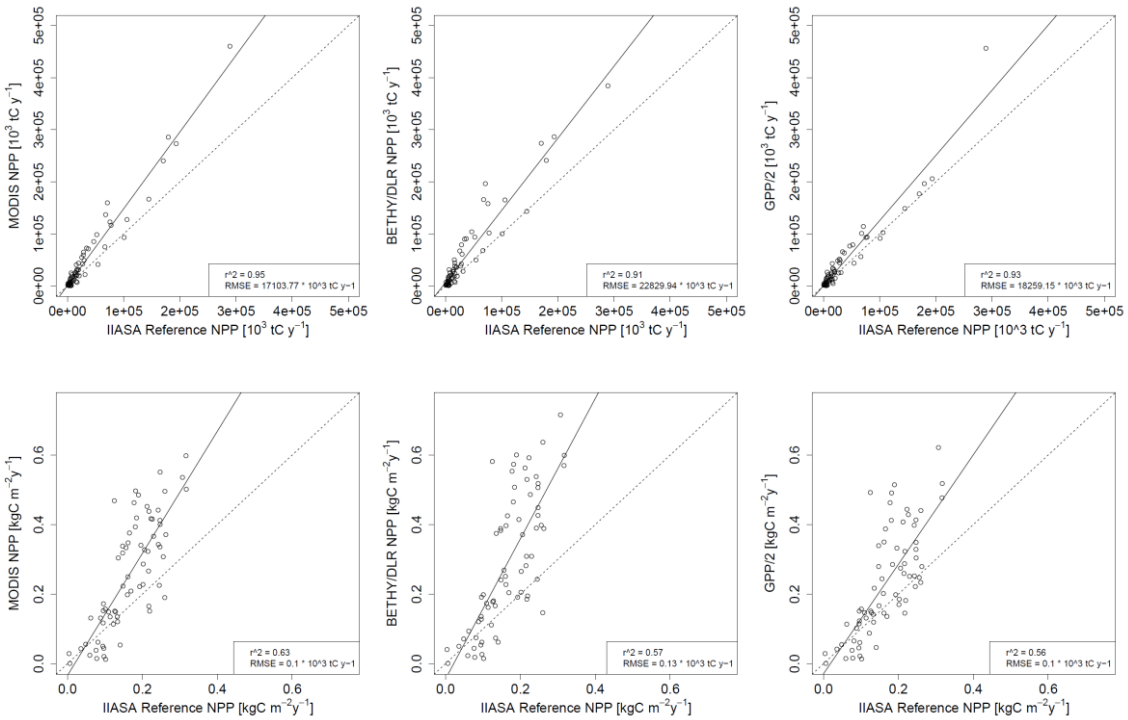

Fig. 3.5: Intercomparison of MODIS NPP (left), BETHY/DLR NPP (centre), and GPP/2 (right) against semi-empirically up-scaled estimates provided by the IIASA based on forest inventory data (Shvidenko *et al.*, 2007a; data obtained from *Shvidenko et al.*, 2007b) for each administrative unit (top) and per area of each administrative unit (bottom)

3.3 Relationships to climate variables

The relationships between *k* and an exhaustive selection of climate variables were analysed, including bioclimatic (BIOCLIM; for a definition of variables see Booth *et al.*, 2014) and climate extreme variables (CLIMDEX; for a definition of variables see Donat *et al.*, 2013). Long-term average values (1981-2010) were calculated for all of these variables based on originally daily climate data from the Water and Global Change programme (WATCH; Weedon *et al.*, 2011), which are available at 0.5° resolution. Boreal and temperate biomes were separated using a biome map (Olson *et al.*, 2001).

In a first step, the Spearman rank correlation between k and the climate variables was computed for each transect (Tables 3.3 and 3.4). In contrast to the Pearson product-moment correlation coefficient, the rank correlation assesses the capability of a monotone function, and not necessarily a linear one, to describe the relationship between two variables. Thus, it is better suited to consider the non-linearity in the relationships between k and climate variables. In addition, significance of the rank correlation was quantified by the p-value at different significance levels. Based on this correlation analysis, climate variables which are consistently (in the same direction) and significantly correlated to k (at a significance level of $p \leq 0.01$ or better) across all boreal or temperate transects could be identified (highlighted in yellow in Tables 3.3 and 3.4). These include

- annual mean temperature (AMT), minimum temperature of coldest month (TCM), mean temperature of driest quarter (TDQ), mean temperature of warmest quarter (TWarmQ), number of frost days (FD), number of icing days (ID), and growing season length (GSL) for boreal forest transects;
- annual mean temperature (AMT), isothermality (ISO), temperature seasonality (TS), maximum temperature of warmest month (TWM), minimum temperature of coldest month (TCM), mean temperature of warmest quarter (TWarmQ), mean temperature of coldest quarter (TCQ), number of frost days (FD), number of summer days (SD), number of icing days (ID), number of tropical nights (TN), growing season length (GSL), simple precipitation intensity index (SPII), and maximum length of warm (maximum temperature ≥ 10°C) –dry (no precipitation) periods (WD10) for temperate forest transects.

Table 3.3: Spearman rank correlation (r_{sp}) between *k* and investigated bioclimatic (BIOCLIM; for a definition of variables see Booth *et al.*, 2014) variables (AMT = annual mean temperature, MDTR = mean diurnal temperature range, ISO = isothermality, TS = temperature seasonality, TWM = maximum temperature of warmest month, TCM = minimum temperature of coldest month, TAR = temperature annual range, TWetQ = mean temperature of wettest quarter, TDQ = mean temperature of driest quarter, TWarmQ = mean temperature of warmest quarter, TCQ = mean temperature of coldest quarter, AP = annual precipitation, PWM = precipitation of wettest month, PDM = precipitation of driest month, PS = precipitation seasonality, PWetQ = precipitation of wettest quarter, PDQ = precipitation of driest quarter, PWarmQ = precipitation of warmest quarter, PCQ = precipitation of coldest quarter) in boreal (b1-b4) and temperate (t1-t4) forest transects. The significance level is quantified by the p-value: "***" $p \leq 0.001$, "**" $0.001 < p \leq 0.01$, "*" $0.01 < p \leq 0.05$, "." $0.05 < p \leq 0.1$, " " $p > 0.1$. Climate variables which are consistently (in the same direction) and significantly correlated to *k* (at a significance level of $p \leq 0.01$ or better) across all boreal or temperate transects are highlighted in yellow.

r_{sp}	b1	b2	b3	b4	t1	t2	t3	t4
AMT	-0.67***	-0.77***	-0.81***	-0.13**	0.59***	0.73***	0.64***	0.70***
MDTR	-0.61***	-0.15*	-0.63***	0.28***	0.31***	0.17**	0.45***	-0.85***
ISO	-0.68***	-0.28***	-0.67***	0.08.	0.59***	0.59***	0.64***	0.67***
TS	0.59***	0.16*	0.69***	0.10*	-0.28***	-0.67***	-0.55***	-0.94***
TWM	-0.47***	-0.77***	-0.67***	-0.10*	0.57***	0.69***	0.52***	0.35***
TCM	-0.66***	-0.76***	-0.76***	-0.12**	0.46***	0.73***	0.71***	0.87***
TAR	0.54***	0.12	0.59***	0.12**	-0.03	-0.61***	-0.23***	-0.94***
TwetQ	-0.55***	-0.47***	-0.52***	-0.01	0.24***	0.49***	-0.10	0.45***
TDQ	-0.36***	-0.77***	-0.64***	-0.13**	0.57***	0.11*	0.62***	0.85***
TWarmQ	-0.52***	-0.78***	-0.69***	-0.15***	0.63***	0.71***	0.51***	0.47***
TCQ	-0.67***	-0.75***	-0.78***	-0.10*	0.50***	0.74***	0.71***	0.83***
AP	0.54***	-0.65***	-0.30***	-0.10*	-0.03	0.29***	-0.12.	0.77***
PWM	-0.21***	-0.38***	-0.46***	-0.11*	0.07	0.49***	0.04	0.61***
PDM	0.45***	-0.39***	0.04	-0.08.	-0.53***	-0.01	-0.50***	0.84***
PS	-0.61***	0.22**	-0.11*	0.09*	0.48***	0.45***	0.37***	-0.48***
PWetQ	-0.08.	-0.52***	-0.45***	-0.11*	0.08	0.49***	0.03	0.60***
PDQ	0.53***	-0.47***	-0.02	-0.14**	-0.51***	0.13*	-0.50***	0.83***
PWarmQ	-0.21***	-0.43***	-0.44***	-0.11*	-0.52***	0.61***	-0.75***	0.60***
PCQ	0.54***	-0.66***	-0.08.	-0.15***	0.15*	0.10.	0.31***	0.83***

Table 3.4: Spearman rank correlation (r_{sp}) between *k* and investigated climate extreme (CLIMDEX; for a definition of variables see Donat *et al.*, 2013) variables (FD = frost days, SD = summer days, ID = icing days, TN = tropical nights, GSL = growing season length, WSDI = warm spell duration index, CSDI = cold spell duration index, MM5P = monthly maximum 5-day precipitation, SPII = simple precipitation intensity index, P10 = days with precipitation ≥ 10 mm, DS = maximum length of dry spell, WS = maximum length of wet spell, WD10 = maximum length of warm (maximum temperature ≥ 10°C) –dry (no precipitation) periods) in boreal (b1-b4) and temperate (t1-t4) forest transects. The significance level is quantified by the p-value: "***" $p \leq 0.001$, "**" $0.001 < p \leq 0.01$, "*" $0.01 < p \leq 0.05$, "." $0.05 < p \leq 0.1$, " " $p > 0.1$.Climate variables which are consistently (in the same direction) and significantly correlated to *k* (at a significance level of $p \leq 0.01$ or better) across all boreal or temperate transects are highlighted in yellow.

r_{sp}	b1	b2	b3	b4	t1	t2	t3	t4
FD	0.62***	0.78***	0.73***	0.15***	-0.47***	-0.74***	-0.67***	-0.67***
SD	-0.46***	-0.78***	-0.75***	-0.02	0.55***	0.71***	0.43***	0.33***
ID	0.69***	0.76***	0.82***	0.12**	-0.55***	-0.77***	-0.72***	-0.72***
TN	0.58***	-0.73***	0.28***	0.01	0.27***	0.71***	0.32***	0.54***
GSL	-0.68***	-0.78***	-0.81***	-0.13**	0.57***	0.74***	0.66***	0.68***
WSDI	0.15**	-0.22**	0.70***	-0.12**	0.06	0.01	-0.05	0.42***
CSDI	-0.42***	0.36***	-0.21***	0.02	-0.54***	0.17**	-0.56***	-0.35***
MM5P	0.15**	-0.69***	-0.52***	-0.14**	0.12*	0.43***	0.20**	0.66***
SPII	0.26***	-0.66***	-0.30***	-0.11*	0.19**	0.37***	0.18**	0.70***
P10	0.51***	-0.60***	-0.36***	-0.10*	0.05	0.39***	-0.02	0.72***
DS	-0.58***	-0.26***	0.08.	0.18***	0.58***	0.69***	0.60***	-0.62***
WS	-0.33***	-0.49***	-0.30***	-0.07	-0.05	0.51***	0.20**	-0.08
WD10	-0.59***	-0.53***	0.13**	-0.27***	0.58***	0.66***	0.76***	0.42***

In boreal forests, it is not plausible which mortality mechanisms could be responsible for the negative correlation between *k* and TDQ (unless the driest quarter is during winter) and TWarmQ. Instead, drought and heat stress would be favoured by higher temperatures during warm and/or dry periods. In addition, no positive relationship between *k* and WD10 becomes apparent in boreal forests. Likely, strong correlations of TDQ and TWarmQ to other climate variables can explain their negative correlation to *k*. The same seems to be true for AMT. All the other climate variables with consistently highly significant correlations to *k* are related to winter temperature and length (TCM,

FD, ID, and GSL), indicating direct and indirect frost stress effects on mortality to be underlying these spatial patterns. These effects are discussed in detail with regard to the literature in Chapter 5.2 of this thesis.
In temperate forests, the climate variables consistently and significantly correlated to *k* can be separated into two major groups:

- climate conditions favouring drought stress effects on mortality (TWM, TWarmQ, SD, TN, WD10)
- and climate conditions favouring insect survival during winter periods (TCM, TCQ, FD, ID)

Other climate indices, including AMT, ISO, TS, GSL, and SPII, again might be correlated to *k* mainly because of their strong correlation to the other climate variables. Nevertheless, additional effects on mortality caused by extreme annual or diurnal temperature ranges (ISO, TS), or by strong precipitation events (SPII), cannot be ruled out. However, the discussion of the underlying mechanisms of the observed spatial patterns in *k* (Chapter 5.2) focuses on climate conditions favouring drought stress and insect epidemics, since these mechanisms have been identified to be of major and global importance in driving broad-scale mortality in temperate forests (Logan *et al.*, 2003; Allen *et al.*, 2010).
Climate variables analysed in detail in the following include ID (in boreal forests), FD and WD10 (in temperate forests). These variables have been selected in order to represent each identified climate-driven mortality mechanism by one climate variable:

- frost stress effects on mortality are represented by ID (in boreal forests),
- drought stress effects on mortality are represented by WD10,
- and insect outbreak effects on mortality are represented by FD (both in temperate forests).

Icing days are defined as the annual count of days with a daily maximum (surface air) temperature below 0°C, whereas frost days are the annual count of days with a daily minimum temperature below 0°C. Warm-dry periods are referred to as both warm (T_{max} ≥ 10°C) and dry (without precipitation) consecutive days, and their maximum length for each year was derived before calculating 30-year averages. Different leaf types (broadleaf / needleleaf, deciduous / evergreen) were separated using GLC2000.

The relationships between the observation based *k* and the climate variables were investigated at 0.5° resolution. In general, exponential functions of the form

$$k = k_{base} + e^{\frac{x - C_{\lim}}{m}} \qquad \text{(Eq. 3.1)}$$

were found to be best suited (in terms of modelling efficiency (MEF; Nash & Sutcliffe, 1970) and ecological interpretability) to model these relationships. MEF is calculated as the variance of the residuals (difference of observed (obs) and modelled (sim) *k*) over the variance in the observed values:

$$MEF = 1 - \frac{\sum (obs - sim)^2}{\sum (obs - mean(obs))^2} \qquad \text{(Eq. 3.2)}$$

While a negative MEF indicates that the mean of the observations is a better predictor than the model, a MEF of 1 corresponds to a perfect match between model and observations (Nash & Sutcliffe, 1970).

k is modelled as a function of a climate variable x, estimating the parameters describing the base turnover rate k_{base}, which is the turnover rate occurring without influence of the climate variable, the climatic limit $C_{\lim}$ where the turnover rate becomes $T_{base} + 1$, and a parameter m defining the slope of the exponential function. These functions were fitted by non-linear least-square regression in R using the port algorithm (Bates & Watts, 1988), which allows defining parameter lower and/or upper boundaries beforehand.

k increases exponentially with ID in boreal forest transects (Fig. 3.6). Also other climate variables related to winter temperatures and length (see discussion above) show similar patterns (see Tables 3.3 and 3.4) due to their high correlation. In temperate forests, *k* increases with WD10 (Fig. 3.7). In Western North-America (t1) and South-Western Europe (t3), there is also a strong increase in *k* for extremely low precipitation levels during the warmest quarter of the year (Table 3.3). However, in South-Eastern North-America (t2) and North-Eastern China / Korea (t4) this relationship cannot be observed, due to relatively high precipitation amounts during summer periods in those regions. In contrast to temperate forests, a consistent relationship between drought and *k* cannot be identified in boreal forests. Moreover, a higher *k* is observed in temperate forests for areas with a lower FD (Fig. 3.8).

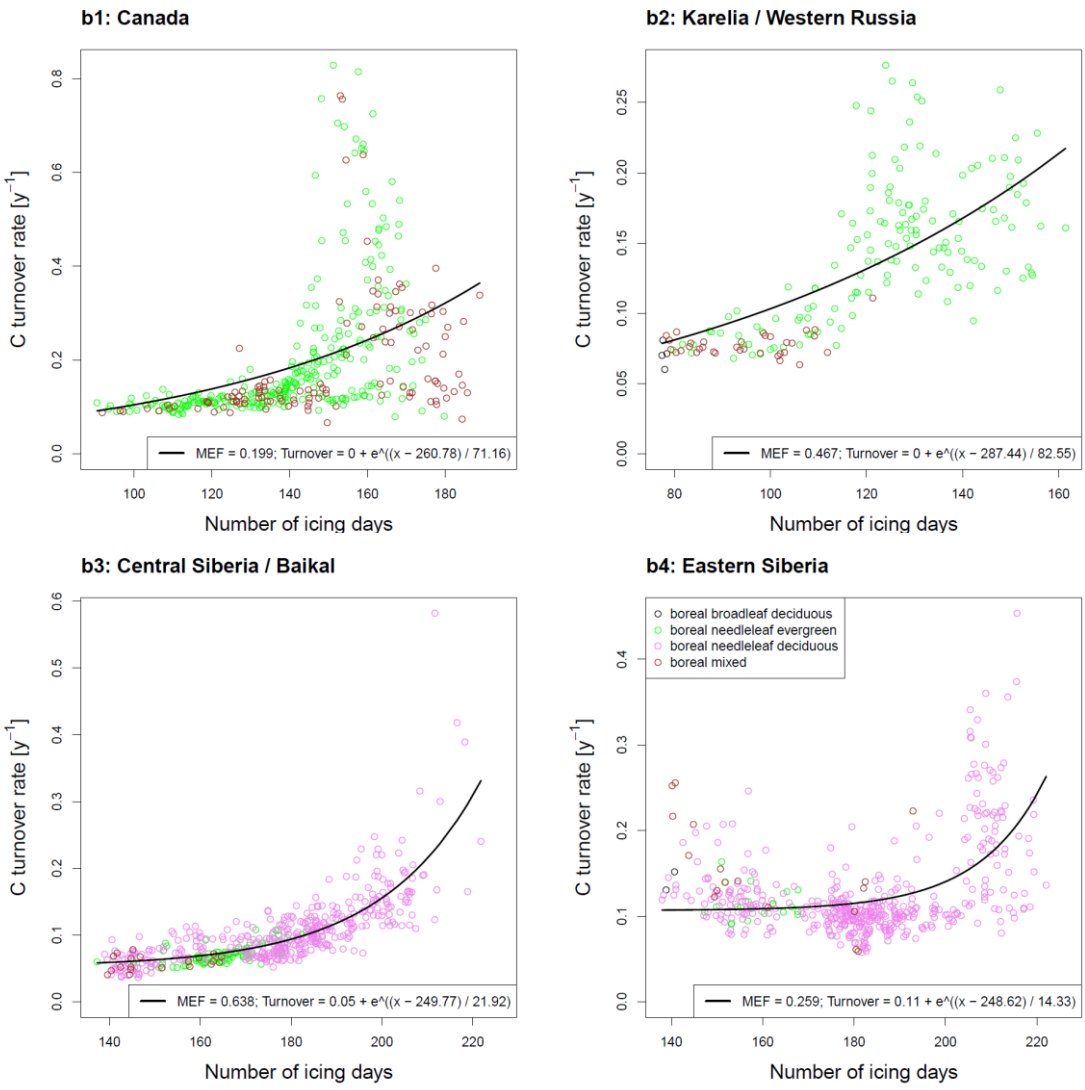

Fig. 3.6: *k* as a function of the number of icing days during a year in boreal forest transects. Points correspond to all 0.5 degree grid cells within the specified transects (cf. Table 3.1) with at least 40 % forest cover (according to GLC2000 land cover dataset; additional use of MODIS MOD12 land cover classification).

Multivariate exponential models adding the influence of both predictor variables (WD10 and FD) lead to a significant increase in MEF in region t3 and a slight increase in the other transects (Table 3.5). Parameters of the relationships of *k* to climate variables, i.e. the climatic limit and steepness of the increase in *k*, are considerably different between regions. On the other hand, only small differences in the low levels of *k* are observed over a wide climatic range within some regions, until a climatic limit is reached, where *k* increases strongly with increasingly extreme climate. For example, in Central Siberia / Baikal (b3) and Eastern Siberia (b4), *k* appears to considerably rise only for more extreme winter lengths and temperatures, but then with a steeper gradient

compared to Canada (b1) and Karelia / Western Russia (b2, Fig. 3.6). Furthermore, no substantially different deviations from the relationships between *k* and climate depending on the leaf type are detected.

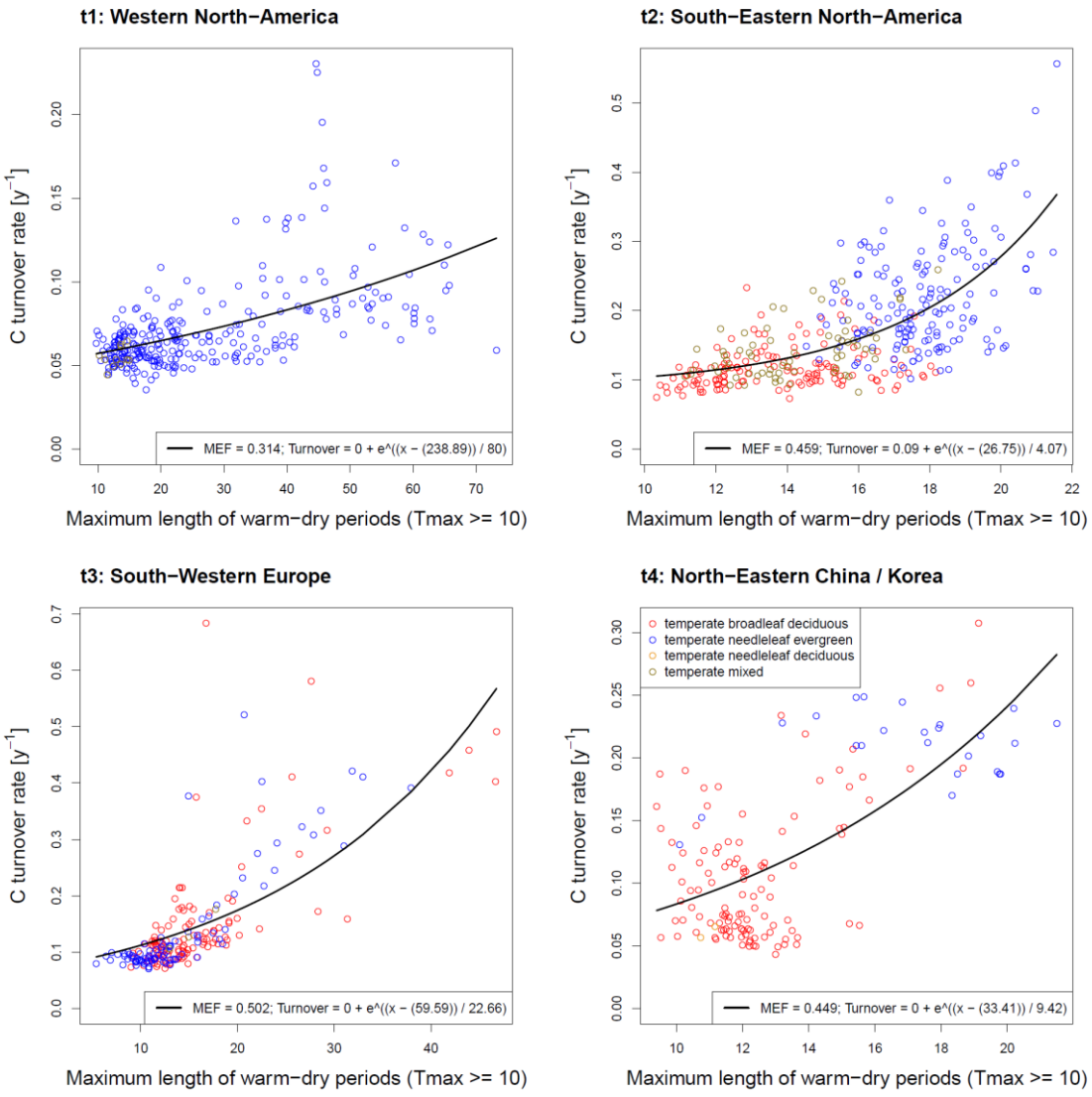

Fig. 3.7: *k* as a function of the maximum length of warm-dry periods (in days) during a year in temperate forest transects. Points correspond to all 0.5 degree grid cells within the specified transects (cf. Table 3.1) with at least 40 % forest cover (according to GLC2000 land cover dataset; additional use of MODIS MOD12 land cover classification).

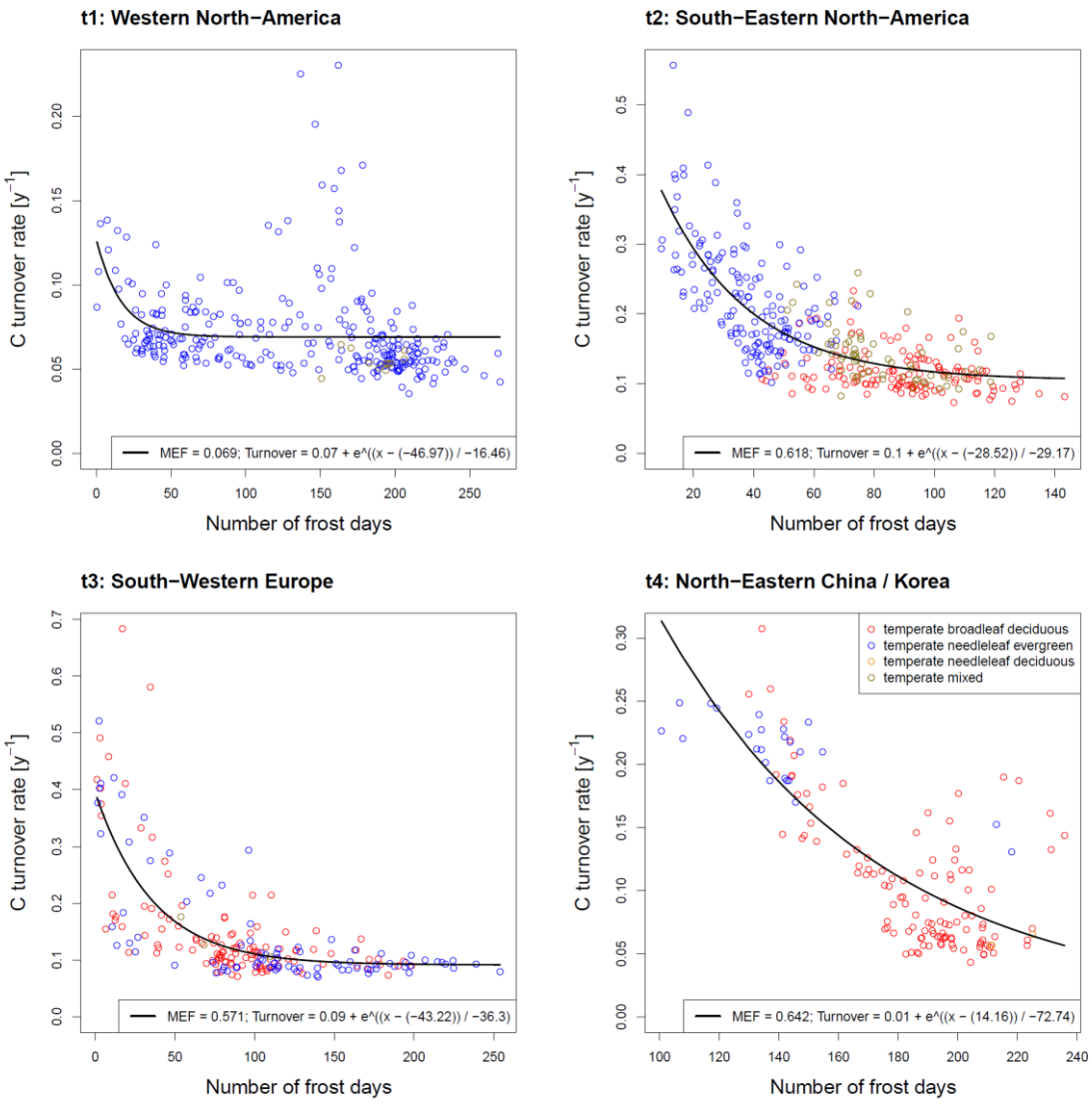

Fig. 3.8: k as a function of the number of frost days during a year in temperate forest transects. Points correspond to all 0.5 degree grid cells within the specified transects (cf. Table 3.1) with at least 40 % forest cover (according to GLC2000 land cover dataset; additional use of MODIS MOD12 land cover classification).

Table 3.5: Modelling Efficiency (MEF) of the exponential model relating k and the WD10, k and FD and k and both predictor variables (applying models of the form $k = k_{base} + e^{\frac{x_1 - C_{\lim_1}}{m_1}} + e^{\frac{x_2 - C_{\lim_2}}{m_2}}$) in temperate forest transects

Transect	MEF WD10	MEF FD	MEF both
t1	0.314	0.069	0.347
t2	0.459	0.618	0.641
t3	0.502	0.571	0.662
t4	0.449	0.642	0.655

3.4 Influence of NPP products on results

MODIS GPP (and thus NPP) is dependent on minimum temperature amongst others. However, GPP (NPP) is decreasing with decreasing minimum temperature by a linear ramp function (Heinsch *et al.*, 2003). In contrast, an elevated *k* (= NPP / Biomass) is found in case of colder winter temperatures in boreal forests (cf. Fig. 3.6). Hence, the MODIS algorithm cannot be primarily responsible for the reported relationships between *k* and climate. Nevertheless, the MODIS algorithm may influence the presented results through its consideration of autotrophic respiration and carbon allocation (cf. Chapter 3.6). In order to evaluate these possible confounding factors, another NPP product and an additional proxy of NPP derived from a data-driven estimate of GPP (Beer *et al.*, 2010) have been tested concerning their impact on the spatial patterns of *k* and the observed relationships to climate indices.

3.4.1 BETHY/DLR NPP

Applying a different NPP product (BETHY/DLR NPP; Wißkirchen *et al.*, 2013) does not reveal lower turnover rates closer to ranges in field measurements ((area weighted) median = 0.101 y^{-1}, first quartile = 0.084 y^{-1}, third quartile = 0.122 y^{-1}). BETHY/DLR integrates remote sensing data (LAI time series from SPOT-VEGETATION, land cover, albedo, digital elevation model, atmospheric CO_2 concentrations), meteorological as well as soil data and the Biosphere Energy Transfer Hydrology (BETHY) (Knorr, 2000; Knorr & Kattge, 2005) model, simulating GPP and plant respiration. In BETHY, photosynthesis, respiration and transpiration are modelled by a combined approach of Farquhar *et al.* (1980) and Collatz *et al.* (1992). Maintenance respiration is driven by temperature and is directly proportional to the maximum carboxylation rate. BETHY/DLR has been validated for Europe using FLUXNET data (Wißkirchen *et al.*, 2013) and statistical yield and national forest inventory data (Tum & Günther, 2011; Tum *et al.*, 2011). Similar to MODIS NPP, long-term averages have been derived from originally daily NPP estimates during 2001-2010 and aggregated from 1 km to 0.5 degrees.

In general, BETHY/DLR shows similar spatial patterns like MODIS NPP (compare Figs. 3.9 and 3.1). Nevertheless, absolute and relative differences are visible between these two products (Fig. 3.9). No general over- or underestimations of MODIS with respect to BETHY/DLR NPP become apparent at biome scale, instead these deviations

are rather fragmented in space. Relatively higher MODIS NPP for instance at the northern edge of the boreal transect b4 might nevertheless overemphasize the increase in *k* along this gradient.

Despite differences in the spatial patterns of NPP between MODIS and BETHY/DLR, the effects on gradients in *k* (Fig. 3.10) and its relationships to climate (compare Figs. 3.11-3.13, Figs. 3.6-3.8) are rather small. Applying a different NPP estimate based on other remote sensing datasets and a state-of-the-art biosphere model does not result in substantially different relationships between *k* and climate, increasing the confidence in these results.

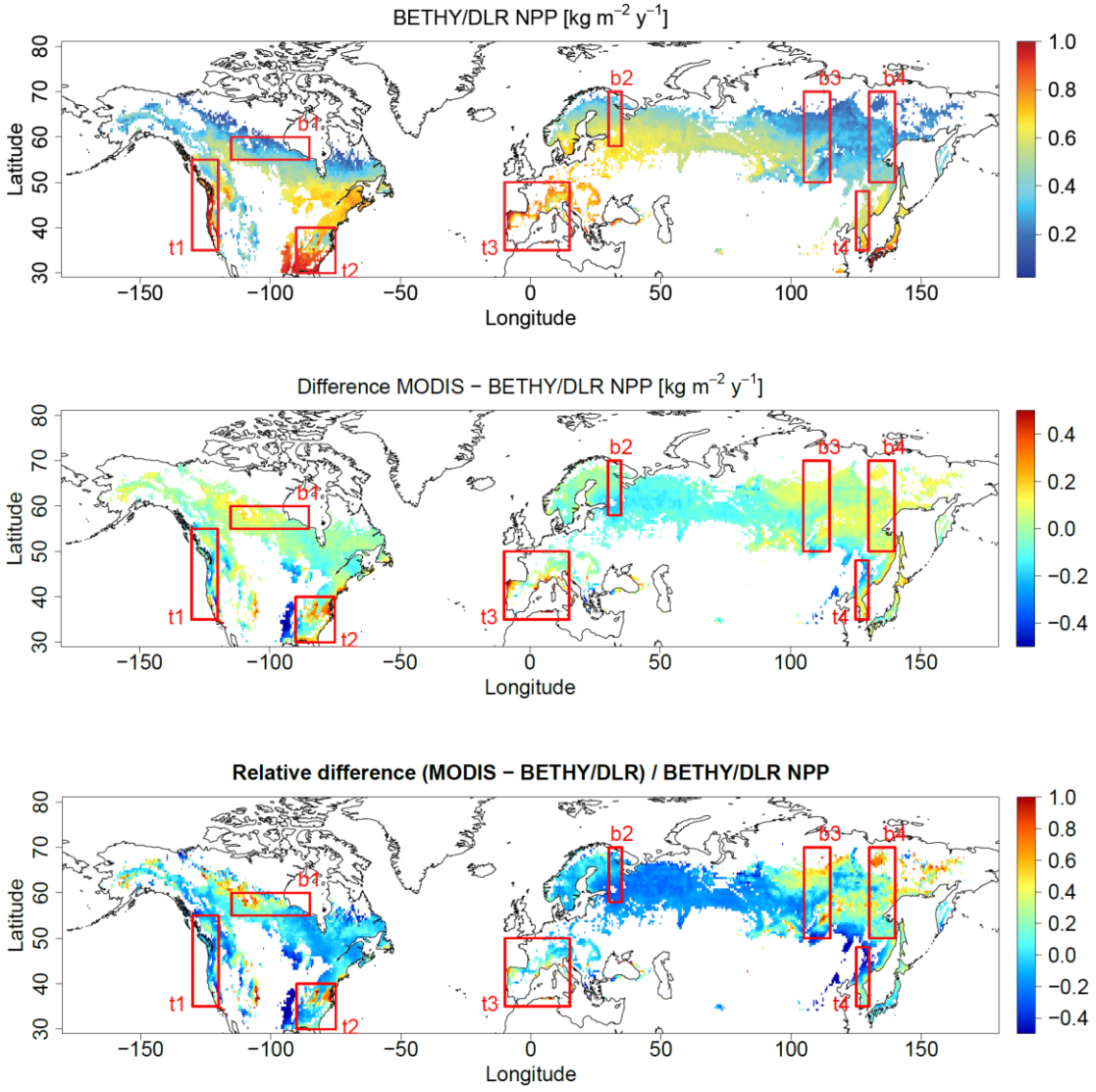

Fig. 3.9: Spatial patterns of BETHY/DLR NPP [kg m^{-2} y^{-1}], for all areas with at least 40 % forest cover (according to GLC2000 land cover dataset; additional use of MODIS MOD12 land cover classification) (top). Absolute (centre) and relative (bottom) difference to MODIS NPP.

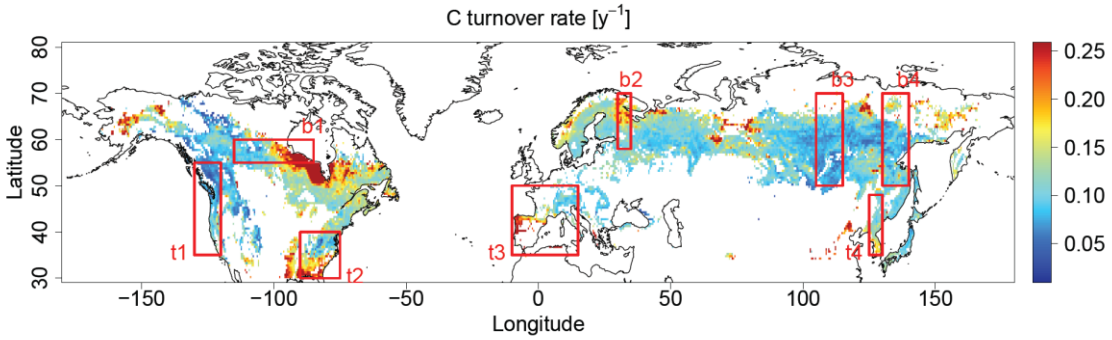

Fig. 3.10: Spatial patterns of k [y^{-1}] as the ratio of BETHY/DLR NPP over biomass, including areas with at least 40 % forest cover

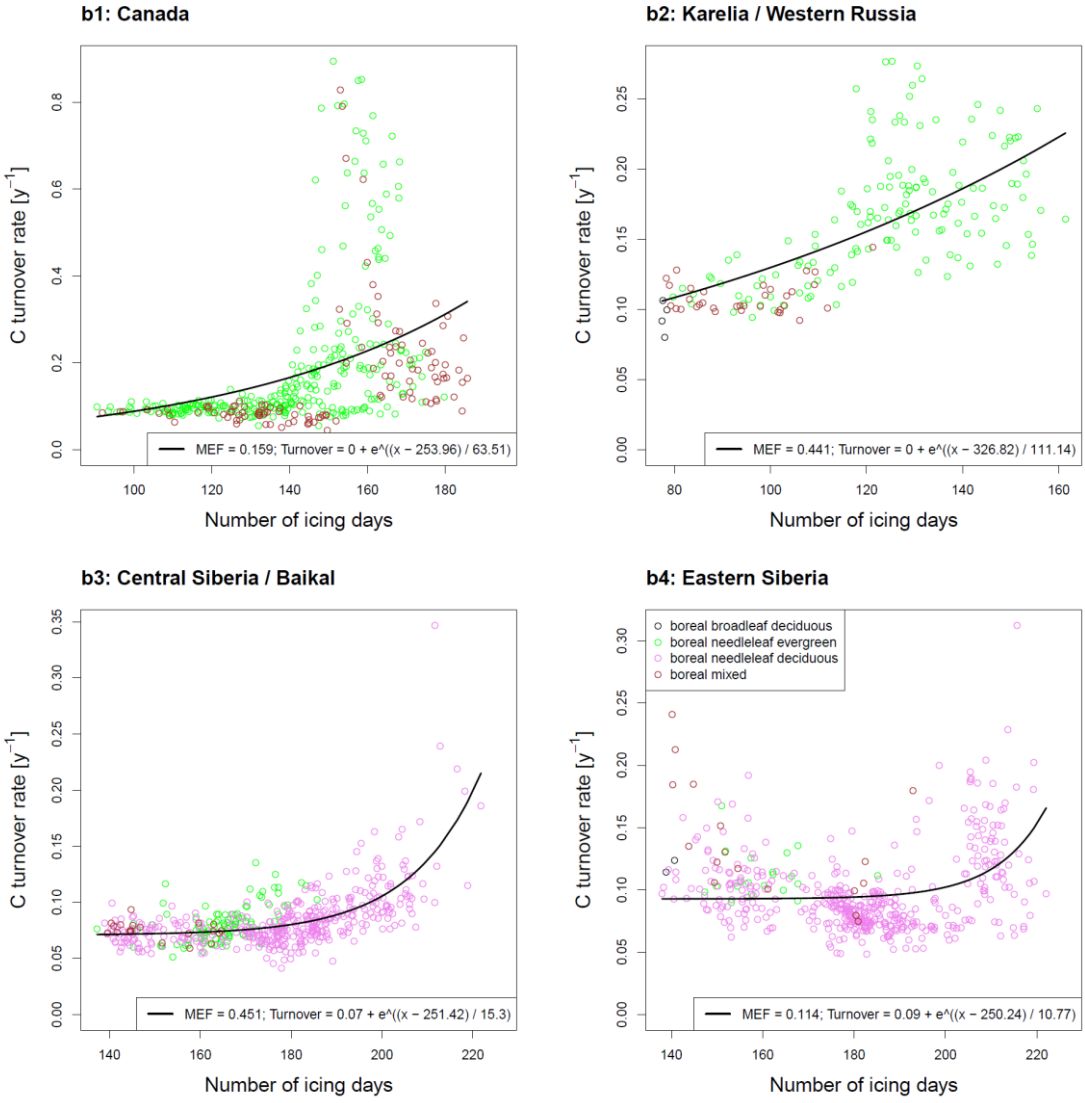

Fig. 3.11: k (= (BETHY/DLR NPP) / biomass) as a function of the number of icing days during a year in boreal forest transects

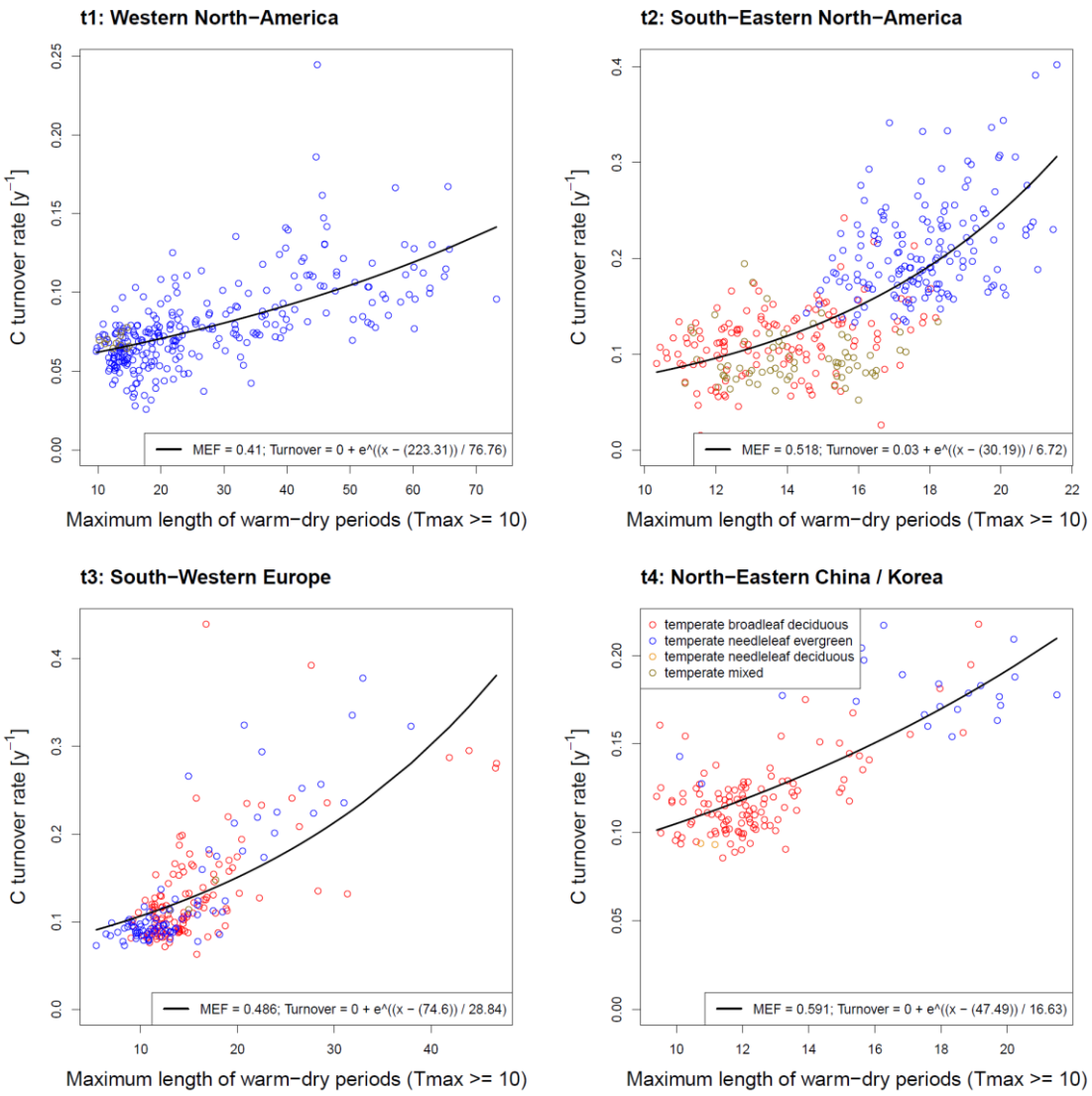

Fig. 3.12: *k* (= (BETHY/DLR NPP) / biomass) as a function of the maximum length of warm-dry periods (in days) in temperate forest transects

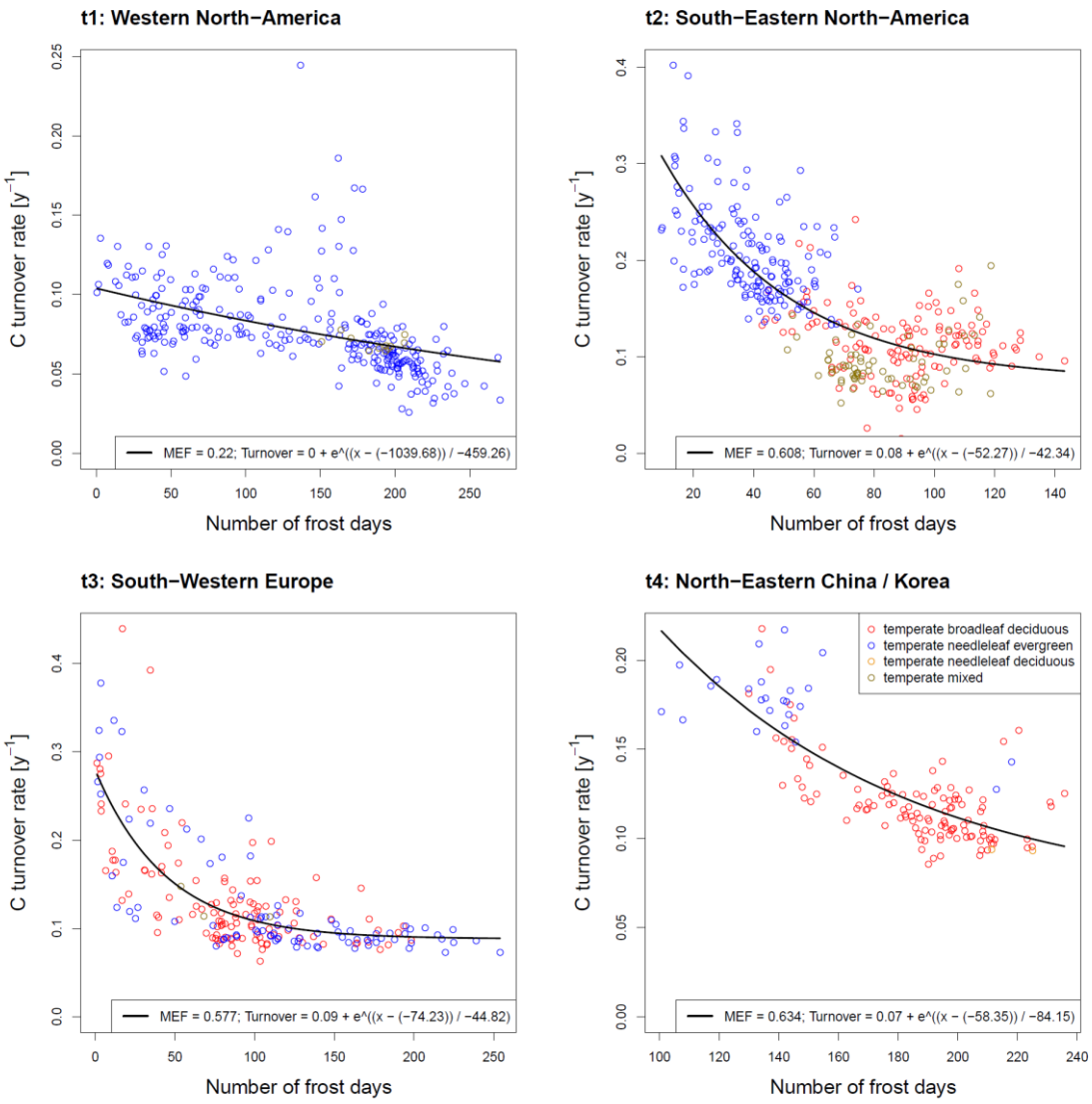

Fig. 3.13: *k* (= (BETHY/DLR NPP) / biomass) as a function of the number of frost days during a year in temperate forest transects

3.4.2 GPP/2 as a proxy for NPP

Furthermore, GPP divided by 2 was used as a simple proxy for NPP, since carbon use efficiency (= NPP / GPP) in forests has been reported to be around 50 % on average, while there is still a debate concerning its range (Waring *et al.*, 1998; DeLucia *et al.*, 2007; van Oijen *et al.*, 2010; Vicca *et al.*, 2012). For this purpose, a global GPP product derived from eddy covariance data and different diagnostic models (Beer *et al.*, 2010) is employed. This GPP estimate does not solely contain forest GPP, however it is applied to derive *k* at forested pixels only (according to GLC2000 at 0.5° resolution).

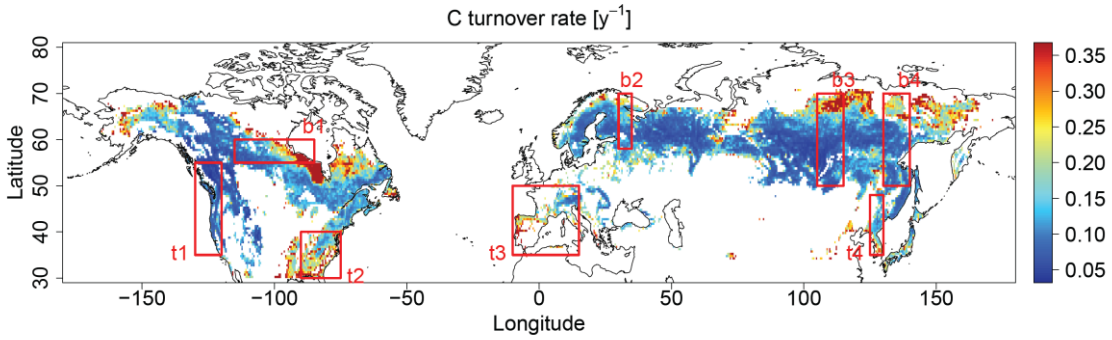

Fig. 3.14: Spatial patterns of k [y^{-1}] as the ratio of total GPP divided by 2 over biomass, including areas with at least 40 % forest cover

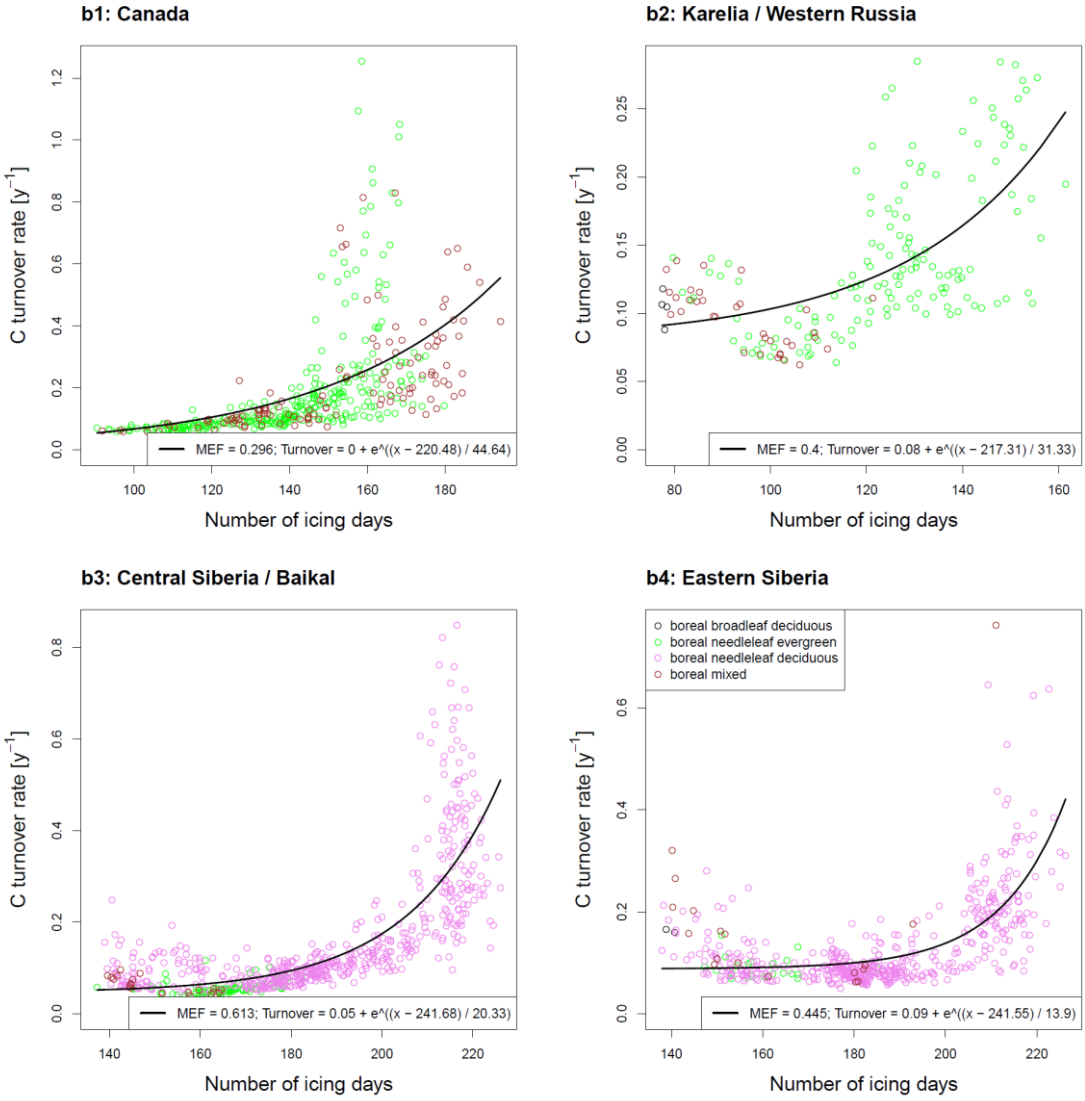

Fig. 3.15: k (= (GPP/2) / biomass) as a function of the number of icing days during a year in boreal forest transects

Again, spatial patterns in *k* based on GPP/2 (Fig. 3.14) do not substantially differ from those observed when making use of MODIS NPP (cf. Fig. 3.1). Although in some cases scatter increases, which might also be due to the very simplifying assumption of a globally constant fraction of plant respiration and the inclusion of non-forest productivity, the general patterns in the relationships between *k* and climate stay the same (compare Figs. 3.15-3.17, Figs. 3.6-3.8).

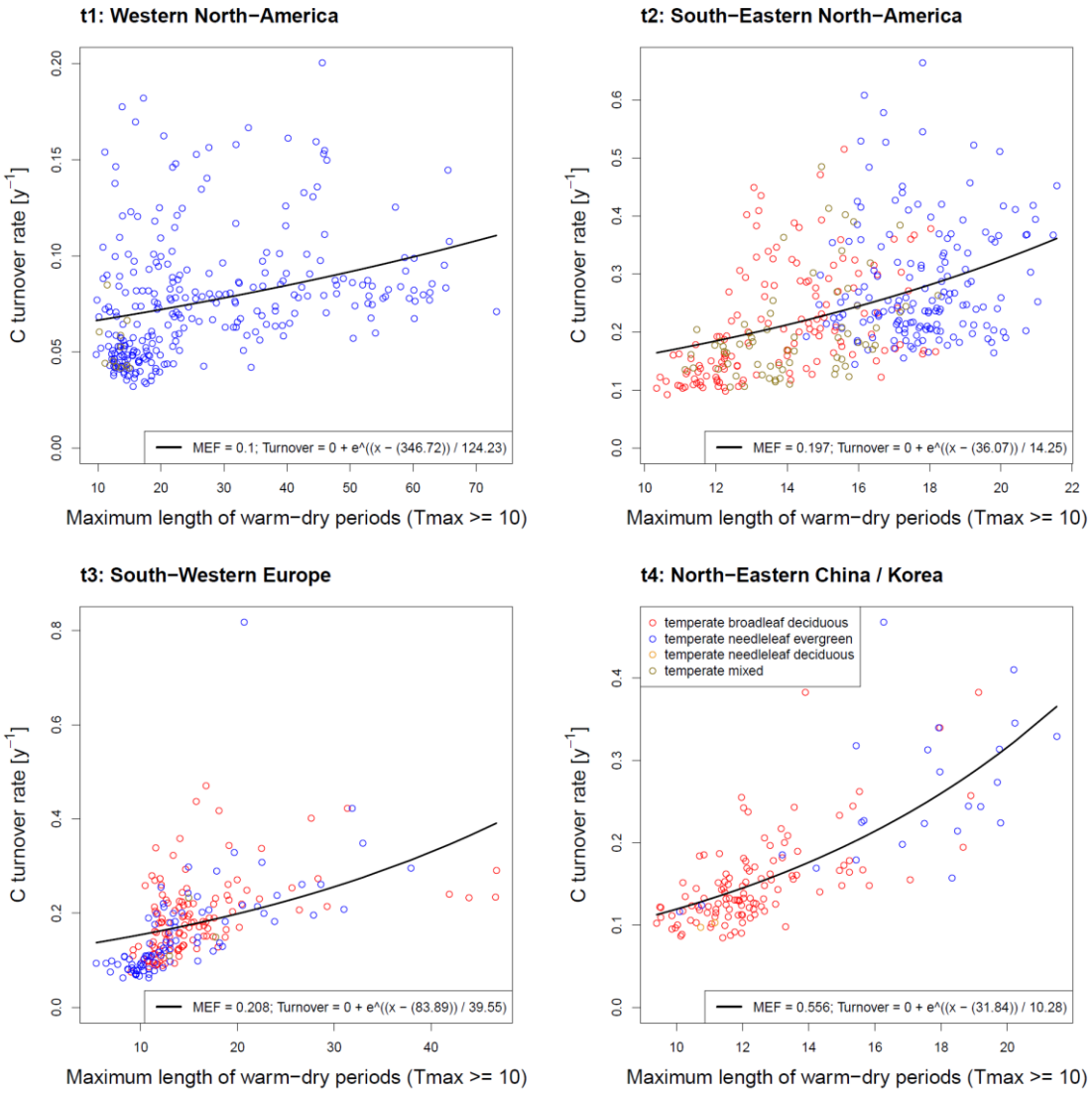

Fig. 3.16: *k* (= (GPP/2) / biomass) as a function of the maximum length of warm-dry periods (in days) in temperate forest transects

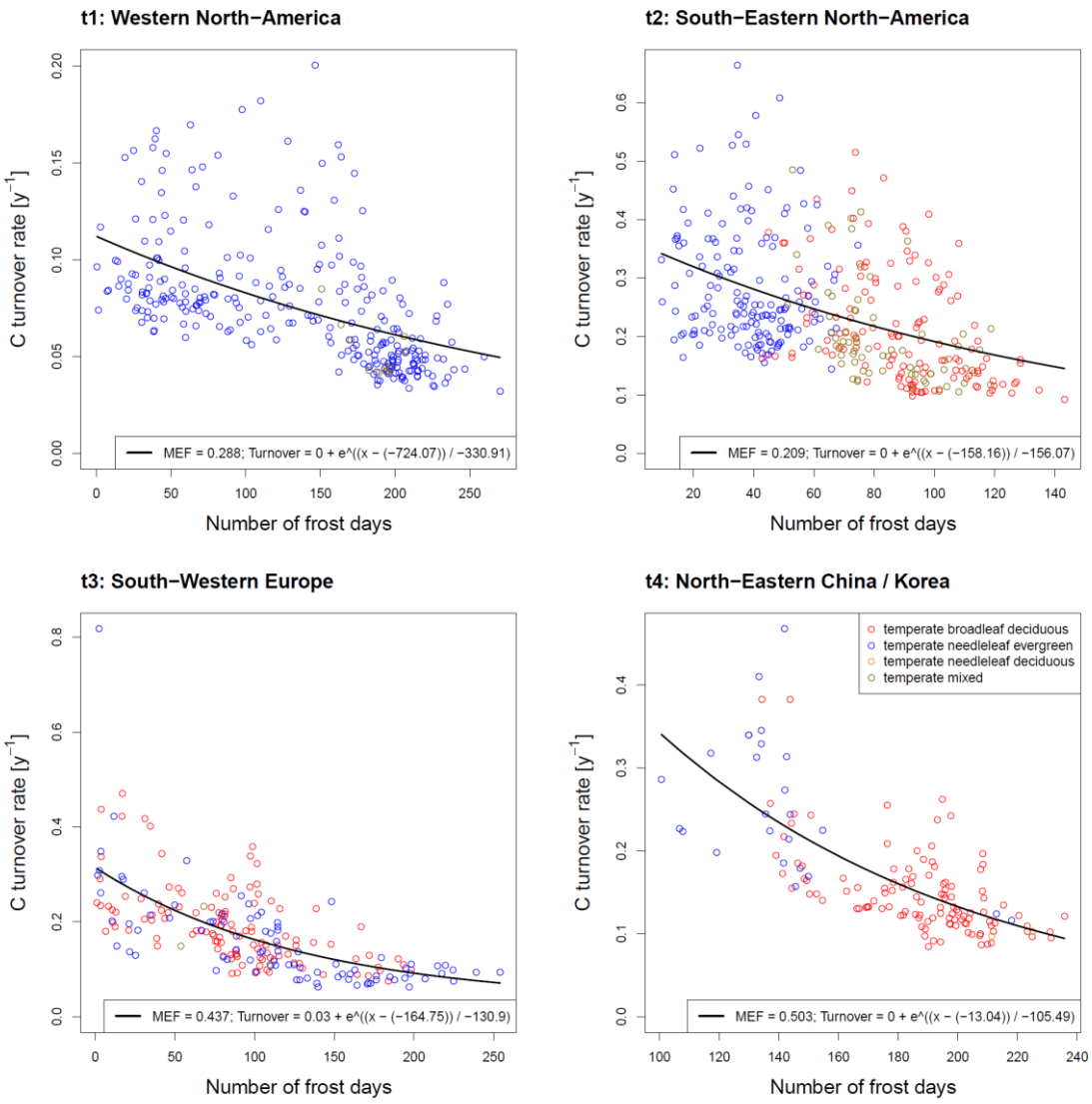

Fig. 3.17: *k* (= (GPP/2) / biomass) as a function of the number of frost days during a year in temperate forest transects

3.5 A first-order uncertainty estimate

The reliability of the observed patterns in *k* and of the relationships to climate variables could be even better evaluated by the consideration of their uncertainty. While there are uncertainty estimates given for the forest biomass map (Thurner *et al.*, 2014), unfortunately such information is missing for MODIS NPP. However, MODIS NPP was used here, since other available global NPP products (Zaks *et al.*, 2007; del Grosso *et al.*, 2008) come with a coarser spatial resolution (10´ and 0.5°, respectively), which does not allow for a detailed differentiation between forest and non-forest NPP at the required spatial scale of this study. There is a need for more observation based global

NPP maps with high spatial resolution and corresponding uncertainty information. However, evaluation studies of the MODIS NPP product have demonstrated the validity of this product in boreal and temperate forests, although relying on a limited number of test sites (Turner *et al.*, 2005, 2006; Zhao *et al.*, 2005). Potentially overestimations in MODIS NPP might be introduced in boreal ecosystems by the non-consideration of the lower photosynthetic capacity of mosses (Yuan *et al.*, 2014).

Higher levels of uncertainty in the biomass product have been estimated in low biomass areas in the northern taiga, potentially contributing to the uncertainty in the observed gradients in k in these regions. Furthermore, dead standing trees as well as the topography in mountainous areas potentially impact the retrieval accuracy of the underlying GSV product (Santoro *et al.*, 2015). However, aggregation to 0.5° is expected to diminish this uncertainty, and, most importantly, intercomparison to up-scaled forest inventory data at regional scales has not revealed systematic offsets (cf. Chapter 2.3).

The aggregation of biomass and NPP to 0.5° resolution reduces the risk of high random errors in these products. However, consistent biases could potentially influence the results of this investigation, but have not been reported beside for extremely high values. Since both biomass and NPP products might underestimate extremely high biomass and NPP values respectively (Thurner *et al.*, 2014; Turner *et al.*, 2006), the ratio of biomass to NPP might be less influenced by such a bias in case of both very high biomass and NPP values. Additionally, also the uncertainty in climate data is potentially contributing to the overall uncertainty of the presented results, especially in remote and/or mountainous areas where observations are sparse and/or the spatial variation is high (Hijmans *et al.*, 2005). But since 30-year average climate is applied here, these uncertainties can be considered reasonably low.

Although no information on uncertainty is available for the individual NPP products, the possible range of NPP can be estimated from NPP values of different products. Based on the BETHY/DLR NPP product in addition to MODIS, and the uncertainty in biomass (u_B) derived in Chapter 2.2, a first uncertainty estimate for k can be derived. Half the range between NPP values from MODIS and BETHY/DLR is used as a first-order estimate for the uncertainty in NPP (u_{NPP}). Assuming them to be independent and random, the uncertainties in NPP and biomass are propagated (Taylor, 1997) in order to derive an uncertainty estimate for turnover rate (u_k):

$$u_k = \sqrt{\left(\frac{dTR}{dNPP} \cdot u_{NPP}\right)^2 + \left(\frac{dTR}{dB} \cdot u_B\right)^2} = \sqrt{\left(\frac{1}{B} \cdot u_{NPP}\right)^2 + \left(\frac{NPP}{B^2} \cdot u_B\right)^2} \qquad \text{(Eq. 3.3)}$$

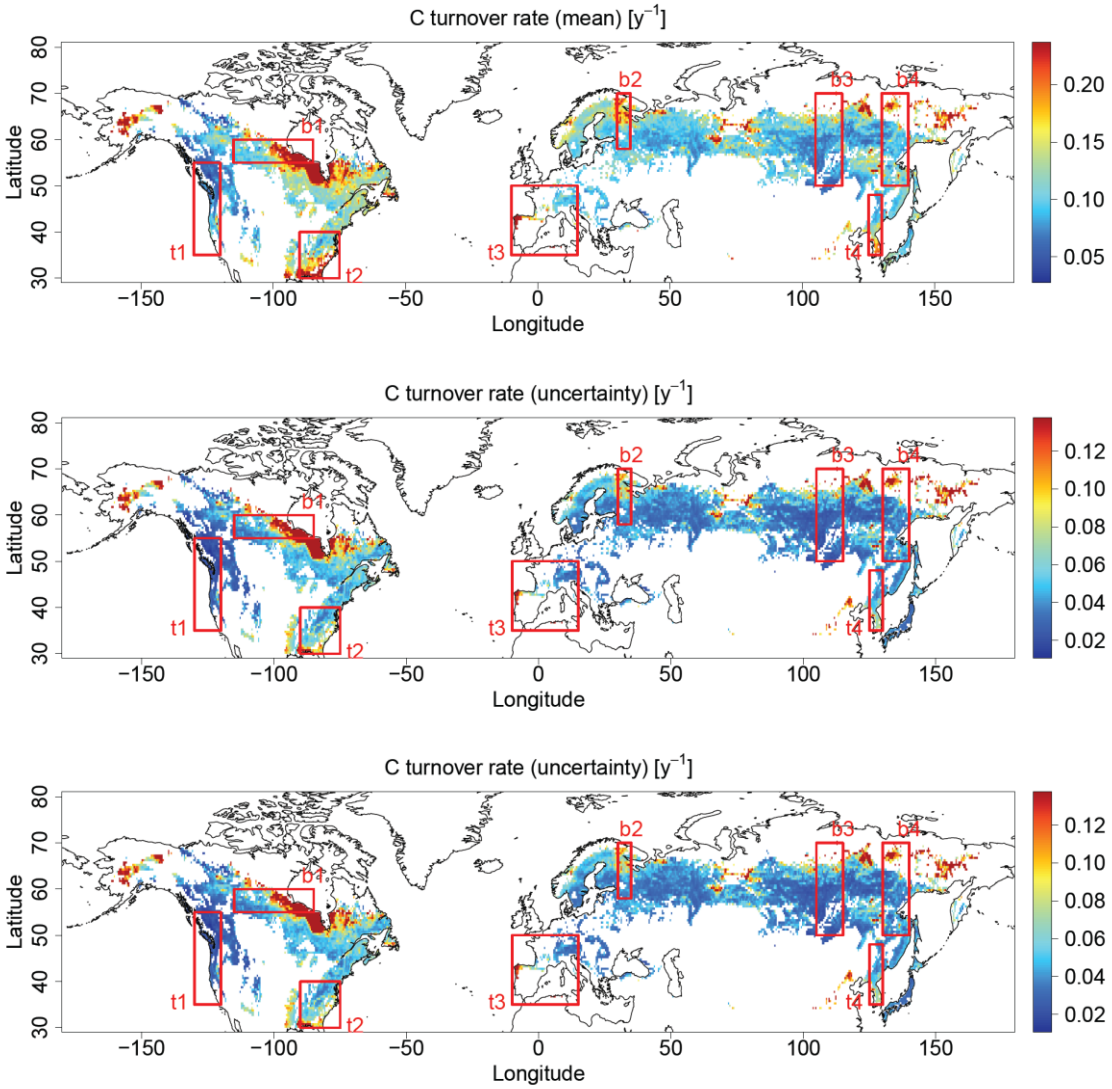

Fig. 3.18: Spatial patterns of k [y^{-1}] as the ratio of NPP (mean of MODIS and BETHY/DLR NPP) over biomass, including areas with at least 40 % forest cover (top). Corresponding absolute (centre) and relative (bottom) uncertainty.

Since only two NPP products (which are based on spatial information from remote sensing) could be used for this estimate, it can only serve as a first proxy of uncertainty. The k derived from the mean of the two different NPP products (Fig. 3.18) is very similar in terms of spatial patterns to the product based on MODIS NPP only (cf. Fig. 3.2). Absolute and relative uncertainties generally increase in areas of low biomass (cf. Fig. 2.11). Figures 3.19-3.21 show the relationships of k to climate variables in the selected transects with uncertainties in k added. The relatively high uncertainties are

partly due to the conservative uncertainty estimate for biomass, which is overestimating its actual uncertainty (cf. Chapter 2.2.3, Fig. 2.12). Nevertheless, changes in *k* with climate indices are in general not explainable by the uncertainty, demonstrating the validity of the observed relationships. In addition, the 90 % confidence interval of the regression, which was derived based on bootstrap samples (Efron, 1979) of the grid cells, is relatively narrow (Figs. 3.19-3.21). This confidence interval could be further improved by accounting at the same time for both the uncertainty arising from the samples of grid cells used for establishing the relationships and the uncertainty in *k* of each grid cell.

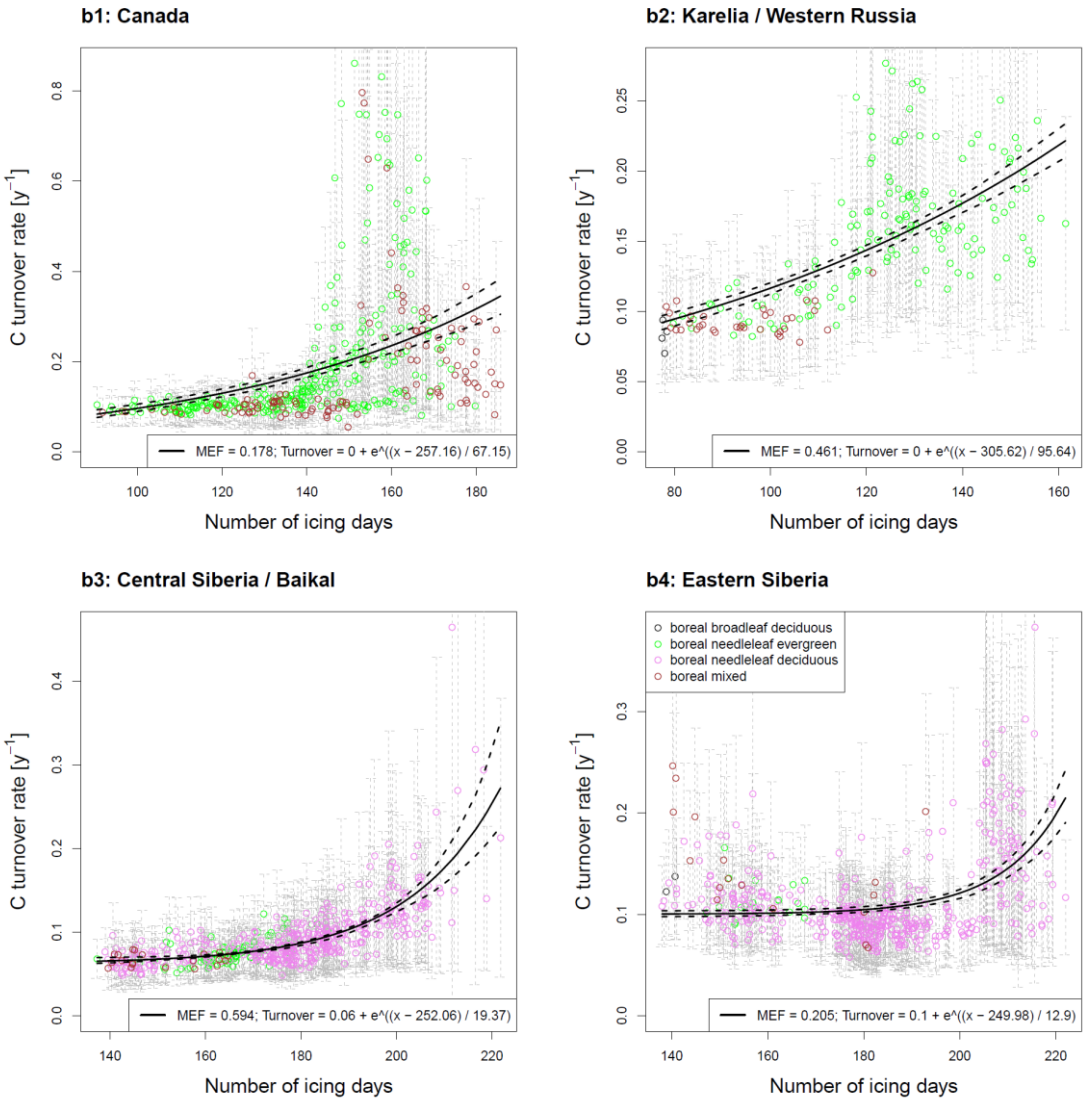

Fig. 3.19: *k* (derived from mean of MODIS and BETHY/DLR NPP) as a function of the number of icing days during a year in boreal forest transects. Dotted error bars indicate the estimated uncertainty in *k* for each grid cell. The solid line is the fitted non-linear regression line using all grid cells. The dotted lines delimit the 90 % confidence interval of the regression using bootstrap samples of the grid cells.

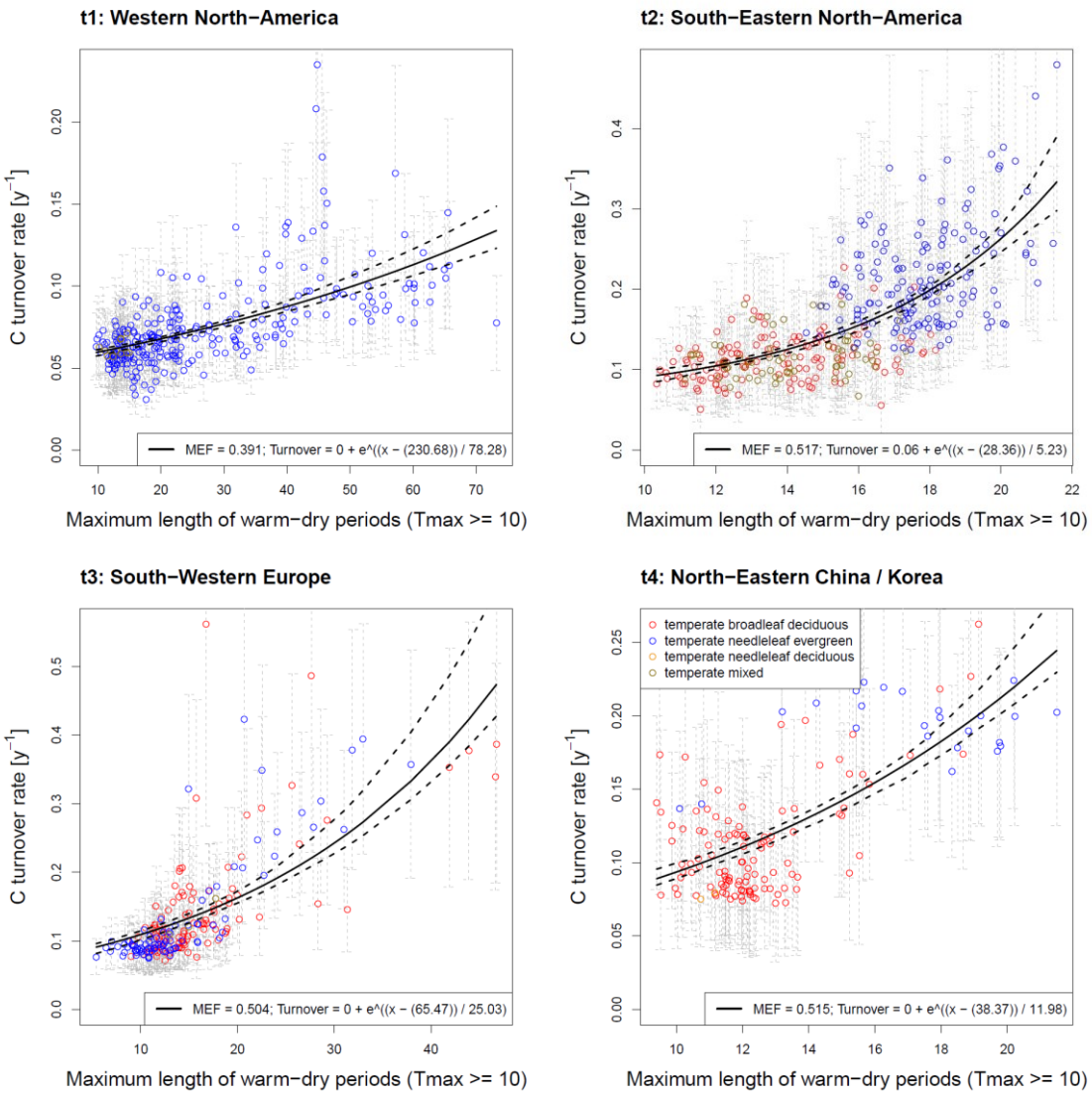

Fig. 3.20: *k* (derived from mean of MODIS and BETHY/DLR NPP) as a function of the number of maximum length of warm-dry periods (in days) during a year in temperate forest transects. Dotted error bars indicate the estimated uncertainty in *k* for each grid cell. The solid line is the fitted non-linear regression line using all grid cells. The dotted lines delimit the 90 % confidence interval of the regression using bootstrap samples of the grid cells.

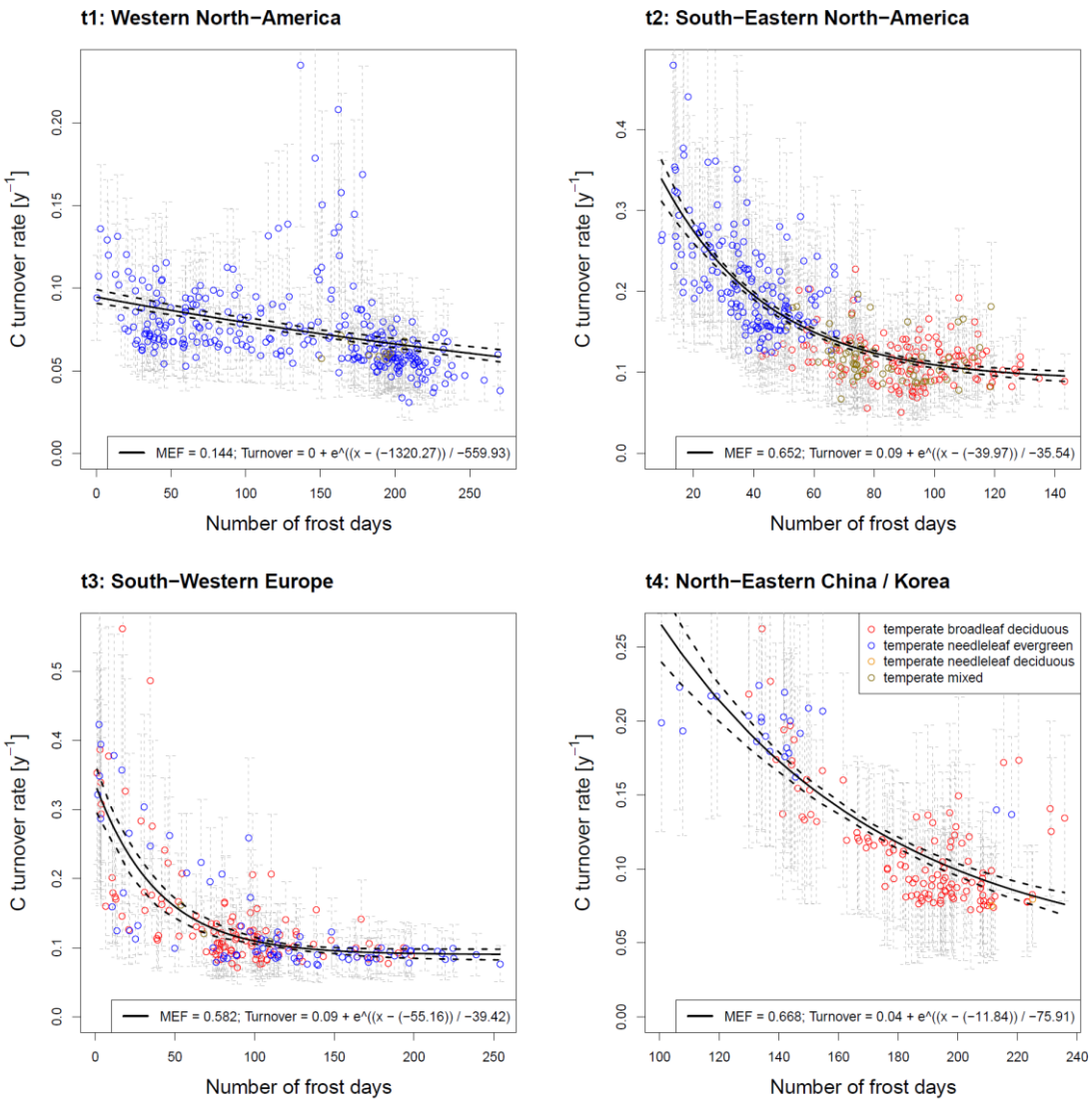

Fig. 3.21: *k* (derived from mean of MODIS and BETHY/DLR NPP) as a function of the number of frost days during a year in temperate forest transects. Dotted error bars indicate the estimated uncertainty in *k* for each grid cell. The solid line is the fitted non-linear regression line using all grid cells. The dotted lines delimit the 90 % confidence interval of the regression using bootstrap samples of the grid cells.

3.6 Potential confounding factors

The presented results may be influenced by a variety of possible confounding factors. Potentially other processes than climate-driven mortality mechanisms (discussed in detail in Chapter 5.2) may cause indirectly the observed relationships of *k* to climate indices. The following analyses, in addition to the implemented tests with different NPP products, provide evidence for the reliability of these findings. The possible

confounding factors which are accounted for in this chapter include soil conditions, fire, tree cover, and uncertainties in autotrophic respiration and carbon allocation.

These processes can contribute to the noise in the climate-*k* relationships; however, most of such potential confounding factors can hardly explain the observed spatial gradients. For instance, there is no evidence that forest management is more extensive towards the northern boundary of boreal forests or towards drier regions of temperate forests. Furthermore, differences in the deviation from steady state between grid cells can potentially have an influence on the results, but again this would require a spatial correlation between forest successional state and the investigated climate variables. For example, it is possible that changes in winter length and temperature in the northern edge of boreal forests lead to a shift of the treeline further to the North and thus forests are in a successional state (Urban *et al.*, 2014), resulting in a currently higher *k* compared to steady state forests. The impact of the steady state assumption on the estimated *k* is covered by Chapter 4.6.1 in detail.

3.6.1 Soil conditions

Soil variables were extracted from the Harmonized World Soil Database (HWSD) (FAO/IIASA/ISRIC/ISSCAS/JRC, 2012), including the available water content and topsoil bulk density, clay content, organic carbon content and silt content. No consistent correlations between *k* and those investigated soil related variables were detected across the selected transects, with the exception of a weak positive correlation between *k* and the topsoil organic carbon content in boreal forest transects (Table 3.6). However, it is not obvious why a higher soil organic carbon content should cause higher *k*, instead it may be itself the result of an increased *k*, since higher vegetation carbon turnover goes hand in hand with elevated introduction of dead plant material into litter and soil. Nevertheless, regional effects of soil variables on *k* cannot be excluded in some of the transects.

Table 3.6: Spearman rank correlation (r_{sp}) between *k* and soil variables obtained from the HWSD (FAO/IIASA/ISRIC/ISSCAS/JRC, 2012; AWC = available water content, BD = topsoil bulk density, CC = topsoil clay content, OCC = topsoil organic carbon content, SC = topsoil silt content) in boreal (b1-b4) and temperate (t1-t4) forest transects. The significance level is quantified by the p-value: "***" $p \leq 0.001$, "**" $0.001 < p \leq 0.01$, "*" $0.01 < p \leq 0.05$, "." $0.05 < p \leq 0.1$, " " $p > 0.1$

r_{sp}	b1	b2	b3	b4	t1	t2	t3	t4
AWC	0.21***	-0.05	-0.12**	0.09*	0.12*	0.20***	-0.11	-0.77***
BD	-0.19***	0.18*	0.10*	-0.22***	-0.44***	0.22***	-0.25***	0.29***
CC	0.07	-0.09	-0.12**	0.20***	0.47***	-0.14**	0.16*	-0.01
OCC	0.13**	0.21**	0.25***	0.22***	-0.23***	-0.12*	0.01	-0.37***
SC	0.43***	-0.21**	-0.06	0.22***	0.03	-0.63***	0.25***	-0.67***

3.6.2 Fire

Recent fires could potentially lead to local increases in the estimated *k*. Forest fires are considered to be related to drought conditions, but due to stochastic influences on their spatial occurrence and spread, burned area or the time since last fire are not found to explain observed broad-scale gradients in *k* (Fig. 3.22). For this purpose, the Global Fire Emissions Database (GFED4; Giglio *et al.,* 2013) was applied to study the relationships between *k* and these fire related variables globally. In a more detailed investigation, the time since last fire could be extracted from regional fire datasets for Alaska (Kasischke *et al.*, 2002) and Canada (Canadian Forest Service, 2010), dating back longer in time (Fig. 3.23). A correlation coefficient of 0.4 is estimated between *k* and the year of last fire in Canada, indicating that recent fires can explain increases in the observed *k* in some grid cells. However, looking at the spatial distribution of these fires in Canada (not shown), they cannot be responsible for the observed broad-scale gradient in *k* in transect b1.

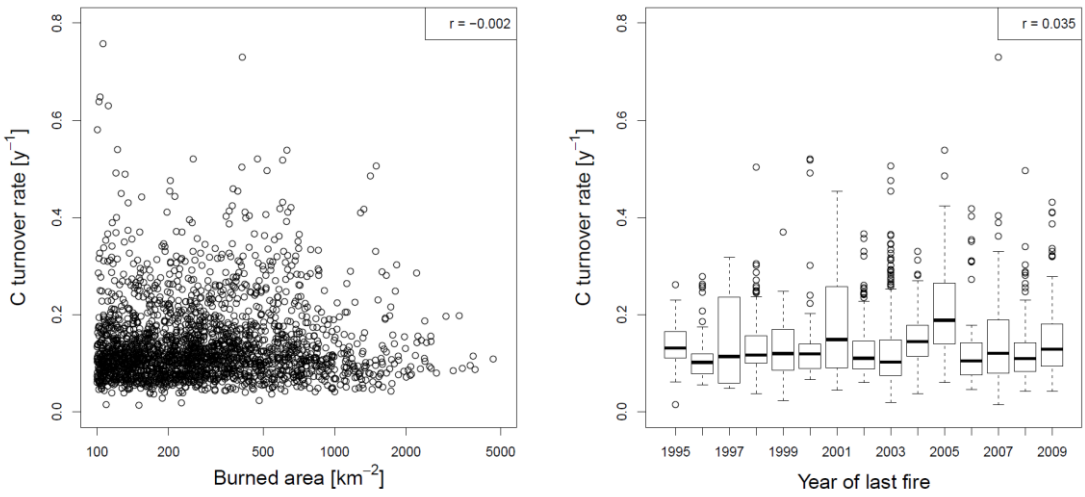

Fig. 3.22: *k* versus burned area (sum of burned area during 1995-2009) and the year of last fire, taking into account major fires covering at least 100 km², derived from the Global Fire Emissions Database (GFED4) (Giglio *et al.,* 2013)

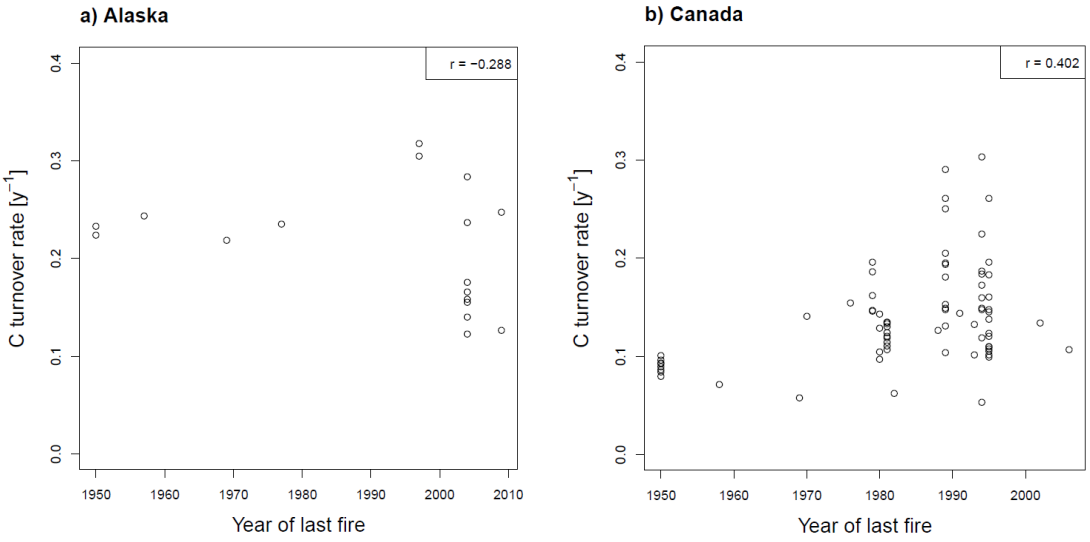

Fig. 3.23: *k* versus the year of last fire derived from regional fire datasets for a) Alaska (Kasischke *et al.,* 2002) and b) Canada (Canadian Forest Service, 2010), taking into account major fires covering at least 50 % of the grid cell

3.6.3 Changes in tree cover

In order to not include grid cells with only sparse forest cover in the analysis, different land cover products and an additional forest cover threshold have been applied. Nevertheless, changes in tree cover at subpixel scale have not been accounted for. In

order to test the relation between *k* and tree cover, tree cover at 0.5° was estimated from the MODIS Vegetation Continuous Field (VCF) tree cover product (Hansen *et al.*, 2002; Townshend *et al.*, 2011). Only forested pixels (according to GLC2000 and MODIS MOD12 land cover classifications) were taken into account when aggregating from 0.01° resolution. Furthermore, only grid cells with at least 40 % forest cover (according to GLC2000, at 0.5°) were included. Based on MODIS VCF, similar relationships between *k* and tree cover like with climate variables are found in boreal forests (Fig. 3.24). Elevated levels of *k* are observed in case of sparse tree cover. This phenomenon is only to some extent detected in temperate forests, especially in region t2 (Fig. 3.25). There are two possible interpretation options of these results:

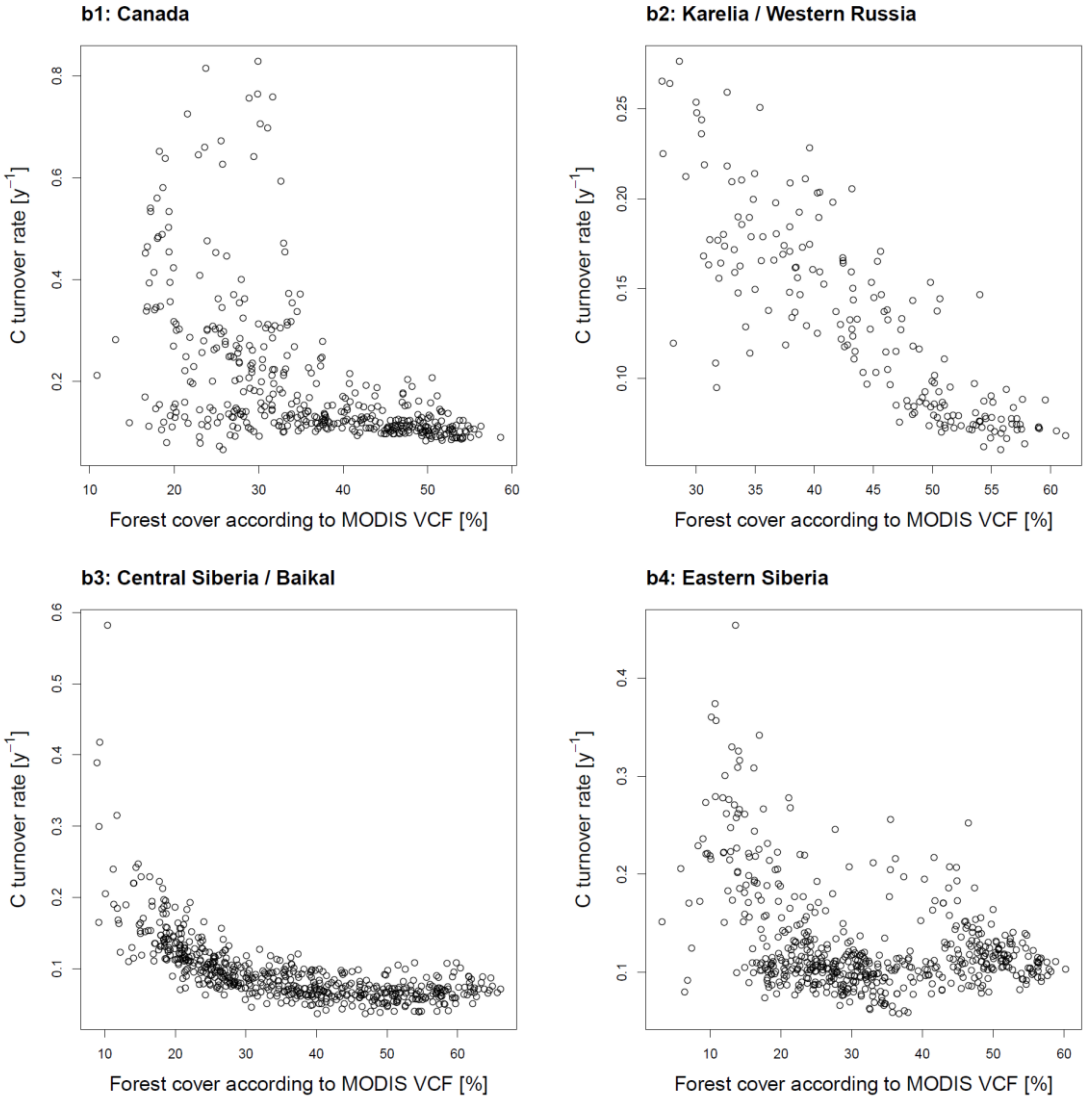

Fig. 3.24: *k* as a function of forest cover (according to the MODIS VCF tree cover product (Hansen *et al.,* 2002; Townshend *et al.,* 2011)) in boreal forest transects

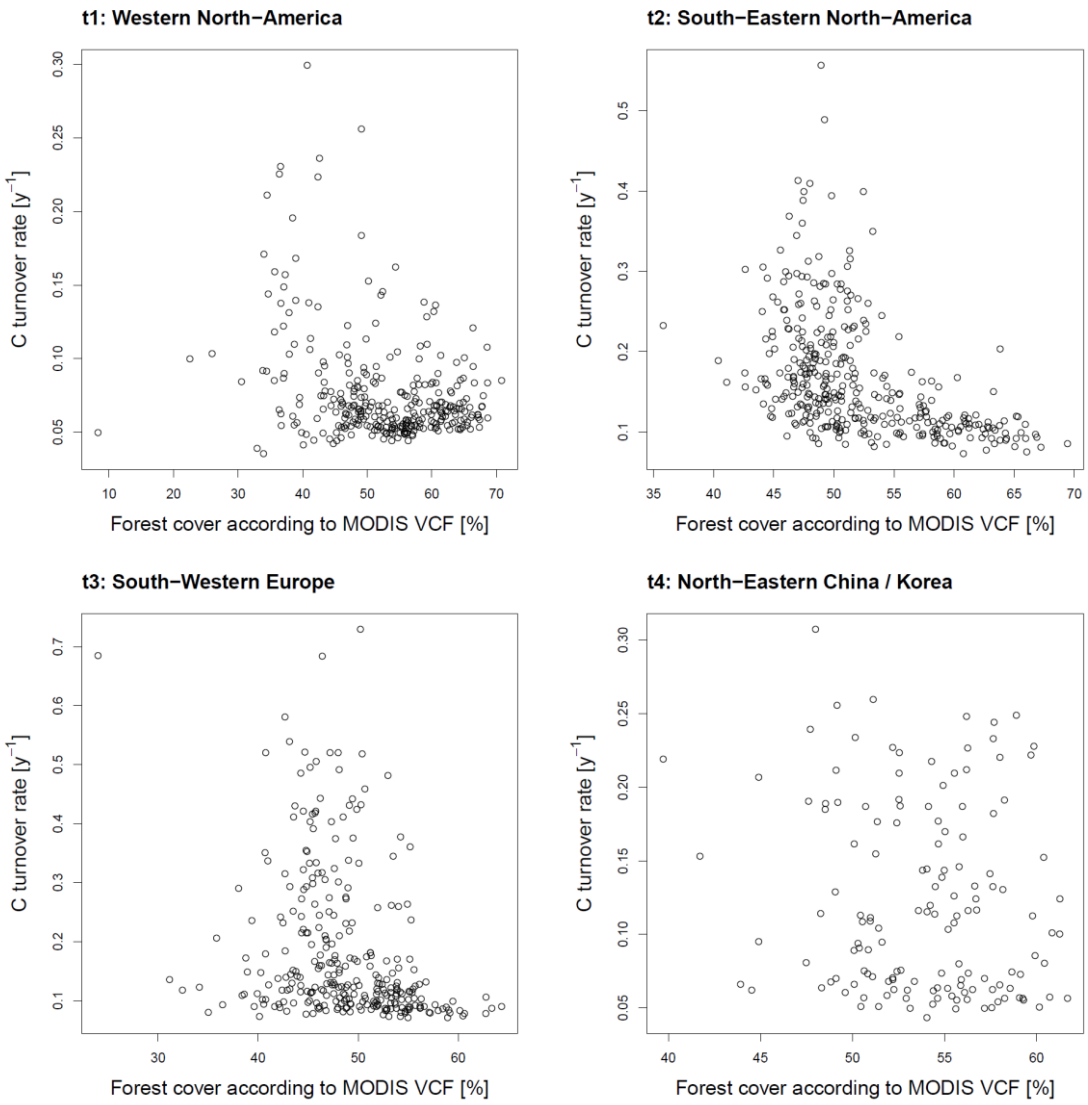

Fig. 3.25: *k* as a function of forest cover (according to the MODIS VCF tree cover product (Hansen *et al.,* 2002; Townshend *et al.,* 2011)) in temperate forest transects

1. Sparse tree cover could introduce a consistent bias in MODIS NPP. NPP (and thus *k*) is overestimated by the MODIS algorithm in pixels consisting of mixed land cover, because complete forest coverage is assumed and reflected in the parameterization (Heinsch *et al.*, 2003). However, in areas of fragmented forest landscapes, pixels with different forms of forest and non-forest vegetation might also present biased estimates of biomass as a consequence of the interplay of different radar backscatter levels. Furthermore, the observed relationships between *k* and climate have been confirmed using different NPP estimates (cf. Chapter 3.4), enhancing the confidence in the following interpretation:

2. Tree cover is highly correlated with climate variables because climate is not only driving *k*, but also tree cover. *k* and tree cover change along the same climatic gradients in unmanaged regions. In this respect, tree cover can also be interpreted as a consequence of climatic conditions and a result of climate-induced *k*. The mechanisms driving the spatial distribution of trees and, in specific, treeline dynamics, are not entirely understood, including hypotheses of growth limitation as well as mortality effects (Harsch & Bader, 2011).

In a second approach, forest cover at 0.5° was estimated as the percentage of forested grid cells at 0.01° according to GLC2000. Consistently, only grid cells with at least 40 % forest cover were included. Based on GLC2000, a relationship between *k* and tree cover does not become visible, neither in boreal nor in temperate forests (not shown). However, such an approach does not account for changes in tree cover at sub-pixel scale.

3.6.4 Autotrophic respiration

Potentially, an oversimplified representation of autotrophic respiration in the MODIS algorithm could introduce biases in estimated NPP and thus also in *k*. There are still important open research questions on the dependency of plant respiration on environmental conditions (e.g. Atkin & Tjoelker, 2003; Piao *et al.*, 2010; Smith & Dukes, 2013). However, as already shown in the corresponding studies (Luyssaert *et al.*, 2007; Vicca *et al.*, 2012), based on the analysis of an exhaustive database of carbon fluxes (and stocks) in forest ecosystems (Luyssaert *et al.*, 2007), there is no evidence that the in general linear relationship between R_a and GPP would be strongly influenced by climate in forests outside the tropics (Fig. 3.26). The strong linear regression between GPP and R_a supports the similarity in the spatial patterns of *k* estimated from NPP and GPP/2. The robustness of the spatial patterns in *k* against the uncertainty in R_a has been demonstrated by the use of different NPP products and proxies relying on different assumptions regarding R_a.

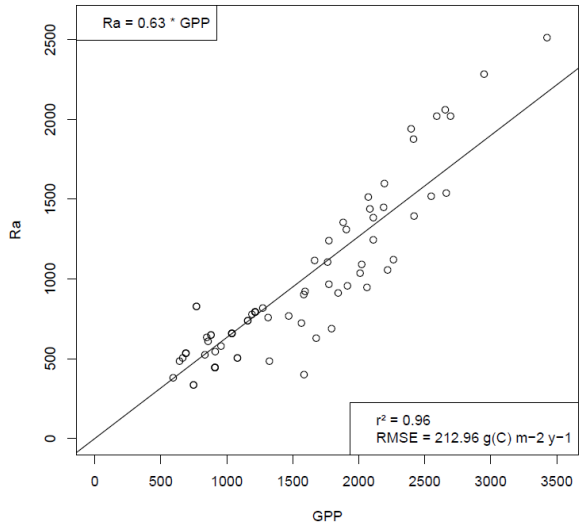

Fig. 3.26: Autotrophic respiration (R_a) as a function of GPP in boreal and temperate forests derived from the Luyssaert database (Luyssaert *et al.*, 2007)

3.6.5 Carbon allocation

Not accounting for climate dependencies of biomass allocation may possibly affect the presented gradients, since different biomass compartments imply unequal *k*. However, the proportions of foliage and root carbon, the two compartments with significantly higher *k* compared to stem and branches carbon, are reported to be related to mean annual temperature in opposite directions (Reich *et al.*, 2014). In addition, using an exhaustive database based on field measurements (Global Biomass Compartment Database; JRC, 2009), no strong correlations between biomass allometry and the investigated climate variables are found in boreal and temperate forests (Figs. 3.27 and 3.28). For this purpose, the ratios of leaf biomass / stem biomass, branches biomass / stem biomass and root biomass / stem biomass were related to the same climate variables which have been related to *k*. The relationship between allometry and climate can serve as a proxy for the relationship between allocation and climate. Hence, it can be concluded that the observed relationships between *k* and climate are unlikely mainly attributable to climate dependencies of allocation; nevertheless spatial patterns in allocation may influence the results, for instance if driven by spatial gradients in light or nutrient availability (Poorter *et al.*, 2012).

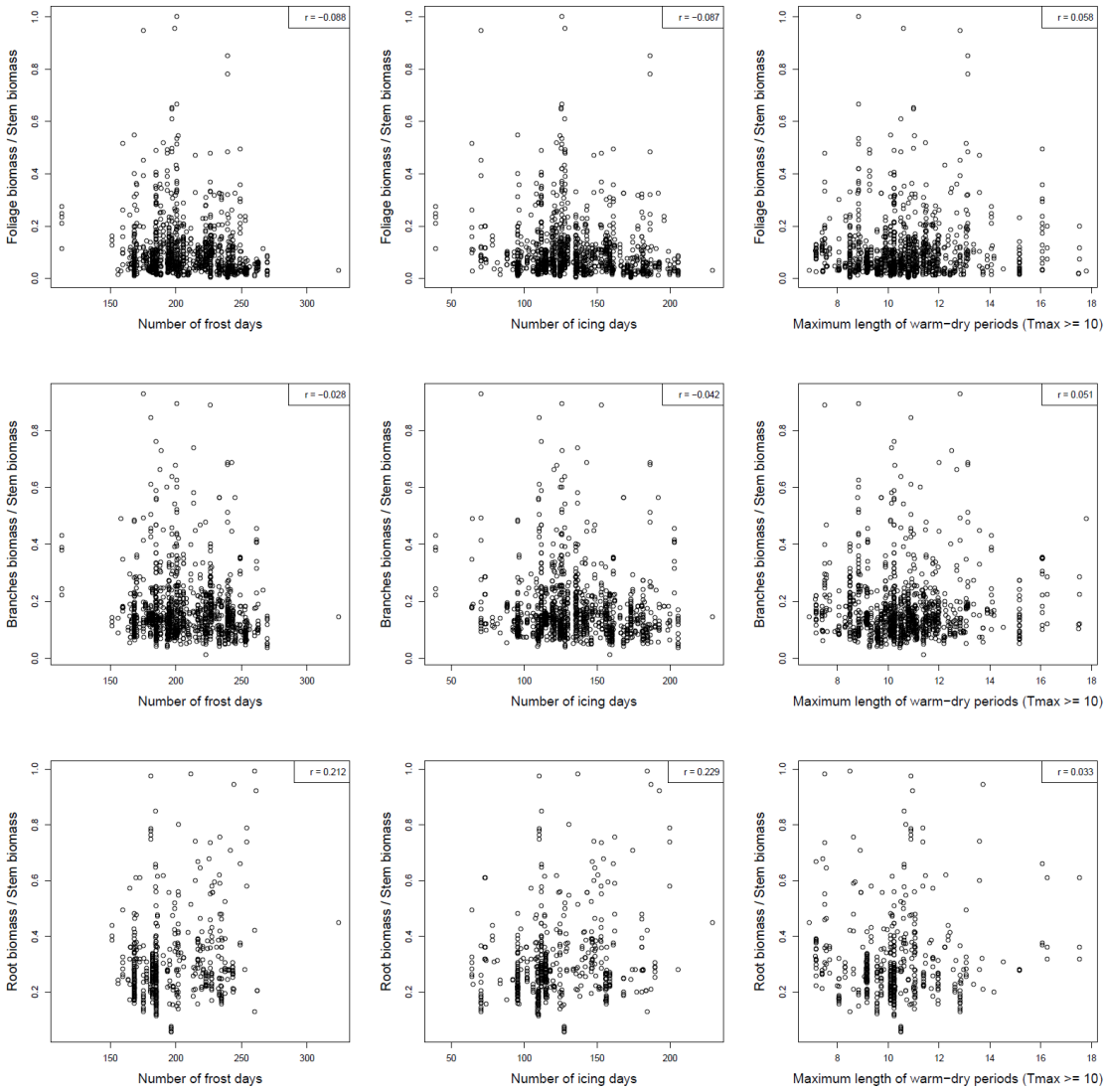

Fig. 3.27: Biomass allometry derived from the Global Biomass Compartment Database as a function of climate variables in boreal forests

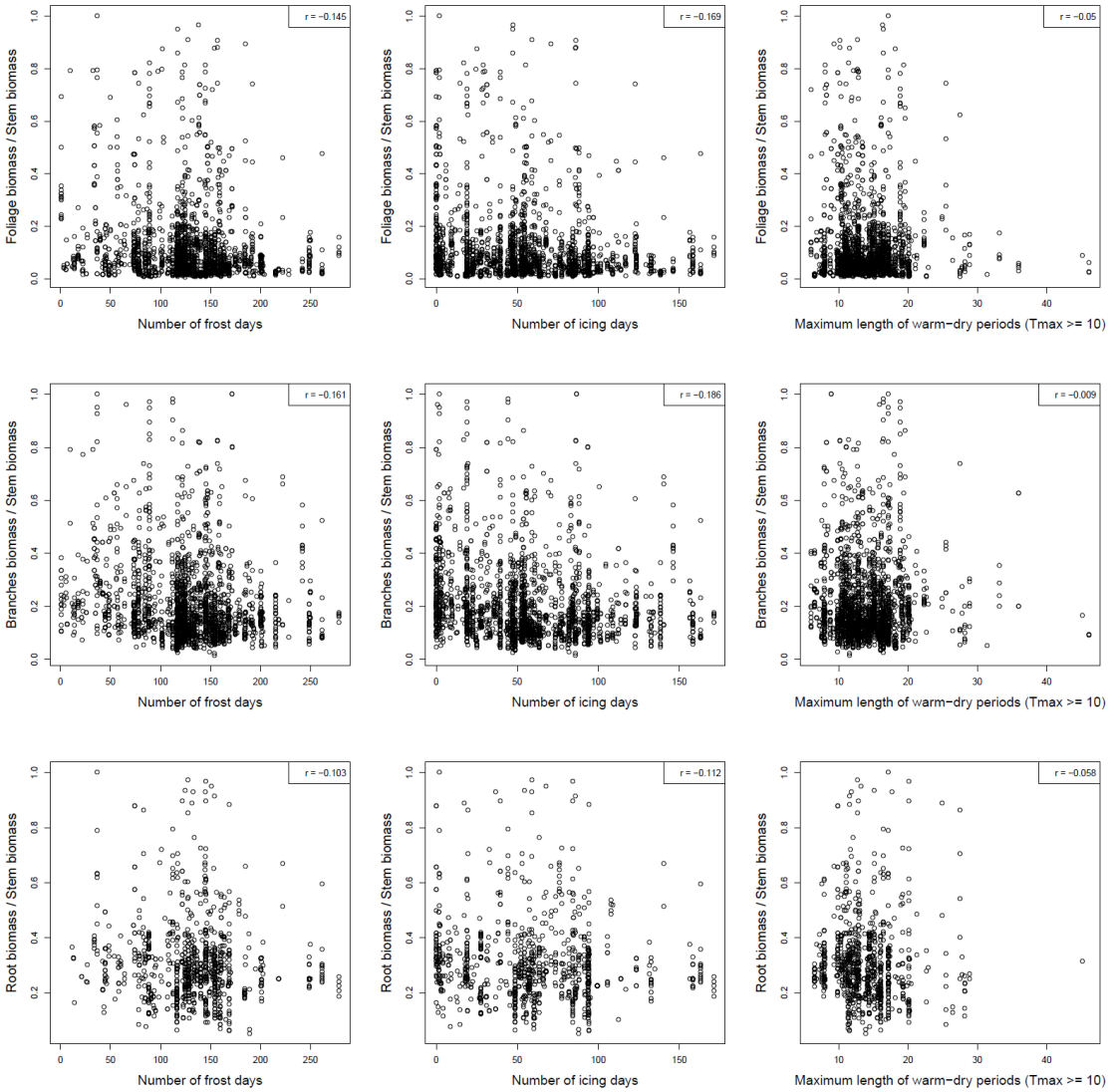

Fig. 3.28: Biomass allometry derived from the Global Biomass Compartment Database as a function of climate variables in temperate forests

3.7 Impact of NPP timespans on observation based turnover rate

Agreement of observation based *k* derived from different NPP timespans (2000-2010, as presented in this chapter, vs. 2000-2004, as applied in Chapter 4) is very high, in terms of relative differences (Fig. 3.29), correlations (Fig. 3.30), and spatial variations (Fig. 3.31). These findings are equally valid for the use of MODIS and BETHY/DLR NPP. The presented relationships between *k* and climate variables hold true if average NPP of 2000-2004 is used instead of 2000-2010 (not shown), allowing for a direct comparison to model results (Chapter 4), which have been available only until 2004. Differences in

k derived from different NPP timespans are considerably smaller than differences in *k* caused by the use of different NPP products (BETHY/DLR vs. MODIS).

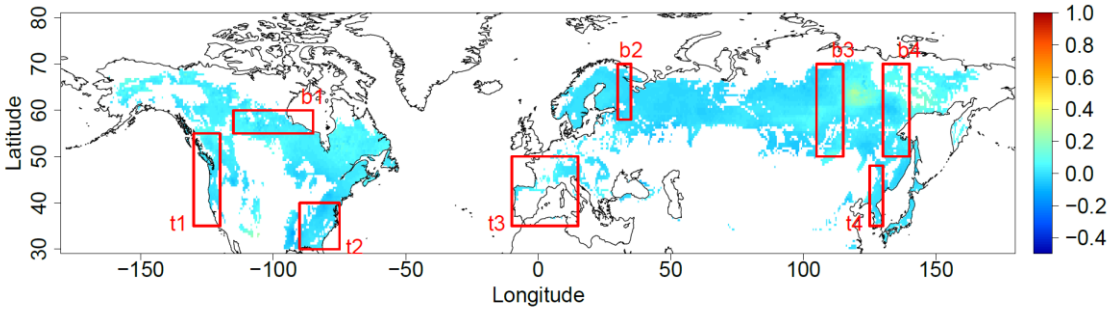

Fig. 3.29: Relative difference between *k* derived from long-term average MODIS NPP for 2000-2010 compared to 2000-2004

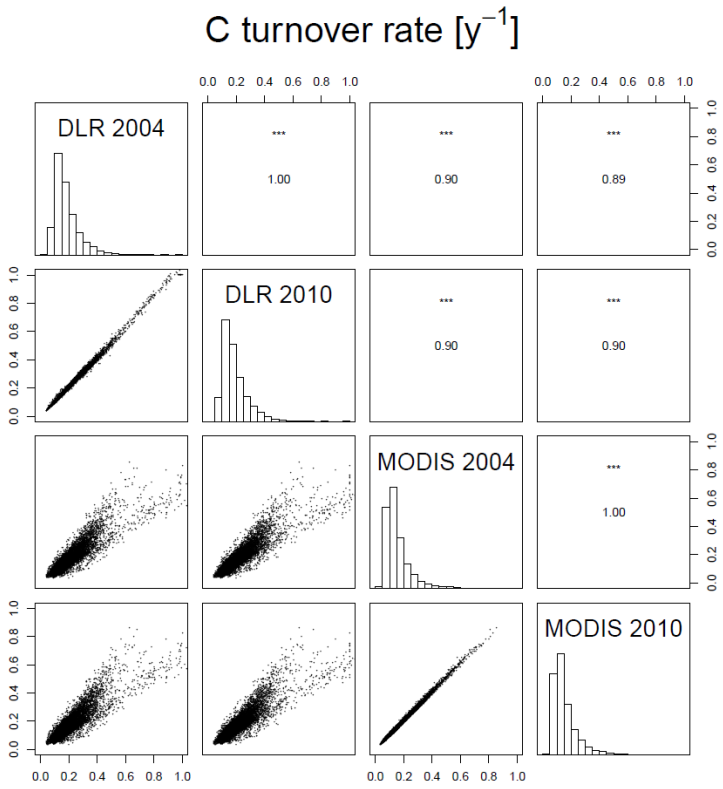

Fig. 3.30: Correlation between *k* derived from long-term average BETHY/DLR NPP and MODIS NPP for 2000-2004 ("DLR 2004", "MODIS 2004") and 2000-2010 ("DLR 2010", "MODIS 2010")

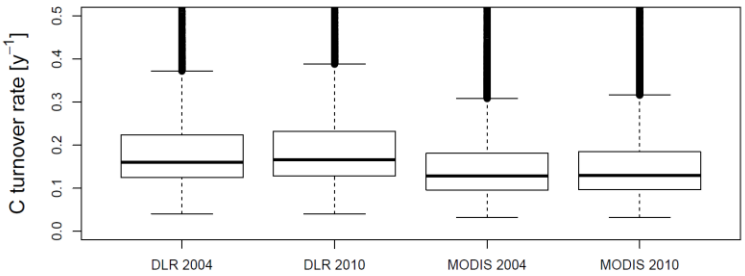

Fig. 3.31: Spatial variation in observed *k* derived from different NPP products (BETHY/DLR vs. MODIS) and for different timespans (2000-2004 vs. 2000-2010). The box–whisker plots show the median and the interquartile range of values. The whiskers extend up to the most extreme data point which is no more than 1.5 times the interquartile range away from the box. Outliers are drawn as circles.

3.8 Comparability to ISI-MIP GVMs

In order to improve comparability to ISI-MIP model output, the spatial relationships between observed *k* and climate variables had to be reinvestigated. For this purpose, similar settings like in the ISI-MIP simulations were used, and the main differences to the investigation presented above were:

(I) Use of long-term average climate variables for the time period 1975-2004 based on bias-corrected Met Office Hadley Centre Global Environment Model version 2 – Earth System (HadGEM2-ES; Collins *et al.*, 2011) climate data.

(II) Use of 5-year average NPP for the time period 2000-2004, applying both MODIS and BETHY/DLR products, and accounting for both forest and non-forest vegetation.

(III) Use of the biomass product aggregated from the original 0.01° resolution to 0.5° while accounting for both forest and non-forest vegetation. Non-forest vegetation was assumed to have a turnover time of 1 year, and thus biomass of non-forest vegetation was assumed to equal (BETHY/DLR) NPP per year.

The observation based relationships between *k* and the climate variables did not change substantially. The fitted non-linear functions to these relationships are shown in Figs. 4.8-4.10, where they are directly compared to the model results.

CHAPTER 4

Evaluation of climate-related forest carbon turnover in global vegetation models

Within this chapter, the observation based *k* (cf. Chapter 3) is used to evaluate the spatial patterns in *k* simulated by GVMs participating in ISI-MIP (Warszawski *et al.*, 2014), including HYBRID4 (Friend *et al.*, 1997; Friend & White, 2000), JeDi (Pavlick *et al.*, 2013), JULES (Clark *et al.*, 2011), LPJml (Sitch *et al.*, 2003), ORCHIDEE (Krinner *et al.*, 2005; Delbart *et al.*, 2010), SDGVM (Woodward & Lomas, 2004) and VISIT (Ito & Oikawa, 2002; Inatomi *et al.*, 2010). ISI-MIP comprises a wide range of state-of-the-art GVMs operated at the same spatial resolution like the observation based findings are based on (0.5° x 0.5°). Among the variety of processes determining vegetation carbon turnover rates (photosynthesis, autotrophic respiration, carbon allocation, carbon turnover including litterfall, background mortality, and disturbances), especially the climate effects on simulated turnover processes are explored. Furthermore, the deviations in *k* caused by mismatches in productivity are separated from those related to incomplete representation of turnover processes.

4.1 Carbon turnover concepts ISI-MIP GVMs

The investigated GVMs comprise different levels of complexity of implemented mortality processes (Table 4.1). Vegetation is not necessarily in steady state given the simulation of vegetation dynamics in response to changes in climate and atmospheric CO_2. All the models simulate background carbon turnover as a constant rate, usually varying between plant functional types (PFTs) and separating between compartments. SDGVM in addition prescribes mortality at a maximum forest age. Such simple carbon turnover concepts do not respond to climate or other environmental factors. However, in JULES leaf turnover increases under low temperatures (Clark *et al.*, 2011). Similarly, in HYBRID4 phenology is affected by drought and frost in dry- and cold-deciduous

forests, respectively. In the version of ORCHIDEE used for ISI-MIP, soil moisture stress and low temperatures also modulate leaf longevity, which in turn changes LAI and the average leaf age related to the inception of senescence (Krinner *et al.*, 2005). Although in most of the models many climate-driven mortality processes are not explicitly treated, temperature and precipitation directly or indirectly influence several implemented mortality algorithms.

In HYBRID4, individual trees compete for light, water and nitrogen, and mortality is finally dependent on the carbon balance as a result of insufficient labile carbon in foliage, fine root and storage pools (Friend & White, 2000). In LPJml, competition between PFTs for light leads to mortality (self-thinning) when an upper threshold of canopy cover is exceeded (Sitch *et al.*, 2003). Thinning as a result of competition is also considered by SDGVM, whereas forest cohorts compete within each individual PFT. Also in JULES, competition for light is considered, thus mortality is increasing at higher vegetation densities.

Fire schemes dependent on fuel availability and moisture are incorporated in LPJml (Thonicke *et al.*, 2001), ORCHIDEE (Thonicke *et al.*, 2001; Krinner *et al.*, 2005), SDGVM (Woodward & Lomas, 2004), and VISIT (fire scheme of Thonicke *et al.*, 2001). Moisture (in general litter moisture) is directly influenced by climatic conditions including precipitation and temperature. LPJml is the only ISI-MIP GVM accounting for mortality due to low growth efficiency and to heat stress. The former is inversely related to growth efficiency, which is defined as the ratio of annual biomass increment to leaf area. In boreal forests, heat stress occurs when the annual degree-day sum exceeds a PFT-specific threshold and increases linearly with further increasing annual degree-day sum (Sitch *et al.*, 2003). Mortality is dependent on NPP or the carbon balance and thus indirectly on temperature and precipitation in HYBRID4, JeDi and SDGVM. Differing from amore mechanistic implementation in HYBRID4, where drought-induced embolism and frost damage affect the available labile carbon in addition to phenology (Friend & White, 2000), in JeDi (Pavlick *et al.*, 2013) a negative overall carbon balance is considered to lead to increased mortality. SDGVM combines these two NPP dependent mortality concepts. Death of forest cohorts occurs when the storage carbon pool is depleted, and in addition low annual NPP causes increased mortality.

Table 4.1: Implemented mortality algorithms in investigated GVMs (modified from Friend *et al.*, 2014 and McDowell *et al.*, 2011).

Model	Mortality algorithms					
	Background rate[1]	**Competition**	**Fire**	**Growth efficiency, NPP dependence, or carbon balance**	**Heat stress**	**Phenology affected by climate**
*HYBRID4**[a]	+	Forest gap model; Competition for light, water and N; Controls mortality of individuals due to the carbon balance of the tree (see on the right)	-	Mortality of individual trees if insufficient C available in foliage + storage C or fine root + storage C; effects of drought-induced embolism and frost damage on NPP	-	Phenology of dry- and cold-deciduous trees is affected by drought and frost
*JeDi**[b]	Turnover times are affected by functional trait parameters	-	-	Increased leaf and fine root turnover if current NPP < 0 and long-term NPP < 0	-	-
*JULES**[c]	Division into disturbance and turnover rate	Density dependent competition for light	-	-	-	Leaf turnover increases in case of low temperatures
*LPJml**[d]	+	Competition for light (canopy cover upper threshold)	f(Fuel load, Litter moisture) (Thonicke *et al.*, 2001)	Growth-efficiency dependent mortality = f(Biomass increment / Leaf area)	f(Annual degree-days above a PFT-specific threshold); linear; only in boreal forests	-
ORCHIDEE[e]	PFT-specific background rate (including rate lost due to herbivory; fraction of leaves and fine roots lost dependent on leaf age)	-	f(Fuel load, Litter moisture) (Thonicke *et al.*, 2001; Krinner *et al.*, 2005)	-	-	Leaf longevity is reduced in case of soil moisture stress, atmospheric dryness and very high temperatures
SDGVM[f]	Maximum age and fixed rate	Thinning as a result of competition between cohorts within each individual PFT	f(Monthly averages of precipitation and temperature)	Mortality of cohort if storage C depleted; Mortality = 1 for annual NPP < 10 g m^{-2} y^{-1} which decreases up to 0 for NPP ≥ 600 g m^{-2} y^{-1}	-	-
VISIT[g]	+	-	f(Fuel load, litter moisture) (Thonicke *et al.*, 2001)	-	-	-

+ Implemented mortality algorithm
- Mortality algorithm not implemented
* DGVM
[1] Background mortality rate = Biomass / Turnover time; usually divided between foliage, wood, and fine root turnover and different PFTs
[a] Friend & White (2000); Friend *et al.* (1997)
[b] Pavlick *et al.* (2013)
[c] Clark *et al.* (2011)
[d] Sitch *et al.* (2003)
[e] Krinner *et al.* (2005); Delbart *et al.* (2010)
[f] Woodward & Lomas (2004)
[g] Ito & Oikawa (2002); Inatomi *et al.* (2010)

Instead of PFTs, JeDi uses a large set of functional trait combinations, with some traits affecting turnover rates of carbon pools as well as NPP feedbacks on senescence. The response time to favourable growing conditions and the turnover time of structural, leaf and fine root pools are considered as traits which differ between plant growth strategies. Furthermore, in dynamic GVMs (DGVMs), including HYBRID4, JeDi, JULES, and LPJml, exceeding bioclimatic tolerances over long time periods (or, in case of HYBRID4, competition between PFTs) leads to a redistribution of PFTs (or, in case of JeDi, plant growth strategies) and thus turnover rates are influenced indirectly. Overall, direct frost and drought stress effects on the simulated carbon balance and thus finally on mortality are only considered in HYBRID4, but only indirectly or not at all in the other GVMs. Insects and pathogens are not explicitly accounted for in any ISI-MIP GVM.

4.2 Simulated carbon turnover rate

As described in Chapter 1.3 and applied to observation based NPP and biomass in Chapter 3, here model output of GVMs participating in ISI-MIP is used to derive k from simulated NPP and biomass (cf. Eq. 1.4). Again, this calculation requires the assumption of steady state, but for the models it is also possible to derive k based on the carbon out- instead of the influx for comparison purposes (cf. Chapter 4.6.1). Here simulated 5-year average NPP (2000-2004; kgC m^{-2} y^{-1}) and biomass (or vegetation carbon density; kgC m^{-2}; accounting for stem, branch, root, and foliage biomass) in 2004 from historical model runs are used, focusing on the Northern Hemisphere boreal and temperate forests (30-80°N). These settings provide the best possible comparability to the observation based investigations presented in Chapter 3, since model outputs are only available until 2004 (cf. Chapter 3.8). For JeDi, JULES, ORCHIDEE and VISIT,

monthly model output is available, and biomass is obtained as the average from June-August biomass in order to account for the maximum leaf biomass during that year. Simulations based on the bias-corrected HadGEM2-ES (Collins *et al.*, 2011) climate data and CO_2 forcing have been applied within ISI-MIP at 0.5° resolution. Boreal and temperate ecoregions are separated according to Olson *et al.* (2001). Only grid cells containing at least 40% forest (according to GLC2000) are considered to be dominated by forest and included in the analysis. Nevertheless, in some grid cells non-forest vegetation might contribute significantly to the carbon stocks and fluxes simulated by the GVM. However, underlying PFT distributions are not available for all of the ISI-MIP GVMs, since JeDi is based on individual plant strategies rather than a PFT concept. In order to further minimize the influence of non-forest vegetation on the results, grid cells with biomass less than 1 kgC m^{-2} are masked out in all of the model outputs. Furthermore, grid cells with simulated $k < 0$ or $k > 1$ are excluded from the analysis.

While increasing spatial gradients in forest k have been detected towards the northern edges of boreal and the southern edges of temperate forests using observation based estimates (cf. Chapter 3), spatial patterns in k are very different between models (Fig. 4.1). Across all models, the spatial variation in k is more strongly related to the spatial variation in biomass than to the spatial variation in NPP, in boreal as well as in temperate forests (Tables 4.2 and 4.3).

In HYBRID4, patterns in k are very patchy (Fig. 4.1a), mostly in accordance with distinct jumps in simulated biomass in several regions (Fig. 1.11a). Isolated spots of very high biomass density occur in the far North, for example in Siberia in transects b3 and b4. This indicates that the implemented mortality algorithms introduce spatial patterns in forest carbon density which are very different from observations (cf. Fig. 2.11). On the other hand, NPP values are surprisingly high in boreal compared to temperate regions; for instance, NPP is much higher in Eastern Canada than in the South-East US (Fig. 1.10a). This may be related to the high aridity in some temperate forest regions since HYBRID4 is strongly affected by high vapour pressure deficits compared to other models, but could also be due to the missing consideration of frost hardening requirements in boreal forests.

In JeDi, simulated k in boreal forests is relatively uniform with highest values in European Russia, which are related to very low biomass values there (Fig. 4.1b). In temperate forests, JeDi generally shows lower k towards the South, contradicting the observations. Modelled relative increases in biomass (Fig. 1.11b) are larger than in NPP

(Fig. 1.10b) along these spatial gradients. The lower *k* in southern temperate forests might be explained by lowest leaf and fine root turnover rates in these regions due to sufficiently high NPP, which does not seem to be very much affected by drier conditions.

In *k* simulated by JULES, small increases are visible towards the North in boreal and the South in temperate forests (Fig. 4.1c), generally similar to the observations. These findings can be explained by density dependent mortality due to competition and in addition by increased leaf turnover caused by low temperatures in boreal forests, hence limiting biomass (Fig. 1.11c) in both forest ecosystems.

Spatial patterns in *k* simulated by LPJml are relatively uniform with higher values in some boreal (especially Central and East Siberia) and temperate (especially South-West and South-East US) forests (Fig. 4.1d). These areas coincide with low biomass regions (Fig. 1.11d) whereas less pronounced spatial anomalies in NPP are visible (Fig. 1.10d), indicating effects of mortality related to growth efficiency and fire. In boreal forests heat stress also affects mortality.

ORCHIDEE is able to reproduce observed spatial patterns in *k* to some extent (Fig. 4.1e), especially in the Northern edges of boreal forests. There elevated *k* corresponds to low biomass areas (Fig. 1.11e). Similar relationships can be observed in the temperate forest transect t4. However, ORCHIDEE uses a constant PFT-specific mortality, so that its spatial patterns of *k* can only reflect spatial patterns of climate stress on phenology and leaf longevity within a given PFT.

SDGVM simulates relatively uniform low values of *k*, with the exception of the Southern boundaries of some temperate forest regions, especially in the South-West US (Fig. 4.1f). Implemented mortality by drought-driven fires is likely causing elevated mortality and lower biomass (Fig. 1.11f) in these regions. *k* also increases slightly towards the North in boreal forests, again related to decreasing biomass, which is explained by the NPP dependent mortality considered by the model.

k spatial patterns produced by VISIT are very patchy, with isolated patches of very high values mostly in the transition region between boreal and temperate forests (Fig. 4.1g), again coinciding with low biomass areas (Fig. 1.11g). This patchiness seems to be related to the application of different turnover rates in deciduous than in evergreen forests.

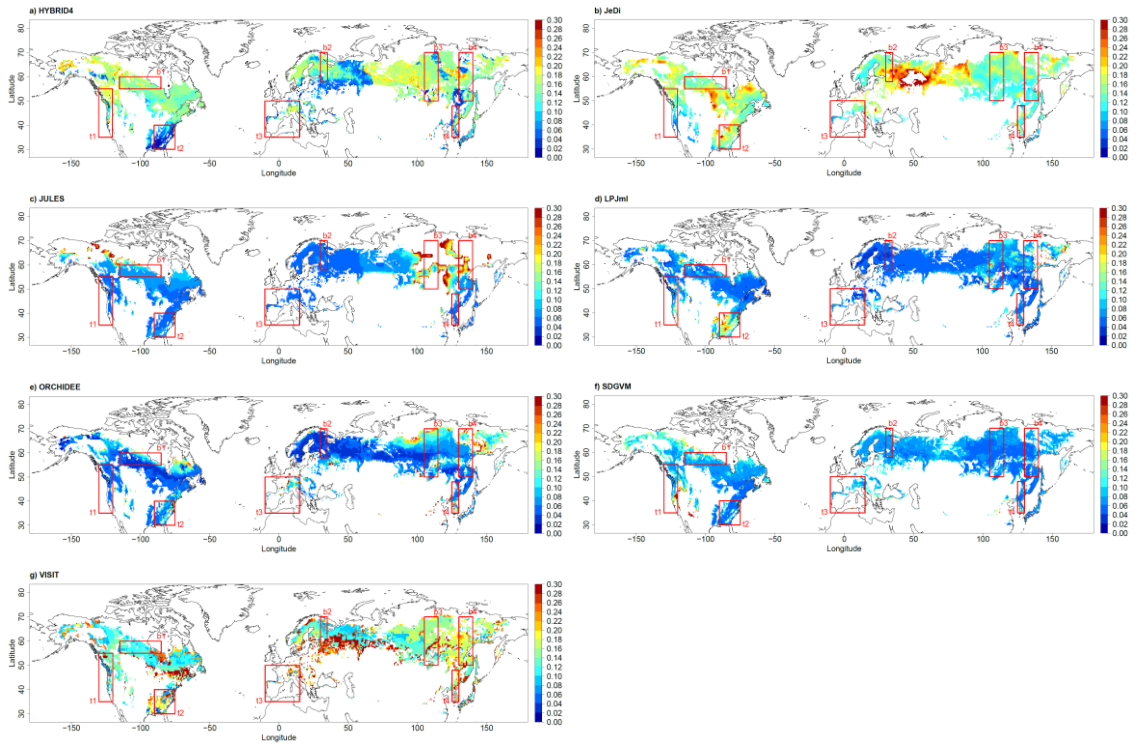

Fig. 4.1: Spatial patterns of k [y^{-1}] as the ratio of NPP over biomass simulated by ISI-MIP GVMs (a) HYBRID4, b) JeDi, c) JULES, d) LPJml, e) ORCHIDEE, f) SDGVM, g) VISIT), including areas with at least 40 % forest cover and at least 1 kgC m^{-2} biomass. Red boxes show selected transects (cf. Table 3.1).

Table 4.2: Variation coefficient (VC) of modelled k, NPP and biomass in boreal forests

VC boreal	HYBRID4	JeDi	JULES	LPJml	ORCHIDEE	SDGVM	VISIT
k	29.0	25.6	72.9	55.3	68.7	31.6	39.7
NPP	25.2	18.5	17.5	13.9	15.1	14.8	29.1
Biomass	48.9	28.3	48.2	38.9	47.3	30.4	54.0

Table 4.3: Variation coefficient (VC) of modelled k, NPP and biomass in temperate forests

VC temperate	HYBRID4	JeDi	JULES	LPJml	ORCHIDEE	SDGVM	VISIT
k	49.2	30.0	55.1	59.8	97.8	53.1	41.4
NPP	36.8	26.2	26.9	18.5	22.0	18.7	48.0
Biomass	54.5	41.7	35.8	36.9	37.1	39.2	116.7

4.3 Comparison to observation based turnover rate, NPP and biomass

In addition to the spatial patterns of *k* and their relationships to climate variables (Chapter 4.4), modelled *k*, NPP and biomass are evaluated at ecosystem scale (boreal and temperate forests) in terms of average values and correlation with observations. Comparing modelled and observed *k*, NPP and biomass can reveal systematic biases in the modelled carbon fluxes and stocks. Here model results are compared to the observation based estimates of *k* presented in Chapter 3, derived from biomass (Thurner *et al.*, 2014) and NPP products including MODIS (Running *et al.*, 2004; Zhao *et al.*, 2005; Zhao & Running, 2010), BETHY/DLR (Wißkirchen *et al.*, 2013) and an average of both.

4.3.1 Biome averages

Although HYBRID4 compares reasonably to the observed average *k* in both boreal (Table 4.4) and temperate forests (Table 4.7), this is associated with serious overestimation of both NPP (Tables 4.5 and 4.8) and biomass (Tables 4.6 and 4.9) in these forest ecosystems. HYBRID4 overestimates NPP (in boreal forests) and biomass (in both boreal and temperate forests) by more than 100% of the observed values. Hence a correction of the NPP simulated by HYBRID4 might suffice to match observed mean biomass. All the other model results agree well with the observation based estimate in terms of NPP. Except for ORCHIDEE and JULES in boreal forests, the simulated NPP is always within 20 % of the observed values. On the other hand, biomass is severely overestimated by most of the models with the exception of JeDi and VISIT, which match the observed mean biomass very closely in both forest ecosystems. Hence, only JeDi and VISIT reproduce the mean observed *k* almost perfectly, since they do not simulate important deviations from both observed mean NPP and biomass.

Table 4.4: Percentage deviation of modelled ***k*** in **boreal** forests compared to observation based *k*. ISI-MIP GVMs including HYBRID4, JeDi, JULES, LPJml, ORCHIDEE, SDGVM, and VISIT. Observation based *k* derived from MODIS, BETHY/DLR or an average (Obs mean) of both NPP products, and biomass from Thurner *et al.* (2014).

% dev. *k* in boreal forests	HYBRID4	JeDi	JULES	LPJml	ORCHIDEE	SDGVM	VISIT
MODIS	-8.1	3.4	-37.7	-57.3	-53.2	-50.9	1.1
BETHY/DLR	-24.5	-14.9	-48.8	-64.9	-61.5	-59.6	-16.9
Obs mean	-17.1	-6.6	-43.8	-61.5	-57.8	-55.7	-8.8

Table 4.5: Percentage deviation of modelled **NPP** in **boreal** forests compared to observation based NPP. ISI-MIP GVMs including HYBRID4, JeDi, JULES, LPJml, ORCHIDEE, SDGVM, and VISIT. Observation based NPP including MODIS, BETHY/DLR or an average (Obs mean) of both products.

% dev. NPP in boreal forests	HYBRID4	JeDi	JULES	LPJml	ORCHIDEE	SDGVM	VISIT
MODIS	184.2	6.7	43.5	29.3	58.0	14.7	12.9
BETHY/DLR	121.7	-16.8	11.9	0.9	23.2	-10.5	-11.9
Obs mean	149.1	-6.5	25.8	13.3	38.5	0.5	-1.0

Table 4.6: Percentage deviation of modelled **biomass** in **boreal** forests compared to observed biomass. ISI-MIP GVMs including HYBRID4, JeDi, JULES, LPJml, ORCHIDEE, SDGVM, and VISIT.

% dev. biomass in boreal forests	HYBRID4	JeDi	JULES	LPJml	ORCHIDEE	SDGVM	VISIT
Observed	156.4	-18.9	135.2	166.9	234.5	88.4	-3.0

Table 4.7: Percentage deviation of modelled ***k*** in **temperate** forests compared to observation based *k*. ISI-MIP GVMs including HYBRID4, JeDi, JULES, LPJml, ORCHIDEE, SDGVM, and VISIT. Observation based *k* derived from MODIS, BETHY/DLR or an average (Obs mean) of both NPP products, and biomass from Thurner *et al.* (2014).

% dev. *k* in temperate forests	HYBRID4	JeDi	JULES	LPJml	ORCHIDEE	SDGVM	VISIT
MODIS	-25.6	1.3	-54.2	-43.5	-40.6	-41.3	27.4
BETHY/DLR	-43.2	-22.7	-65.1	-56.9	-54.7	-55.2	-2.8
Obs mean	-35.6	-12.3	-60.3	-51.1	-48.6	-49.2	10.3

Table 4.8: Percentage deviation of modelled **NPP** in **temperate** forests compared to observation based NPP. ISI-MIP GVMs including HYBRID4, JeDi, JULES, LPJml, ORCHIDEE, SDGVM, and VISIT. Observation based NPP including MODIS, BETHY/DLR or an average (Obs mean) of both products.

% dev. NPP in temperate forests	HYBRID4	JeDi	JULES	LPJml	ORCHIDEE	SDGVM	VISIT
MODIS	61.4	-2.8	18.5	0.3	29.8	-6.4	11.3
BETHY/DLR	22.1	-26.4	-10.3	-24.1	-1.7	-29.2	-15.7
Obs mean	39.0	-16.2	2.1	-13.6	11.8	-19.4	-4.1

Table 4.9: Percentage deviation of modelled **biomass** in **temperate** forests compared to observed biomass. ISI-MIP GVMs including HYBRID4, JeDi, JULES, LPJml, ORCHIDEE, SDGVM, and VISIT.

% dev. biomass in temperate forests	HYBRID4	JeDi	JULES	LPJml	ORCHIDEE	SDGVM	VISIT
Observed	136.9	-9.0	157.1	87.3	146.2	63.9	8.4

4.3.2 Correlation

Correlation analyses show that none of the models can reproduce observed spatial patterns in *k* in boreal (Fig. 4.2) and temperate (Fig. 4.5) forests. The Pearson correlation coefficient (r) between mean observation based (Obs mean) and simulated *k* is never higher than 0.42 (SDGVM) in boreal and 0.19 (LPJml) in temperate forests, respectively. In addition, there are important disagreements between models, with

highest correlations between JULES, LPJml and ORCHIDEE (r = 0.33-0.36) in boreal and between JeDi and VISIT (r = 0.20) in temperate forests. In many cases, significant negative correlations occur between models and (in temperate forests) also between models and observations. Although there are large differences in modelled NPP, spatial correlations to the observation based NPP are in general much higher than between simulated and observed *k* (Figs. 4.3 and 4.6), beside for HYBRID4. In both investigated forest ecosystems, r between the mean of the NPP observations (Obs mean) and some models is ≥ 0.65 (LPJml and SDGVM in boreal forests; JeDi, JULES and SDGVM in temperate forests). For biomass, correlation between models and between models and observations is relatively weak (Figs. 4.4 and 4.7). While in boreal forests SDGVM (r = 0.72) and ORCHIDEE (r = 0.58) show the highest agreement with observations, models compare worse in temperate forests, with ORCHIDEE, SDGVM and VISIT (r = 0.22-0.25) most closely matching the observed biomass.

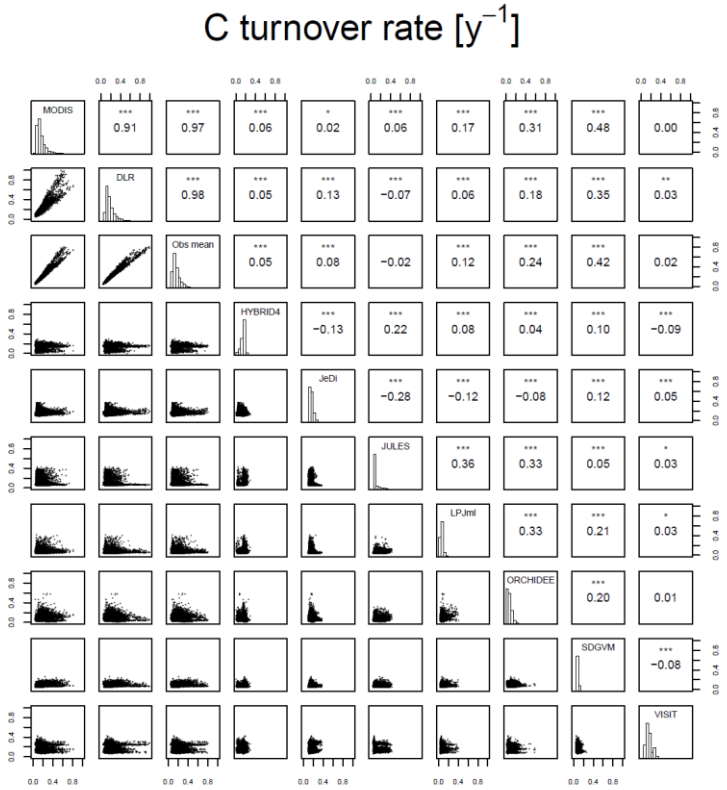

Fig. 4.2: Correlation between modelled and observation based ***k*** in **boreal** forests. ISI-MIP GVMs including HYBRID4, JeDi, JULES, LPJml, ORCHIDEE, SDGVM, and VISIT. Observation based *k* derived from derived from MODIS, BETHY/DLR or an average (Obs mean) of both NPP products, and biomass from Thurner *et al.* (2014).
The lower left panel shows the scatterplots. The upper right panel shows the corresponding Pearson correlation coefficients and the significance level. The significance level is quantified by the p-value: "***" $p \leq 0.001$, "**" $0.001 < p \leq 0.01$, "*" $0.01 < p \leq 0.05$, "." $0.05 < p \leq 0.1$, " " $p > 0.1$. The histograms plotted in the diagonal show the frequency distribution of *k* values.

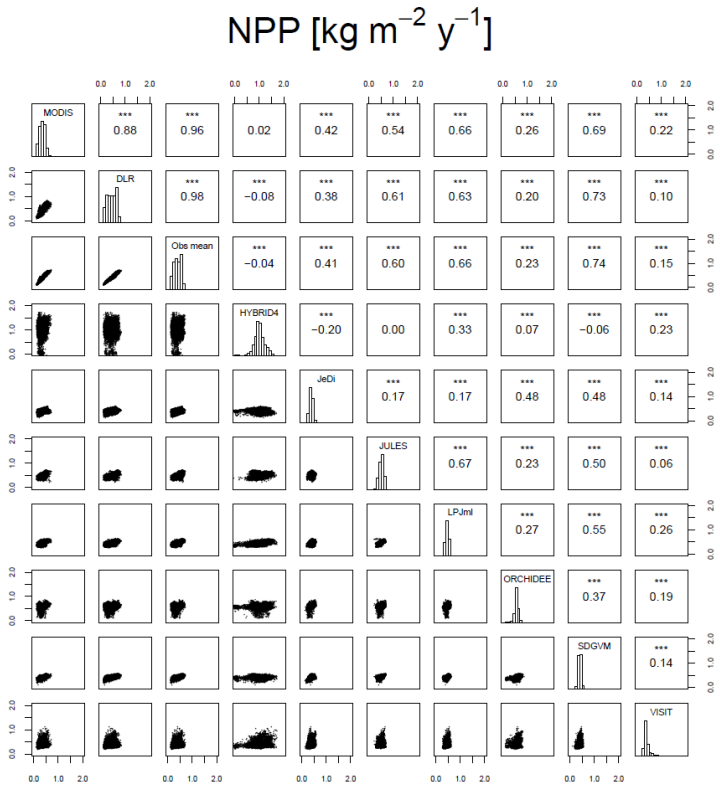

Fig. 4.3: Correlation between modelled and observation based **NPP** in **boreal** forests. ISI-MIP GVMs including HYBRID4, JeDi, JULES, LPJml, ORCHIDEE, SDGVM, and VISIT. Observation based NPP including MODIS, BETHY/DLR or an average (Obs mean) of both products. For further explanations see Fig. 4.2.

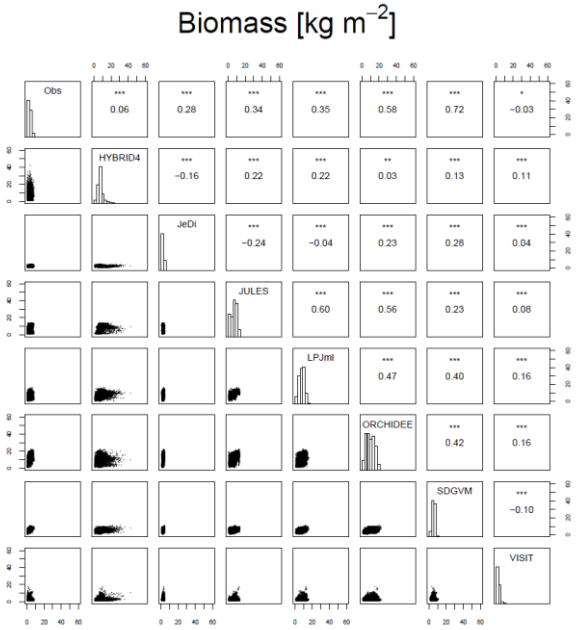

Fig. 4.4: Correlation between modelled and observed **biomass** (Obs) in **boreal** forests. ISI-MIP GVMs including HYBRID4, JeDi, JULES, LPJml, ORCHIDEE, SDGVM, and VISIT. For further explanations see Fig. 4.2.

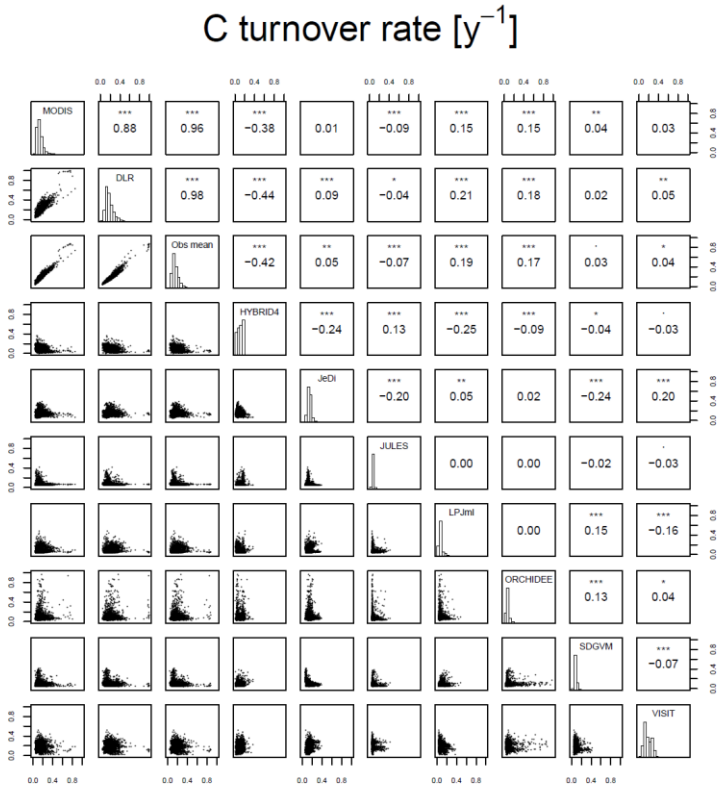

Fig. 4.5: Correlation between modelled and observation based ***k*** in **temperate** forests. ISI-MIP GVMs including HYBRID4, JeDi, JULES, LPJml, ORCHIDEE, SDGVM, and VISIT. Observation based *k* derived from derived from MODIS, BETHY/DLR or an average (Obs mean) of both NPP products, and biomass from Thurner *et al.* (2014). For further explanations see Fig. 4.2.

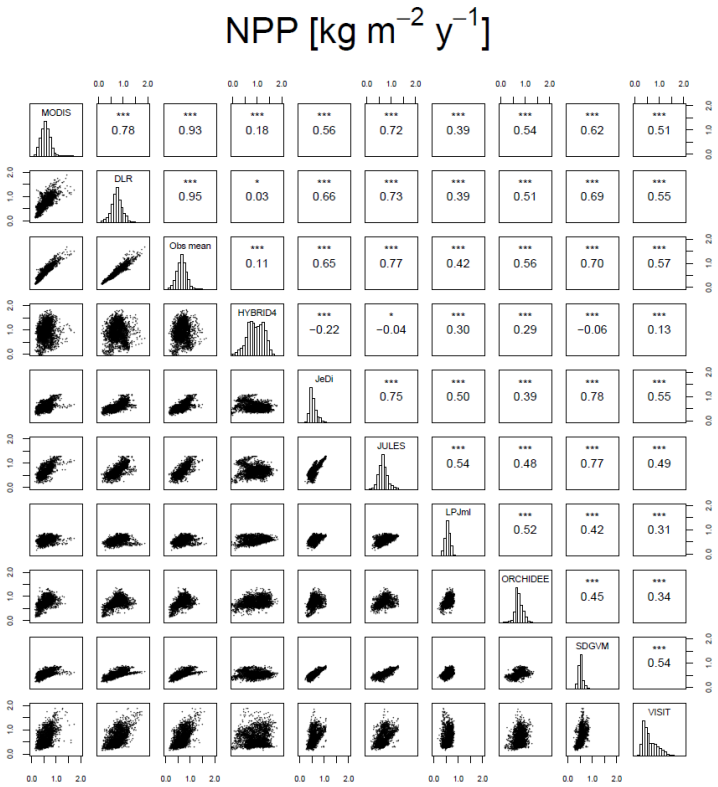

Fig. 4.6: Correlation between modelled and observation based **NPP** in **temperate** forests. ISI-MIP GVMs including HYBRID4, JeDi, JULES, LPJml, ORCHIDEE, SDGVM, and VISIT. Observation based NPP including MODIS, BETHY/DLR or an average (Obs mean) of both products. For further explanations see Fig. 4.2.

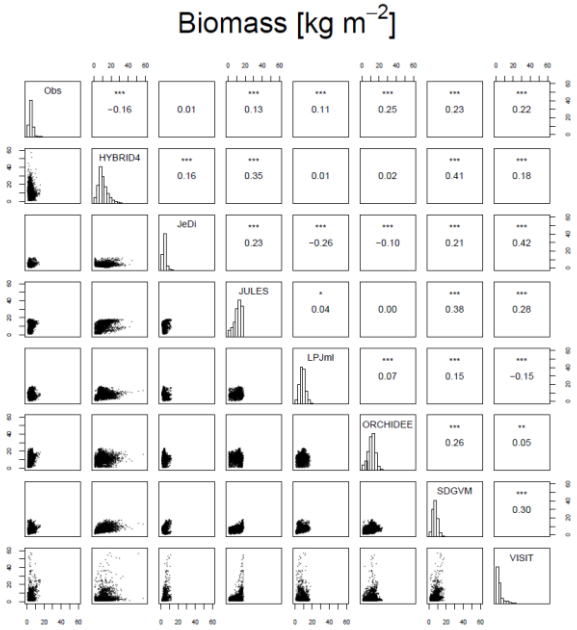

Fig. 4.7: Correlation between modelled and observed **biomass** (Obs) in **temperate** forests. ISI-MIP GVMs including HYBRID4, JeDi, JULES, LPJml, ORCHIDEE, SDGVM, and VISIT. For further explanations see Fig. 4.2.

4.4 Modelled relationships to climate variables

Climate variables considered include the number of icing days (ID), the number of frost days (FD) and the maximum length of warm-dry periods (WD10). These are selected since they have been identified to be related to observation based *k* in boreal and temperate forest transects (cf. Chapter 3.3). Long-term average values (1975-2004) are calculated for these variables based on daily bias-corrected HadGEM2-ES climate data (Collins *et al.*, 2011) at 0.5° resolution.

The applicability of relationships between *k* and bioclimatic variables derived from observations (as in Chapter 3.3) to ISI-MIP model simulations is evaluated by their modelling efficiency (MEF; Nash & Sutcliffe, 1970), defined as :

$$MEF = 1 - \frac{\sum (isimip - obs)^2}{\sum (isimip - mean(isimip))^2} \qquad \text{(Eq. 4.1)}$$

where $isimip$ is a modelled value of *k* and obs is its value calculated from the observed relationship. Negative MEF indicates that the mean of the modelled *k* values is a better predictor than the *k* calculated from the observed relationship, while a MEF of 1 indicates a perfect match between model and observations (Nash & Sutcliffe, 1970).

Observed increases in *k* with increasing ID (cf. Fig. 3.6) are hardly reproduced by any of the models in the selected boreal forest transects (Fig. 4.8). An always negative MEF indicates that the observed *k* = f(ID) relationships are not suitable to predict the model output. Although all models show deviations from observed relationships, in most models the simulated *k* is positively correlated to ID in some of the boreal forest transects ($r > 0.3$ for JULES in all transects; HYBRID4 in b2; JeDi in b3 and b4; LPJml in b4; ORCHIDEE in b1, b3 and b4; SDGVM in b1, b2 and b4). In general, NPP decreases only slightly with increasing ID, whereas the decrease in biomass is more pronounced (not shown). For LPJml, increased mortality as a direct function of growth efficiency is expected to be mainly responsible for the simulated patterns. In the northern boreal regions, permafrost dynamics determine soil water availability, which in turn influences growth. Frost damage effects on the carbon balance can lead to an increased *k* simulated by HYBRID4. In JeDi, only leaf and fine root turnover is affected by negative NPP, leading to less pronounced effects on the simulated *k*. Elevated leaf turnover caused by low temperatures can explain the patterns modelled by JULES, whereas distinct jumps in *k* in the boreal transects b3 and b4 are likely caused by

changes in the PFT distribution. In SDGVM, increasing mortality in case of low NPP or depleted storage carbon can explain the modelled relationship between *k* and ID. The processes underlying the positive correlation between *k* and ID simulated by ORCHIDEE remain unclear, since such mortality mechanisms are not implemented in the model version used in ISI-MIP (cf. Table 4.1).

The observed increases in *k* related to drought in temperate forest transects are not reproduced by any of the models, with the exception of LPJml (MEF = 0.21) and SDGVM (MEF = 0.176) in transect t1. Nevertheless JULES (t2 and t3), LPJml (t1 and t4), ORCHIDEE (t4), and SDGVM (t1, t3 and t4) show a relationship with $r > 0.3$ in some of the transects (Fig. 4.9). It is surprising that, apart from HYBRID4, LPJml and ORCHIDEE in several regions, NPP is increasing along spatial gradients with longer WD10 (not shown). This is a sign of little effect of dry conditions on productivity in most of the models. Distinct decreases in biomass with longer drought periods are only visible in LPJml (not shown). In addition to mortality from fire, water stress effects on NPP (Schaphoff *et al.*, 2006) can lead to increased mortality related to low growth efficiency. Small increases in *k* with drought simulated by JULES might be introduced by the coincidence of increasing biomass with WD10 (not shown), causing increased mortality through competition in high vegetation density regions. In ORCHIDEE, drought conditions can lead to decreased leaf longevity and, as in SDGVM, also to elevated fire occurrence.

None of the investigated GVMs reproduces the observed increase in *k* related to fewer FD in temperate forest transects (Fig. 4.10; MEF < 0). JeDi (t4), JULES (t2 and t3), LPJml (t4), ORCHIDEE (t4) and SDGVM (t4) show negative correlations ($r < -0.3$) in some of the transects, but this might be caused by high correlation between FD and other bioclimatic variables in these areas. Furthermore, in JeDi, JULES, SDGVM and VISIT, NPP is negatively correlated to FD. These temperature effects on productivity propagate to the spatial gradients in biomass simulated by these models (not shown). Overall, none of the investigated GVMs incorporates effects of winter length and temperature on the survival of insect populations, which in turn would affect forest mortality. There are also no other processes implemented in those models which could cause increased mortality rates in case of fewer FD.

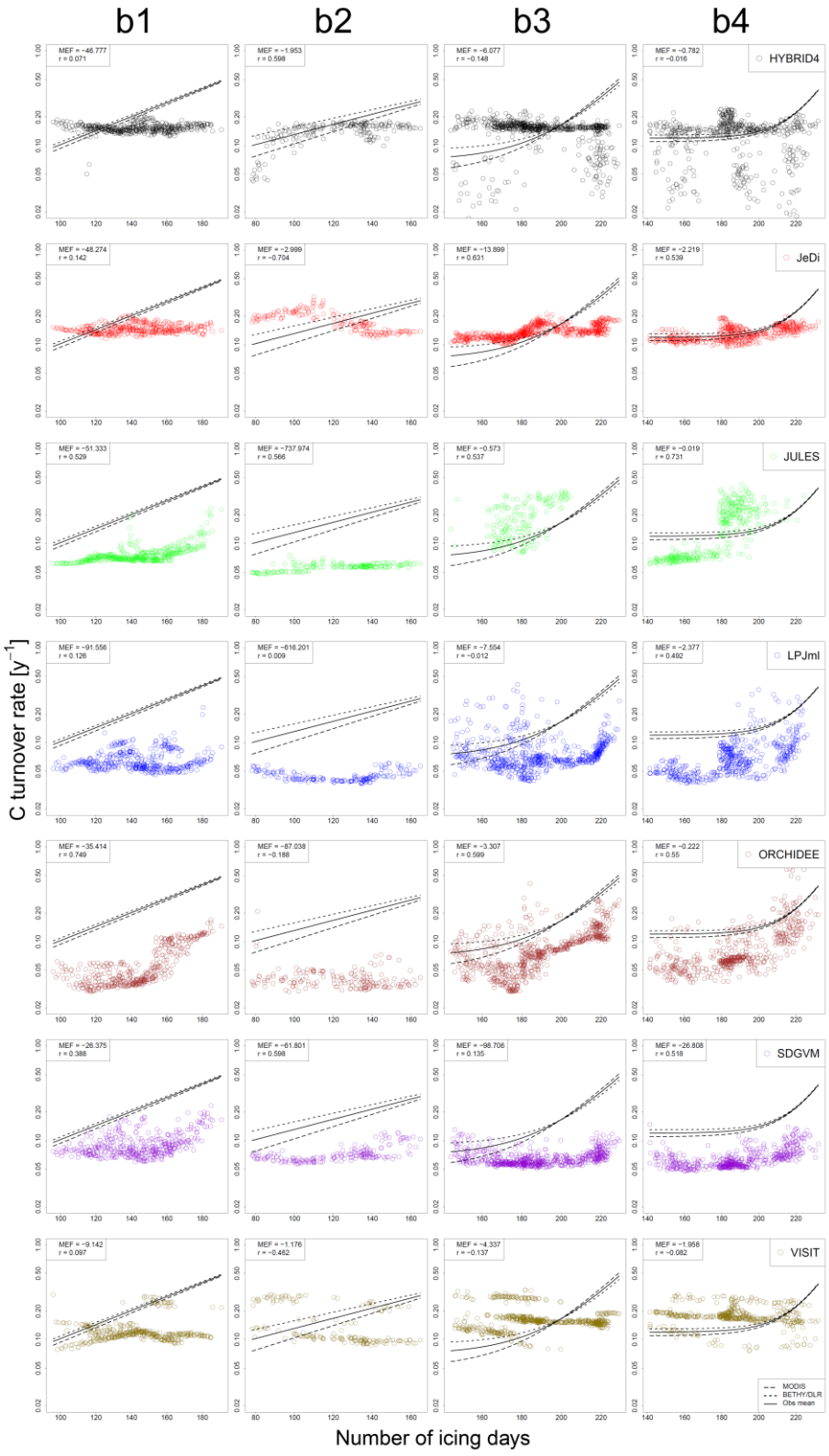

Fig. 4.8: *k* modelled by ISI-MIP GVMs as a function of the number of icing days during a year in boreal forest transects (cf. Table 3.1). Lines indicate observation based relationships (cf. Fig. 3.6), with longdashed lines corresponding to the use of MODIS NPP, dashed lines to BETHY/DLR NPP and solid lines to an average (Obs mean) of both products. Modelling efficiency (MEF) refers to the ability of the observation based relationships to describe the *k* simulated by ISI-MIP models as a function of the climate variable. The correlation coefficient (r) denotes the correlation between *k* simulated by ISI-MIP models and the climate variable.

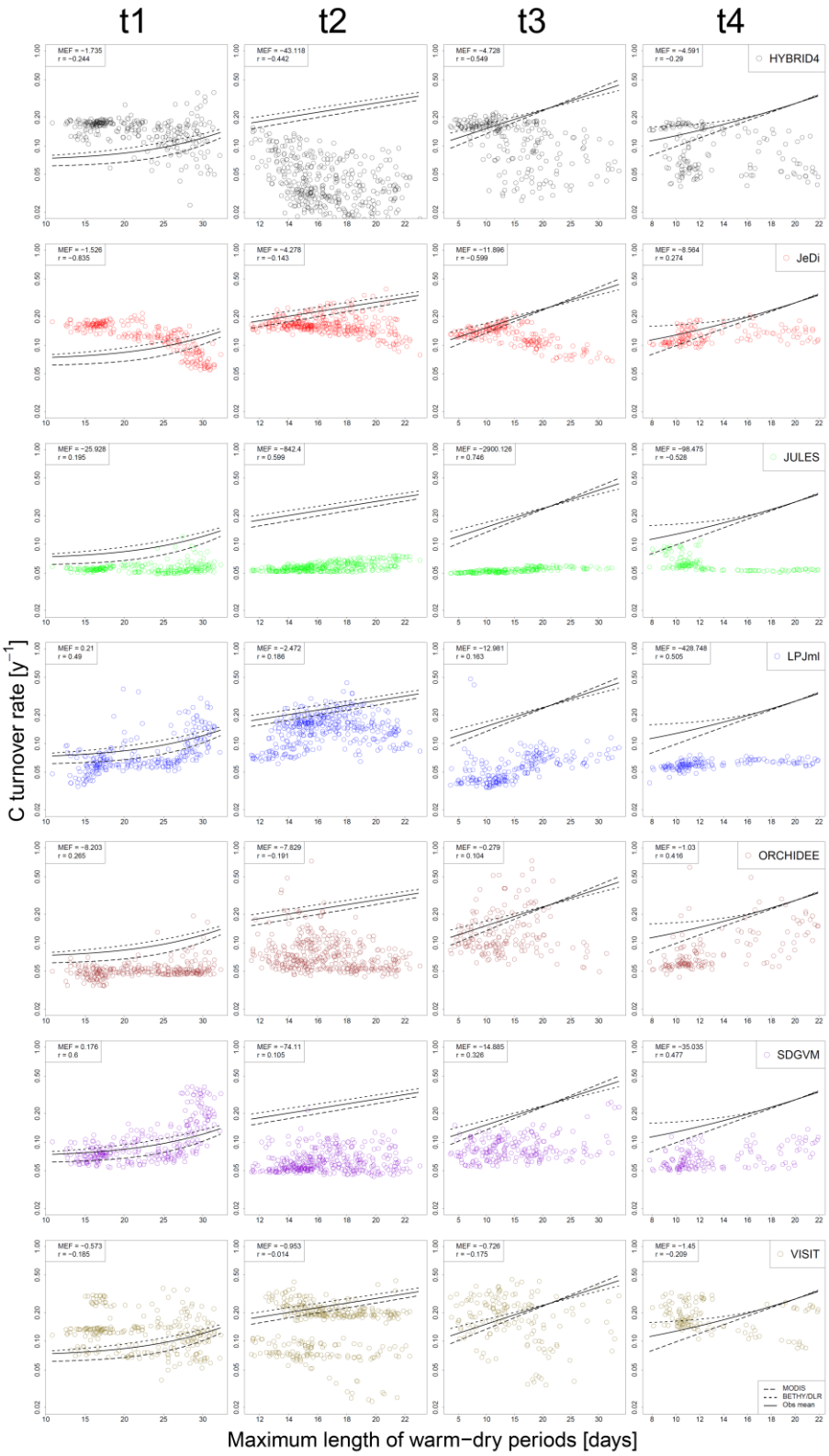

Fig. 4.9: *k* modelled by ISI-MIP GVMs as a function of the maximum length of warm-dry periods (in days) during a year in temperate forest transects (cf. Table 3.1). Lines indicate observation based relationships (cf. Fig. 3.7), with longdashed lines corresponding to the use of MODIS NPP, dashed lines to BETHY/DLR NPP and solid lines to an average (Obs mean) of both products. Modelling efficiency (MEF) refers to the ability of the observation based relationships to describe the *k* simulated by ISI-MIP models as a function of the climate variable. The correlation coefficient (r) denotes the correlation between *k* simulated by ISI-MIP models and the climate variable.

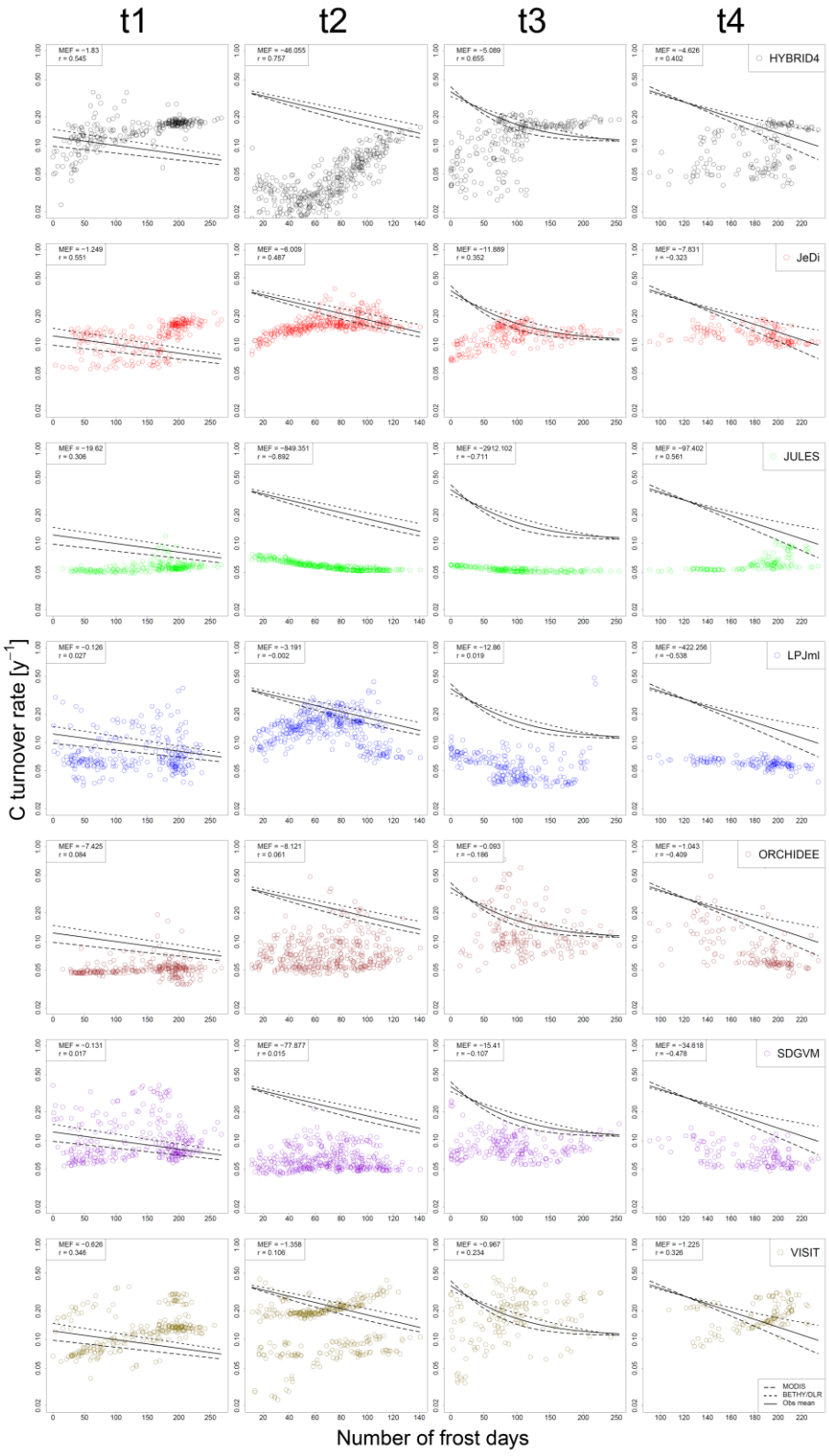

Fig. 4.10: *k* modelled by ISI-MIP GVMs as a function of the number of frost days during a year in temperate forest transects (cf. Table 3.1). Lines indicate observation based relationships (cf. Fig. 3.8), with longdashed lines corresponding to the use of MODIS NPP, dashed lines to BETHY/DLR NPP and solid lines to an average (Obs mean) of both products. Modelling efficiency (MEF) refers to the ability of the observation based relationships to describe the *k* simulated by ISI-MIP models as a function of the climate variable. The correlation coefficient (r) denotes the correlation between *k* simulated by ISI-MIP models and the climate variable.

4.5 Attribution of errors in modelled turnover rate to errors in NPP and biomass

In boreal forests, the negative correlation between errors (difference between model and observations) in *k* and NPP as well as the negative correlation between errors in *k* and biomass (shown for LPJml in Fig. 4.11, and summarized for all models in Table 4.10) reveal that biases in NPP (exception: ORCHIDEE) and biomass always occur in the same direction. This is due to the high correlation between NPP and biomass, since NPP directly influences biomass. For all models, the errors in *k* are more strongly related to the errors in biomass than to the errors in NPP. In other words, an underestimation of NPP and an even stronger underestimation of biomass are related to an overestimation of *k*, and vice versa. This indicates that the errors in *k* are not only caused by disagreements in NPP, but also by other not correctly represented processes influencing biomass, like mortality processes.

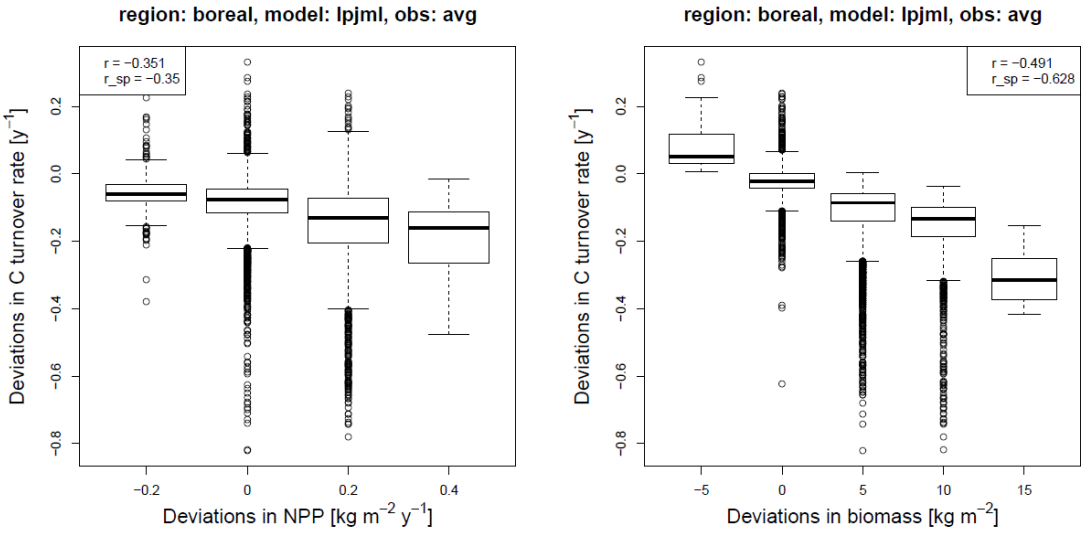

Fig. 4.11: Correlation between errors in *k* and NPP (left) as well as *k* and biomass (right) in boreal forests (model: LPJml; observed NPP: average of MODIS and BETHY/DLR; r…Pearson correlation coefficient; r_sp…Spearman's rank correlation coefficient)

Table 4.10: Correlation between errors in *k* and NPP as well as *k* and biomass in boreal forests for all ISI-MIP GVMs (observed NPP: average of MODIS and BETHY/DLR; r_{sp}…Spearman's rank correlation coefficient)

Model	HYBRID4	JeDi	JULES	LPJml	ORCHIDEE	SDGVM	VISIT
$r_{sp}(k, NPP)$	-0.212	-0.338	-0.378	-0.35	0.063	-0.279	-0.33
$r_{sp}(k,$ biomass)	-0.737	-0.843	-0.761	-0.628	-0.504	-0.549	-0.821

In temperate forests, the errors in *k* and biomass are again negatively correlated for all models, whereas the errors in *k* and NPP are sometimes positively, sometimes negatively, and sometimes not at all correlated (shown for LPJml in Fig. 4.12, and summarized for all models in Table 4.11). Like in boreal forests, the errors in *k* are always more strongly related to the errors in biomass than to the errors in NPP. These findings again demonstrate that the errors in *k* are only to a minor extent related to errors in productivity and instead are mainly caused by not correctly represented processes influencing biomass, like mortality processes. For HYBRID4 it becomes apparent that the errors in NPP and biomass are correlated to the errors in *k* in the opposite direction, indicating important shortcomings in both modelled productivity and mortality processes.

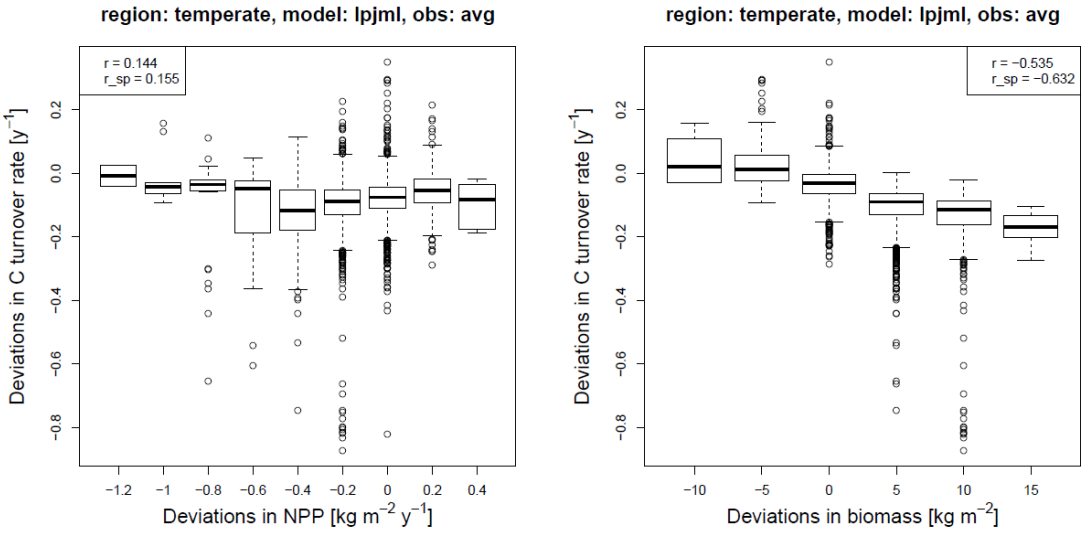

Fig. 4.12: Correlation between errors in *k* and NPP (left) as well as *k* and biomass (right) in temperate forests (model: LPJml; observed NPP: average of MODIS and BETHY/DLR; r…Pearson correlation coefficient; r_sp…Spearman's rank correlation coefficient)

Table 4.11: Correlation between errors in *k* and NPP as well as *k* and biomass in temperate forests for all ISI-MIP GVMs (observed NPP: average of MODIS and BETHY/DLR; r_{sp}…Spearman's rank correlation coefficient)

Model	HYBRID4	JeDi	JULES	LPJml	ORCHIDEE	SDGVM	VISIT
r_{sp}(*k*, NPP)	0.519	-0.086	-0.181	0.155	0.256	0.238	-0.336
r_{sp}(*k*, biomass)	-0.834	-0.852	-0.838	-0.632	-0.679	-0.782	-0.816

4.6 Potential confounding factors

The spatial differences in the NPP/biomass ratio can be explained by effects of mortality processes on biomass (as above), but may also be confounded by the potential impact of non-forest vegetation on *k*, by differences in the ecosystem state (steady state vs. succession), and by uncertainty in the modelled NPP. Moreover, differences in modelled and observation based NPP and biomass, caused by either forest management effects or mismatches in the considered timespans, may influence the comparison of models and observations. Elevated *k* in areas of very low biomass might be influenced by the possibly high contribution of non-forest vegetation especially in northern boreal forests, which might correlate with winter length and thus influence the simulated relationships between *k* and climate. However, by applying a forest cover threshold and, in addition, by masking out very low biomass areas, the influence of ecosystem state and non-forest vegetation has been minimized as far as possible. The other possible confounding factors are investigated below and/or discussed in Chapters 5.3 and 5.5.

4.6.1 Assessment of the steady state assumption

Apart from recent disturbances, differences in the ecosystem state between grid cells can be caused by recent shifts in the PFT or plant growth strategy composition in DGVMs (including HYBRID4, JeDi, JULES, LPJml). For example in LPJml, mortality of PFTs occurs if long-term climate exceeds climatic tolerances, whereas already a short-term exceedance of a maximum temperature threshold leads to mortality of boreal forests. In addition, DGVMs simulate a potential natural vegetation distribution and thus do not account for land use (e.g. agriculture). The differences in the spatial patterns in *k* between observations and the other GVMs (ORCHIDEE, SDGVM, VISIT), which apply a prescribed vegetation distribution based on observed land use, are supposed to be less affected by the influence of ecosystem state and non-forest vegetation.

However, the spatial patterns between *k* calculated as the ratio of NPP over biomass (as presented above) and *k* derived from the carbon outflux from vegetation carbon stocks (i.e., the sum of carbon fluxes to the litter, the soil and the atmosphere) do not substantially differ (Table 4.12). Instead of applying Eq. 1.4, for this purpose *k* has been derived as follows:

$$k = \text{outflux} / \text{biomass} \quad \text{(Eq. 4.2)}$$

The annual outflux can be derived as the difference between yearly NPP and the change in biomass between years as described in Friend *et al.* (2014). 5-year average *k* is calculated as the mean of annual turnover rates between 2000 and 2004. All processes considered by the model which are contributing to a carbon loss from vegetation are thus included in this measure. The agreement between *k* derived from the two different methods is very high for all models in terms of correlations ($r > 0.95$) and MEF (> 0.9). These results suggest that the impact of the steady state assumption on the presented results is rather small and strengthen the validity of the interpretation of spatial patterns in *k* in terms of turnover processes.

Table 4.12: Pearson correlation coefficient (r) and modelling efficiency (MEF) between *k* calculated based on carbon in- and outflux (Eqs. (1.4) and (4.2))

Model	HYBRID4	JeDi	JULES	LPJml	ORCHIDEE	SDGVM	VISIT
r	0.984	0.958	1.000	0.982	0.990	0.997	0.998
MEF	0.964	0.917	0.996	0.955	0.979	0.982	0.996

4.6.2 Forest management

Furthermore, the influence of forest management on NPP and biomass can affect the presented results. While forest management contributes to the observation based NPP, biomass and *k*, it is not considered by the models, which instead simulate potential natural vegetation. Based on global databases of site measurements, NPP has been found to be relatively similar in managed and unmanaged forests, whereas management has been documented to lead to an important decrease of about 50 % in biomass and to a higher allocation of assimilated carbon to aboveground carbon pools (Noormets *et al.*, 2015). However, these results are integrated over all forest ecosystems and age classes. Missing management effects in the investigated GVMs could thus partly explain the

overestimation of biomass compared to the observations, and might also lead to an underestimation of simulated *k* in managed forests. At continental scale, biomass has been reported to increase linearly with NPP over time in highly managed forests in Europe (Ciais *et al.*, 2008), suggesting rather little influence of forest management on *k*. Inabilities of a GVM (ORCHIDEE) to reproduce observed biomass dynamics despite matching NPP have been interpreted in terms of forest management effects (Ciais *et al.*, 2008), but could also be due to structural shortcomings in modelling mortality dynamics.

In addition, forest management can hardly explain observed spatial gradients in *k* and the spatial patterns in the deviations of modelled from observed *k*. Along the investigated boreal forest gradients, in many (but not all) transects and in case of many (but not all) models, with an increasing ID the underestimation of (modelled compared to observation based) *k* is getting more pronounced, whereas the overestimation of both NPP and biomass are getting more serious (shown as an example for transect b1 in Fig. 4.13). Along the investigated temperate forest gradients, with an increasing WD10 the underestimation of *k* is getting more pronounced, whereas the relationships between errors in NPP and biomass and this bioclimatic variable differ strongly between transects and models (not shown). With a decreasing FD the underestimation of *k* is getting more pronounced, whereas the relationships between errors in NPP and biomass and the number of frost days again differ strongly between transects and models (not shown). These results emphasize that the investigated bioclimatic variables are strongly related to the biases in modelled *k*, since the models do not reproduce the observation based relationships. Other factors like forest management are unlikely to be the main reason of these biases, unless they would correlate with climate.

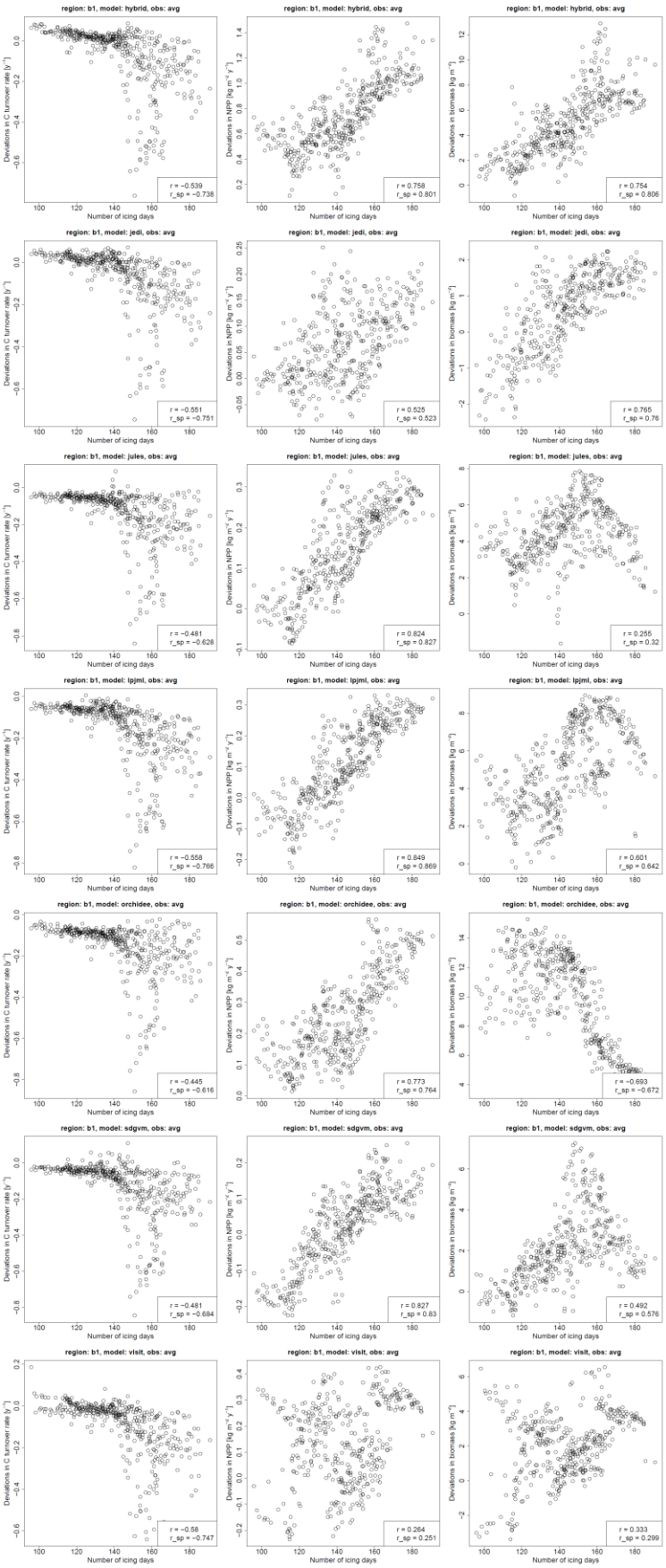

Fig. 4.13: Spatial relationships between errors in *k* (left), NPP (centre) and biomass (right) and the number of icing days during a year in the boreal forest transect b1 (observed NPP: average of MODIS and BETHY/DLR; r…Pearson correlation coefficient; r_sp…Spearman's rank correlation coefficient)

4.6.3 Impact of NPP timespans on modelled turnover rate

The robustness of the presented approach with respect to the influence of inter-annual variability could be improved by a longer overlap in NPP from ISI-MIP models (until 2004) and from observations (MODIS and BETHY/DLR time series starting in 2000). However, the agreement between modelled *k* derived for different timespans (1995-2004 vs. 2000-2004) is in general very high in terms of relative differences (Fig. 4.14), correlations (Table 4.13) and spatial variations (Fig. 4.15). Only for HYBRID4 might recent shifts in the PFT distribution cause important changes in modelled *k* in some regions. The influence of the deviation in biomass retrieval time between models (2004) and observation (2010) on the findings is considered relatively small at the applied spatial scale.

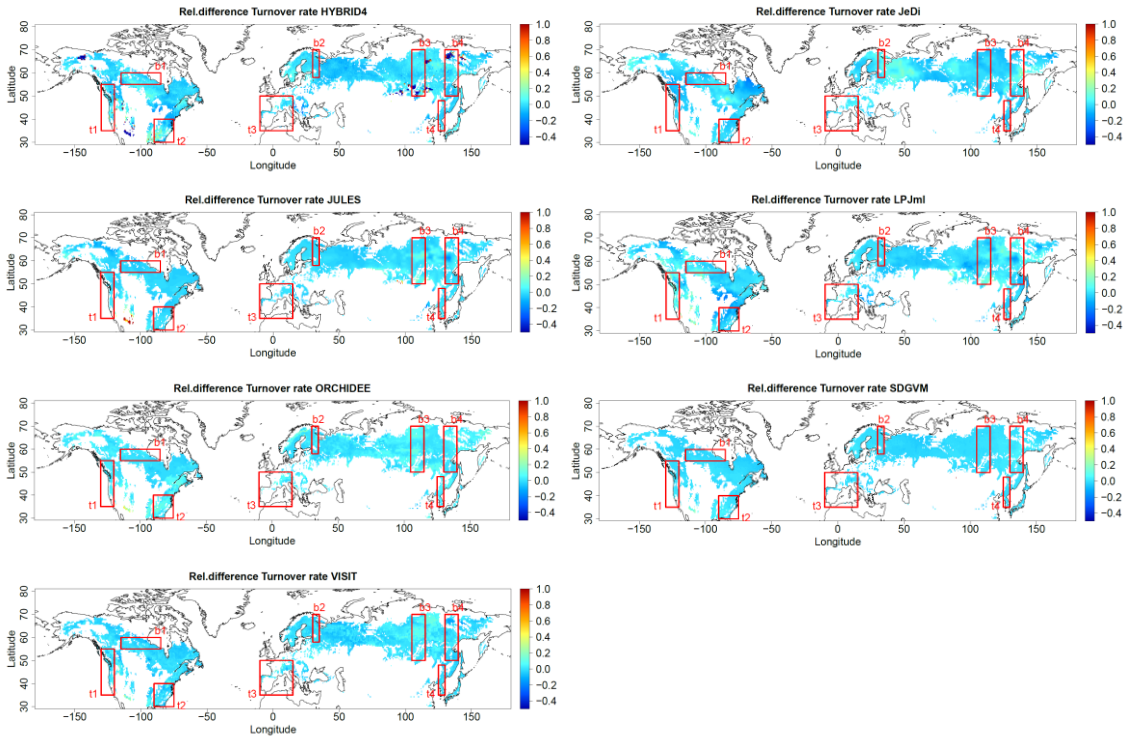

Fig. 4.14: Relative difference between modelled *k* derived for different timespans (1995-2004 vs. 2000-2004)

Table 4.13: Pearson correlation coefficient (r) between modelled *k* derived for different timespans (1995-2004 vs. 2000-2004)

Model	HYBRID4	JeDi	JULES	LPJml	ORCHIDEE	SDGVM	VISIT
r	0.84	0.99	0.99	0.99	1.00	0.99	1.00

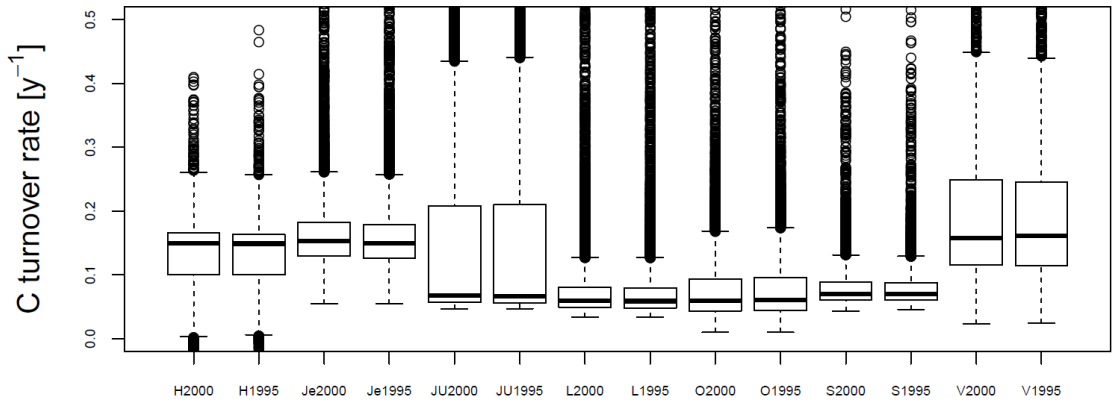

Fig. 4.15: Spatial variation in modelled *k* derived for different timespans (1995-2004 vs. 2000-2004). H…HYBRID4, Je…JeDi, JU…JULES, L…LPJml, O…ORCHIDEE, S…SDGVM, V…VISIT. 1995…1995-2004, 2000…2000-2004. The box–whisker plots show the median and the interquartile range of values. The whiskers extend up to the most extreme data point which is no more than 1.5 times the interquartile range away from the box. Outliers are drawn as circles.

CHAPTER 5

Discussion

Within the framework of this thesis, remote sensing biomass data allowed for benchmarking the absolute amount and spatial distribution of carbon stock in boreal and temperate forests. Subsequently, information from earth observation and GVMs on biomass and NPP have been used to study carbon turnover rate (k), a fundamental property of the carbon cycle, in these ecosystems. The significance of remote sensing products related to vegetation structure and dynamics for an improved understanding of the carbon cycle in forests has been demonstrated. In light of future threats to forest ecosystems, i.e. likely intensified forest mortality, this knowledge is extremely important to improve the representations of mortality mechanisms in GVMs in order to enable a better informed prediction of future land carbon cycle feedbacks to climate change. In the following, the implications of the presented findings are discussed with respect to the literature and an outlook is given on possible improvements of the applied methodology and the next research steps to be taken.

5.1 BIOMASAR-II – A new benchmark of forest carbon stocks

The presented carbon density map derived from BIOMASAR-II GSV data can serve as a new benchmark for estimating forest carbon stocks at regional to global scales. The derived carbon stock values in boreal forests are very well in line with former estimates of Pan *et al.* (2011), who derived forest carbon stocks based on up-scaling of inventory data (compare Tables 5.1 and 2.3). In contrast, Pan *et al.* (2011) reported higher carbon stocks in boreal forests, but, with the exception of North-America, still within the uncertainty range of the BIOMASAR-II based value. Other rough estimates by Saugier *et al.* (2001) seem to be far too high, especially in temperate forests. Interestingly, continental carbon stocks reported in Goodale *et al.* (2002) and Liski *et al.* (2003), both based on national inventory data, match the estimated values very closely.

Table 5.1: Total forest carbon values reported in other studies (TBMF = Temperate Broadleaf and Mixed Forests, TCF = Temperate Conifer Forests, BFT = Boreal Forests / Taiga). Pan *et al.* (2011) distinguished between continents and biomes. Goodale *et al.* (2002) and Liski *et al.* (2003) distinguished between continents only. Saugier *et al.* (2001) distinguished between biomes only.

Other Studies	Total Forest Carbon [Pg(C)]	N-America	Europe	Asia	Sum of 3 Continents	Saugier *et al.* (2001) ****
Pan *et al.* (2011) *	TBMF	**19.4**	**10.5**	**8.3**	**38.2**	139
	TCF					
	BFT	**14.0**	**12.1**	**27.9**	**53.9**	57
	Sum of 3 Biomes	**33.4**	**22.6**	**36.2**	**92.1**	196
Goodale *et al.* (2002) **	Sum of 3 Biomes	31.3	52.2		83.5	
Liski *et al.* (2003) ***	Sum of 3 Biomes	31	49		80	

* Forest total living biomass from 2007; understorey vegetation may be excluded if very small compared to total biomass; excluding Australia, New Zealand and "other countries"
** Live vegetation from 1990; including understorey vegetation
*** Woody biomass on forest and other wooded land in temperate and boreal forests; including dead trees; including shrubs and bushes; from early/mid 1990s; China, Korea and Japan excluded
**** Carbon in living phytomass; including understorey vegetation; based on different studies

In terms of carbon density, the values stated by Pan et al. (2011) are most often within the uncertainty of the estimates derived from BIOMASAR-II, but they report higher values in North-America, especially in boreal forests (compare Tables 5.2 and 2.4). Saugier *et al.* (2001) again strongly overestimate the carbon density in temperate, but not in boreal forests. Carbon density estimates by Goodale *et al.* (2002) and Liski *et al.* (2003) are very close to the derived carbon density in North-America, but slightly lower in Eurasia. Such comparisons are, however, always influenced by differences in the biomass retrieval method, the considered forest area and biomass compartments (including or not understorey biomass) as well as the investigation period (Thurner *et al.*, 2014). The proven accuracy of the carbon density map would also allow for the derivation of carbon stock and density estimates at finer spatial (e.g. for regions or countries instead of continents) and thematic (e.g. for tree species instead of leaf types) scales.

Table 5.2: Carbon density values calculated from other studies (TBMF = Temperate Broadleaf and Mixed Forests, TCF = Temperate Conifer Forests, BFT = Boreal Forests / Taiga). Pan *et al.* (2011) distinguished between continents and biomes. Goodale *et al.* (2002) and Liski *et al.* (2003) distinguished between continents only. Saugier *et al.* (2001) distinguished between biomes only.

Other Studies	Carbon Density [kg(C) m-2 (Forest)]	N-America	Europe	Asia	Mean of 3 Continents	Saugier *et al.* (2001) ****
Pan *et al.* (2011) *	TBMF	**7.55**	**7.27**	**4.47**	**6.51**	13.35
	TCF					
	BFT	**6.10**	**5.28**	**4.12**	**4.76**	4.15
	Mean of 3 Biomes	**6.87**	**6.05**	**4.20**	**5.35**	8.13
Goodale *et al.* (2002) **	Mean of 3 Biomes	4.46	3.88		4.07	
Liski *et al.* (2003) ***	Mean of 3 Biomes	4.3	4.3		4.3	

* Forest total living biomass and forest area data from 2007; understorey vegetation may be excluded if very small compared to total biomass; excluding Australia, New Zealand and "other countries"
** Live vegetation and total forest and woodland area from 1990; including understorey vegetation
*** woody biomass on forest and other wooded land in temperate and boreal forests; including dead trees; including shrubs and bushes; from early/mid 1990s; China, Korea and Japan excluded
**** Carbon in living phytomass; including understorey vegetation; based on different studies; using biome area instead of forest area

While the uncertainty of the carbon density product has been estimated to be within 20 – 40 % in high carbon density areas, very high uncertainties occur in low carbon density regions. However, the applied uncertainty analysis gives a conservative uncertainty estimate and should be interpreted as an upper bound. Total uncertainty is calculated as the sum of biomass compartment uncertainties, potentially leading to an overestimation (Taylor, 1997; cf. Fig. 2.12). The independent evaluation has shown that the carbon density map is valid even in areas where a high relative uncertainty has been estimated. The accuracy of the product has been demonstrated by a comparison to up-scaled forest inventory data at a regional scale. A slight underestimation of very high carbon density values may occur as a result of the application of C-band radar data with its relatively short wavelength, however such high GSV values (> 300 m^3 ha^{-1}) rarely exist in the study region (Santoro *et al.*, 2015).

Uncertainties associated with the applied land use – land cover dataset (GLC2000) could not be accounted for in the uncertainty estimate. On the one hand, pixels might be

misclassified, influencing the applied wood density and allometric relationship as well as the calculated forest area. On the other hand, sub-pixel heterogeneities cannot be considered. The relatively low tree cover threshold of 15 % used in GLC2000 for classification of forests (Bartholomé & Belward, 2005) ensures including also sparsely forested areas, where GSV is expected to be small as well.

5.2 Frost, drought and insects as forest mortality agents

Along spatial gradients in boreal forests, *k* has been found to be explained by climate variables describing winter length and winter temperature. These results suggest that *k* is related to frost damage effects and the trade-off between growth and frost adaptation in boreal forest ecosystems. Minimum winter temperature is considered the most important bioclimatic limit determining the global distribution of (tree) species (Sakai & Weiser, 1973; Woodward & Williams, 1987; Harrison *et al.*, 2010). Different species have different cold tolerances, below which mortality levels increase as a result of complex effects of low temperatures, including biochemical and structural effects of freezing plant and soil water on plant cells, which can be modified by snow cover insulation (Sakai & Larcher, 1987).

A detailed overview on frost stress induced mortality mechanisms and feedbacks is visualized in Fig. 5.1. Winter temperatures below 0°C lead to soil freezing, limiting the soil water availability to roots. The resulting desiccation of the xylem can lead to tree mortality by hydraulic failure (Sakai & Larcher, 1987), which can also occur as a result of xylem embolism caused by frequent freeze-thaw cycles of the water taken up by the roots (Sperry & Sullivan, 1992). In general, desiccation and xylem embolism decrease the resistance of the forest towards other mortality agents, during the autumn-winter-spring season most importantly wind throw (Schlyter *et al.,* 2006). Wind can also further intensify desiccation itself (Sakai & Larcher, 1987). Furthermore, the occurrence of spring frost can lead to physical damage if new shoots already have been developed (Cannell & Smith, 1986). Mortality from physical damage of the whole tree can also be caused by ice storms (Sun *et al.,* 2012). In addition, a long period of chilly days require a long dormancy during winter, diminishing the available growing season length (Harrison *et al.,* 2010). This way, mortality can occur as an indirect consequence of winter length due to decreases in GPP and growth efficiency, for instance preventing trees from developing the required resistance to frost and winter desiccation (Tranquillini, 1979). According to this hypothesis dating back to Michaelis (1934a,b), the short growing season does not permit for the differentiation of new shoots and the

full development of the cuticular resistance to transpiration in trees along alpine timberlines, facilitating desiccation during winter (Wardle, 1971; Tranquillini, 1979). These theories have mainly been established in order to explain the physiological ecology of the alpine timberline, but have also been confirmed at the polar timberline (Holtmeier, 1971). However, so far they have rarely been applied to explain the spatial patterns of *k* along gradients in boreal forests.

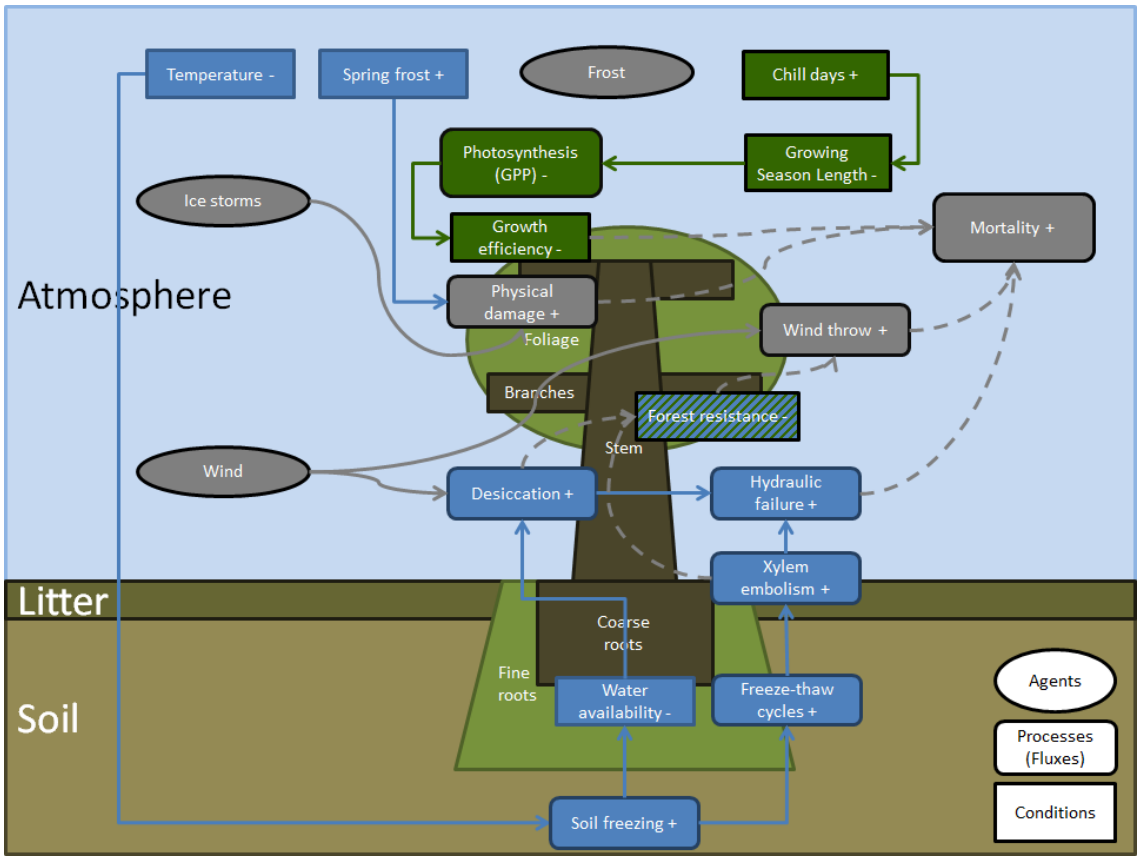

Fig. 5.1: Frost stress induced mortality mechanisms and feedbacks (+ indicates an increase; - indicates a decrease)

Unlike in boreal forests, *k* is found to be explained by climate conditions favouring drought and insect outbreaks along spatial gradients in temperate forests. Drought stress has been reported to lead to an increased mortality in forests all over the world, with numerous examples in temperate, but also boreal forests (Allen *et al.,* 2010). For instance, regionally elevated forest mortality in the South-West USA is very likely driven by drought stress, implying both catastrophic mortality events (Breshears *et al.,* 2005) and long-term forest background mortality (Williams *et al.,* 2010). Increased forest mortality as a consequence of warm and dry conditions has also been observed in

Western Europe (Bréda *et al.,* 2006). Forest mortality has been related to drought in boreal forests as well (Michaelian *et al.,* 2011; Peng *et al.,* 2011; Ma *et al.,* 2012); however, the data used in these field studies are usually located close to the southern boundary of boreal forests, while measurements are underrepresented towards the North, potentially explaining the different findings in this thesis.

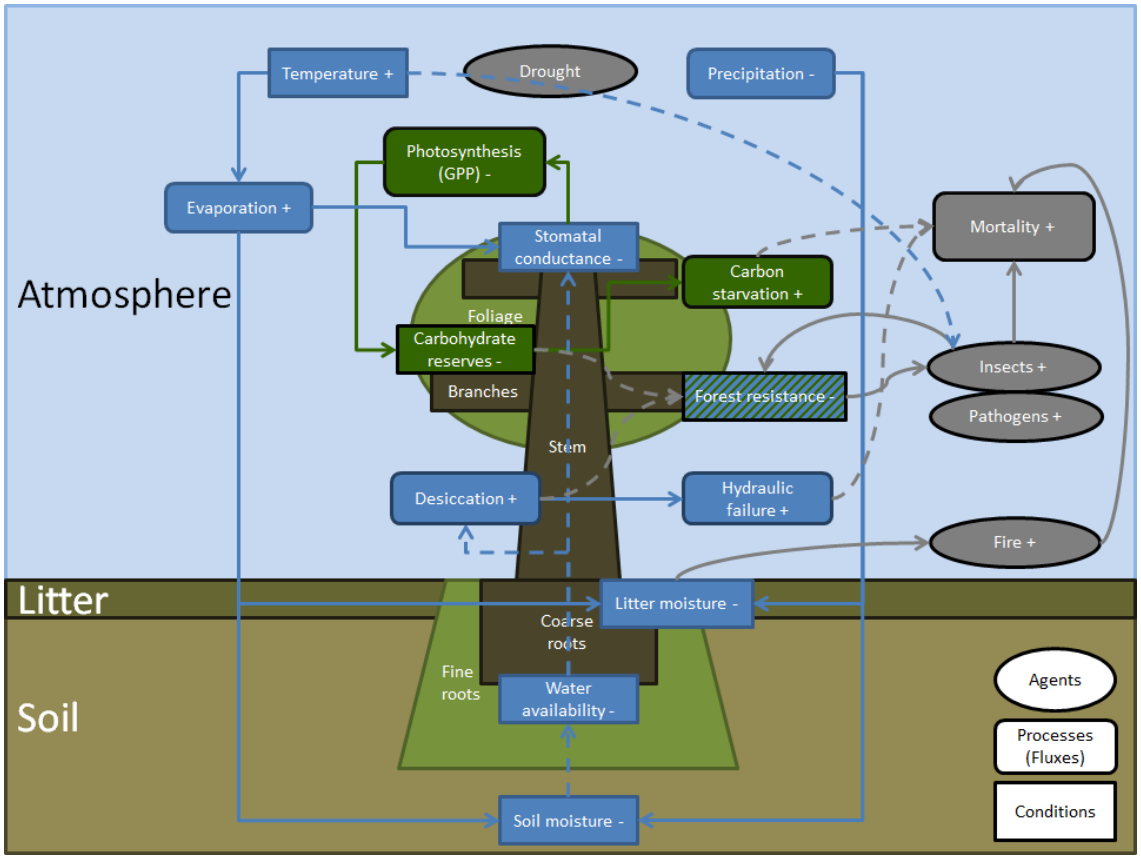

Fig. 5.2: Drought stress induced mortality mechanisms and feedbacks (+ indicates an increase; - indicates a decrease)

Fig. 5.2 illustrates drought stress induced mortality mechanisms and feedbacks. Drought periods, most importantly involving low levels of precipitation, lead to a decrease in soil moisture content, limiting the plant available water. Two mechanisms of drought related mortality are distinguished and are still under debate: Hydraulic failure and carbon starvation (Sala *et al.*, 2010; Mitchell *et al.*, 2013). Hydraulic failure is the direct consequence of xylem desiccation. On the other hand, limited water availability has a negative effect on stomatal conductance, not allowing the tree to assimilate enough carbon required for photosynthesis. Ultimately, this will lead to a depletion of carbohydrate reserves, resulting in mortality by carbon starvation (McDowell *et al.,*

2008; McDowell *et al.,* 2011; Hartmann *et al.*, 2013). Both desiccation and low carbohydrate reserves reduce forest resistance, making the individual trees more susceptible to insect attacks and pathogen infestations, which themselves further amplify this feedback, potentially leading to forest mortality at landscape scale. In addition, drought during the summer season may be accompanied by heat waves, causing increased evaporation, and benefiting the acceleration of the generation cycle of insects (Raffa *et al.,* 2008). Increased evaporation, along with the lack of precipitation, diminishes not only soil, but also litter moisture, facilitating the occurrence of fires (Williams *et al.*, 2010). On the other hand, an increased evaporation rate together with low relative humidity increase the transpiration rate, further reducing the plant water content, or finally leading to stomatal closure (Allen *et al.,* 2010; McDowell *et al.,* 2011).

In North-America, insect outbreaks are considered to be the most important disturbance agent (Logan *et al.,* 2003). Minimum winter temperature is known to be the most important control of insect survival during winter (Bale *et al.,* 2002), bark beetles being studied most intensively (Safranyik & Carroll*,* 2006). In case minimum winter temperatures do not fall below critical lower limits, some insects, for instance bark beetles, can proceed in their generation cycle (Williams & Liebhold*,* 2002). In general, increased temperatures can allow them to produce several generations during one year, favouring an epidemic outbreak if also other conditions are met (Raffa *et al.,* 2008). Similar controls have been observed for pathogens native to temperate forests (Bergot *et al.,* 2004; Chavarriaga *et al.,* 2007), although research on the importance of pathogens is underrepresented. In addition to increases in k and consequent reductions in forest biomass, bark beetle attacks have been found to lead to increases in NPP at landscape level over the long-term, since the beetles prefer attacking the largest trees, enabling surviving understory and smaller trees to grow faster due to reduced competition for light, water and nutrients (Raffa *et al.,* 2008). While increases in mortality might be best explained by drought stress in water-limited temperate forests, mortality in energy-limited temperate forests might be mostly related to insects and pathogens (Das *et al.,* 2013).

In the future, a strong decrease in cold temperature extremes and the number of frost days together with an increase in warm temperature extremes are projected by CMIP5 models in boreal forest regions, whereas the length of drought periods is predicted to decline (cf. Chapter 1.1; Sillmann *et al.*, 2013; in Collins *et al.*, 2013). These projections seem to indicate a diminished exposure of boreal forests to frost stress induced mortality

towards the end of this century. In this context, there are also indications that changes in winter length and temperature in the Northern edge of boreal forests lead to a shift of the treeline further to the North (Urban *et al.,* 2014). Nevertheless, bud break during spring might occur earlier in response to rising temperatures, increasing the vulnerability to temperature backlashes during the early growing season (Cannell & Smith, 1986; Jönsson *et al.*, 2004). Furthermore, the expected reduction in frost days and minimum temperatures will have effects on the life-cycles of insects and their interaction with host tree species, and ultimately this might lead to the expansion of severe insect and also pathogen epidemics towards boreal forests (Kurz *et al.*, 2008). In temperate forest regions, in contrast, the projected increase in warm temperature extremes together with a decrease in cold temperature extremes, a decline in the number of frost days and the predicted rise in the duration of drought periods (cf. Chapter 1.1; Sillmann *et al.*, 2013; in Collins *et al.*, 2013) will likely be intensifying large-scale forest mortality. The frequency and severity of droughts and heat waves as well as insect and pathogen outbreaks are favoured by such climate conditions (Reichstein *et al.*, 2013; Frank *et al.*, 2015).

5.3 A need for improved mortality schemes in global vegetation models

The performance of the investigated GVMs regarding the spatial patterns of k and its relationship to climate variables is very different between models, depending on the ability to reproduce observed NPP and implemented mortality algorithms (cf. Chapter 4). In terms of NPP, most of the models are within 20 % of observed overall averages for boreal and temperate forests. Only HYBRID4 shows a severe overestimation, especially in boreal forests. On the other hand, correlation between models and observations is often weak ($r \leq 0.65$) for NPP, with few exceptions of moderate correlation. For k and biomass, there is a much weaker correlation between all models and also in their comparison to observations. Deviation from observed k ranges from -61.5 to -6.6 % in boreal and from -60.3 to 10.3 % in temperate forests. Most models, except for JeDi and VISIT, severely overestimate biomass, indicating important shortcomings in the considered mortality processes. Although JeDi and VISIT reproduce the observed average biomass, they do not capture its spatial variability. Overall, none of the models compares sufficiently well to the observed spatial patterns in k. The errors in k are more strongly related to the errors in biomass than to the errors in NPP, across all models and in boreal as well as in temperate forests (cf. Chapter 4.5).

These findings illustrate the high uncertainty in carbon turnover processes and, as a consequence, the need for improvements, in addition to existing uncertainties in modelled NPP.

As a next step, mortality agents like frost stress, drought stress and insect epidemics should be considered in GVMs. Processes like frost-induced xylem embolism (Sperry & Sullivan, 1992), desiccation (Sakai & Larcher, 1987) and forest destruction by ice storms (Sun *et al.*, 2012) are considered to be key mortality mechanisms in forest ecosystems (Reichstein *et al.*, 2013). However, direct frost damage effects on mortality are usually not accounted for in GVMs, for instance among the GVMs participating in ISI-MIP only HYBRID4 considered frost stress impacts on the carbon balance potentially leading to tree mortality. Due to growth efficiency (in LPJml) and NPP dependent mortality rates (JeDi, LPJml, SDGVM), some ISI-MIP models already include a kind of trade-off between growth and development of frost resistance. Thus simulated spatial relationships between k and winter length agree relatively well with observations in some of the explored boreal forest transects. Among other improvements, a recent study (Zhu *et al.*, 2015) introduced a tree mortality rate increasing linearly with decreasing winter temperature and a broadleaf tree mortality caused by spring frost after bud break in a new version of ORCHIDEE. Furthermore, cold hardiness and related frost damage has been implemented within the ecosystem model LPJ-GUESS (Rammig *et al.*, 2010). Beside these examples, frost-driven mortality seems to be largely underrepresented in current GVMs and also in forest ecology research in general, although the basic mechanisms are known (Sakai & Larcher, 1987).

Moreover, it has been shown recently that total ecosystem carbon turnover time covaries more strongly with precipitation globally than considered in ESMs (Carvalhais *et al.*, 2014). In temperate forests, NPP was found to further increase despite longer periods of drought in most of the investigated models, indicating missing or insufficient controls of productivity by the water cycle. Concerning mortality processes, soil or litter moisture affect leaf turnover (HYBRID4, ORCHIDEE) or fire (LPJml, OPRCHIDEE, SDGVM, VISIT) in some ISI-MIP models, and indirect feedbacks of water availability are implemented in terms of NPP, growth efficiency, or carbon balance dependent mortality (HYBRID4, JeDi, LPJml, SDGVM). However, further observed hydrological feedbacks are usually not considered by the investigated GVMs, most importantly direct drought effects like carbon starvation or hydraulic failure (only in HYBRID4; Sala *et al.*, 2010; McDowell *et al.*, 2011; Hartmann *et al.*, 2013) or drought-favoured

susceptibility to insect and pathogen epidemics (Raffa *et al.*, 2008; Williams *et al.*, 2010) as well as to wind-throw (Schlyter *et al.*, 2006). In addition, integrating fire modules into GVMs is essential in order to correctly account for long-term fire return intervals in response to moisture conditions (Thonicke *et al.*, 2001). The impact of soil available water on fire occurrence has been shown to substantially affect vegetation carbon density in permafrost regions (Beer *et al.*, 2007).

Modelling turnover dependent on climate conditions favouring insect epidemics can serve as a proxy to reproduce the large-scale spatial impact of these mortality agents. The explicit incorporation of the life-cycle of insects into GVMs would be the ultimate step to be taken. In the field of forestry, research on this problem is already ongoing, and available conceptual frameworks and models representing insect population dynamics (e.g. Logan *et al.*, 2003, Régnière & Bentz, 2007; Kurz *et al.*, 2008; Raffa *et al.*, 2008) should be evaluated concerning their integration into GVMs. This would require the adjustment of processes and parameters in order to cover region-specific differences in insect populations and their dynamics.

Finally, interacting effects of different processes and their importance at global scale also need to be investigated. For instance, first attempts of coupled fire and insect outbreak models have been made (Chen-Charpentier & Leite, 2014). In addition, forest management and its influence on mortality rates needs to be improved in GVMs. Only one example is the effect of human activities in fire modelling (Le Page *et al.*, 2015).

Furthermore, climate-dependent phenology can contribute to overall turnover rates. This is the case in HYBRID4, JULES and ORCHIDEE, where soil moisture stress and/or low temperatures influence leaf longevity and turnover. Phenology limited by cold temperatures, heat stress, light and water availability has already been shown to improve biomass spatial patterns simulated by LPJml compared to the original model version used in ISI-MIP (Forkel *et al.*, 2014). In addition to direct effects on leaf turnover, phenology can also influence mortality indirectly through impacts on productivity (Xia *et al.*, 2015), carbon allocation and the vegetation distribution in DGVMs. Nevertheless, as long as climate-related mortality processes are not considered, a climate-dependent phenology alone does not enable models to correctly reproduce long-term carbon dynamics.

5.4 Impact of carbon turnover uncertainty on the land carbon balance

A process based implementation of mortality agents like frost stress, drought stress and insect epidemics would allow to quantify their impact on the simulated land carbon balance under climate change conditions (Friedlingstein *et al.*, 2006; McDowell *et al.*, 2011; Ahlström *et al.*, 2012). The impact of the uncertainty in carbon turnover on the land carbon balance is underrepresented in the literature, despite its importance (Delbart *et al.*, 2010; Galbraith *et al.*, 2013; Friend *et al.*, 2014). The observed carbon density map can also be used to adjust simulated carbon stocks in models directly, e.g. by adjustments in turnover rate. In a first test, the default woody biomass turnover time (= 40 years in all boreal and temperate PFTs) in JSBACH, the land surface component of the Max Planck Institute (MPI) ESM (Raddatz *et al.*, 2007), was adjusted in order to match the observed average BIOMASAR-II biomass per PFT in 2010.

In most areas across boreal and temperate forests, JSBACH overestimated the observed biomass by default. A lower biomass was achieved by lower turnover rates in temperate broadleaf deciduous and coniferous evergreen forests, resulting in lower simulated litter fluxes, soil carbon, heterotrophic respiration, and finally lower net ecosystem exchange (NEE = - NEP; Fig. 5.3). During 2001-2010, NEE was modified between ca. -110 % and +5 % for 90 % of the study area. Most important decreases in NEE occurred in boreal forests of Canada, Central Siberia and South Scandinavia and also in some temperate forests of Central and East Europe and in the South-East US. Slight increases in NEE are simulated in parts of East Siberia and some other arctic regions due to a higher turnover time implemented for coniferous deciduous forests. Modelled northern-hemispheric total forest NEE was found to decrease significantly from -0.530 PgC y^{-1} to -0.656 PgC y^{-1} when making use of the observation based carbon density map. For 1.86 % of the northern-hemispheric (30-80°N) forest area the change in biomass turnover leads to a switch from a carbon source to a sink. On the other hand, only 0.17 % of the forest area turn from a carbon sink to a source. This example illustrates that even small relative changes in turnover rates and dependent fluxes (litter flux, heterotrophic respiration) can lead to large relative changes in NEE, which is approximately the small difference of two large fluxes, i.e. heterotrophic respiration and NPP (in absence of disturbances; cf. Eq. 1.2). In addition, also (maintenance) autotrophic respiration is dependent on vegetation biomass (Thornley, 1970), but this relationship is not considered by JSBACH.

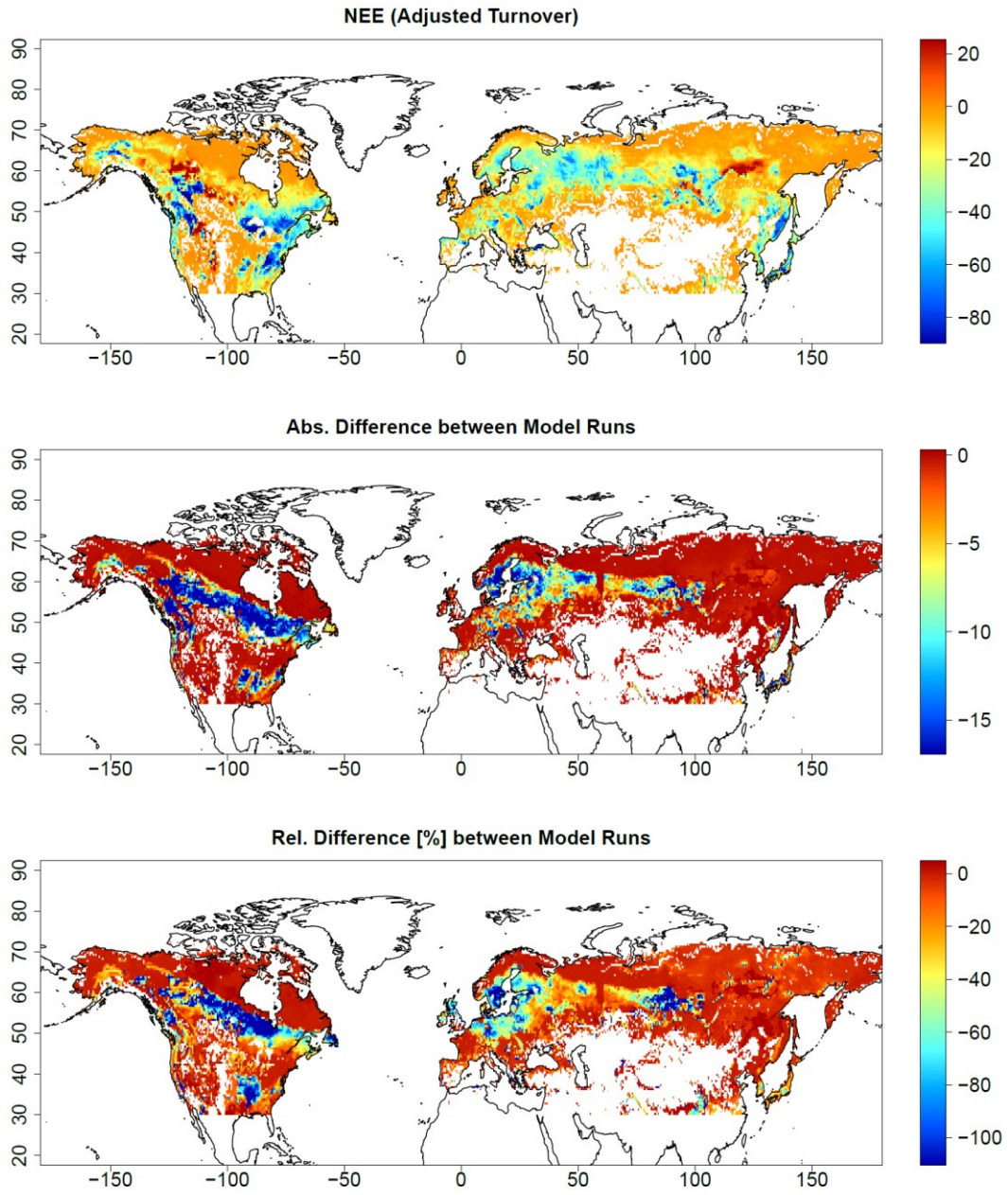

Fig. 5.3: Simulated NEE (gC m^{-2} y^{-1}) by JSBACH after adjusting *k* (top). Negative values indicate carbon sinks, positive values indicate carbon sources. Absolute (gC m^{-2} y^{-1}) (centre) and relative (%) (bottom) differences between model runs with adjusted and default *k*. Negative values indicate a decrease in NEE in the model run with adjusted *k* compared to the model run with default *k*, and vice versa.

5.5 Outlook

Envisat/ASAR data are not perfectly suited to be related to stem volume, but other SAR datasets are currently not available globally and at no cost (Thurner *et al.*, 2014). This situation might improve with the launch of upcoming earth observation missions.

Especially the BIOMASS mission, applying a fully polarimetric P-band SAR sensor (Le Toan *et al.*, 2011), could potentially be very promising in this respect. However, it is very likely that the radar sensor will not be permitted to operate over North America and Europe, due to interference with the US missile warning system, leaving ALOS-2 an option with longer wavelength (L-band) for studies in these areas (ESA, 2012). Other recent and future projects and missions with the potential to improve global carbon stock estimates and distributions include the European Space Agency's (ESA) GlobBiomass project (GlobBiomass, 2016), integrating available earth observation and *in situ* data, and NASA's Global Ecosystem Dynamics Investigation Lidar (GEDI; Neeck, 2015) mission, inferring biomass from forest vertical structure.

The presented carbon density map remains unvalidated at its original resolution (0.01°). A direct comparison to forest inventory biomass usually involves the problem of up-scaling, since field data represent a different spatial scale (Gibbs *et al*., 2007; Saatchi *et al*., 2007, 2011). For such a task, the application of air- or spaceborne LiDAR is considered most promising (Patenaude *et al*., 2004; Saatchi *et al*., 2011). In the future, also GSV products with higher spatial resolution and increased accuracy at finer scales are expected to become available globally from radar remote sensing. First tests using ALOS/PALSAR L-band data at selected study regions already have investigated their potential (Santoro *et al.*, 2014). Such high resolution GSV data could be used to study the spatial scale at which disturbances are occurring, the relationship between forest stand attributes (e.g. forest age) and biomass spatial variation or the impact of the consideration of biomass small-scale heterogeneity in GVMs on the simulated carbon dynamics.

Furthermore, the derived carbon density map could be improved by the use of a global tree species dataset instead of leaf types only. However, such products are not available so far, but could for example be applied over Europe (Köble & Seufert, 2001). This would allow to derive wood densities and allometric relationships for tree species separately. In addition, a better coverage of biomass compartment measurements across tree species and all climate zones would allow for a more detailed exploitation of the Global Biomass Compartment Database and thus improve the accuracy of the carbon density map.

Multi-temporal observations (at times $t1$ and $t2$) of forest biomass from remote sensing, in addition to virtually continuous estimates of NPP, could enable the derivation of k independent of the steady-state assumption:

$$Biomass_{t2} = Biomass_{t1} + \sum_{i=t1}^{t2} NPP_i - \sum_{i=t1}^{t2} (k_i \cdot Biomass_i) \quad \text{(Eq. 5.1)}$$

$$\approx Biomass_{t1} + \sum_{i=t1}^{t2} NPP_i - k \cdot \frac{Biomass_{t1} + Biomass_{t2}}{2}$$

$$\Leftrightarrow k \approx 2 \cdot \frac{Biomass_{t1} - Biomass_{t2} + \sum_{i=t1}^{t2} NPP_i}{Biomass_{t1} + Biomass_{t2}}$$

For such an approach, the uncertainty in biomass observations needs to be considerably smaller than the difference in biomass between observation times $t1$ and $t2$. However, this approach still involves the simplifications of a constant turnover rate over time and of a linear change in biomass over time between $t1$ and $t2$, which might not be met in case of a disturbance occurring at the spatial scale of interest between the two observation times. In general, changes in *k* over time remain unexplored. Observations which would allow to analyse the response of *k* to climate change are not available from remote sensing and require long-term networks of field studies. However, as shown in this thesis, spatial patterns might be used to infer information on temporal processes (space-for-time substitution; e.g. applied in Williams *et al.*, 2013).

The analysis of broad-scale patterns in remote sensing based *k* has enabled the identification of hot-spot regions of increased *k*, which should be investigated in detail in a network of field studies. Here, considerable spatial gradients towards the northern edges of boreal and towards the southern edges of temperate forests have been identified. Only field studies will allow for an improved understanding of the mortality mechanisms underlying these observed gradients. While the information gained in this work can be used to implement empirical relationships between *k* and climate variables in GVMs in order to improve the spatial patterns of simulated biomass, results from field studies will further facilitate a process-based consideration of the underlying mechanisms.

A direct implementation of the spatial relationships between *k* and climate variables in GVMs is hampered by the observed differences between regions. In addition to spatial differences in the interaction with other climate influences, differences in adaptation strategies are likely responsible for these patterns. For instance, geographically marginal populations, which are used to more extreme climatic conditions, have been found to be more strongly adapted to frost (Kreyling *et al.,* 2014) and drought (Thiel *et al.,* 2014) than central populations. The response of mortality rates to drought differs between species and may also change over time, potentially leading to changes in species

composition over the long-term, benefiting the better adapted or adapting species (Barbeta *et al.,* 2013). Adaptation itself is driven by a trade-off between growth and mortality by either frost in boreal (Schreiber *et al.,* 2013) or drought in temperate forests (Thiel *et al.,* 2014). Moreover, the presented results support evidence that the spatial distribution of leaf types can be considered a direct consequence of adaptation to climate (Sakai and Weiser*,* 1973; Woodward and Williams*,* 1987; Harrison *et al.,* 2010), since no substantially different deviations from the relationships between *k* and climate depending on the leaf type have been found. The impact of adaptation and biodiversity on the effects of climate in general and climate extremes in particular on the carbon cycle remain largely unknown (Reichstein *et al.*, 2013).

In addition to the knowledge gaps on mortality processes, GVMs show also large differences in simulated NPP (cf. Chapter 4.3). Concerning the uncertainty in NPP components, there are still important open research questions on the dependency of plant respiration (e.g. Atkin & Tjoelker, 2003; Piao *et al.*, 2010; Smith & Dukes, 2013) and allocation fractions to carbon pools (e.g. Friedlingstein *et al.*, 1999; Litton *et al.*, 2007; Wolf *et al.*, 2011) on environmental conditions, especially at the spatial and temporal scales relevant to GVMs. For instance, the ratio of biomass production to GPP is suggested to be related to nutrient availability (Vicca *et al.*, 2012) or management (Campioli *et al.*, 2015). Carbon allocation results in the ratio of carbon pools having different turnover times (i.e., living tissue pools with shorter turnover times versus woody vegetation components pools with longer turnover times) and hence inherently contributes to faster/slower turnover not directly related to mortality. In contrast to plant respiration and carbon allocation, GPP and its relation to climate is relatively well known at a global scale (Luyssaert *et al.*, 2007; Beer *et al.*, 2010), but there is still considerable uncertainty in simulated GPP between models and their comparison to observations (Schaefer *et al.*, 2012; Piao *et al.*, 2013).

Overall, a process based consideration of forest mortality will allow for an improved assessment of the impact of climate change on forest carbon stocks in the future. Increased mortality in response to more frequent and severe climate extremes might counteract the CO_2 fertilization effect on productivity and turn the World's forests from a carbon sink into a carbon source (Kurz *et al.*, 2008; Reichstein *et al.*, 2013; Frank *et al.*, 2015). Information obtained from remote sensing products is essential to investigate the spatially and temporally variable turnover processes, whereas the sole reliance on field studies is suspected to lead to biases in the estimated carbon balance, since disturbance events might not be covered (Fisher *et al.*, 2008).

CHAPTER 6

Summary

(1) How much carbon is currently stored in Northern Hemisphere boreal and temperate forests? How are forest carbon stock and density spatially distributed?

A carbon density map with a spatial resolution of 0.01° was derived from a GSV product based on radar remote sensing, covering the Northern Hemisphere boreal and temperate forests (30-80°N). For this conversion, forest inventory databases on wood density and biomass allometry have been applied, allowing for detailed information on stem, branches, root and foliage carbon. In addition, a conservative uncertainty estimate has been derived, accounting for the uncertainty in GSV, wood density and allometric relationships. An evaluation of the resulting carbon density map by comparing to up-scaled forest inventory data revealed strong agreement at regional scale (r^2 = 0.70–0.90).

In 2010, 40.7 ± 15.7 PgC are stored in BFT, whereas TBMF and TCF contain 24.5 ± 9.4 PgC and 14.5 ± 4.8 PgC, respectively. In total, these numbers add up to 79.8 ± 29.9 PgC stored in northern boreal and temperate forests. In terms of carbon density, 6.21 ± 2.07 kgC m^{-2} are retained in TCF and 5.80 ± 2.21 kgC m^{-2} in TBMF, whereas BFT have a mean carbon density of 4.00 ± 1.54 kgC m^{-2}. European forests exhibit a higher carbon density across all the three biomes compared with North America and Asia, however these results are not always significant at the 95 % confidence interval. Highest carbon densities are located along the Rocky Mountains in north-west Canada and the USA, the European mountains (both mostly TCF), European Russia, southern central Siberia (TBMF, southern BFT) and Japan (mostly TBMF). The presented carbon density map greatly improves our current knowledge on the absolute amount and spatial distribution of carbon stocks, since it is the first spatially explicit approach covering the entire Northern Hemisphere boreal and temperate forests at a moderate spatial resolution. It

can also be used to derive spatially more detailed carbon stock and density values at the scale of countries or regions.

(2) *How is the spatial variation in boreal and temperate forest carbon turnover rate related to climate? Which mortality agents are responsible for the observed relationships?*

Forest *k* has been derived from remote sensing based products of NPP and carbon density at 0.5° resolution. Based on this approach, for the first time the effects of interacting mortality processes and their relevance at continental scale could be investigated. In contrast to field studies, the whole variety of turnover processes (litterfall, background mortality, and all kinds of disturbances) at landscape scale over long time periods could be captured. In boreal forests, the spatial variation of *k* is found to be related to winter length and temperature, indicating direct and indirect frost damage effects on forest mortality. In temperate forests, in contrast, climatic conditions favouring drought stress and insect or pathogen outbreak related mortality can explain the spatial variation in *k*. Applying different NPP products confirmed these results. Possible confounding factors, including soil conditions and forest management, can hardly explain the observed spatial gradients, however spatial gradients in tree cover correlate with gradients in climate in boreal forests. In addition to forest mortality, (climate) controls on autotrophic respiration and carbon allocation might contribute to the observed spatial patterns in *k* and need to be explored further.

(3) *Are the observation based relationships between turnover rate and climate reproduced by GVMs? Which climate-related mortality processes are represented in GVMs and which are required for an improved simulation of turnover rate spatial patterns?*

Simulated vegetation carbon and NPP by GVMs participating in ISI-MIP (HYBRID4, JeDi, JULES, LPJml, ORCHIDEE, SDGVM, VISIT) have been used to calculate a model based *k* at a spatial resolution (0.5°) and time span comparable to the observation based *k*. The investigated GVMs comprise different levels of complexity of implemented mortality processes, including or not background mortality, competition,

fire, growth efficiency dependent, NPP dependent, or carbon balance dependent mortality, heat stress, and climate effects on phenology. Along the selected transects in boreal and temperate forests, the observation based findings are reproduced by the models only to a limited extent, depending on the ability to match observation based NPP and on the implemented mortality algorithms. Concerning NPP, most of the models are within 20 % of observed overall averages for boreal and temperate forests, although correlation between models and observations is often weak ($r \leq 0.65$) with only few exceptions of moderate correlation. Correlations are even much weaker regarding biomass and *k*. Deviations from observation based *k* range from -61.5 % to -6.6 % in boreal and from -60.3 % to 10.3 % in temperate forests, and can be attributed mostly to severe overestimations of observed biomass. These results highlight the importance of improving mortality concepts in GVMs. Further research should concentrate on incorporating frost damage effects and the trade-off between growth and frost adaptation in boreal forests into mortality schemes of GVMs, whereas the effects of drought and insect epidemics on mortality need to be considered in temperate forests.

Die gefährlichste Weltanschauung ist die Weltanschauung derer,
die die Welt nie angeschaut haben.

Alexander Freiherr von Humboldt (zugeschrieben)

References

Ahlström A, Schurgers G, Arneth A, Smith B (2012) Robustness and uncertainty in terrestrial ecosystem carbon response to CMIP5 climate change projections. Environmental Research Letters, **7**, 044008.

Akaike H (1974) A new look at the statistical model identification. IEEE Transactions on Automatic Control, **AC-19**, 716-723.

Allen CD, Macalady AK, Chenchouni H *et al.* (2010) A global overview of drought and heat-induced tree mortality reveals emerging climate change risks for forests. Forest Ecology and Management, **259**, 660-684.

Allen CD, Breshears DD, McDowell N (2015) On underestimation of global vulnerability to tree mortality and forest die-off from hotter drought in the Anthropocene. Ecosphere, **6**, 1-55.

Atkin O (2003) Thermal acclimation and the dynamic response of plant respiration to temperature. Trends in Plant Science, **8**, 343-351.

Baccini A, Goetz SJ, Walker WS *et al.* (2012) Estimated carbon dioxide emissions from tropical deforestation improved by carbon-density maps. Nature Climate Change, **2**, 182-185.

Bale JS, Masters GJ, Hodkinson ID *et al.* (2002) Herbivory in global climate change research: direct effects of rising temperature on insect herbivores. Global Change Biology, **8**, 1-16.

Barbeta A, Ogaya R, Penuelas J (2013) Dampening effects of long-term experimental drought on growth and mortality rates of a Holm oak forest. Global Change Biology, **19**, 3133-3144.

Bartholomé E, Belward AS (2005) GLC2000: a new approach to global land cover mapping from Earth observation data. International Journal of Remote Sensing, **26**, 1959-1977.

Bates DM, Watts DG (1988) *Nonlinear Regression Analysis and Its Applications*, New York, Wiley.

Beaudoin A, Bernier PY, Guindon L *et al.* (2014) Mapping attributes of Canada's forests at moderate resolution throughkNN and MODIS imagery. Canadian Journal of Forest Research, **44**, 521-532.

Beer C, Lucht W, Schmullius C, Shvidenko A (2006) Small net carbon dioxide uptake by Russian forests during 1981–1999. Geophysical Research Letters, **33**, L15403.

Beer C, Lucht W, Gerten D, Thonicke K, Schmullius C (2007) Effects of soil freezing and thawing on vegetation carbon density in Siberia: A modeling analysis with the Lund-Potsdam-Jena Dynamic Global Vegetation Model (LPJ-DGVM). Global Biogeochemical Cycles, **21**, GB1012.

Beer C, Reichstein M, Tomelleri E *et al.* (2010) Terrestrial gross carbon dioxide uptake: global distribution and covariation with climate. Science, **329**, 834-838.

Bergot M, Cloppet E, Perarnaud V, Deque M, Marcais B, Desprez-Loustau M-L (2004) Simulation of potential range expansion of oak disease caused by Phytophthora cinnamomi under climate change. Global Change Biology, **10**, 1539-1552.

Bindoff NL, Stott PA, AchutaRao KM *et al.* (2013) Detection and Attribution of Climate Change: from Global to Regional. In: *Climate Change 2013: The Physical Science Basis. Contribution of Working Group I to the Fifth Assessment Report of the Intergovernmental Panel on Climate Change*. (eds Stocker TF, Qin D, Plattner G-K *et al.*] pp 867-952, Cambridge, United Kingdom and New York, NY, USA, Cambridge University Press.

Bolin B, Rodhe H (1973) A note on the concepts of age distribution and transit time in natural reservoirs. Tellus, **25**, 1, 58-62.

Bonan GB (2008) Forests and climate change: forcings, feedbacks, and the climate benefits of forests. Science, **320**, 1444-1449.

Bond-Lamberty B, Thomson A (2010) Temperature-associated increases in the global soil respiration record. Nature, **464**, 579-582.

Booth TH, Nix HA, Busby JR, Hutchinson MF, Franklin J (2014) BIOCLIM: the first species distribution modelling package, its early applications and relevance to most current MaxEnt studies. Diversity and Distributions, **20**, 1-9.

Bréda N, Huc R, Granier A, Dreyer E (2006) Temperate forest trees and stands under severe drought: a review of ecophysiological responses, adaptation processes and long-term consequences. Annals of Forest Science, **63**, 625-644.

Breshears DD, Cobb NS, Rich PM *et al.* (2005) Regional vegetation die-off in response to global-change-type drought. PNAS, **102**, 15144-15148.

Campioli M, Vicca S, Luyssaert S *et al.* (2015) Biomass production efficiency controlled by management in temperate and boreal ecosystems. Nature Geoscience, **8**, 843-846.

Canadian Forest Service (2010) National Fire Database - Agency Fire Data, Edmonton, Alberta, Natural Resources Canada, Canadian Forest Service, Northern Forestry Centre (available online at: http://cwfis.cfs.nrcan.gc.ca/en_CA/nfdb).

Cannell MGR (1982) *World forest biomass and primary production data,* London, Academic Press.

Cannell MGR, Smith RI (1986) Climatic warming, spring budburst and frost damage on trees. Journal of Applied Ecology, **23**, 177-191.

Carvalhais N, Forkel M, Khomik M *et al.* (2014) Global covariation of carbon turnover times with climate in terrestrial ecosystems. Nature, **514**, 213-217.

Chapin IIII FS, Matson PA, Mooney HA (2002) *Principles of terrestrial ecosystem ecology,* New York, Springer.

Chavarriaga D, Bodles WJ, Leifert C, Belbahri L, Woodward S (2007) Phytophthora cinnamomi and other fine root pathogens in north temperate pine forests. FEMS Microbiology Letters, **276**, 67-74.

Chave J, Coomes D, Jansen S, Lewis SL, Swenson NG, Zanne AE (2009) Towards a worldwide wood economics spectrum. Ecology Letters, **12**, 351-366.

Chen-Charpentier B, Leite MCA (2014) A model for coupling fire and insect outbreak in forests. Ecological Modelling, **286**, 26-36.

Ciais P, Schelhaas MJ, Zaehle S *et al.* (2008) Carbon accumulation in European forests. Nature Geoscience, **1**, 425-429.

Ciais P, Sabine C, Bala G *et al.* (2013) Carbon and Other Biogeochemical Cycles. In: *Climate Change 2013: The Physical Science Basis. Contribution of Working Group I to the Fifth Assessment Report of the Intergovernmental Panel on Climate Change*. (eds Stocker TF, Qin D, Plattner G-K *et al.*] pp 465-570, Cambridge, United Kingdom and New York, NY, USA, Cambridge University Press.

Clark DA, Brown S, Kicklighter DW, Chambers JQ, Thomlinson JR, Ni J (2001) Measuring net primary production in forests: concepts and field methods. Ecological Applications, **11**, 356-370.

Clark DB, Mercado LM, Sitch S *et al.* (2011) The Joint UK Land Environment Simulator (JULES), model description – Part 2: Carbon fluxes and vegetation dynamics. Geoscientific Model Development, **4**, 701-722.

Collatz GJ, Ball JT, Grivet C, Berry JA (1991) Physiological and environmental regulation of stomatal conductance, photosynthesis and transpiration: a model that includes a laminar boundary layer. Agricultural and Forest Meteorology, **54**, 107-136.

Collatz GJ, Ribas-Carbo M, Berry JA (1992) Coupled photosynthesis-stomatal conductance model for leaves of C4 plants. Aust. J. Plant Physiol., **19**, 519-538.

Collins M, Knutti R, Arblaster J *et al.* (2013) Long-term Climate Change: Projections, Commitments and Irreversibility. In: *Climate Change 2013: The Physical Science Basis. Contribution of Working Group I to the Fifth Assessment Report of the Intergovernmental Panel on Climate Change*. (eds Stocker TF, Qin D, Plattner G-K *et al.*] pp 1029-1136, Cambridge, United Kingdom and New York, NY, USA, Cambridge University Press.

Collins WJ, Bellouin N, Doutriaux-Boucher M *et al.* (2011) Development and evaluation of an Earth-System model – HadGEM2. Geoscientific Model Development, **4**, 1051-1075.

Cramer W, Kicklighter DW, Bondeau A *et al.* (1999) Comparing global models of terrestrial net primary productivity (NPP): overview and key results. Global Change Biology, **5 (Suppl. 1)**, 1-15.

Cubasch U, Wuebbles D, Chen D, Facchini MC, Frame D, Mahowald N, Winther J-G (2013) Introduction. In: *Climate Change 2013: The Physical Science Basis. Contribution of Working Group I to the Fifth Assessment Report of the Intergovernmental Panel on Climate Change*. (eds Stocker TF, Qin D, Plattner G-K *et al.*] pp 119-158, Cambridge, United Kingdom and New York, NY, USA, Cambridge University Press.

Das AJ, Battles J, Stephenson NL, Van Mantgem PJ (2011) The contribution of competition to tree mortality in old-growth coniferous forests. Forest Ecology and Management, **261**, 1203-1213.

Das AJ, Stephenson NL, Flint A, Das T, Van Mantgem PJ (2013) Climatic correlates of tree mortality in water- and energy-limited forests. PloS one, **8**, e69917.

Del Grosso S, Parton W, Stohlgren T *et al.* (2008) Global potential net primary production predicted from vegetation class, precipitation, and temperature. Ecology, **89**, 2117-2126.

Delbart N, Ciais P, Chave J, Viovy N, Malhi Y, Le Toan T (2010) Mortality as a key driver of the spatial distribution of aboveground biomass in Amazonian forest: results from a dynamic vegetation model. Biogeosciences, **7**, 3027-3039.

DeLucia EH, Drake JE, Thomas RB, Gonzalez-Meler M (2007) Forest carbon use efficiency: is respiration a constant fraction of gross primary production? Global Change Biology, **13**, 1157-1167.

Donat MG, Alexander LV, Yang H *et al.* (2013) Updated analyses of temperature and precipitation extreme indices since the beginning of the twentieth century: The HadEX2 dataset. Journal of Geophysical Research: Atmospheres, **118**, 2098-2118.

EFI (2005) LTFRA database, European Forest Institute (available online at: http://www.efi.int/portal/virtual_library/databases/, accessed 2012/06/08).

Efron B (1979) Bootstrap methods: another look at the jackknife. The Annals of Statistics, **7**, 1-26.

ESA (2012) Report for Mission Selection: Biomass, ESA SP-1324/1 (3 volume series). pp 193, Noordwijk, The Netherlands, European Space Agency.

ESRI (2008) Continents shapefile, Baruch College, City University of New York, Baruch Geoportal (available online at: http://www.baruch.cuny.edu/geoportal/data/esri/esri_intl.htm, accessed 2012/12/07).

FAO/IIASA/ISRIC/ISSCAS/JRC (2012) Harmonized World Soil Database (version 1.2), Rome, Italy and Laxenburg, Austria, FAO and IIASA.

Farquhar GD, Von Caemmerer S, Berry JA (1980) A biochemical model of photosynthetic CO2 assimilation in leaves of C3 species. Planta, **149**, 78-90.

Fisher JI, Hurtt GC, Thomas RQ, Chambers JQ (2008) Clustered disturbances lead to bias in large-scale estimates based on forest sample plots. Ecology Letters, **11**, 554-563.

Forkel M, Carvalhais N, Schaphoff S, V. Bloh W, Migliavacca M, Thurner M, Thonicke K (2014) Identifying environmental controls on vegetation greenness phenology through model–data integration. Biogeosciences, **11**, 7025-7050.

Frank D, Reichstein M, Bahn M *et al.* (2015) Effects of climate extremes on the terrestrial carbon cycle: concepts, processes and potential future impacts. Global Change Biology, **21**, 2861-2880.

Friedl MA, Sulla-Menashe D, Tan B, Schneider A, Ramankutty N, Sibley A, Huang X (2010) MODIS Collection 5 global land cover: Algorithm refinements and characterization of new datasets. Remote Sensing of Environment, **114**, 168-182.

Friedlingstein P, Joel G, Field CB, Fung IY (1999) Toward an allocation scheme for global terrestrial carbon models. Global Change Biology, **5**, 755-770.

Friedlingstein P, Cox P, Betts R *et al.* (2006) Climate–Carbon Cycle Feedback Analysis: Results from the C4MIP Model Intercomparison. Journal of Climate, **19**, 3337-3353.

Friend AD, Stevens AK, Knox RG, Cannell MGR (1997) A process-based, terrestrial biosphere model of ecosystem dynamics (Hybrid v3.0). Ecological Modelling, **95**, 249-287.

Friend AD, White A (2000) Evaluation and analysis of a dynamic terrestrial ecosystem model under preindustrial conditions at the global scale. Global Biogeochemical Cycles, **14**, 1173-1190.

Friend AD, Lucht W, Rademacher TT *et al.* (2014) Carbon residence time dominates uncertainty in terrestrial vegetation responses to future climate and atmospheric CO_2. PNAS, **111**, 3280-3285.

Galbraith D, Malhi Y, Affum-Baffoe K *et al.* (2013) Residence times of woody biomass in tropical forests. Plant Ecology & Diversity, **6**, 139-157.

Gibbs HK, Brown S, Niles JO, Foley JA (2007) Monitoring and estimating tropical forest carbon stocks: making REDD a reality. Environmental Research Letters, **2**, 045023.

Giglio L, Randerson JT, Van Der Werf GR (2013) Analysis of daily, monthly, and annual burned area using the fourth-generation global fire emissions database (GFED4). Journal of Geophysical Research: Biogeosciences, **118**, 317-328.

GlobBiomass (2016) Welcome to the ESA DUE Globbiomass project (http://globbiomass.org/, accessed 2016/04/06).

Goll DS, Brovkin V, Parida BR *et al.* (2012) Nutrient limitation reduces land carbon uptake in simulations with a model of combined carbon, nitrogen and phosphorus cycling. Biogeosciences, **9**, 3547-3569.

Goodale CL, Apps MJ, Birdsey RA *et al.* (2002) Forest carbon sinks in the Northern Hemisphere. Ecological Applications, **12**, 891-899.

Guo Z, Fang J, Pan Y, Birdsey R (2010) Inventory-based estimates of forest biomass carbon stocks in China: A comparison of three methods. Forest Ecology and Management, **259**, 1225-1231.

Hansen MC, Defries RS, Townshend JRG, Sohlberg R, Dimiceli C, Carroll M (2002) Towards an operational MODIS continuous field of percent tree cover algorithm: examples using AVHRR and MODIS data. Remote Sensing of Environment, **83**, 303-319.

Harrison SP, Prentice IC, Barboni D, Kohfeld KE, Ni J, Sutra J-P (2010) Ecophysiological and bioclimatic foundations for a global plant functional classification. Journal of Vegetation Science, **21**, 300-317.

Harsch MA, Bader MY (2011) Treeline form - a potential key to understanding treeline dynamics. Global Ecology and Biogeography, **20**, 582-596.

Hartmann H, Ziegler W, Kolle O, Trumbore S (2013) Thirst beats hunger - declining hydration during drought prevents carbon starvation in Norway spruce saplings. New Phytologist, **200**, 340-349.

Hastie TJ, Tibshirani RJ (1990) *Generalized additive models*, Boca Raton, FL, Chapman & Hall/CRC.

Heinsch FA, Reeves M, Votava P *et al.* (2003) User's Guide. GPP and NPP (MOD17A2/A3) products. NASA MODIS land algorithm. pp 57.

Henry M, Bombelli A, Trotta C *et al.* (2013) GlobAllomeTree: international platform for tree allometric equations to support volume, biomass and carbon assessment. iForest - Biogeosciences and Forestry, **6**, 326-330.

Hijmans RJ, Cameron SE, Parra JL, Jones PG, Jarvis A (2005) Very high resolution interpolated climate surfaces for global land areas. International Journal of Climatology, **25**, 1965-1978.

Holtmeier FK (1971) Waldgrenzenstudien im nördlichen Finnisch-Lappland und angrenzenden Nordnorwegen. Rep. Kevo Subarctic Res. Stat., **8**, 53-62.

Holzwarth F, Kahl A, Bauhus J, Wirth C, Zuidema P (2013) Many ways to die - partitioning tree mortality dynamics in a near-natural mixed deciduous forest. Journal of Ecology, **101**, 220-230.

Inatomi M, Ito A, Ishijima K, Murayama S (2010) Greenhouse Gas Budget of a Cool-Temperate Deciduous Broad-Leaved Forest in Japan Estimated Using a Process-Based Model. Ecosystems, **13**, 472-483.

Ito A, Oikawa T (2002) A simulation model of the carbon cycle in land ecosystems (Sim-CYCLE): a description based on dry-matter production theory and plot-scale validation. Ecological Modelling, **151**, 143-176.

Jenkins JC, Chojnacky DC, Heath LS, Birdsey RA (2003) National-scale biomass estimators for United States tree species. Forest Science, **49**, 12-35.

Jones GS, Stott PA, Christidis N (2013) Attribution of observed historical near-surface temperature variations to anthropogenic and natural causes using CMIP5 simulations. Journal of Geophysical Research: Atmospheres, **118**, 4001-4024.

Jönsson AM, Linderson M-L, Stjernquist I, Schlyter P, Bärring L (2004) Climate change and the effect of temperature backlashes causing frost damage in Picea abies. Global and Planetary Change, **44**, 195-207.

JRC (2003) Global Land Cover 2000 database, European Commission, Joint Research Centre (available online at: http://bioval.jrc.ec.europa.eu/products/glc2000/glc2000.php, accessed 2012/07/03).

JRC (2009) The Biomass Compartment Database of the GHG-AFOLU project of the European Commission, Joint Research Centre (available online at: http://afoludata.jrc.ec.europa.eu/index.php/public_area/biomass_compartments, accessed 2012/01/06).

Kasischke ES, Williams D, Barry D (2002) Analysis of the patterns of large fires in the boreal forest region of Alaska. International Journal of Wildland Fire, **11**, 131-144.

Kattge J, Díaz S, Lavorel S *et al.* (2011) TRY - a global database of plant traits. Global Change Biology, **17**, 2905-2935.

Keith H, Mackey BG, Lindenmayer DB (2009) Re-evaluation of forest biomass carbon stocks and lessons from the world's most carbon-dense forests. PNAS, **106**, 11635-11640.

Kellndorfer JM, Walker WS, Lapoint E, Kirsch K, Bishop J, Fiske G (2010) Statistical fusion of lidar, InSAR, and optical remote sensing data for forest stand height characterization: A regional-scale method based on LVIS, SRTM, Landsat ETM+, and ancillary data sets. Journal of Geophysical Research: Biogeosciences, **115**, G00E08.

Kellndorfer J, Walker W, LaPoint E *et al.* (2012) NACP aboveground biomass and carbon baseline data (NBCD 2000), USA 2000 data set, Oak Ridge, TN, ORNL DAAC (available online at: http://daac.ornl.gov, accessed 2012/11/07).

Knorr W (2000) Annual and interannual CO2 exchanges of the terrestrial biosphere: process-based simulations and uncertainties. Global Ecology and Biogeography, **9**, 225-252.

Knorr W, Kattge J (2005) Inversion of terrestrial ecosystem model parameter values against eddy covariance measurements by Monte Carlo sampling. Global Change Biology, **11**, 1333-1351.

Knutson TR, Zeng F, Wittenberg AT (2013) Multimodel Assessment of Regional Surface Temperature Trends: CMIP3 and CMIP5 Twentieth-Century Simulations. Journal of Climate, **26**, 8709-8743.

Köble R, Seufert G (2001) Novel maps for forest tree species in Europe. pp 6, Ispra, JRC.

Kottek M, Grieser J, Beck C, Rudolf B, Rubel F (2006) World Map of the Köppen-Geiger climate classification updated. Meteorologische Zeitschrift, **15**, 259-263.

Kreyling J, Buhk C, Backhaus S *et al.* (2014) Local adaptations to frost in marginal and central populations of the dominant forest tree Fagus sylvatica L. as affected by temperature and extreme drought in common garden experiments. Ecology and Evolution, **4**, 594-605.

Krinner G, Viovy N, De Noblet-Ducoudré N *et al.* (2005) A dynamic global vegetation model for studies of the coupled atmosphere-biosphere system. Global Biogeochemical Cycles, **19**, GB1015.

Kurz WA, Dymond CC, Stinson G *et al.* (2008) Mountain pine beetle and forest carbon feedback to climate change. Nature, **452**, 987-990.

Le Page Y, Morton D, Bond-Lamberty B, Pereira JMC, Hurtt G (2015) HESFIRE: a global fire model to explore the role of anthropogenic and weather drivers. Biogeosciences, **12**, 887-903.

Le Quéré C, Moriarty R, Andrew RM *et al.* (2015) Global Carbon Budget 2015. Earth System Science Data, **7**, 349-396.

Le Toan T, Quegan S, Davidson MWJ *et al.* (2011) The BIOMASS mission: Mapping global forest biomass to better understand the terrestrial carbon cycle. Remote Sensing of Environment, **115**, 2850-2860.

Liski J, Korotkov AV, Prins CFL, Karjalainen T, Victor DG, Kauppi PE (2003) Increased carbon sink in temperate and boreal forests. Climatic Change, **61**, 89-99.

Litton CM, Raich JW, Ryan MG (2007) Carbon allocation in forest ecosystems. Global Change Biology, **13**, 2089-2109.

Lo E (2005) Gaussian error propagation applied to ecological data: post-ice-storm-downed woody biomass. Ecological Monographs, **75**, 451-466.

Logan JA, Régnière J, Powell JA (2003) Assessing the impacts of global warming on forest pest dynamics. Frontiers in Ecology and the Environment, **1**, 130-137.

Luyssaert S, Inglima I, Jung M *et al.* (2007) CO2balance of boreal, temperate, and tropical forests derived from a global database. Global Change Biology, **13**, 2509-2537.

Ma Z, Peng C, Zhu Q *et al.* (2012) Regional drought-induced reduction in the biomass carbon sink of Canada's boreal forests. PNAS, **109**, 2423-2427.

McDowell N, Pockman WT, Allen CD *et al.* (2008) Mechanisms of plant survival and mortality during drought: why do some plants survive while others succumb to drought? New Phytologist, **178**, 719-739.

McDowell NG, Beerling DJ, Breshears DD, Fisher RA, Raffa KF, Stitt M (2011) The interdependence of mechanisms underlying climate-driven vegetation mortality. Trends in Ecology and Evolution, **26**, 523-532.

Metla (2013) File service for publicly available data, Finnish Forest Research Institute Metla (http://kartta.metla.fi/index-en.html, accessed 2016/04/02).

Michaelian M, Hogg EH, Hall RJ, Arsenault E (2011) Massive mortality of aspen following severe drought along the southern edge of the Canadian boreal forest. Global Change Biology, **17**, 2084-2094.

Michaelis P (1934a) Ökologische Studien an der alpinen Baumgrenze. IV. Zur Kenntnis des winterlichen Wasserhaushaltes. Jahrb. Wiss. Bot., **80**, 169-298.

Michaelis P (1934b) Ökologische Studien an der alpinen Baumgrenze. V. Osmotischer Wert und Wassergehalt während des Winters in den verschiedenen Höhenlagen. Jahrb. Wiss. Bot., **80**, 337-362.

Mitchell PJ, O'Grady AP, Tissue DT, White DA, Ottenschlaeger ML, Pinkard EA (2013) Drought response strategies define the relative contributions of hydraulic dysfunction and carbohydrate depletion during tree mortality. New Phytologist, **197**, 862-872.

Mokany K, Raison RJ, Prokushkin AS (2006) Critical analysis of root:shoot ratios in terrestrial biomes. Global Change Biology, **12**, 84-96.

Moss RH, Edmonds JA, Hibbard KA *et al.* (2010) The next generation of scenarios for climate change research and assessment. Nature, **463**, 747-756.

Myhre G, Shindell D, Bréon F-M *et al.* (2013) Anthropogenic and Natural Radiative Forcing. In: *Climate Change 2013: The Physical Science Basis. Contribution of Working Group I to the Fifth Assessment Report of the Intergovernmental Panel on Climate Change*. (eds Stocker TF, Qin D, Plattner G-K *et al.*] pp 659-740, Cambridge, United Kingdom and New York, NY, USA, Cambridge University Press.

Nash JE, Sutcliffe JV (1970) River flow forecasting through conceptual models part I - a discussion of principles. Journal of Hydrology, **10**, 282-290.

Neeck SP (2015) The NASA Earth Science Flight Program: an update. Proc. SPIE, **9639**, Sensors, Systems, and Next-Generation Satellites XIX, 963907 (October 12, 2015); doi:10.1117/12.2199919.

Nemani RR, Keeling CD, Hashimoto H *et al.* (2003) Climate-driven increases in global terrestrial net primary production from 1982 to 1999. Science, **300**, 1560-1563.

Noormets A, Epron D, Domec JC, Mcnulty SG, Fox T, Sun G, King JS (2015) Effects of forest management on productivity and carbon sequestration: A review and hypothesis. Forest Ecology and Management, **355**, 124-140.

Norby RJ (1998) Nitrogen deposition: a component of global change analyses. New Phytologist, **139**, 189-200.

Olson DM, Dinerstein E, Wikramanayake ED *et al.* (2001) Terrestrial ecoregions of the world: A new map of life on Earth. BioScience, **51**, 933-938.

Pan Y, Birdsey RA, Fang J *et al.* (2011) A large and persistent carbon sink in the world's forests. Science, **333**, 988-993.

Patenaude G, Hill RA, Milne R, Gaveau DLA, Briggs BBJ, Dawson TP (2004) Quantifying forest above ground carbon content using LiDAR remote sensing. Remote Sensing of Environment, **93**, 368-380.

Pavlick R, Drewry DT, Bohn K, Reu B, Kleidon A (2013) The Jena Diversity-Dynamic Global Vegetation Model (JeDi-DGVM): a diverse approach to representing terrestrial biogeography and biogeochemistry based on plant functional trade-offs. Biogeosciences, **10**, 4137-4177.

Peng C, Ma Z, Lei X *et al.* (2011) A drought-induced pervasive increase in tree mortality across Canada's boreal forests. Nature Climate Change, **1**, 467-471.

Penuelas J (2005) A big issue for trees. Nature, **437**, 965-966.

Piao S, Luyssaert S, Ciais P *et al.* (2010) Forest annual carbon cost: a global-scale analysis of autotrophic respiration. Ecology, **91**, 652-661.

Piao S, Sitch S, Ciais P *et al.* (2013) Evaluation of terrestrial carbon cycle models for their response to climate variability and to CO2 trends. Global Change Biology, **19**, 2117-2132.

Pinheiro J, Bates D (2000) *Mixed-effects models in S and S-PLUS*, New York, Springer.

Poorter H, Niklas KJ, Reich PB, Oleksyn J, Poot P, Mommer L (2012) Biomass allocation to leaves, stems and roots: meta-analyses of interspecific variation and environmental control. New Phytologist, **193**, 30-50.

Raddatz TJ, Reick CH, Knorr W *et al.* (2007) Will the tropical land biosphere dominate the climate–carbon cycle feedback during the twenty-first century? Climate Dynamics, **29**, 565-574.

Raffa KF, Aukema BH, Bentz BJ, Carroll AL, Hicke JA, Turner MG, Romme WH (2008) Cross-scale Drivers of Natural Disturbances Prone to Anthropogenic Amplification: The Dynamics of Bark Beetle Eruptions. BioScience, **58**, 501.

Rammig A, Jönsson AM, Hickler T, Smith B, Bärring L, Sykes MT (2010) Impacts of changing frost regimes on Swedish forests: Incorporating cold hardiness in a regional ecosystem model. Ecological Modelling, **221**, 303-313.

Reese H, Nilsson M, Granqvist Pahlén T *et al.* (2003) Countrywide estimates of forest variables using satellite data and field data from the national forest inventory. Ambio, **32**, 542-548.

Regniere J, Bentz B (2007) Modeling cold tolerance in the mountain pine beetle, Dendroctonus ponderosae. Journal of Insect Physiology, **53**, 559-572.

Reich PB, Luo Y, Bradford JB, Poorter H, Perry CH, Oleksyn J (2014) Temperature drives global patterns in forest biomass distribution in leaves, stems, and roots. PNAS, **111**, 13721-13726.

Reichstein M, Bahn M, Ciais P *et al.* (2013) Climate extremes and the carbon cycle. Nature, **500**, 287-295.

Rodhe H (1992) Modeling biogeochemical cycles. In: *Global biogeochemical cycles.* (eds Butcher SS, Charlson RJ, Orians GH, Wolfe GV) pp 55-72, London, Academic Press.

Rosenqvist A, Shimada M, Ito N, Watanabe M (2007) ALOS PALSAR: a Pathfinder mission for global-scale monitoring of the environment. IEEE Transactions on Geoscience and Remote Sensing, **45**, 3307-3316.

Running SW, Nemani RR, Heinsch FA, Zhao M, Reeves M, Hashimoto H (2004) A continuous satellite-derived measure of global terrestrial primary production. BioScience, **54**, 547-560.

Saatchi SS, Houghton RA, Dos Santos Alvalá RC, Soares JV, Yu Y (2007) Distribution of aboveground live biomass in the Amazon basin. Global Change Biology, **13**, 816-837.

Saatchi SS, Harris NL, Brown S *et al.* (2011) Benchmark map of forest carbon stocks in tropical regions across three continents. PNAS, **108**, 9899-9904.

Safranyik L, Carroll AL (2006) The biology and epidemiology of the mountain pine beetle in lodgepole pine forests. In: *The mountain pine beetle. A synthesis of biology, management, and impacts on lodgepole pine.* (eds Safranyik L, Wilson B) pp 3-66, Victoria, BC, Natural Resources Canada, Canadian Forest Service, Pacific Forestry Centre.

Sakai A, Weiser CJ (1973) Freezing resistance of trees in North America with reference to tree regions. Ecology, **54**, 118-126.

Sakai A, Larcher W (1987) *Frost survival of plants. Responses and adaptation to freezing stress,* Berlin, Springer.

Sala A, Piper F, Hoch G (2010) Physiological mechanisms of drought-induced tree mortality are far from being resolved. New Phytologist, **186**, 274-281.

Santoro M, Beer C, Cartus O *et al.* (2011) Retrieval of growing stock volume in boreal forest using hyper-temporal series of Envisat ASAR ScanSAR backscatter measurements. Remote Sensing of Environment, **115**, 490-507.

Santoro M, Wegmüller U, Carvalhais N, Thurner M, Beer C, Fransson JES, Schmullius C (2014) K&C Final Report – Phase 3. Coupling radar-based estimates of forest information with biosphere models for improved carbon flux estimation. pp 15, Gümligen, Gamma Remote Sensing.

Santoro M, Beaudoin A, Beer C *et al.* (2015) Forest growing stock volume of the northern hemisphere: Spatially explicit estimates for 2010 derived from Envisat ASAR. Remote Sensing of Environment, **168**, 316-334.

Saugier B, Roy J, Mooney HA (2001) Estimations of global terrestrial productivity: converging toward a single number? In: *Terrestrial global productivity* (eds Roy J, Saugier B, Mooney HA) pp 543-557. San Diego, CA, Academic Press.

Schaefer K, Schwalm CR, Williams C *et al.* (2012) A model-data comparison of gross primary productivity: Results from the North American Carbon Program site synthesis. Journal of Geophysical Research: Biogeosciences, **117**, G03010.

Schaphoff S, Lucht W, Gerten D, Sitch S, Cramer W, Prentice IC (2006) Terrestrial biosphere carbon storage under alternative climate projections. Climatic Change, **74**, 97-122.

Schepaschenko D, Mccallum I, Shvidenko A, Fritz S, Kraxner F, Obersteiner M (2011) A new hybrid land cover dataset for Russia: a methodology for integrating statistics, remote sensing and in situ information. Journal of Land Use Science, **6**, 245-259.

Schlyter P, Stjernquist I, Bärring L, Jönsson AM, Nilsson C (2006) Assessment of the impacts of climate change and weather extremes on boreal forests in northern Europe, focusing on Norway spruce. Climate Research, **31**, 75-84.

Schreiber SG, Ding C, Hamann A, Hacke UG, Thomas BR, Brouard JS, Saura S (2013) Frost hardiness vs. growth performance in trembling aspen: an experimental test of assisted migration. Journal of Applied Ecology, **50**, 939-949.

Schwartz SE (1979) Residence times in reservoirs under non-steady-state conditions: application to atmospheric SO, and aerosol sulfate. Tellus, **31**, 530-547.

Shinozaki K, Yoda K, Hozumi K, Kira T (1964) A quantitative analysis of plant form - the pipe model theory. I. Basic analyses. Japanese Journal of Ecology, **14**, 97-105.

Shvidenko A, Schepaschenko D, Nilsson S, Bouloui Y (2007a) Semi-empirical models for assessing biological productivity of Northern Eurasian forests. Ecological Modelling, **204**, 163-179.

Shvidenko A, Schepaschenko D, McCallum I, Nilsson S (2007b) CD-ROM "Russian Forests and Forestry", Laxenburg, Austria, International Institute for Applied Systems Analysis and the Russian Academy of Science.

Shvidenko A, Schepaschenko D, Mccallum I, Nilsson S (2010) Can the uncertainty of full carbon accounting of forest ecosystems be made acceptable to policymakers? Climatic Change, **103**, 137-157.

Sillmann J, Kharin VV, Zwiers FW, Zhang X, Bronaugh D (2013) Climate extremes indices in the CMIP5 multimodel ensemble: Part 2. Future climate projections. Journal of Geophysical Research: Atmospheres, **118**, 2473-2493.

Sitch S, Smith B, Prentice IC *et al.* (2003) Evaluation of ecosystem dynamics, plant geography and terrestrial carbon cycling in the LPJ dynamic global vegetation model. Global Change Biology, **9**, 161-185.

Sitch S, Huntingford C, Gedney N *et al.* (2008) Evaluation of the terrestrial carbon cycle, future plant geography and climate-carbon cycle feedbacks using five Dynamic Global Vegetation Models (DGVMs). Global Change Biology, **14**, 2015-2039.

Sitch S, Friedlingstein P, Gruber N *et al.* (2015) Recent trends and drivers of regional sources and sinks of carbon dioxide. Biogeosciences, **12**, 653-679.

Smith NG, Dukes JS (2013) Plant respiration and photosynthesis in global-scale models: incorporating acclimation to temperature and CO2. Global Change Biology, **19**, 45-63.

Somogyi Z, Teobaldelli M, Federici S, Matteucci G, Pagliari V, Grassi G, Seufert G (2008) Allometric biomass and carbon factors database. iForest, **1**, 107-113.

Sperry JS, Sullivan JEM (1992) Xylem embolism in response to freeze-thaw cycles and water stress in ring-porous, diffuse porous, and conifer species. Plant Physiology, **100**, 605-613.

Sun Y, Gu L, Dickinson RE, Zhou B (2012) Forest greenness after the massive 2008 Chinese ice storm: integrated effects of natural processes and human intervention. Environmental Research Letters, **7**, 035702.

Taylor JR (1997) *An introduction to error analysis. The study of uncertainties in physical measurements*, Sausalito, CA, University Science Books.

Teobaldelli M, Somogyi Z, Migliavacca M, Usoltsev VA (2009) Generalized functions of biomass expansion factors for conifers and broadleaved by stand age, growing stock and site index. Forest Ecology and Management, **257**, 1004-1013.

Thiel D, Kreyling J, Backhaus S *et al.* (2014) Different reactions of central and marginal provenances of Fagus sylvatica to experimental drought. European Journal of Forest Research, **133**, 247-260.

Thomas SC, Martin AR (2012) Carbon Content of Tree Tissues: A Synthesis. Forests, **3**, 332-352.

Thonicke K, Venevsky S, Sitch S, Cramer W (2001) The role of fire disturbance for global vegetation dynamics: coupling fire into a Dynamic Global Vegetation Model. Global Ecology and Biogeography, **10**, 661-677.

Thornley JHM (1970) Respiration, growth and maintenance in plants. Nature, **227**, 304-305.

Thurner M, Beer C, Santoro M *et al.* (2014) Carbon stock and density of northern boreal and temperate forests. Global Ecology and Biogeography, **23**, 297-310.

Torres R, Snoeij P, Geudtner D *et al.* (2012) GMES Sentinel-1 mission. Remote Sensing of Environment, **120**, 9-24.

Townshend JRG, Hansen MC, Carroll M, Dimiceli C, Sohlberg R, Huang C (2011) User Guide for the MODIS Vegetation Continuous Fields product Collection 5 version 1. pp 12, University of Maryland.

Tranquillini W (1979) *Physiological ecology of the Alpine timberline. Tree existence at high altitudes with special reference to the European Alps,* Berlin, Springer.

Tum M, Buchhorn M, Günther KP, Haller BC (2011) Validation of modelled forest biomass in Germany using BETHY/DLR. Geoscientific Model Development, **4**, 1019-1034.

Tum M, Günther KP (2011) Validating modelled NPP using statistical yield data. Biomass and Bioenergy, **35**, 4665-4674.

Turner DP, Ritts WD, Cohen WB *et al.* (2005) Site-level evaluation of satellite-based global terrestrial gross primary production and net primary production monitoring. Global Change Biology, **11**, 666-684.

Turner DP, Ritts WD, Cohen WB *et al.* (2006) Evaluation of MODIS NPP and GPP products across multiple biomes. Remote Sensing of Environment, **102**, 282-292.

UN-REDD (2011) UN-REDD Programme, Support to National REDD+ Action, Global Programme Framework 2011–2015, adopted as of 9 August 2011, The United Nations Collaborative Programme on Reducing Emissions from Deforestation and Forest Degradation in Developing Countries, FAO, UNDP, UNEP.

Urban M, Forkel M, Eberle J, Hüttich C, Schmullius C, Herold M (2014) Pan-Arctic Climate and Land Cover Trends Derived from Multi-Variate and Multi-Scale Analyses (1981–2012). Remote Sensing, **6**, 2296-2316.

USDA (2012) Forest inventory and analysis national program, United States Department of Agriculture (available online at: http://www.fia.fs.fed.us/, accessed 2012/11/07).

Usoltsev VA (2001) *Forest biomass of northern Eurasia*, Yekaterienburg, Russian Academy of Sciences, Ural Branch, Botanical Garden and Ministry of Education of Russian Federation, Ural State Forest Engineering University (in Russian).

Van Oijen M, Schapendonk A, Hoglind M (2010) On the relative magnitudes of photosynthesis, respiration, growth and carbon storage in vegetation. Annals of Botany, **105**, 793-797.

Van Vuuren DP, Edmonds J, Kainuma M *et al.* (2011) The representative concentration pathways: an overview. Climatic Change, **109**, 5-31.

Vicca S, Luyssaert S, Penuelas J *et al.* (2012) Fertile forests produce biomass more efficiently. Ecology Letters, **15**, 520-526.

Wardle P (1971) An explanation for alpine timberline. New Zealand Journal of Botany, **9**, 371-402.

Waring RH, Landsberg JJ, Williams M (1998) Net primary production of forests: a constant fraction of gross primary production? Tree Physiology, **18**, 129-134.

Warszawski L, Frieler K, Huber V, Piontek F, Serdeczny O, Schewe J (2014) The Inter-Sectoral Impact Model Intercomparison Project (ISI-MIP): project framework. PNAS, **111**, 3228-3232.

Weedon GP, Gomes S, Viterbo P *et al.* (2011) Creation of the WATCH Forcing Data and Its Use to Assess Global and Regional Reference Crop Evaporation over Land during the Twentieth Century. Journal of Hydrometeorology, **12**, 823-848.

Williams AP, Allen CD, Millar CI, Swetnam TW, Michaelsen J, Still CJ, Leavitt SW (2010) Forest responses to increasing aridity and warmth in the southwestern United States. PNAS, **107**, 21289-21294.

Williams DW, Liebhold AM (2002) Climate change and the outbreak ranges of two North American bark beetles. Agricultural and Forest Entomology, **4**, 87-99.

Williams M, Hill TC, Ryan CM (2013) Using biomass distributions to determine probability and intensity of tropical forest disturbance. Plant Ecology & Diversity, **6**, 87-99.

Wißkirchen K, Tum M, Günther KP, Niklaus M, Eisfelder C, Knorr W (2013) Quantifying the carbon uptake by vegetation for Europe on a 1 km² resolution using a remote sensing driven vegetation model. Geoscientific Model Development, **6**, 1623-1640.

Wolf A, Field CB, Berry JA (2011) Allometric growth and allocation in forests: a perspective from FLUXNET. Ecological Applications, **21**, 1546-1556.

Wood SN (2006) *Generalized additive models: an introduction with R*, Boca Raton, FL, Chapman & Hall/CRC.

Woodward FI, Williams BG (1987) Climate and plant distribution at global and local scales. Vegetatio, **69**, 189-197.

Woodward FI, Lomas MR (2004) Vegetation dynamics – simulating responses to climatic change. Biological Reviews, **79**, 643-670.

Wutzler T, Wirth C, Schumacher J (2008) Generic biomass functions for Common beech (Fagus sylvatica) in Central Europe: predictions and components of uncertainty. Canadian Journal of Forest Research, **38**, 1661-1675.

Xia J, Niu S, Ciais P *et al.* (2015) Joint control of terrestrial gross primary productivity by plant phenology and physiology. PNAS, **112**, 2788-2793.

Yuan W, Liu S, Dong W *et al.* (2014) Differentiating moss from higher plants is critical in studying the carbon cycle of the boreal biome. Nature Communications, **5**, 4270.

Zak DR, Pregitzer KS, Kubiske ME, Burton AJ (2011) Forest productivity under elevated CO(2) and O(3): positive feedbacks to soil N cycling sustain decade-

long net primary productivity enhancement by CO_2. Ecology Letters, **14**, 1220-1226.

Zaks DPM, Ramankutty N, Barford CC, Foley JA (2007) From Miami to Madison: Investigating the relationship between climate and terrestrial net primary production. Global Biogeochemical Cycles, **21**, GB3004.

Zanne AE, Lopez-Gonzalez G, Coomes DA *et al.* (2009) Data from: towards a worldwide wood economics spectrum, Dryad Digital Repository (available online at: http://datadryad.org/handle/10255/dryad.234, accessed 2011/11/02).

Zhao M, Heinsch FA, Nemani RR, Running SW (2005) Improvements of the MODIS terrestrial gross and net primary production global data set. Remote Sensing of Environment, **95**, 164-176.

Zhao M, Running SW (2010) Drought-induced reduction in global terrestrial net primary production from 2000 through 2009. Science, **329**, 940-943.

Zhu D, Peng SS, Ciais P *et al.* (2015) Improving the dynamics of northern vegetation in the ORCHIDEE ecosystem model. Geoscientific Model Development Discussions, **8**, 2213-2270.

Zianis D, Muukkonen P, Mäkipää R, Mencuccini M (2005) Biomass and stem volume equations for tree species in Europe. Silva Fennica Monographs, **4**, 63 p.

Zuur AF, Ieno EN, Walker NJ, Saveliev AA, Smith GM (2009) *Mixed effects models and extensions in ecology with R*, New York, Springer.

Selbständigkeitserklärung

Ich erkläre, dass ich die vorliegende Arbeit selbständig und unter Verwendung der angegebenen Hilfsmittel, persönlichen Mitteilungen und Quellen angefertigt habe.

Jena, 08.04.2016 Martin Thurner